University of Alberta

Conditions of Diamond Formation and Preservation from On- and Off-Craton Settings

by

Lucy Catherine Hunt

A thesis submitted to the Faculty of Graduate Studies and Research
in partial fulfillment of the requirements for the degree of

Doctor of Philosophy

Department of Earth and Atmospheric Sciences

©Lucy Hunt

Fall 2011
Edmonton, Alberta

Permission is hereby granted to the University of Alberta Libraries to reproduce single copies of this thesis and to lend or sell such copies for private, scholarly or scientific research purposes only. Where the thesis is converted to, or otherwise made available in digital form, the University of Alberta will advise potential users of the thesis of these terms.

The author reserves all other publication and other rights in association with the copyright in the thesis and, except as herein before provided, neither the thesis nor any substantial portion thereof may be printed or otherwise reproduced in any material form whatsoever without the author's prior written permission.

Dedication

This thesis is dedicated to my parents, whose love, support and “gentle nudges in the right direction” never go unappreciated.

Abstract

The Renard kimberlites (52°48’26N, 72°14’52W: Quebec, Canada) are typical for primary diamond deposits: being located within Archean basement (Superior craton). Pb-Pb isotope data of clinopyroxenes also suggests an Archean age (~2.7Ga) for the subcratonic lithospheric mantle (SCLM). The Carolina Kimberlite (11°29’5S, 61°1’30W: Rondônia State, Brazil) is unconventional, being located within Proterozoic basement (Amazon “craton”). Whilst there are no age constraints on the SCLM, a post-Archean setting is consistent with a lack of harzburgitic garnets.

Renard xenolith/xenocryst geothermobarometry suggests, at the time of kimberlite emplacement (~632Ma), an ~190km thick lithosphere with a “cold” (38mW/m2) model conductive geotherm was present. Geothermobarometry on Carolina clinopyroxene grains derived from surficial samples and from kimberlite core indicates two geothermal gradients: a hotter 44mW/m2, and a colder 38mW/m2 geotherm. Grains from the kimberlite core exclusively reflect the colder geotherm, whereas clinopyroxene from surficial samples derive from both gradients. It is proposed that the implied change in geotherm reflects a large scale heating episode which may relate to the opening of the South Atlantic. Diamond inclusion and nitrogen thermometry data from both Renard and Carolina indicate normal mantle residence temperatures, predominantly between 1100-1200oC.

At Renard, the xenoliths/xenocrysts and diamond inclusions indicate a peridotite dominated SCLM, with only a minor eclogitic population. Mineral

inclusions also document an unusually high abundance of coesite. We propose the presence of SiO2 was caused by an extreme influx of CO2 into peridotitic SCLM, causing progressive carbonation reactions, locally consuming all olivine, orthopyroxene, and clinopyroxene and leaving free SiO2.

Diamonds from Carolina have high nitrogen contents and, in part, highly negative carbon isotopic values suggesting an eclogitic paragenesis. This is also indicated by eclogitic garnet xenocrysts (13% of the garnet population), of which just over half have high sodium (>0.07wt% Na2O), considered to be an indication of increased depth and higher diamond potential.

Xenoliths/xenocrysts sampled by the Renard kimberlites indicate an evolving melt pervasively re-fertilized an originally strongly depleted lithospheric mantle with respect to highly and moderately incompatible trace elements. Less pervasive fluid style metasomatism, as indicated by selective re-enrichment of highly incompatible elements, occurred within a depth range of 125-170km.

Acknowledgements

When I began this journey I knew I would need help, but I didn't know just how much. Before everybody else, I would like to thank my parents. If it hadn't have been for their continued love and support I would not be where I am today. They gave me my love for all things geology, they taught me to work hard but to enjoy life, they gave me hugs when I needed them and kicks up the bum when they were required too. I hope one day to be as determined as my Mummy and as patient as my Daddy, I couldn't ask for two better parents.

Thank you to my sister. Whilst I think my love for rocks amuses you to no end, you have always been there when I needed you – a shoulder to cry on, a friend to gossip with or sister to love. Also a huge thank you to my grandparents, I couldn't have asked for a better Nanny or Gaga. You have always been there for me, and supported me in whatever I have taken on. Now that I am done, you can finally tell your friends at the golf club that you have a doctor in the family, and not a perpetual student!

Being so far from home has been hard at times, and if it wasn't for Thomas I don't know if I would always have had the strength to keep my ears up and keep plugging away. Your support as a supervisor is unmatched, even at your busiest you have always made time for me. But, your support as a friend, mentor and surrogate dad when needed is what I am most thankful for.

My research would not have been possible without help from many people along the way. In particular I would like to thank Herman Grütter, who has provided so much help and support throughout the course of my research. Thank you to Jeff Harris and Tom McCandless who patiently taught me everything you need to know about describing diamonds. My research would not have been possible if it hadn't have been for Roger Morton, Tom McCandless and John Armstrong who provided me with all my samples. Finally, so many people gave me so much help along the way; including Bob Luth, Karlis Muehlenbachs, Toni Simonetti, Sergei Matveev, Sebastian Tappe, GuangCheng Chen and Andrew Locock to name but a few.

I have made many friends throughout my journey who helped make Canada feel like home, and I am eternally grateful to them all. I would like to especially thank, my big brother Steve Creighton, who always makes me laugh, and has helped whenever I have asked – which was a lot! Thank you to Katie – the Canadian version of me! You were always there for academic discussions over coffee, wine, cocktails and lots of great food. Thank you also to Karen, I have loved getting to know you, and appreciate all the help you have given.

Last, but by no means least, I would like to thank Jeremy. You have always been so supportive of everything that I do and I love you so much. As I got to the end of writing this thesis, I have not always been the cheeriest of people, but you have been so understanding. You make me laugh when I feel like crying, you keep me going on when I feel at my most overwhelmed, and you tell me when I am being ridiculous, when I may be being slightly ridiculous! This past year has had the lowest of lows and the highest of highs and you have been by my side through them all, thank you.

Table of Contents

List of Tables

List of Figures

List of Symbols and Abbreviations

agg.	Aggregate
%B	The proportion of nitrogen aggregation in the B centre in diamond
^{o}C	Degrees Celsius
cc	Calcite
chr	Chromite
CITZAF	A matrix correction programme for electron microprobe data
cpx	Clinopyroxene
cm	Centimetre
Cr#	Chrome number: Molar ration of Cr/(Cr+Al)*100
δ^{13}C	Carbon isotope composition expressed relative to known standard
dm	Dolomite
dodec.	Dodecahedral
EDS	Energy dispersion x-ray spectrometry
EPMA	Electron probe microanalysis
Fo	Forsterite
frag.	Fragment
FTIR	Fourier transform infrared spectrometry
G0	Unidentified garnets
G1	Megacrystic garnets
G3	Eclogitic garnets
G4	Pyroxenitic garnets
G9	Lherzolitic garnets
G10	Harzburgitic garnets
G11	Ti-metasomatised garnets
G12	Wehrlitic garnets
G?D	A “D” suffix indicates a strong association with diamond
Ga	Billions of years
gnt	Garnet
GPa	Gigapascal
HREE	Heavy rare earth element
irr.	Irregular

Kα	X-Ray emission arising from electron transfer from L to K shells
km	Kilometres
kV	Kilovolts
Lα	X-Ray emission arising from electron transfer from M to L shells
LA-MC-ICP-MS	Laser Ablation-Multi-collector-Inductively Coupled Plasma-Mass Spectrometer
LREE	Light rare earth elements
Ma	Millions of years
Mg#	Mg number: Molar ratio of Mg/(Mg+Fe)*100
Mol.%	Molecular percent
MREE	Middle rare earth elements
MSWD	Mean standard weighted deviates
µm	Micron
mW/m^2	Milliwatts per metre squared (unit of heat flow)
nA	Nanoampere
NIST	Standard from the National Institute of International Standards
octa.	Octahedral
ol	Olivine
opx	Orthopyroxene
‰	Per mil
ppb	Concentration expressed as parts per billion
ppm	Concentration expressed as parts per million
r^2	Correlation coefficient
REE	Rare earth elements
REE_N	Subscript “N” indicates normalisation values
σ	Error expressed as 1 standard deviation from the mean
SCLM	Subcontinental lithospheric mantle
Type IaA	Nitrogen aggregation expressed in A centre
Type IaAB	Nitrogen aggregation expressed in both A and B centres
Type IaB	Nitrogen aggregation expressed in B centre
Type II	Nitrogen free diamonds
V-PDB	Vienna PeeDee Belemnite carbon isotope standard
WDS	Wavelength dispersion spectrometry
wt%	Concentration in weight percent

CHAPTER 1

INTRODUCTION

1.1 Introduction

The root of the word diamond comes from the Greek words “diaphanes” and “adamas”, meaning “transparent” and “unconquerable”. Due to diamonds’ “fire” and brilliance, they are a sought after gemstone. Properties such as their extreme hardness and high thermal conductivity make them a valuable industrial mineral. Beyond their marketable attributes, however, diamonds provide invaluable information on the deep Earth. Diamonds form within the lithospheric mantle; a thermal, chemical and mechanical boundary layer within the Earth. This layer is thicker and colder beneath continental crust relative to its occurrence beneath oceanic crust (Jordan, 1978; Boyd, 1989). In particular, subcratonic lithospheric mantle – located beneath continental regions that were stabilised in the Archean (>2.5Ga) and termed cratons – is of greatest thickness, up to ~250km (e.g. Pearson *et al.*, 2004 and references therein), and is the dominant host for diamonds. The more depleted the lithosphere is the more diamond prospective (Gurney, 1984). Partial melting of primitive mantle leads to depletion in easily fusible components (lowered Si, Ti, Al, Ca and Na).

This thesis builds on decades of research which has focused on understanding the composition of the source of natural, terrestrial diamonds and, ultimately, the deep underlying sub-continental lithospheric mantle (SCLM). To do this, a number of methods and materials have been utilised. Along with diamonds, other mantle materials termed xenoliths and xenocrysts are brought to the surface by volcanic rocks such as kimberlites. The two main types of mantle derived rocks are peridotite and eclogite. The peridotitic suite is characterised by the presence of olivine, orthopyroxene, clinopyroxene, Cr-rich garnet and Mg-chromite. The eclogitic suite typically contains Cr-poor grossular garnet, omphacitic clinopyroxene (Na-rich) as well as minor phases such as rutile, kyanite, coesite and sanidine. The major element composition of these minerals can provide an insight into processes that led to craton

formation. Their incompatible trace elements are highly sensitive to secondary events, providing information on processes which have modified the lithospheric mantle after its assembly. Thus, xenoliths and xenocrysts are extremely useful in identifying the specific conditions controlling growth, survival and destruction of diamonds, however, due to a complex history of modification (Stachel *et al.*, 1998; Griffin *et al.*, 1999) they may not be representative of the SCLM at the time of diamond formation.

The study of diamonds and the mineral inclusions within them provides an alternative means of directly sampling the Earth's upper mantle. Diamonds are composed of nearly pure carbon and therefore provide only a limited amount of information about their origin in the SCLM. Minor impurities of nitrogen can be studied to provide an approximate residence temperature or age of individual diamonds within the mantle, but little information on the broader composition of the SCLM can be determined. However, during the growth of diamonds, syngenetic mineral inclusions (typically silicates, oxides and sulphides) can be trapped and enclosed within them (Harris, 1968). As diamonds are chemically inert during their mantle residence and transport to the surface, inclusions are protected from chemical alteration, preserving their original mantle signature. Inclusions, therefore, provide the only pristine information on the components and conditions of the cratonic mantle at the time of diamond formation.

1.2 Layout of Thesis

This thesis contains the detailed study of diamonds and their mineral inclusions, and xenocrysts and xenoliths from:

1) The Carolina Kimberlite, Rondônia State, Brazil, South America (Chapter 2)
2) The Renard Kimberlites, Quebec, Canada (Chapters 3 and 4)

This study focuses on mantle-derived xenoliths/xenocrysts and diamonds from two relatively poorly studied diamond bearing regions: the Otish mountains region

of the eastern Superior craton (Renard kimberlites) of Canada, and the Rondônia kimberlite province of the western Amazon "craton" (Carolina kimberlite) in Brazil. This research will improve our understanding of both the Superior Craton and the Amazon "craton" and will help contribute to understanding diamond provenance in these regions.

Brazil has had a long history in the diamond industry. In 1725 it became the third country to produce diamonds after India and Borneo, and was the world's leading supplier until the discoveries in South Africa in 1866. The diamonds were recovered from secondary deposits (such as river sediments) with the primary source(s) being unknown. The lack of primary deposits has been interpreted to be the result of erosion (e.g. Chaves *et al.*, 1993) or a derivation of the diamonds from sources outside of Brazil (e.g. Reid, 1974). More recently discoveries of diamondiferous kimberlites in Brazil (including the Carolina kimberlite) and adjacent countries (e.g. Svisero *et al.*, 1984; Bizzi *et al.*, 1994; Tompkins, 1994) show that primary sources are more common that previously suggested. However, their discovery is difficult, due to the low preservation potential of many kimberlite indicator minerals in tropical environments.

In contrast, diamond exploration in Canada only began in the 1960s, with major kimberlite discoveries not being made until the 1980s. In 1991, the first economically viable diamond deposit was discovered in the Lac de Gras area of the Northwest Territories (Kjarsgaard, 1996). Since the opening of Canada's first diamond mine - Ekati - in 1998, the diamond industry in Canada has grown considerably, with a production value of $2.1 billion in 2008. Canada is now the world's third largest diamond producer by value after Botswana and Russia (e.g. Read and Janse, 2009).

The two regions under study are similar in their relative lack of information on the underlying SCLM. However, whilst the Archean Superior craton is typical for a diamondiferous region, the Amazon "craton" in unconventional. Historically, Clifford's rule (Clifford, 1966) has been guiding diamond exploration for the last four decades. Clifford (1966) recognised two tectono-metallogenic units in Africa

containing distinct metallogenic associations, with primary diamond deposits being restricted to cratonic areas that have remained stable throughout younger periods of tectonism. This empirical rule was subsequently modified by Janse (1994) who stated that diamondiferous kimberlites are restricted to Archean (>2.5 billion year old) cratons ("Archons"). The Renard kimberlites follow this rule and are typical for diamondiferous primary deposits, being located on Archean basement rocks. In contrast, the presence of the diamondiferous Carolina kimberlite appears to be in "violation" of Clifford's rule being located within Proterozoic crustal rocks (1.8 to 1.2 billion years old). This study of the Carolina kimberlite and its diamonds will significantly advance our basic understanding of the origin and composition of deep (>140 km) and apparently stable Proterozoic cratonic keels.

1.3 Geological Background

1.3.1 Geology of the Amazon Craton

The South American platform of Brazil is underlain by two cratons; the Amazon craton and the São Francisco craton. The Amazon "craton" is one of the largest cratonic areas in the world and forms the northern part of the platform (Teixeira *et al.*, 1989; Tassinari and Macambira, 1999). The "Craton" can be divided into two Precambrian shields: The Guaporé Shield to the south and the Guiana Shield to the north, which are separated by the Paleozoic Amazonian Sedimentary Basin (Teixeira *et al.*, 1989; Tassinari and Macambira, 1999). Six major geochronological provinces have been identified (Fig. 1.1) and comprise a stable Archean nucleus: Central Amazonian Province; and five Paleoproterozoic and Mesoproterozoic Provinces: Maroni-Itacaiúnas (2.2 to 1.95Ga); Ventuari-Tapajós (1.95–1.8Ga); Rio Negro-Juruena (1.8–1.55Ga); Rondônian-San Ignácio (1.55–1.30Ga) and Sunsás (1.30–1.0Ga) (Teixeira *et al.*, 1989; Tassinari and Macambira, 1999 and references therein). The Rondônia kimberlite province, including the Carolina pipe, is located within the Rio Negro-Juruena province.

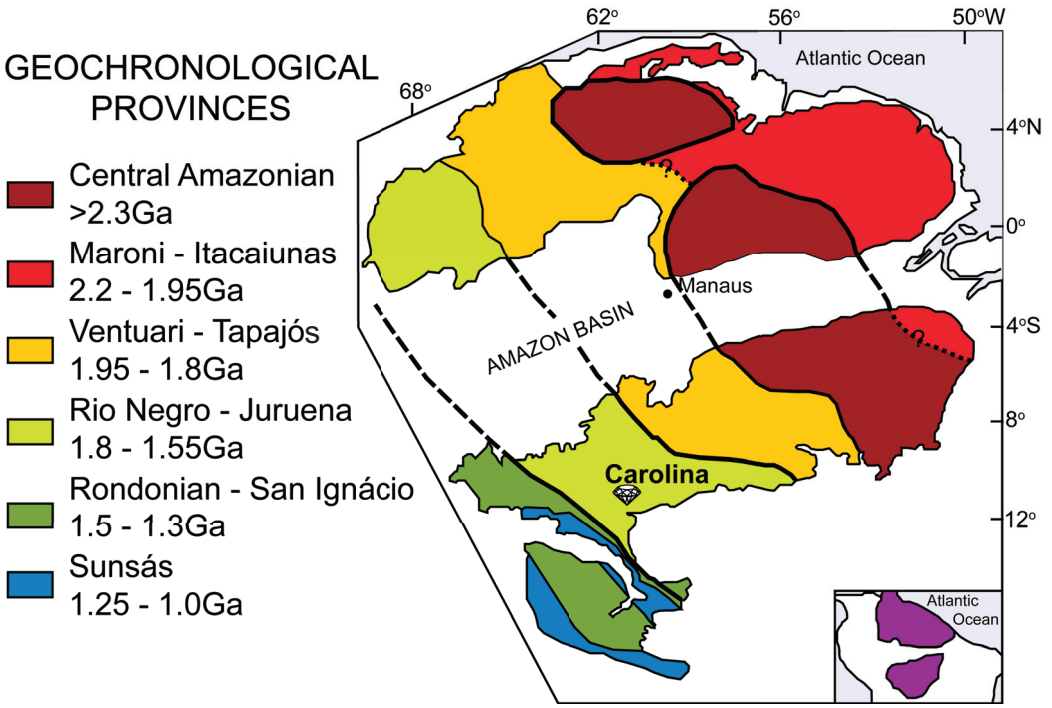

Figure 1.1. Geochronological provinces of the Amazon craton. Redrawn from Tassinari and Macambira (1999).

The Central Amazonian Province contains Archean basement rocks which are thought to have been stable since at least the lower Proterozoic (Teixeira *et al.*, 1989). The Maroni-Itacaiunas Province is characterised by large portions of supracrustal rocks associated with gneisses and migmatites predominantly accreted during the early Proterozoic, whilst the Ventuari-Itacaiunas Province comprises mainly of calc-alkaline granitoids. The Rio Negro-Juruena Province is composed almost entirely of granite-gneisses and granitoids metamorphosed to amphibolite facies with minor granulite facies also present. The units are thought to be mantle-derived magmatic arc rocks (Teixeira *et al.*, 1989; Tassinari and Macambira, 1999). In contrast, the Rondônia and Sunsas provinces are silica and alumina rich in character and record evidence of reworking of pre-existing continental material.

At least fifteen kimberlite provinces have been recognised throughout Brazil (Tompkins and Gonzaga, 1989; Kaminsky *et al.*, 2010). Along with other ultramafic alkaline activity, the majority occur along three major continental-scale lineaments (Herz, 1977; Svisero and Haralyi, 1983; Gibson *et al.*, 1995). The lineaments

were reactivated during the break-up of western Gondwana and the opening of the Atlantic Ocean (Turner *et al.*, 1994). Structurally, the Rondônia kimberlite province (including the Carolina kimberlite) is associated with the Paleozoic Pimenta Bueno- and Colorado-grabens which are aligned with the 125°AZ lineament. This lineament stretches 3000km from Rio de Janeiro to Rondônia, and is interpreted to be a continental extension of oceanic fractures in the South Atlantic and contains other kimberlite clusters (e.g. Tompkins and Gonzaga, 1989; Turner *et al.*, 1994). Approximately 200km further south-east along the lineament lie a number of Cretaceous kimberlites of the Juina area, Mato Grosso (Heaman *et al.*, 1998; Andreazza *et al.*, 2008). The Juina field is one of a number of Cretaceous alkaline volcanic centres developed along the lineament that may be attributed to the passage of the Brazilian continent over the Trindade mantle plume (Bulanova *et al.*, 2008).

1.3.2 Geology of the Superior Craton

The Superior Province in Eastern Canada is the world's largest Archean cratons. Along with other Archean provinces (e.g. Slave, Rae, Hearne, Nain) and Proterozoic orogens (e.g. Trans-Hudson, Thelon, Torngat) it makes up the majority of the Canadian Shield (Hoffman, 1988). Isotopic age determinations show that volcanic and plutonic rocks of the Superior Province range from 3.1Ga to 2.6Ga and that within this range there is evidence for several major magmatic episodes at about 3.0Ga and 2.7Ga (Card, 1990). During these episodes, tholeitic, calc-alkaline, komatiitic and alkaline volcanogenic clastic and chemical sediments of the greenstone belts were deposited, as were turbidites of intervening metasedimentary subprovinces (Card, 1990).

Within the Superior craton deep-seated mantle-derived igneous rocks, including kimberlite and ultramafic lamprophyre, form widespread diatremes and dikes (Birkett *et al.*, 2004 and references therein). The eruption centres are distributed in seven distinct fields, with the Renard kimberlite cluster being located within the Otish Mountains. The Renard kimberlites are located in the Opinaca subprovince composed predominantly of metasedimentary rocks with lesser amounts of

metavolcanics, intruded by biotite granites, and metamorphosed to greenschist to amphibolite-grade facies.

The age of sediment deposition of the Opinaca-Nemiscau subprovince is poorly understood. The minimum deposition age is best constrained by the 2674 ± 12Ma, U-Pb zircon crystallisation age (Gouthier *et al.*, 2001) of the Bezier pluton, which intrudes the Opinaca metasediments. The upper age limit of sediment deposition, ~2700Ma, is constrained by several U-Pb ages obtained from deformed plutons and volcanic rocks at the edge of the Opinaca subprovince (Moukhsil *et al.*, 2003).

The bounding subprovinces of the Opanica-Nemiscau have been the subject of numerous geochronological studies. To the north lies the La Grande subprovince. It is unusual in the eastern Superior craton as it exposes felsic gneisses and plutons which formed over a protracted period of at least 250Ma (2.88-2.62Ga), based on U-Pb age determinations (Isnard and Gariepy, 2004). Some of the older basement gneiss contain inherited zircons with ages up to 3.0Ga (Parent, 1998). To the south, the Opinaca-Nemiscau subprovince is bounded by the Abitibi-Opatica terrane. The Abitibi-Opatica terrane includes granite-greenstone belts of the Abitibi subprovince (e.g. Card and Poulsen, 1998) and gneisses and plutons of the Opatica domain (e.g. Sawyer and Benn, 1993; Davies *et al.*, 1995). The stratigraphy of the Abitibi Subprovince is the best dated and characterised sequence of Archean supracrustal rocks. It consists of several well-developed periods of volcanism between ca. 2760 and 2698Ma followed by two cycles of siliciclastic sedimentation between 2696 and 2675Ma (Ayer *et al.*, 2002).

The geological evidence suggests that deposition of thick turbidite sequences of the Opinaca metasediments occurred at ~2.71-2.70Ga ago (Fig. 1.2). This coincided with the end of major volcanism and the onset of polyphase deformation and a period of major crust formation (Card, 1990). This occurred with the collision of the Abitibi-Opatica terrane and the La Grande subprovince. This large scale subduction created the crust of the Superior province and likely, the thick underlying cratonic lithosphere below the Renard kimberlites.

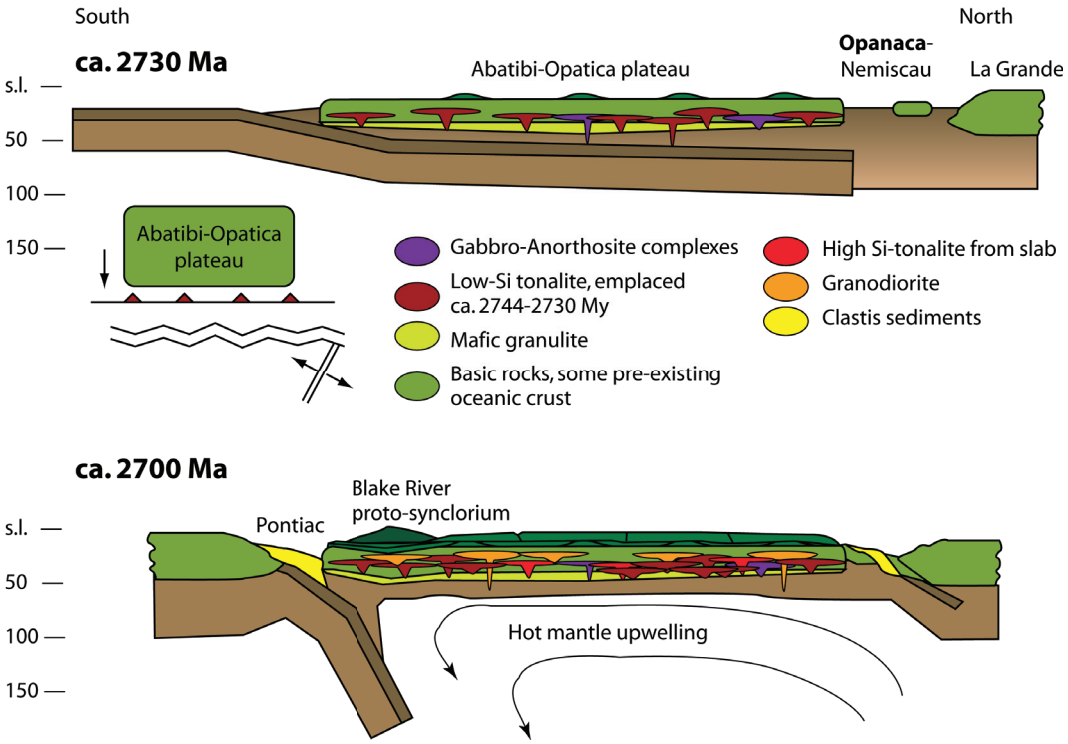

Figure 1.2. Schematic diagram showing a model of crust formation in the western Superior province, including the Opinaca domain. Redrawn from Benn and Moyen (2008).

Regional geologic syntheses (e.g. Card, 1990) complemented by comprehensive U-Pb age data (e.g. Corfu and Davies, 1992) have led to the interpretation that the elongate belts of the southern Superior province are accreted island arcs, oceanic plateaus, microcontinents and accretionary prisms amalgamated in the interval 2.75-2.70Ga - formerly collectively known as the Kenoran orogeny. Isotopic data also indicate that widespread mantle metasomatism occurred at least 2.7Ga ago and hence is probably connected with large-scale melt extraction and crustal recycling during formation of the Superior crust (Shirey and Carlson, 1986; Card, 1990).

References

Andreazza, P., Kaminsky, F.V., Sablukov, S.M., Belousova, E.A., Tremblay, M. and Griffin, W.L., 2008. Kimberlitic sources of super-deep diamonds in the Juina area, Mato Grosso State, Brazil, Extended Abstract No. 9IKC-A-00004, 9th International Kimberlite Conference, Frankfurt.

Ayer, J., Amelin, Y., Corfu, F., Kamo, S., Ketchum, J., Kwok, K. and Trowell, N., 2002. Evolution of the southern Abitibi greenstone belt based on U-Pb geochronology: autochthonous volcanic construction followed by plutonism, regional deformation and sedimentation. Precambrian Research, 115(1): 63-95.

Benn, K. and Moyen, J.F., 2008. The Late Archean Abitibi-Opatica terrane, Superior Province: A modified oceanic plateau. In: K.C. Condie and V. Pease (Editors), When Did Plate Tectonics Begin on Planet Earth. The Geological Society of America, Inc., pp. 173-197.

Birkett, T.C., McCandless, T.E. and Hood, C.T., 2004. Petrology of the Renard igneous bodies: host rocks for diamond in the northern Otish Mountains region, Quebec. Lithos, 76(1-4): 475-490.

Bizzi, L., Smith, C.B., DeWit, M.J., Armstrong, R. and Meyer, H.O.A., 1994. Mesozoic kimberlites and related alkalic rocks in south-western Sao Francisco craton, Brazil: A case for local mantle reservoirs and their interaction. Brasilia, Companhia de Pesquisa de Recursos Minerais (CPRM) Special Publication, 94/1A: 156-171.

Boyd, F.R., 1989. Compositional distinction between oceanic and cratonic lithosphere. Earth and Planetary Science Letters, 96(1-2): 15-26.

Bulanova GP, Smith CB, Walter MJ, Blundy J, Gobbo L, EIMF, Kohn SC (2008) Proto-kimberlitic ultra-deep diamonds from Collier 4 kimberlite pipe, Juina, Brazil. Extended Abstract 9IKC-A-00227, 9th International Kimberlite Conference, Frankfurt.

Card, K.D., 1990. A review of the Superior Province of the Canadian Shield, a product of Archean accretion. Precambrian Research, 48(1-2): 99-156.

Card, K.D. and Poulsen, k.H., 1998. Archean and Paleoproterozoic geology and metallogeny of the southern Canadian Shield. Exploration and Mining Geology, 7(3): 181-215.

Chaves, M.L.C.S., Dupont, H., Karfunkel, J. and Svisero, D.P., 1993. Depósitos diamantíferos de Minas Gerais: Uma revisão: Anais I Simpósio Brasileiro de Geologia do Diamante, Cuiabá. 79-100.

Clifford, T.N., 1966. Tectono-metallogenic units and metallogenic provinces of Africa. Earth and Planetary Science Letters, 1(6): 421-434.

Corfu, F. and Davies, D.W., 1992. U-Pb geochronological framework for the western Superior Province, Ontario. In: P.C. Thurston, H.R. Williams, R.H. Sutcliffe and G.M. Stott (Editors), Geology of Ontario, Ontario Geological Survey Special Volumes, 4, 1135–1346.

Davies, W.J., Machado, N., Garièpy, C., Sawyer, E.W. and Benn, K., 1995. U-Pb geochronology of the Opatica tonalite-gneiss belt and its relationship to the Abitibi greenstone belt, Superior Province, Quebec. Canadian Journal of Earth Sciences, 32: 113–127.

Gibson, S.A., Thompson, R.N., Leonardos, O.H., Dickin, A.P. and Mitchell, J.G., 1995. The Late Cretaceous Impact of the Trindade Mantle Plume - Evidence from Large-Volume, Mafic, Potassic Magmatism in Se Brazil. Journal of Petrology, 36(1): 189-229.

Gouthier, J., Dion, C., Ouellet, M.-C., Davis, D.W., David, J. and Parent, M., 2001. Géologie de la région du Lac Guyer (33G/05, 33/G06 et 33G/11). Ministère des Ressources Naturelles du Québec, RG 2001--15, Quebec.

Griffin, W.L., Shee, S.R., Ryan, C.G., Win, T.T. and Wyatt, B.A., 1999. Harzburgite to lherzolite and back again: metasomatic processes in ultramafic xenoliths from the Wesselton kimberlite, Kimberley, South Africa. Contributions to Mineralogy and Petrology, 134(2-3): 232-250.

Gurney, J.J., 1984. A correlation between garnets and diamonds in kimberlites, Publications of the Geology Department & Extension Service, University of Western Australia, pp. 143-166.

Harris, J.W., 1968. Recognition of Diamond Inclusions .1. Syngenetic Mineral Inclusions. Industrial Diamond Review, 28(334): 402.

Heaman, L.M., Teixeira, N.A., Gobbo, L. and Gaspar, J.C., 1998. U-Pb mantle zircon ages for kimberlites from the Juina and Paranatinga provinces, Brazil, VIIth International Kimberlite Conference, Extended abstracts, Cape Town, pp. 322-324.

Herz, N., 1977. Timing of Spreading in South-Atlantic - Information from Brazilian Alkalic Rocks. Geological Society of America Bulletin, 88(1): 101-112.

Hoffman, P.F., 1988. United Plates of America, the Birth of a Craton - Early Proterozoic Assembly and Growth of Laurentia. Annual Review of Earth and Planetary Sciences, 16: 543-603.

Isnard, H. and Gariepy, C., 2004. Sm-Nd, Lu-Hf and Pb-Pb signatures of gneisses and granitoids from the La Grande belt: Extent of late Archean crustal recycling in the northeastern Superior Province, Canada. Geochimica Et Cosmochimica Acta, 68(5): 1099-1113.

Janse, A.J.A., 1994. Is Clifford's rule still valid? Affirmative examples from around the world. In: H.O.A. Meyer and O.H. Leonardos (Editors), Diamonds: Characterization, Genesis and Exploration. CPRM — Special Publication Jan/94, Brasilia, pp. 215–235.

Jordan, T.H., 1978. Composition and Development of Continental Tectosphere. Nature, 274(5671): 544-548.

Kaminsky, F.V., Sablukov, S.M., Belousova, E.A., Andreazza, P., Tremblay, M. and Griffin, W.L., 2010. Kimberlitic sources of super-deep diamonds in the Juina area, Mato Grosso State, Brazil. Lithos, 114(1-2): 16-29.

Kjarsgaard BA (1996) Slave Province kimberlites, N.W.T. In: LeCheminant AN, Richardson DG, DiLabio RNW, Richardson KA (eds) Searching for

Diamonds in Canada, Open File 3228. Geological Survey of Canada, pp 55-60.

Moukhsil, A., Legault, M., Boily, M., Doyon, J., Sawyer, E.W. and Davis, W.D., 2003. Synthèse géologique et métallogénique de la ceinture de roches vertes de la moyenne et de la Basse-Eastmain, Baie James, Québec. Ministère des Ressources Naturelles du Québec.

Pearson, D.G., Canil, D. and Shirey, S.B., 2004. Mantle samples included in volcanic rocks: xenoliths and diamonds. In: R.W. Carlson (Editor), Treatise on Geochemistry. Volume 2: The Mantle and Core. Elsevier-Pergamon, Oxford, pp. 171-275.

Percival, J.A., 1989. A Regional Perspective of the Quetico Meta-Sedimentary Belt, Superior Province, Canada. Canadian Journal of Earth Sciences, 26(4): 677-693.

Read, G.H. and Janse, A.J.A., 2009. Diamonds: Exploration, mines and marketing. Lithos, 112(1): 1-9

Reid, A.R., 1974. Proposed origin for Guianian diamonds. Geology, 2: 67-68.

Sawyer, E.W. and Benn, K., 1993. Structure of the High-Grade Opatica Belt and Adjacent Low-Grade Abitibi Subprovince, Canada - an Archean Mountain Front. Journal of Structural Geology, 15(12): 1443-1458.

Shirey, S.B. and Carlson, R.W., 1986. Rb and Nd isotope evolution of the Archean Superior Province mantle enrichment and present subcontinental mantle reservoirs. Terra Cognita, 6: 237.

Stachel, T., Viljoen, K.S., Brey, G. and Harris, J.W., 1998. Metasomatic processes in lherzolitic and harzburgitic domains of diamondiferous lithospheric mantle: REE in garnets from xenoliths and inclusions in diamonds. Earth and Planetary Science Letters, 159(1-2): 1-12.

Svisero, D.P. and Haralyi, N.L.E., 1983. The Kimberlitic Province of the Upper Paranaiba, Minas-Gerais. Anais Da Academia Brasileira De Ciencias, 55(1): 137-138.

Svisero, D.P., Meyer, H.O.A., Haralyi, N.L.E. and Hasui, Y., 1984. A Note on the Geology of Some Brazilian Kimberlites. Journal of Geology, 92(3): 331-338.

Tassinari, C.C.G. and Macambira, M.J.B., 1999. Geochronological provinces of the Amazonian Craton. Episodes, 22: 174–182.

Teixeira, W., Tassinari, C.C.G., Cordani, U.G. and Kawashita, K., 1989. A Review of the Geochronology of the Amazonian Craton - Tectonic Implications. Precambrian Research, 42(3-4): 213-227.

Tompkins, L.A., 1994. Tectono-structural environments of primary diamond source rocks in Brazil: A reveiw. Brasilia, Companhia de Pesquisa de Recursos Minerais (CPRM) Special Publication, 94/1B: 259-267.

Tompkins, L.A. and Gonzaga, G.M., 1989. Diamonds in Brazil and a Proposed Model for the Origin and Distribution of Diamonds in the Coromandel Region, Minas-Gerais, Brazil. Economic Geology, 84(3): 591-602.

Turner, S., Regelous, M., Kelley, S., Hawkesworth, C. and Mantovani, M., 1994. Magmatism and continental break-up in the South Atlantic: high precision ^{40}Ar-^{39}Ar geochronology. Earth and Planetary Science Letters, 121(3-4): 333-348.

CHAPTER 2

THE CAROLINA KIMBERLITE, BRAZIL – INSIGHTS INTO AN UNCONVENTIONAL DIAMOND DEPOSIT

The content of this chapter, in modified form, has been published in *Lithos* as:
Lucy Hunt, Thomas Stachel, Roger Morton, Herman Grütter, Robert A. Creaser (2009): The Carolina kimberlite, Brazil – Insights into an unconventional diamond deposit

2.1. Introduction

Historically diamond exploration has been guided by Clifford's rule (Clifford, 1966); which states that diamondiferous kimberlites are restricted to areas of the Earth's crust that have been stable for at least 2Ga. Clifford (1966) recognised two tectono-metallogenic associations in Africa represented by distinct mineral deposits, with primary diamond deposits being restricted to cratonic areas that have been stable throughout younger periods of tectonism. This empirical rule was subsequently modified by Janse (1994) who concluded that primary diamond deposits are restricted to cratons with an age >2.5Ga ("Archons").

Clifford's rule has recently been challenged through the discovery of primary diamondiferous deposits in terranes with metamorphic ages <2Ga. These include the Argyle lamproites, emplaced within the Paleoproterozoic Halls Creek Mobile Zone along the SE edge of the Kimberley craton (Jaques *et al.*, 1986), and the Buffalo Hills kimberlites in northern Alberta (Canada), located in the Paleoproterozoic Buffalo Head Terrane (Hood and McCandless, 2004).

The diamondiferous kimberlites in the Pimenta Bueno area of Brazil provide a further challenge, since they are located in a province of the Amazon craton stabilised ≤1.8Ga (Fig. 2.1), without any indications of an Archean crustal prehistory. We have studied diamonds and mantle xenocrysts from the Carolina kimberlite in the Pimenta

Bueno area to determine if this unconventional Proterozoic setting is associated with unusual lithospheric signatures. Whilst alluvial deposits in the Pimenta Bueno were known for some time, exploration for the primary sources of these diamonds only began in 1974, with the Carolina kimberlite being found in 2002 (Maunula, 2006).

2.2. Geological Setting

The South American platform of Brazil is underlain by two cratons, the Amazon and the São Francisco (Fig. 2.1). The Rondônia kimberlite province, including the

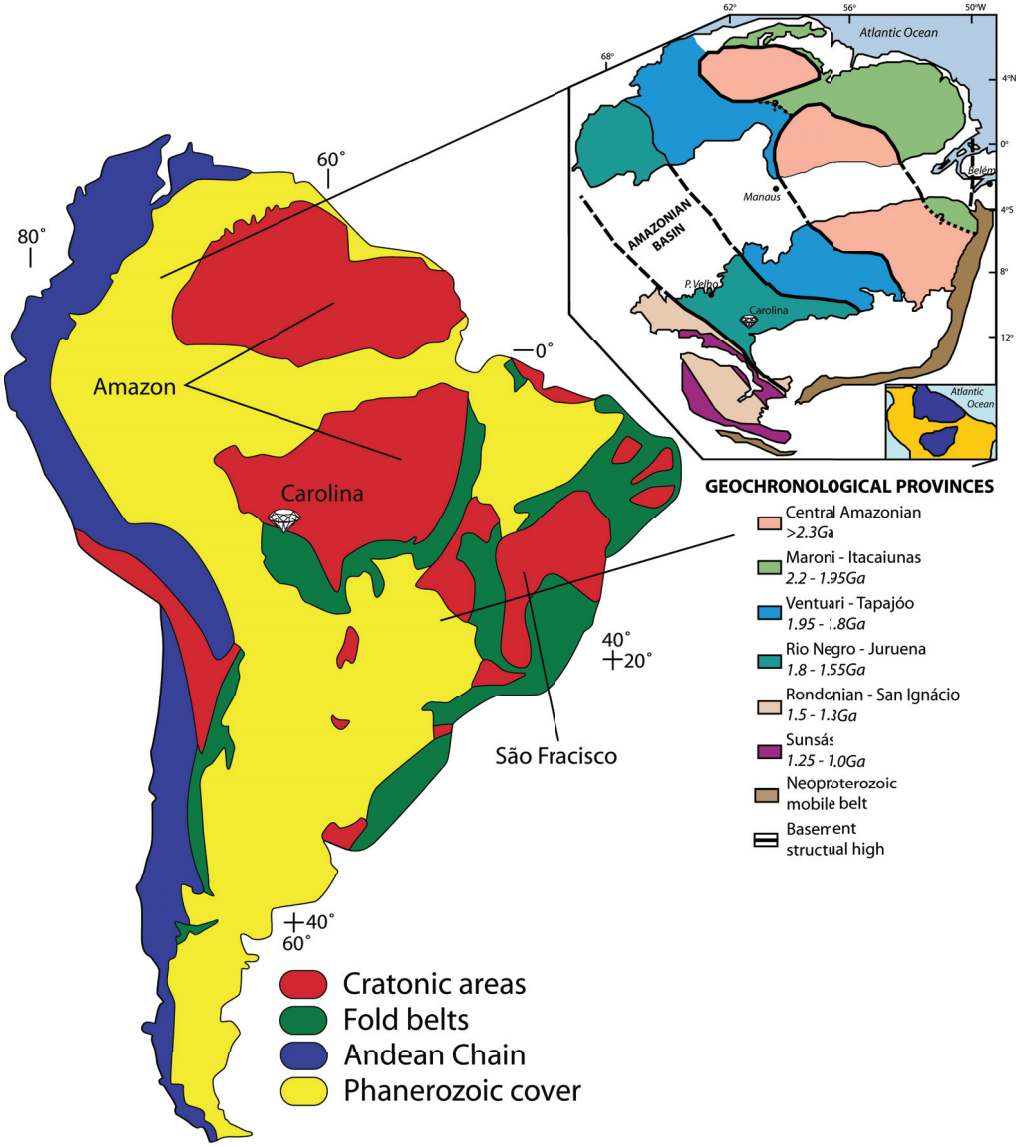

Figure 2.1. Geological setting of the Carolina kimberlite. Inset adapted from Tassinari and Macambira (1999).

Carolina pipe, is located on the Amazon craton within basement rocks of Proterozoic age (1.8 to 1.55Ga). The ages of these crustal rocks have been tightly constrained by a number of studies (Tohver *et al.*, 2005 and references therein). Little work has been carried out to establish the age of the underlying lithospheric mantle. A Paleoproterozoic age of lithospheric mantle may be inferred from the observation that crust and mantle in cratonic areas generally remain coupled since their formation (Pearson, 1999). Bulanova *et al.* (2008a) have shown the presence of harzburgitic G10 garnets in concentrates from Pimenta Bueno kimberlites (Maunula, 2006) in the same tectonic region, which implies the presence of underlying depleted mantle.

A number of ultramafic and alkaline intrusive centres, comprising kimberlites (including Carolina), kamafugites, ugandites and carbonatites (Herz, 1977; Svisero and Haralyi, 1983; Gibson *et al.*, 1995) are correlated with a pre-existing continental-scale lineament. The lineament, referred to as the 125°AZ, trends NW-SE across a large portion of the South American platform, stretching 3,000 km from Rio de Janeiro to Rondônia.

Thirty-two kimberlites occur to the east of the Carolina property, 15 of which are diamondiferous (Evans, 2005), with cross-cutting relationships and limited age dating indicating Carboniferous (~360-300Ma) ages (Manuela, 2006). The majority of the kimberlites are moderately well-preserved and typically of crater or diatreme facies (Evans, 2005). Structurally the kimberlites within the Rondônia kimberlite province show an association with the Paleozoic Pimenta Bueno- and Colorado-grabens which are themselves structurally associated and aligned with the 125°AZ lineament. Approximately 200 km further south-east along the lineament lie a number of Cretaceous kimberlites of the Juina area, Mato Grosso (Heaman *et al.*, 1998; Andreazza *et al.*, 2008). The Juina Field is one of a number of Cretaceous alkaline volcanic centres developed along the lineament attributed to the passage of the Brazilian continent over the Trindade Plume (Bulanova *et al.*, 2008b).

2.3. Samples and Analytical Methods

2.3.1. Samples

Twenty-five diamond samples ranging from 3.0 to 31.7mg were provided for destructive analysis, a further 230 diamonds were obtained for non-destructive nitrogen analysis (~3-50mg). The diamonds were recovered from the Carolina kimberlite pipe during exploration bulk sampling. Before analysis, the samples were cleaned in an ultrasonic bath using petroleum ether to remove surface contamination.

Diamonds collected for destructive analysis were crushed in a steel breaker and fragments were selected for FTIR (Fourier Transform Infrared) analyses to quantify nitrogen concentrations and characterise nitrogen aggregation states. These fragments were then further analysed for carbon isotopic composition.

Garnet and clinopyroxene xenocrysts were selectively picked from heavy mineral concentrate derived from both kimberlite drill core, separated by dense medium separation (DMS), and surficial samples, collected by gaimpeiros from panned concentrate from east of the Carolina kimberlite.

2.3.2 Analytical Techniques

Nitrogen concentrations and aggregation states in the Carolina diamonds were determined using a Thermo-Nicolet FTIR spectrometer coupled with a Continuum microscope equipped with a KBr beam splitter. Sample spectra (650 to 4000 cm^{-1}) were collected for 250 seconds with a spectral resolution of $4cm^{-1}$, and, after subtraction of a pure Type II diamond spectrum, converted to absorption coefficient. The spectra were deconvoluted into A, B and D components using software provided by David Fisher (Diamond Trading Company (DTC) Research Centre, Maidenhead, UK). The nitrogen concentrations, in atomic ppm, were calculated from absorption values at 1282 cm^{-1} for the A- and B-centre (Boyd *et al.*, 1994; 1995). Transmission analysis on all but 25 samples was carried out on whole diamonds. Due to a

combination of large sample thickness and high nitrogen contents, the nitrogen peak reached saturation for some samples. As such, calculated nitrogen concentrations for these diamonds represent minimum values, these analyses were not included in the final data set.

Hydrogen (at 3107cm^{-1}) and platelet peak intensities were quantified by determining the areas beneath the respective peaks on spectra converted to absorption coefficient (i.e. normalised to a sample thickness of 1cm). The peak areas were measured using the diamond spectrum as a base line.

Nitrogen detection limits are 10-20 ppm, depending largely on the spectral quality of the sample. Precision of the reported nitrogen concentrations and aggregation states is generally within 10-20% relative (1σ) (Banas *et al.*, 2007).

Carbon isotope ratios were determined on a subset of 25 stones. Inclusion-free diamond fragments (0.7-1.9mg) were combusted together with 1.0-2.0g CuO in an evacuated and sealed silica glass tube for a minimum of 10 hours at 950ºC. Carbon isotope ratios ($\delta^{13}C$) were measured using a Finnigan MAT 252 mass spectrometer, with a total analytical precision better than ±0.1‰ (1 sigma, see Donnelly *et al.*, 2007). Data are reported in standard per mille (‰) notation relative to the V-PDB standard (Vienna Pee Dee Belemnite):

$$\delta^{13}C\ ‰ = \frac{(^{13}C/^{12}C)_{sample} - (^{13}C/^{12}C)_{standard}}{(^{13}C/^{12}C)_{standard}} \times \mathbf{1000}$$

The silicate xenocrysts were embedded in Araldite® epoxy resin and final polish was achieved using 0.05µm alumina suspension on a polishing wheel. The major and minor element compositions were determined by wavelength-dispersion spectrometry (WDS) on a JEOL JXA-8900 Superprobe using silicate, oxide and metal standards. The results obtained represent averages of multiple analyses. Operating with an accelerating voltage of 20kV and a beam current of 20nA, counts for each element were collected for 30-60 seconds (peak) and for half the time on each peak side.

The age of the kimberlite was determined using phlogopite macrocrysts taken from kimberlitic drill core. Samples were picked after careful inspection to ensure no alteration or leaching had occurred. Due to the pervasive nature of tropical weathering in the area, representative samples were analysed using a Rigaku Geigerflex Power Diffractometer XRD machine with a Co tube and a graphite monochromator to determine the purity of a powdered bulk sample. Absence of alteration along cleavage boundaries was verified using EMPA transects over small portions of the phlogopite grains. The analytical procedures for Rb-Sr phlogopite dating and sequential leaching techniques are outlined in Creaser *et al.* (2004).

2.4. Results

2.4.1. Kimberlite Phlogopite Macrocryst Rb-Sr Model Age

Fresh phlogopite macrocryst samples were analysed to determine the age of kimberlite emplacement. The samples show high Rb and low Sr contents typical of kimberlitic phlogopite. Both analyses yield identical model ages within their quoted uncertainties of ± 1% of 232.0 and 231.1 +/- 2.3Ma (Table 2.1). A Triassic (~Ladinian) emplacement age is thus implied for the Carolina kimberlite.

Sample	weight (g)	Rb (ppm)	Sr (ppm)	$^{87}Rb/^{86}Sr$	$^{87}Sr/^{86}Sr$	+/- 2SE	Model Age (0.705)
CAD-04x-A	0.00480	717.0	9.85	225.8	1.45017	0.00003	232.0
CAD-04x-B	0.00277	672.5	12.90	159.0	1.22755	0.00007	231.1

Table 2.1. Table showing the results of the rubidium strontium model age dating of the phlogopite samples.

2.4.2. Diamonds

2.4.2.1. Diamond Characteristics

The subset of 25 diamonds for destructive analysis was characterised based on their colour, morphology and surface features. The diamonds have a range of colours from colourless to yellow, pink, brown and grey. Grey diamonds are dominant, comprising 48% of the sample set, colourless diamonds made up 24%,

with the remaining 28% consisting of yellow (16%), brown (8%), and pink (4%). Brown and pink colouration indicates plastic deformation of the diamond (Harris, 1987). However, the features indicative of deformation, such as deformation lines on dodecahedral faces, are absent in the majority of diamonds.

Morphologically, the 255 Carolina diamonds examined in this study comprise irregular crystals, octahedra, rounded dodecahedra and octahedral macles. Irregular shapes dominate and include fragments and aggregates. Where possible, irregular stones were classed according to residual octahedral and dodecahedral faces. Dodecahedral crystals make up 32% of the sample set, with another 26% comprising of irregular dodecahedra. A further 26% classify as irregular with no original morphology being identified. The breakage surfaces of these stones often show no evidence of secondary resorption indicating breakage post kimberlite emplacement, most likely during recovery. The remaining 16% comprise octahedral stones with 3% of those being octahedral macles.

Surface features are related to the morphology of the diamond, with certain features found on dodecahedral faces, and others found exclusively on octahedral faces. As a consequence of the abundance of dodecahedral stones in the sample set, features restricted to these faces dominate and mainly consist of terraces and hillocks of varying forms. Ruts and corrosion sculptures are also noted on more resorbed faces.

Graphite is commonly observed within the diamonds studied, occurring mostly as small thin flakes. The mineral inclusion assemblage in this small selection of 25 diamonds is limited, with only sulphides visible in a few (6) samples.

2.4.2.2. Carbon Isotopic Values

The diamond samples have a range in carbon isotopic composition from -22.4 to -3.7‰, with a high proportion (68%) of the diamonds having mantle-like carbon isotopic signatures ($\delta^{13}C$ near -5.5‰), analogous to diamonds worldwide (Fig. 2.2). Worldwide, peridotitic diamonds have a narrow range in $\delta^{13}C$ (about −10 to −2‰),

whilst eclogitic diamonds have isotopic compositions that extend to very negative values (-38.4‰) (Cartigny et al., 2004). In this limited sample set there was no correlation observed between carbon isotopic composition and morphology or colour.

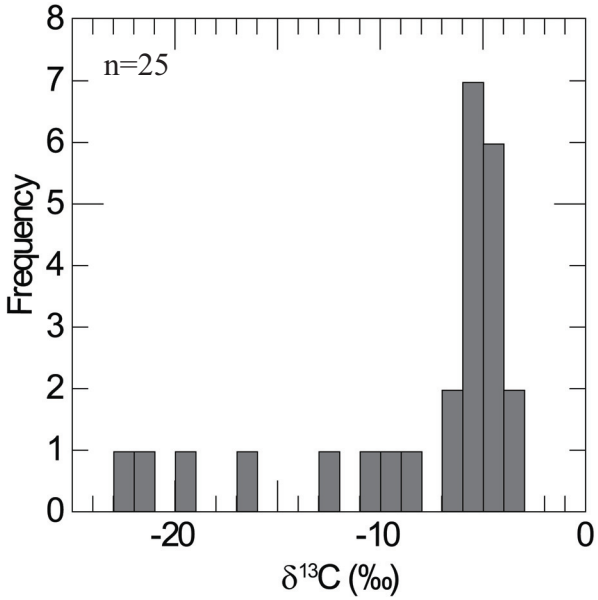

Figure 2.2. The carbon isotopic values for the Carolina diamonds. A mode at -5‰ is seen, with a tail stretching to much more negative values.

2.4.2.3. Nitrogen Content and Aggregation State

Nitrogen is the most abundant impurity in diamond (Kaiser and Bond, 1959), substituting for carbon atoms in the crystal lattice. All the diamonds studied from the Carolina pipe contained measurable nitrogen, and for the 222 samples with spectra suitable for quantitative analysis, the concentrations range from 42 to 2124 atomic ppm, and consequently classify as Type I (Fig. 2.3). Using the same methods, worldwide lithospheric inclusion bearing diamonds without detectable nitrogen (Type II) comprise 20% of all samples (Stachel, 2007). This is an order of magnitude higher than the commonly quoted 2% (e.g. (Dyer *et al.*, 1965). The lack of Type II diamonds at Carolina is unexpected, particularly in view of their abundance from the Machado River alluvials 35km downstream (Bulanova *et al.*, 2008a).

Type I diamonds may be further subdivided based on the aggregation state

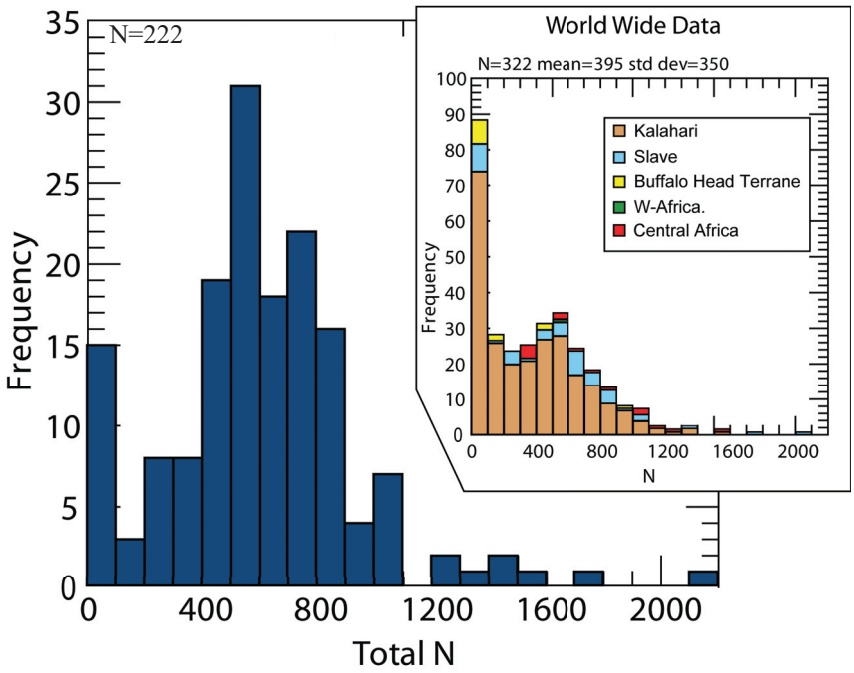

Figure 2.3. Histogram of nitrogen contents of the 222 Carolina diamonds with spectra suitable for quantitative analysis. Insert shows nitrogen contents for diamonds with eclogitic inclusions from worldwide sources (data base of Stachel and Harris, 2008).

of their nitrogen impurities (Evans *et al.*, 1981). Diamonds with singly substituted nitrogen are classified as Type Ib and are very rare in nature. Diamonds with aggregated nitrogen (Type Ia) reflect a temporal evolution from the single substitutional state through aggregation into pairs (Type IaA) to four nitrogen atoms surrounding a vacancy (Type IaB) (Davies, 1976; Evans *et al.*, 1981). Intermediate aggregation states (10-90% of nitrogen in B centres) are termed Type IaAB.

Aggregation of nitrogen occurs during mantle residence and depends on time, total nitrogen content and temperature. At mantle temperatures the transition from Type Ib to IaA occurs very rapidly, whilst aggregation from Type IaA to IaB generally takes hundreds of millions to billions of years (Evans *et al.*, 1981). Ninety-three percent of the Carolina diamonds analysed classify as Type IaAB, indicating intermediate aggregation states. This is common amongst diamonds from other localities (Stachel, 2007). Type IaA diamonds comprise 6% of this diamond population, with just 0.5% classifying as Type IaB.

Time averaged mantle residence temperatures can be determined for an assumed mantle residence time using the aggregation state and known concentration of nitrogen (calculated from Taylor *et al.*, 1990; Leahy and Taylor, 1997). These temperatures normally show acceptable agreement with inclusion geothermobarometry (e.g. Leahy and Taylor, 1997). Whilst the exact residence time of the Carolina diamonds is unclear, it has been shown that mantle residence temperatures are fairly insensitive to the approximated residence time (Leahy and Taylor, 1997). Calculated for a mantle residence of 1.5 Ga, the majority of Carolina diamonds indicate residence temperatures between 1100-1150°C (Fig. 2.4.).

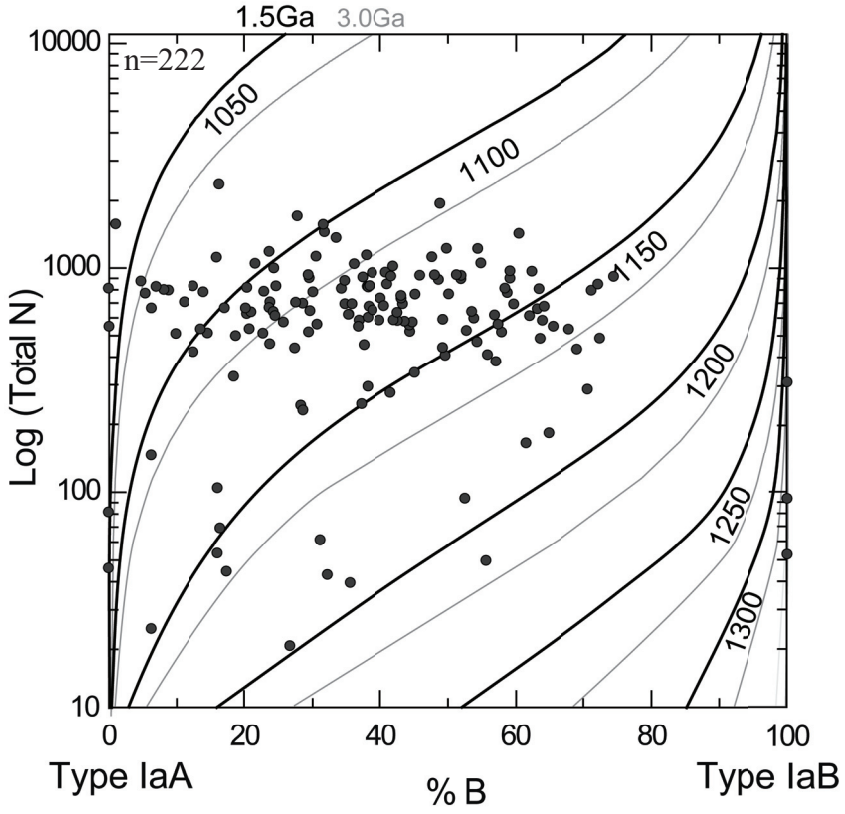

Figure 2.4. Time averaged mantle residence temperatures determined from nitrogen content and aggregation state for the Carolina diamonds with spectra suitable for quantitative analysis. Nitrogen aggregation (%B) is expressed as the relative proportion of nitrogen in the B centre - determined as atomic percent of nitrogen in the B centre divided by the sum of the atomic percents of the nitrogen in the A and B centres. Isotherms based on 1.5Ga mantle residence time (isotherms for 3Ga mantle residence time are shown as thin grey lines) are calculated after (Taylor *et al.*, 1990; Leahy and Taylor, 1997).

2.4.2.4. Platelet Peak

With the aggregation of nitrogen from the A to B centre comes the concurrent growth of B´ centres, with an absorbance peak between 1358 to 1380cm^{-1}. These centres are defects within the crystal lattice caused by platelets, the composition of which has been heavily debated in the literature. Most authors now regard platelets as interstitial carbon atoms which are likely displaced in the diamond lattice with the aggregation of nitrogen (Woods, 1986; Goss, et al. 2003). The nitrogen, detected in variable amounts, likely reflects a contaminant rather than an essential component (Goss *et al.*, 2003).

Previous work (Woods, 1986) has determined a linear relationship between the intensity of the peak (I(B´)), normalised to the nitrogen content, and the relative proportion of nitrogen present in the B centre (%B) for regular specimens. A subset of irregular specimens was also identified where this relationship was not observed, and for these diamonds 'catastrophic platelet degradation' (Woods, 1986) was proposed as a consequence of short lived heating events (Evans *et al.*, 1995) and possible strain (Woods, 1986).

For the 222 samples with spectra suitable for quantitative analysis of nitrogen there was no measurable platelet peak component in 11% of the stones. In addition, the intensity of the peak component of all but 10 of the samples, when plotted against %B, fell below the linear relationship proposed for regular diamonds (Fig. 2.5.a). Consequently, the diamonds are classified as irregular, and may have suffered a themal event (Evans *et al.*, 1995) or strain (Woods, 1986).

2.4.2.5. 3107cm-1 Hydrogen Peak

A number of peaks in the absorbance spectrum of diamond have been attributed to hydrogen impurities within the diamond lattice (Woods and Collins, 1983). In this study, only the intensity of the hydrogen peak at 3107cm^{-1} was determined. The weaker hydrogen peaks at 1405, 2786, 4169 and 4469cm^{-1} are only observable at high intensities of the 3107cm^{-1} peak. The 3107cm^{-1} peak likely relates to stretching

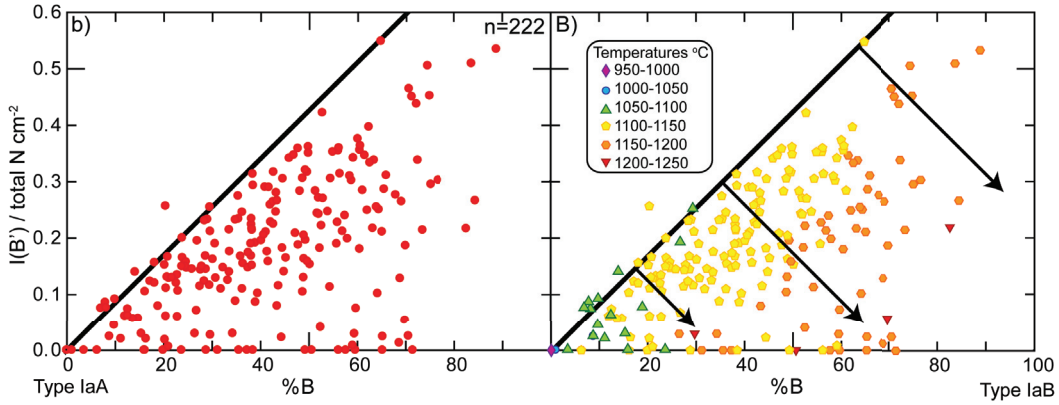

Figure 2.5. a) A plot of the intensity of the platelet peak (I(B´)) versus the percentage of nitrogen aggregated into the B component for the Carolina diamonds with spectra suitable for quantitative analysis. The solid line represents the linear relationship between platelet peak intensity and %B for regular diamonds (Woods, 1986). b) The same plot separating samples according to their time averaged mantle residence temperatures. Arrows indicate increasing platelet degradation with increasing temperature.

vibrations of $C=CH_2$ (vinylidene) bonds (Woods and Collins, 1983). The hydrogen peak intensity (measured as a peak area) varied from 0 to 86cm^{-2} although most (91% of diamonds) fell in the range of 0 to 10cm^{-2} (Fig. 2.6).

For Argyle diamonds a linear relationship was observed between nitrogen content and the 3107cm^{-1} hydrogen absorption peak (Iakoubovskii and Adriaenssens, 2002). Such a correlation is not visible for Carolina diamonds (Fig. 2.6). Iakoubovskii and Adriaenssens (2002) suggest that relatively nitrogen rich and hydrogen poor diamonds (as observed for Carolina) could relate to a purely nitrogen-rich growth environment, as opposed to a proposed ammonium-rich growth medium for the Argyle stones.

2.4.3. Xenocrysts

2.4.3.1. Garnet Xenocrysts

Garnet xenocrysts from coarse concentrate derived from garimpeiro diggings east of the Carolina kimberlite (n=349) and from drill core (n=147) have been analysed. Electron microprobe analyses (EPMA) show the garnets to be derived

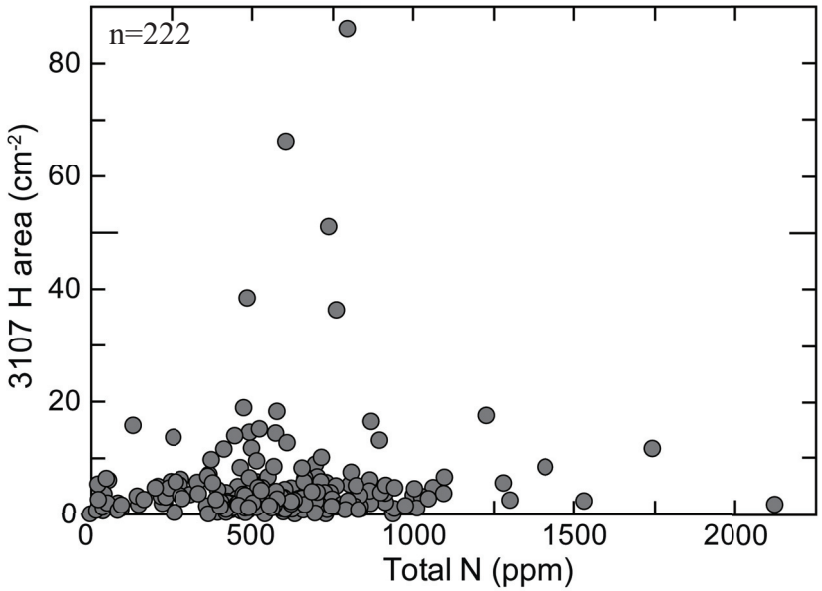

Figure 2.6. Plot showing the relationship of the 3107cm^{-1} hydrogen peak area and total nitrogen content for Carolina diamonds. with spectra suitable for quantitative analysis

predominantly from a peridotitic source (87%), which is exclusively lherzolitic (G9) in paragenesis (Fig. 2.7). Grütter *et al.* (2004) showed that lherzolitic garnets plotting close to the G10/G9 divide are typically associated with cool cratonic lithospheric mantle (G9A), whereas garnets removed towards the Ca rich side of the divide are characteristic of off-craton kimberlites (G9B). Garnets derived from the surfacial concentrate of the kimberlite typically plot in the G9B field whereas garnets taken from the core predominantly plot in the G9A field (Fig. 2.7).

Thirteen percent of the 496 garnets belong to the eclogitic suite. Eclogitic garnets are distinctly more abundant in core (28% of 147) compared to surficial samples (9% of 349) and derive from distinct sources, with 96% of the garnets from core classifying as Group I (>0.07wt% Na_2O; Gurney, 1984) as opposed to only 28% of surficial garnets. High sodium (>0.07wt% Na_2O) in garnet has been identified as a characteristic of diamond facies eclogites and hence is considered an indication for increased diamond potential of the host kimberlite (Gurney, 1984; Gurney *et al.*, 1993).

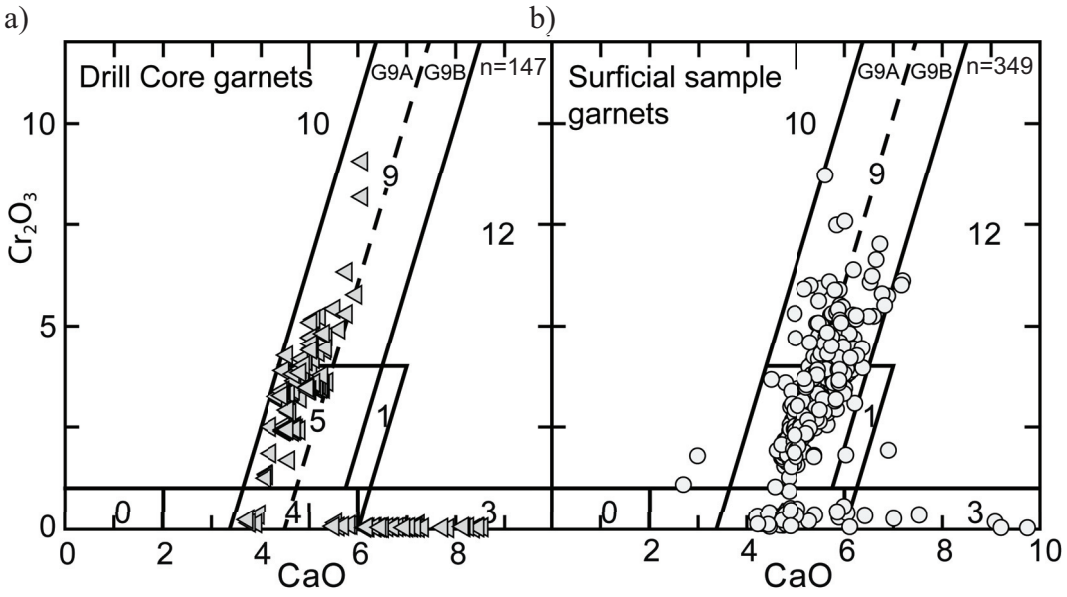

Figure 2.7. Plots of Cr_2O_3 versus CaO (wt%) for core and surficial concentrate garnet, with fields for garnet classes (G1 to G12) after Grütter *et al.* (2004). G9A garnets are typically associated with cool cratonic lithospheric mantle, whilst G9B garnets are characteristic of off-craton kimberlites (Grütter *et al.*, 2004). a) Garnets from kimberlitic core. b) Garnets from surficial samples.

2.4.3.2. Clinopyroxene Xenocrysts

All but 4 of 129 clinopyroxene xenocrysts recovered from surficial samples and drill core fall within the 'on-craton' garnet peridotite field in the Cr_2O_3/Al_2O_3 discrimination diagram of Ramsay (1992) (Fig. 2.8). The majority of clinopyroxene from the kimberlite have lower Al_2O_3 wt% than those from the surface concentrate.

For clinopyroxene from garnet lherzolites, pressure and temperature conditions of last equilibration may be estimated using the single crystal geothermobarometer of Nimis and Taylor (2000). This empirical thermobarometer satisfies experimental and phase-compatibility constraints to within acceptable error for a wide variety of peridotitic bulk compositions and a broad range of pressures and temperatures (Grütter and Moore, 2003). A number of filters were applied to the data to ensure that any batch analytical effects were removed (Fig. B.1.).

Using well studied Canadian localities for comparison (Grütter and Moore, 2003 and references therein), the pressure-temperature conditions calculated for

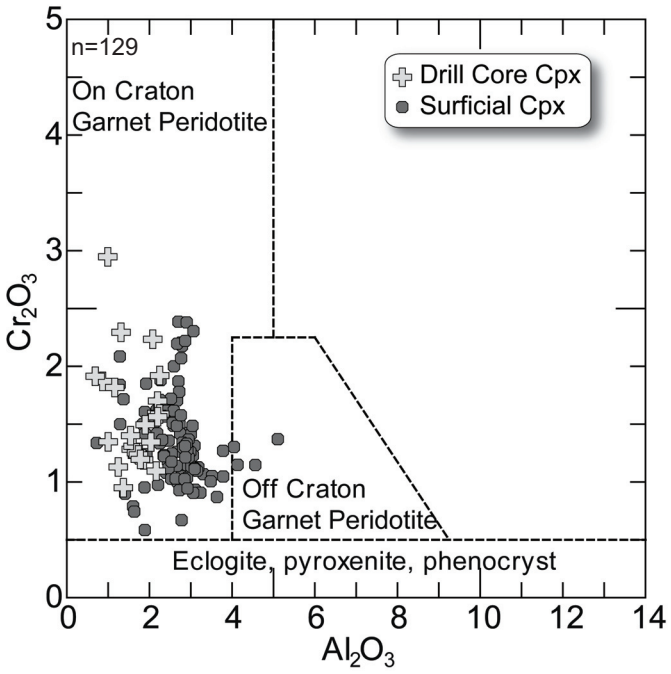

Figure 2.8. Plot of Cr_2O_3 versus Al_2O_3 (wt%) for core and surficial concentrate clinopyroxenes with the compositional fields of Ramsay (1992). The majority of grains plot in the "on craton garnet peridotite" field. The xenocrysts are separated based on whether they were derived from kimberlitic drill core or surficial samples.

the Carolina material reflect two distinct geotherms: a hot "Somerset Island type" geotherm (44mW/m^2), and a colder "Slave type" geotherm (38mW/m^2) (Fig. 2.9). Clinopyroxenes from kimberlite core exclusively fall on the colder model geotherm whilst surficial clinopyroxenes predominantly delineate the hotter geotherm.

2.5. Discussion

2.5.1. Diamond Source Region

Using the Cr_2O_3/Al_2O_3 discrimination diagram of Ramsay (1992), the composition on the clinopyroxene xenocrysts from the Carolina kimberlite indicate derivation from cratonic garnet peridotites (Fig. 2.8). Garnet xenocryst compositions are atypical for diamond prospective cratonic source regions. The complete absence of harzburgitic (G10) garnets (Fig. 2.7) is unusual for a diamondiferous kimberlite,

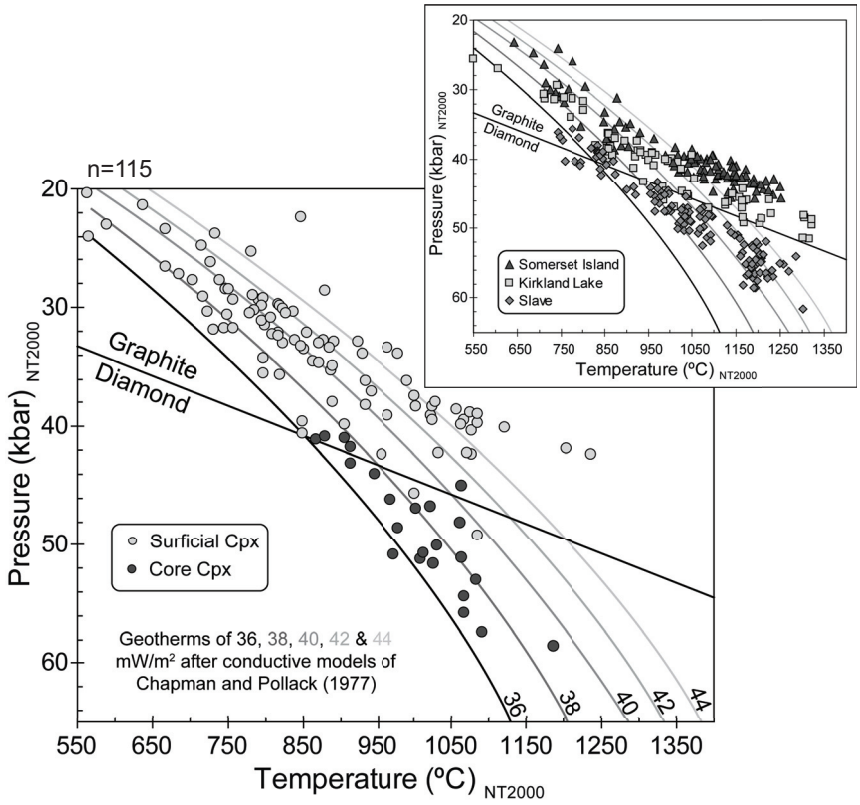

Figure 2.9. Core and surficial concentrate clinopyroxene P-T estimates based on the thermobarometer of Nimis and Taylor (2000). Data from the Slave Craton, Kirkland Lake and Somerset Island are shown for reference to indicate low, intermediate and high cratonic geotherms (Grütter and Moore, 2003 and references therein).

but is consistent with the post-Archean setting of the area (c.f. Griffin *et al.*, 1999; Griffin *et al.*, 2003; Hood and McCandless, 2003). This is believed to relate to secular cooling of the earth, with mantle potential temperatures subsequent to the Archean being too low to allow for the high degrees of melt extraction required to create harzburgitic-dunitic residues (e.g. Stachel *et al.*, 1998; Walter, 1998; Shirey *et al.*, 2004).

Basement rocks of the area are dated at 1.8-1.55Ga (e.g. Tassinari and Macambira, 1999), the absence of harzburgitic garnets thus is not suggestive of a decoupled origin of crust and mantle beneath the Carolina kimberlite, and may be taken to imply that the underlying lithospheric mantle has a similar age. There is some evidence for a depleted lithosphere, with trace harzburgitic G10 garnets having been found in nearby kimberlites in the Pimenta Bueno area (Manuela, 2006).

The absence of G10 garnets, as has been suggested previously for other localities (Gurney, 1984), suggests that Carolina diamonds are not derived from peridotitic sources but rather points to an eclogitic diamond population. Eclogitic garnet xenocrysts are present at Carolina (13% of garnets) and are particularly abundant in kimberlite core (28% of garnets). Compositions of most eclogitic garnets from kimberlite core corrspond to the field of diamond facies eclogites (>0.07wt% Na_2O, Gurney, 1984; Gurney *et al.*, 1993). In surficial samples a large (72%) proportion of eclogitic garnets are Na poor and hence related to sources with low diamond potential. The notion of an eclogitic diamond population at Carolina is consistent with the observation of highly negative carbon isotopic values and overall high nitrogen contents (e.g. Cartigny, 2005; Stachel, 2007). This also conforms with their presence in Machado River alluvials downstream, as identified by Bulanova *et al.* (2008a) from diamond inclusion studies.

2.5.2. Thermal evolution of the Source Region

The nitrogen contents and aggregation states of the diamonds indicate that, for an assumed mantle residence of 1.5 Ga, the majority of Carolina diamonds resided at temperatures between 1100-1150°C (Fig. 2.4). The observed range in values from ~1050-1300°C is consistent with previously observed diamond populations (Taylor *et al.*, 1995). The observed range in temperatures likely relates to sampling of diamonds by the kimberlite at different depths in the lithospheric mantle, with deeper diamonds residing at higher temperatures. The small range in temperatures for the majority of diamonds indicates preferred sampling over a restricted depth range from sources with a uniform thermal history (e.g. the diamond population from the Point Lake kimberlite, Canada: Taylor and Milledge, 1995).

Whilst the diamonds appear to have resided at fairly uniform conditions, the observation of common platelet degradation among Carolina diamonds is evidence for thermal perturbations and/or strain affecting the diamond source regions prior to kimberlite emplacement. Almost no work has been carried out on determining the effect of strain, and relatively little is known about the temperatures required for

catastrophic platelet degradation to occur. Evans *et al.* (1995) showed experimentally that platelets become unstable at temperatures of between 2500-2700°C. The number of transient events that affected the diamond source regions and their timing, e.g. a possible temporal relationship with the initiation of kimberlite magmatism, cannot be constrained from the nitrogen data. However, any heating events must have been short lived or occurred just prior to eruption of the kimberlite else the aggregation state of the diamonds would be higher. Plotting platelet degradation in conjunction with nitrogen based mantle residence temperatures clearly shows that strong degradation correlates with high residence temperatures and, by inference, with great depths of origin (Fig. 2.5B). This is consistent with the heat source for platelet degradation being upwelling asthenospheric melts (~1300°C), and/or with increased strain with depth.

The largest change to the diamond source region occurred after the eruption of the Carolina kimberlite. Evidence of a much larger heating event postdating emplacement of the Carolina kimberlite is provided by the clinopyroxene geothermobarometry: Whilst clinopyroxenes from the Carolina kimberlite itself imply a "Slave type" geotherm (38mW/m^2) typically associated with stable cratonic areas, P-T data for grains collected from the surface define a second fairly hot "Somerset Island type" geotherm (44mW/m^2), indicative of massive lithosphere heating and hence reduced diamond potential (Fig. 2.9). This implies that in surficial samples, clinopyroxene from younger volcanic sources associated with a higher geothermal gradient are mixed with material derived from Carolina itself. This heating event is also evidenced by the garnet xenocrysts. Garnets from the kimberlite core plot predominantly in the G9A field of Grütter *et al.* (2004), indicative of a cool cratonic geotherm, whilst xenocrysts taken from the surface show a shift to more CaO rich values, at a given Cr_2O_3 content, (G9B field) typical of more off-craton kimberlites and a hotter geotherm. Given the Triassic age of the Carolina kimberlite, it is speculated that a younger generation of Cretaceous-Tertiary kimberlites in the Pimenta Bueno area could represent this second source of clinopyroxene and garnet xenocrysts. These may or may not be related to the Cretaceous kimberlites

of the Juina area, Mato Grosso which lie 200km south-east along the same 125°AZ lineament (Heaman *et al.*, 1998; Andreazza *et al.*, 2008).

Maunula (2006) noted a similar difference between samples from the Vaaldiam Pepper and Tumeleiro kimberlite provinces and those taken from ~10 km downstream. Alluvial garnet samples showed a more enriched mantle signature, whilst the clinopyroxene geotherm for the alluvial grains was elevated by comparison to those grains from the kimberlites. Maunula (2006) speculated the presence of yet undiscovered kimberlites as the source for the alluvial grains.

By implication, in the time span between the Triassic and Cretaceous, heating of lithospheric mantle beneath the south-eastern Amazon Craton occurred. Similar observations have previously been made (e.g. for the São Francisco Craton), where thermal erosion of the deep mantle lithosphere occurred in a time window between 95-85 Ma (Read *et al.*, 2004). Lithosphere extension and incipient rifting during the opening of the South Atlantic or impact of a plume have been suggested as possible causes for the thermal erosion of the lithospheric root beneath the São Francisco Craton, but the evidence is inconclusive (Read *et al.*, 2004).

During the Cretaceous, South America underwent major crustal evolution with the break-up of Gondwanaland and associated plume activity. In the Early Cretaceous, the impact of the Tristan and St Helena plume heads beneath Gondwana is believed to have been responsible for the extensive Paraná-Etendeka magmatism (White and Mckenzie, 1989) during the final stages of supercontinent break-up and opening of the South Atlantic. In addition, large-volume mafic, potassic magmatism in south-east Brazil between the Amazon and São Francisco cratons (Gibson *et al.*, 1995) has also been linked to plume activity in the late Cretaceous. Gibson *et al.* (1995) proposed that the Alto Paranaíba Province alkaline magmatism was caused by impingement of the Trindade plume on the base of the lithosphere. Any of these events may have transported sufficient heat into the lithospheric mantle beneath the Pimenta Bueno area to cause the observed increase in geothermal gradient from 38 to 44mW/m^2 surface heat flow.

2.6. Conclusions

With its setting in a basement province ≤1.8 Ga, the Carolina kimberlite represents an unconventional diamond deposit. A complete absence of harzburgitic garnet xenocrysts is consistent with this post Archean setting, although G10 garnets have been reported from neighbouring kimberlites. Eclogitic garnet xenocrysts with high sodium contents (Na_2O >0.07wt%), indicative of the presence of diamond facies eclogite at depth, combined with high nitrogen contents and in part highly negative carbon isotopic values of the diamonds themselves, suggest derivation of Carolina diamonds from eclogitic source regions. Mantle storage of the diamonds occurred at temperatures that are typical for cratonic mantle sources (1100-1150°C). One or more short-lived heating event(s) during mantle storage are revealed by platelet peak degradation in the majority of diamonds.

A typical cratonic model geotherm (~38 mW/m^2 surface heat flow) is recorded by clinopyroxene xenocrysts derived directly from the Carolina kimberlite. Clinopyroxenes sourced from a nearby garimpeiro digging, likely derived from both local and regional sources, correspond to a hotter 44mW/m^2 model geotherm. This suggests that after eruption of the determined Triassic (~Ladinian) Carolina kimberlite a large scale heating event affected the underlying lithospheric mantle and its previously existing diamond source regions. This heating event may relate to intense plume activity affecting the Amazon Craton throughout the Cretaceous.

References

Andreazza, P., Kaminsky, F.V., Sablukov, S.M., Belousova, E.A., Tremblay, M. and Griffin, W.L., 2008. Kimberlitic sources of super-deep diamonds in the Juina area, Mato Grosso State, Brazil, Extended Abstract No. 9IKC-A-00004, 9th International Kimberlite Conference, Frankfurt.

Banas, A., Stachel, T., Muehlenbachs, K. and McCandless, T.E., 2007. Diamonds from the Buffalo Head Hills, Alberta: Formation in a non-conventional setting. Lithos, 93(1-2): 199-213.

Boyd, S.R., Kiflawi, I. and Woods, G.S., 1994. The Relationship between Infrared-Absorption and the a Defect Concentration in Diamond. Philosophical Magazine B-Physics of Condensed Matter Statistical Mechanics Electronic Optical and Magnetic Properties, 69(6): 1149-1153.

Boyd, S.R., Kiflawi, I. and Woods, G.S., 1995. Infrared-Absorption by the B-Nitrogen Aggregate in Diamond. Philosophical Magazine B-Physics of Condensed Matter Statistical Mechanics Electronic Optical and Magnetic Properties, 72(3): 351-361.

Bulanova GP, Smith CB, Kohn SC, Walter MJ, Gobbo L, Kearns S (2008a) Machado River Brazil, Brazil - a newly recognised ultradeep diamond occurrence. Extended Abstract 9IKC-A-00233, 9th International Kimberlite Conference, Frankfurt

Bulanova GP, Smith CB, Walter MJ, Blundy J, Gobbo L, EIMF, Kohn SC (2008b) Proto-kimberlitic ultra-deep diamonds from Collier 4 kimberlite pipe, Juina, Brazil. Extended Abstract 9IKC-A-00227, 9th International Kimberlite Conference, Frankfurt

Cartigny, P., 2005. Stable isotopes and the origin of diamond. Elements, 1(2): 79-84.

Cartigny, P., Stachel, T., Harris, J.W., Javoy, M., 2004. Constraining diamond metasomatic growth using C- and N-stable isotopes: examples from Namibia. Lithos 77 (1–4), 359–373.

Chapman, D.S. and Pollack, H.N., 1977. Regional geotherms and lithospheric thickness. Geology, 5(5): 265-268.

Clifford, T.N., 1966. Tectono-metallogenic units and metallogenic provinces of Africa. Earth and Planetary Science Letters, 1(6): 421-434.

Creaser, R.A., Grutter, H., Carlson, J. and Crawford, B., 2004. Macrocrystal phlogopite Rb-Sr dates for the Ekati property kimberlites, Slave Province, Canada: evidence for multiple intrusive episodes in the Paleocene and Eocene. Lithos, 76(1-4): 399-414.

Davies, G., 1976. A-Nitrogen Aggregate in Diamond - Its Symmetry and Possible Structure. Journal of Physics C-Solid State Physics, 9(19): L537-L542.

Donnelly, C.L., Stachel, T., Creighton, S., Muehlenbachs, K. and Whiteford, S., 2007. Diamonds and their Mineral Inclusions from the A154 South pipe, Diavik Diamond Mine, Northwest Territories, Canada. Lithos, 98(1-4): 160-176.

Dyer, H.B., Raal, F.A., Dupreez, L. and Loubser, J.H.N., 1965. Optical Absorption Features Associated with Paramagnetic Nitrogen in Diamond. Philosophical Magazine, 11(112): 763-&.

Evans, B.T., 2005. Technical Report on the Diamond Exploration Potential of the Carolina Property, Rondônia State, Brazil., Sola Resources Corporation.

Evans, T., Kiflawi, I., Luyten, W., Vantendeloo, G. and Woods, G.S., 1995. Conversion of Platelets into Dislocation Loops and Voidite Formation in Type Iab Diamonds. Proceedings of the Royal Society of London Series a-Mathematical and Physical Sciences, 449(1936): 295-313.

Evans, T., Qi, Z. and Maguire, J., 1981. The Stages of Nitrogen Aggregation in Diamond. Journal of Physics C-Solid State Physics, 14(12): L379-L384.

Gibson, S.A., Thompson, R.N., Leonardos, O.H., Dickin, A.P. and Mitchell, J.G., 1995. The Late Cretaceous Impact of the Trindade Mantle Plume - Evidence from Large-Volume, Mafic, Potassic Magmatism in Se Brazil. Journal of Petrology, 36(1): 189-229.

Goss, J.P., Coomer, B.J., Jones, R., Fall, C.J., Briddon, P.R. and Oberg, S., 2003. Extended defects in diamond: The interstitial platelet. Physical Review B, 67(16): 165208.

Griffin, W.L., O'Reilly, S.Y., Abe, N., Aulbach, S., Davies, R.M., Pearson, N.J., Doyle, B.J. and Kivi, K., 2003. The origin and evolution of Archean lithospheric mantle. Precambrian Research, 127(1-3): 19-41.

Griffin, W.L., O'Reilly, S.Y. and Ryan, C.G., 1999. The composition and origin of subcontinental lithospheric mantle. In: Y. Fei, C.M. Bertka and B.O. Mysen (Editors), Mantle Petrology: Field Observations and High Pressure Experimentation: A tribute to Francis R. (Joe) Boyd. Special Publication. The Geochemical Society, Houston: 13–45.

Grütter, H. and Moore, R.O., 2003. Pyroxene geotherms revisited - an empirical approach based on Canadian xenoliths. Extended Abstract - 8th International Kimberlite Conference, CD-ROM: 272.

Grütter, H.S., Gurney, J.J., Menzies, A.H. and Winter, F., 2004. An updated classification scheme for mantle-derived garnet, for use by diamond explorers. Lithos, 77(1-4): 841-857.

Gurney, J.J., 1984. A correlation between garnets and diamonds in kimberlites, Publications of the Geology Department & Extension Service, University of Western Australia: 143-166.

Gurney, J.J., Helmstaedt, H. and Moore, R.O., 1993. A Review of the Use and Application of Mantle Mineral Geochemistry in Diamond Exploration. Pure and Applied Chemistry, 65(12): 2423-2442.

Harris, J.W., 1987. Recent physical, chemical, and isotopic research of diamonds. In: P.H. Nixon (Editor), Mantle Xenoliths. John Wiley and Sons.

Heaman, L.M., Teixeira, N.A., Gobbo, L. and Gaspar, J.C., 1998. U-Pb mantle zircon ages for kimberlites from the Juina and Paranatinga provinces, Brazil, VIIth International Kimberlite Conference, Extended abstracts, Cape Town: 322-324.

Herz, N., 1977. Timing of Spreading in South-Atlantic - Information from Brazilian Alkalic Rocks. Geological Society of America Bulletin, 88(1): 101-112.

Hood, C. and McCandless, T., 2003. Systematic variations in xenocryst mineral composition at the province scale, Buffalo Hills kimberlites, Alberta, Canada, 8th International Kimberlite Conference, Victoria (BC), Canada: 3.

Hood, C.T.S. and McCandless, T.E., 2004. Systematic variations in xenocryst mineral composition at the province scale, Buffalo Hills kimberlites, Alberta, Canada. Lithos, 77(1-4): 733-747.

Iakoubovskii, K. and Adriaenssens, G.J., 2002. Optical characterization of natural Argyle diamonds. Diamond and Related Materials, 11(1): 125-131.

Janse, A.J.A., 1994. Is Clifford's rule still valid? Affirmative examples from around the world. In: H.O.A. Meyer and O.H. Leonardos (Editors), Diamonds: Characterization, Genesis and Exploration. CPRM — Special Publication Jan/94, Brasilia: 215–235.

Jaques, A.L., Lewis, J.D. and Smith, C.B., 1986. The kimberlites and lamproites of Western Australia:. Geological Survey of Western Australia Bulletin: 132-268.

Kaiser, W. and Bond, W.L., 1959. Nitrogen, a Major Impurity in Common Type-I Diamond. Physical Review, 1(4): 857-863.

Kirkley, M.B., Gurney, J.J., Otter, M.L., Hill, S.J. and Daniels, L.R., 1991. The Application of C Isotope Measurements to the Identification of the Sources of C in Diamonds - a Review. Applied Geochemistry, 6(5): 477-494.

Leahy, K. and Taylor, W.R., 1997. The influence of the Glennie domain deep structure on the diamonds in Saskatchewan kimberlites. Geologiya I Geofizika, 38(2): 451-460.

Maunula T (2006) Technical report on the Pimenta Bueno diamond project, Brazil. Report to Vaaldiam Resources Ltd. www.vaaldiam.com/mining/pimenta-bueno.html.

Nimis, P. and Taylor, W.R., 2000. Single clinopyroxene thermobarometry for garnet peridotites. Part I. Calibration and testing of a Cr-in-Cpx barometer and an enstatite-in-Cpx thermometer. Contributions to Mineralogy and Petrology, 139(5): 541-554.

Pearson, D.G., 1999. Evolution of cratonic lithospheric mantle: an isotopic perspective. In: Y. Fei, C.M. Bertka and B.O. Mysen (Editors), Mantle Petrology Field Observations and High-Pressure Experimentation. A Tribute to Francis, R. (Joe) Boyd, The Geochemical Society Special Publications, Houston, TX: 57-78.

Ramsay, R.R., 1992. Geochemistry of Diamond Indicator Minerals. PhD Thesis, University of Western Australia, Perth.

Read, G., Grutter, H., Winter, S., Luckman, N., Gaunt, F. and Thomsen, F., 2004.

Stratigraphic relations, kimberlite emplacement and lithospheric thermal evolution, Quiricó Basin, Minas Gerais State, Brazil. Lithos, 77(1-4): 803-818.

Shirey, S.B., Richardson, S.H. and Harris, J.W., 2004. Integrated models of diamond formation and craton evolution. Lithos, 77(1-4): 923-944.

Stachel, T., 2007. Diamond. Mineralogical Association of Canada Short Course Series, 37: 1-22.

Stachel, T., Viljoen, K.S., Brey, G. and Harris, J.W., 1998. Metasomatic processes in lherzolitic and harzburgitic domains of diamondiferous lithospheric mantle: REE in garnets from xenoliths and inclusions in diamonds. Earth and Planetary Science Letters, 159(1-2): 1-12.

Svisero, D.P. and Haralyi, N.L.E., 1983. The Kimberlitic Province of the Upper Paranaiba, Minas-Gerais. Anais Da Academia Brasileira De Ciencias, 55(1): 137-138.

Tassinari, C.C.G. and Macambira, M.J.B., 1999. Geochronological provinces of the Amazonian Craton. Episodes, 22: 174–182.

Taylor, W.R., Gurney, J.J. and Milledge, H.J., 1995. Nitrogen aggregation and cathodoluminescence characteristics of diamonds from the Point Lake kimberlite pipe, Slave Province, NWT, Canada, Sixth International kimberlite Conference (Novosibirsk), Extended Abstracts: 614-615.

Taylor, W.R., Jaques, A.L. and Ridd, M., 1990. Nitrogen-defect aggregation characteristics of some Australasian diamonds; time-temperature constraints on the source regions of pipe and alluvial diamonds. American Mineralogist, 75(11-12): 1290-1310.

Taylor, W.R. and Milledge, H.J., 1995. Nitrogen aggregation character, thermal history and stable isotope composition of some xenolith-derived diamonds from Roberts Victor and Finch, Sixth International Kimberlite Conference (Novosibirsk), Extended Abstracts: 620-622.

Tohver, E., van der Pluijm, B.A., Mezger, K., Scandolara, J.E. and Essene, E.J., 2005. Two stage tectonic history of the SW Amazon craton in the late

Mesoproterozoic: identifying a cryptic suture zone. Precambrian Research, 137(1-2): 35-59.

Walter, M.J., 1998. Melting of garnet peridotite and the origin of komatiite and depleted lithosphere. Journal of Petrology, 39(1): 29-60.

White, R. and Mckenzie, D., 1989. Magmatism at Rift Zones - the Generation of Volcanic Continental Margins and Flood Basalts. Journal of Geophysical Research-Solid Earth and Planets, 94(B6): 7685-7729.

Woods, G.S., 1986. Platelets and the Infrared-Absorption of Type-Ia Diamonds. Proceedings of the Royal Society of London Series a-Mathematical Physical and Engineering Sciences, 407(1832): 219-238.

Woods, G.S. and Collins, A.T., 1983. Infrared-Absorption Spectra of Hydrogen Complexes in Type-I Diamonds. Journal of Physics and Chemistry of Solids, 44(5): 471-475.

CHAPTER 3

MANTLE-DERIVED MICROXENOLITHS AND XENOCRYSTS FROM THE RENARD KIMBERLITES, QUEBEC: A RECORD OF MANTLE LITHOSPHERE FORMATION AND MODIFICATION BENEATH THE EASTERN SUPERIOR CRATON

The content of this chapter, in modified form, has been submitted for publication in *Journal of Petrology* as:

Lucy Hunt, Thomas Stachel, Herman Grütter, John Armstrong, Tom E. McCandless, Antonio Simonetti and Sebastian Tappe: Mantle-derived microxenoliths and xenocrysts from the Renard kimberlites, Quebec: A record of mantle lithosphere formation and modification beneath the eastern Superior craton

3.1. Introduction

Mantle xenoliths and xenocrysts provide a means to directly study the Earth's upper mantle. Whilst their major element compositions provide insights into processes that led to cratonic lithosphere formation, their incompatible trace element record is highly sensitive to secondary events that may have modified the lithospheric mantle after its assembly. Thus, they can be employed, firstly, to better understand craton evolution, and secondly, to identify the specific conditions controlling growth, survival and destruction of diamonds.

The diamondiferous Renard kimberlites are located in the eastern Superior Province of Canada (Fig. 3.1), within the northern Otish Mountains of Quebec. Compared to the Slave craton, (e.g. Griffin *et al.*, 1999a; MacKenzie and Canil, 1999; Kopylova and Russell, 2000; Aulbach *et al.*, 2003; Stachel *et al.*, 2003; Menzies *et al.*, 2004 and references therein) the formation and geological history of the Superior subcratonic lithospheric mantle (SCLM) is poorly known.

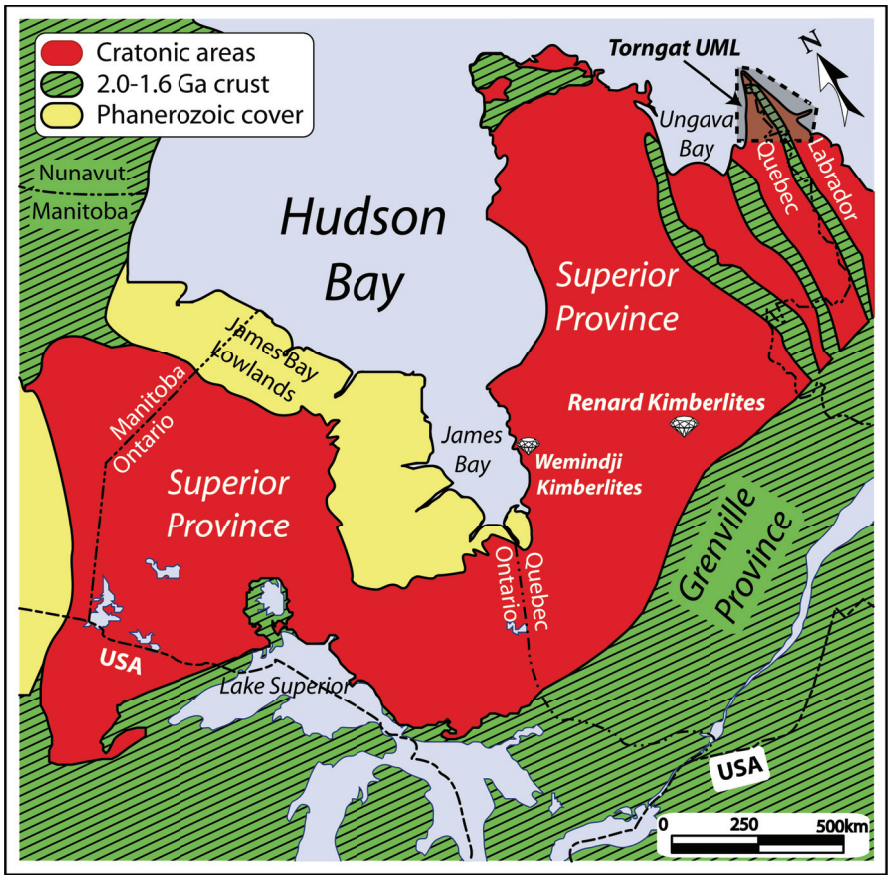

Figure 3.1. Simplified geological map of the Superior Province and adjacent areas showing the location of the Renard Kimberlites (redrawn using information from: Hoffman, 1988; Card, 1990; Percival *et al.*, 1992). Torngat UML –Torngat Neoproterozoic Ultramafic Lamprophyres of Quebec and Labrador (Tappe *et al.*, 2007).

In this study we report major and trace element compositions of mantle xenoliths and xenocrysts from the Renard kimberlites. We discuss the composition of the underlying lithospheric mantle at the time of Neoproterozoic kimberlite emplacement and the possible diamond source regions. We determine some of the processes which have affected the cratonic mantle throughout its evolution. A number of thermometers and barometers were applied to place the samples in a "stratigraphic" context, looking for evidence of mantle layering as has been suggested for other areas of the Superior Craton (Scully *et al.*, 2004). These thermobarometric calculations establish whether a deep SCLM and a cold cratonic geotherm (diamond favourable conditions) were present at the time of kimberlite emplacement.

Additionally, we present Pb isotopic compositions of xenocrystic mantle-derived clinopyroxenes determined by *in situ* laser ablation-multicollector-inductively coupled plasma mass spectrometry (LA-MC-ICPMS). The observed range of common Pb isotopic compositions and their Pb contents allows us to fingerprint the origin of the Pb component and to evaluate its age significance. Constraints on the age of lithospheric mantle stabilisation beneath the eastern Superior Province allow a comprehensive assessment of the paragenesis of Renard diamonds and their formation. The age of the lithosphere is often suggestive of the paragenesis of the diamonds. Peridotitic diamonds are typically associated with cratonic mantle roots formed in the Archean. During this period, high mantle potential temperatures allowed the creation of extremely depleted melting residues, that, once emplaced as SCLM, are favourable for diamond growth (e.g. Gurney, 1984; Boyd and Gurney, 1986). Conversely, eclogitic diamonds are often associated with cratonic areas modified during the Proterozoic (Shirey *et al.*, 2004).

3.2. Geological Background

The Superior Province in Eastern Canada is one of the world's largest Archean cratons. Along with other Archean provinces (e.g. Slave, Rae, Hearne, Wyoming, Nain) and Proterozoic orogens (e.g. Trans-Hudson, Thelon, Torngat) it makes up the majority of the Canadian Shield (Hoffman, 1988). To the east of the Renard kimberlites lie Proterozoic rocks of the Labrador fold belt, to the north the Cape Smith fold belt, and in the south the Grenville Province (Fig. 3.1). Radiometric dating of both extrusive and intrusive magmatic rocks of the Superior Province provide ages ranging from ~3.1 to 2.6Ga (Card, 1990), with evidence for periods of intense magmatism at 3.0 and 2.7Ga. The latter were associated with periods of major crust forming that occurred in accretionary settings, thought to result from processes similar to those existing within parts of the Pacific rim today (Card, 1990).

Within the Superior craton mantle-derived igneous rocks, including kimberlite and ultramafic lamprophyre, form widespread diatremes and dikes (Birkett *et al.*, 2004 and references therein). The eruption centres are distributed in seven distinct

fields, with the Renard kimberlite cluster being located within the Otish Mountains Field. The Renard kimberlites are emplaced into Archean granitic and gneissic rocks of the Opinaca Subprovince (Percival, 2007), which recorded amphibolite and local granulite facies metamorphism (Percival *et al.*, 1994) during the late Archean (Moorhead *et al.*, 2003).

Exploration during 2001 to 2003 identified ten kimberlite pipes at Renard. They align roughly northwest-southeast in a 2km^2 area (Fig. D1). The pipes were named Renards 1 to 10, with subsequent work, in 2003, determining that the diatremes beneath Renard 5 and 6 join at depth (consequently renamed Renard 65). Four pipes (2, 3, 4 and 9) are of particular interest due to high initial diamond grades. Currently, economic diamond content at Renard is estimated to be ~30 million carats (NI 43-101 Technical Report, 2011). During 2003 and 2005, respectively, the diamondiferous Lynx and Hibou dykes were discovered a few kilometres west of the Renard pipe cluster (Fig. D1).

Whole rock trace element compositions (Birkett *et al.*, 2004) and petrographic analyses (Fitzgerald *et al.*, 2008) of the Renard kimberlites support a Group I kimberlite classification, although affinities to ultramafic lamprophyres have also been suggested (Birkett *et al.*, 2004). U-Pb perovskite dating of hypabyssal kimberlite from Renard 1 indicates Neoproterozoic emplacement, with a $^{206}Pb/^{238}U$ age of 631.6±3.5Ma (2σ) (Birkett *et al.*, 2004). A later U-Pb groundmass perovskite study on the main phases in Renard 2 and 3 gave a similar emplacement age of 640.5±2.8Ma (Fitzgerald *et al.*, 2008). The Renard kimberlite field is one of the oldest in Canada, similar in eruption age to the Wemindji kimberlites on the same craton (629 Ma, Letendre *et al.*, 2003). The Renard bodies are part of the Late Neoproterozoic to Cambrian kimberlite and carbonatite province of eastern Canada (Girard, 2001; Moorhead *et al.*, 2002; Letendre *et al.*, 2003; Tappe *et al.*, 2006; Tappe *et al.*, 2008), which formed as a distal effect to Late Neoproterozoic lithosphere extension along the then-active St. Laurence and Labrador Sea rifts (Tappe *et al.*, 2007, and references therein).

3.3. Samples

Sixty-three microxenoliths and 50 xenocrysts from Renards 2, 3, 4 and 65 were collected for this study during final observation of DMS concentrate during 2007/08. The samples range in weight from 1.2mg to 2.2g, and size from ~2mm to 2cm. The microxenoliths are typically bimineralic (26) and trimineralic (30). The dominant assemblage is peridotitic, composed mainly of purple garnet and emerald green clinopyroxene with less abundant orthopyroxene and minor olivine and chromite. A few pink and red garnets were also observed. A minor eclogitic assemblage consists predominantly of orange garnets with lesser amounts of clinopyroxene. The eclogitic samples, in particular the clinopyroxenes, were affected by intense secondary alteration characterised by a white fine-grained aggregate, likely consisting of diopside-rich clinopyroxene and plagioclase (Harte and Kirkley, 1997).

3.4. Analytical Methods

3.4.1. Major and Minor Element Analysis

The xenocrysts were embedded in Araldite® epoxy resin and finished to a final polish using 0.05μm alumina suspension on a polishing wheel. Analysis of minor and major element compositions was undertaken at the University of Alberta microprobe facility by wavelength-dispersion spectrometry (WDS) on a JEOL JXA-8900 Superprobe, using silicate, oxide and metal standards. Operating with an accelerating voltage of 20kV and a beam current of 20nA, counts for each element were collected for 30-60 seconds (peak) and for half the time on each background. Based on a minimum of three point analyses for each geochemical datum, detection limits (DL) of microprobe analyses are <100ppm for all oxides with the exception of Na_2O (DL of 200ppm) and P_2O_5 (DL of 250ppm).

The multiple spots analysed per grain were subsequently averaged if found homogeneous and unaltered. The microxenoliths were checked for internal homogeneity before averaging of multiple analysed grains.

3.4.2. Trace Element Analysis

Trace element analysis was carried out at the University of Alberta's Radiogenic Isotope Facility (RIF). The analyses were obtained on grain mounts by laser ablation ICP-MS, using a New Wave Research Nd:YAG UV213 laser system coupled to a Perkin Elmer Elan 6000 Quadrupole ICP-MS. Laser spot diameter for all minerals was 160μm, with individual analyses consisting of a 20 second measurement of background levels followed by 50 seconds of ion signal acquisition, with a fluence (energy density) of ~10J/cm^2. Where possible, multiple spots were studied per grain, and a minimum of six grains per xenolith were analysed. After checking for homogeneity only average results per xenocryst/xenolith are reported here.

The NIST 612 standard was used as the external calibration standard. Two megacrystic garnet standards (PN1, PN2, Tappert *et al.* 2005) were employed to monitor analytical accuracy. These grains have been well characterised compositionally by a number of analytical techniques (INAA, SIMS, LA-ICPMS) in several laboratories world-wide (e.g. Canil *et al.*, 2003; Tappert *et al.*, 2005). Repeated measurements of the same grains on different days yielded an external reproducibility (relative standard deviation (RSD)) well within the 2σ precision.

Calcium contents determined by electron microprobe analysis were used as an internal standard for monitoring, and correction of, instrumental drift. Data were reduced using the GLITTER® software (van Achterbergh *et al.*, 2001). Analytical precision at the 2σ level ranges between 7 and 40% (relative), but is generally better than 10%. Relative uncertainties >10% are typical for elements present in ultra low abundances (e.g. <<1 ppm; U, Th in garnet and HREEs in clinopyroxene). Concentrations below detection limits are indicated where appropriate. Further details on the techniques employed here can be found in Schmidberger *et al.* (2007).

3.4.3. In-situ Pb Isotopic Analysis

In situ Pb isotope data were obtained using a New Wave Research Nd:YAG UP213 laser system coupled to a NuPlasma MC-ICP-MS instrument at the

University of Alberta RIF. The low abundance of Pb (< 1 ppm) in the clinopyroxene grains investigated precluded the use of Faraday detectors for the acquisition of the Pb ion signals during the *in situ* analyses (e.g. Schmidberger *et al.*, 2007). Thus, a new protocol was developed using the Faraday–multiple ion counter (n=3) collector block. A detailed description of the collector configuration array, laser and ICP-MS instrument configurations are provided in Simonetti *et al.* (2005). In brief, the sample-out line from the laser ablation cell was 'y'-connected to the sample-out line from the desolvating nebuliser system (DSN-100 from Nu instruments) to allow for simultaneous aspiration of a dilute Tl solution (NIST SRM 997 standard in 2% HNO_3). The latter was used to monitor and correct for instrumental mass bias of the measured Pb isotope ratios (Longerich *et al.*, 1987).

Prior to the start of ablation, a 30 second on-peak baseline measurement was conducted in order to correct for the background ^{207}Pb, ^{206}Pb and ^{204}Hg and ^{204}Pb ion signals. Following the start of laser ablation, the acquisition sequence consisted of a two-step peak-jumping routine; in the first sequence the isotopes simultaneously measured were ^{207}Pb, ^{206}Pb, ^{205}Tl, ^{204}Pb, and ^{203}Tl, and the second sequence consisted solely of measuring the $^{202}Hg/^{204}Hg$ ratio. The purpose of the acquisition sequence is to primarily ensure the removal of any isobaric ^{204}Hg, present in trace amounts in the Ar gas, using a $^{204}Hg/^{202}Hg$ ratio of 0.22988 (Rosman and Taylor, 1999). Data acquisition consisted of 8 cycles of 10 second and 5 second integration intervals for sequences 1 and 2 (with 3 second magnet settling time) respectively, resulting in a total ablation time of ~3 minutes. Thus, in order to minimise the volume of sample consumed, clinopyroxene grains were ablated in raster mode using a 320µm by 320µm area, with a scan speed of 160µm/s, a 20Hz repetition rate, and 15J/cm^2 fluence.

Accuracy and external reproducibility was verified at the start of each session through multiple ablations of the NIST SRM 614 standard. This standard was chosen as its certified Pb concentration (2.32ppm: Reed, 1992) is close to that of the clinopyroxene grains investigated here. Repeated measurements (n=4) of the NIST SRM 614 standard, ablated using the same analytical settings as for the

clinopyroxene grains, indicate that the 'per session' external reproducibility (2σ, %RSD) for $^{206}Pb/^{204}Pb$ and $^{207}Pb/^{204}Pb$ ratios is better than 1% (for 6 sessions). The Pb/Pb ratios obtained here are also within 1% of the accepted values for NIST SRM 614.

3.4. Results

3.4.1. Major Elements

3.4.1.1. Garnet

Garnet occurs in 88 of the 113 samples analysed (28 as xenocrysts and 60 within microxenoliths). Electron microprobe analysis of the garnet grains showed that the majority (75) are derived from peridotitic sources (G9 or lherzolitic, G10 or harzburgitic, and G12 or wehrlitic). The remainder comprise two megacrystic (G1), one Ti-metasomatised lherzolitic (G11), five websteritic (G4), three eclogitic (two G3, and one G4) and two unclassified (G0) garnet grains (following the classification scheme of Grütter *et al.*, 2004) (Table 3.1). The websteritic garnets were distinguished from eclogitic G4 garnets based on the presence of orthopyroxene in two xenolith samples. Two more xenocrystic garnets showed near identical compositions to the garnets from websteritic xenoliths, all differing from eclogitic garnets in their higher MgO and Cr_2O_3 contents, and lower FeO (websteritic garnets: mean Mg-number (Mg# = 100Mg/[Mg+Fe^{2+}]) 84.0, Cr-number (Cr# = (100Cr/[Cr+Al])) 1.7; eclogitic garnets: mean Mg# 73.5, Cr# 0.5).

The peridotitic garnets are chrome pyropes, with average concentrations of 5.2wt% CaO, 6.4wt% Cr_2O_3, 20.6wt% MgO and 7.2wt% FeO. The exception is a wehrlitic (G12) garnet with very high CaO (19.5wt%) and low MgO (10.9wt%) (Table 3.1).

The majority of the peridotitic garnets plot in the lherzolitic field (53), with a sub-population deriving from harzburgitic (18) and wehrlitic (4) sources (Fig. 3.2).

Table 3.1. Major element data of the Renard microxenoliths and xenocrysts. $Mg\#_{Ca\text{-}corr}$ after Stachel *et al.* (2008). Garnet class following the Grütter *et al.* (2004) garnet classification scheme. Olivine Mg# calculated from peridotitic garnet composition and Ni in garnet temperature using an inversion of the Fe-Mg exchange thermometer of O'Neil and Wood (1979).

Min.	Xeno. #	Weight (mg)	Pipe #	P_2O_5	SiO_2	TiO_2	Al_2O_3	Cr_2O_3	V_2O_3	FeO	MnO	NiO	MgO	CaO	Na_2O	K_2O	Total	Mg#	Mg# Ca_corr	Cr#	Gnt Class	Ol Mg# from perid. Gnt
gnt	1b.1	2158.90	3	0.01	41.96	0.24	22.72	1.62	0.02	7.34	0.28	0.01	21.79	4.14	0.06	0.00	100.18	84.1	85.4	4.6	G9	92.4
cpx	1b.1	-	3	0.01	54.31	0.38	3.42	1.15	0.06	1.77	0.06	0.05	15.62	19.43	2.49	0.01	98.77	94.0	-	18.6	-	-
opx	1b.1	-	3	0.00	57.21	0.11	0.60	0.13	0.01	4.49	0.08	0.13	35.91	0.30	0.08	0.00	99.06	93.4	-	12.5	-	-
rutile	1b.1	-	3	0.00	0.14	98.05	0.08	1.34	0.92	0.18	0.02	0.00	0.21	0.44	0.02	0.00	101.42	0.0	-	0.0	-	-
gnt	1b.2	1141.40	3	0.03	41.47	0.36	22.14	1.88	0.03	7.43	0.36	0.01	21.67	4.48	0.08	0.00	99.93	83.9	85.2	5.4	G9	91.8
cpx	1b.2	-	3	0.01	53.74	0.38	3.53	1.15	0.06	2.14	0.09	0.04	15.85	19.95	2.39	0.02	99.34	93.0	-	19.1	-	-
opx	1b.2	-	3	0.01	57.00	0.12	0.56	0.12	0.00	4.69	0.10	0.09	36.17	0.36	0.10	0.00	99.32	93.2	-	13.0	-	-
gnt	2b.1	1449.60	4	0.02	41.18	0.26	19.62	5.41	0.04	7.30	0.41	0.01	20.42	5.23	0.06	0.00	99.96	83.3	84.9	15.6	G9	92.5
gnt	2b.2	669.10	4	0.01	42.45	0.06	23.72	0.71	0.02	7.30	0.28	0.01	21.90	4.06	0.03	0.00	100.55	84.2	-	2.0	G4	-
cpx	2b.2	-	4	0.01	55.00	0.04	2.32	0.37	0.04	1.98	0.06	0.08	16.94	20.75	1.52	0.01	99.13	93.8	-	9.7	-	-
opx	2b.2	-	4	0.01	57.45	0.02	0.65	0.05	0.01	4.68	0.09	0.16	35.43	0.40	0.08	0.00	99.03	93.1	-	5.2	-	-
gnt	1	989.50	1	0.03	41.03	0.17	17.33	8.21	0.04	8.67	0.50	0.01	17.74	6.86	0.03	0.01	100.63	78.5	80.6	24.1	G9	-
cpx	1	-	1	0.02	54.69	0.06	1.50	1.93	0.03	2.39	0.11	0.04	16.70	20.64	1.42	0.01	99.54	92.6	-	48.0	-	-
opx	1	-	1	0.01	53.75	0.04	4.43	1.27	0.02	5.49	0.20	0.04	30.42	2.00	0.30	0.75	98.73	90.8	-	16.1	-	-
gnt	2.1	77.70	2	0.02	41.08	0.27	17.23	8.59	0.05	7.10	0.43	0.01	18.82	6.94	0.04	0.00	100.58	82.5	84.7	25.1	G9	92.3
cpx	2.1	-	2	0.01	54.54	0.14	1.21	2.06	0.04	1.80	0.08	0.04	16.93	20.80	1.39	0.02	99.06	94.4	-	53.3	-	-
opx	2.1	-	2	0.00	57.65	0.09	0.51	0.35	0.01	4.56	0.12	0.09	35.73	0.42	0.08	0.00	99.61	93.3	-	31.4	-	-
olv	2.1	-	2	0.01	40.82	0.03	0.01	0.03	0.00	7.60	0.10	0.35	51.33	0.02	0.02	0.00	100.32	92.3	-	66.2	-	-
chr	2.1	-	2	0.01	0.22	1.80	7.45	60.89	0.32	17.46	0.50	0.12	13.91	0.18	0.01	0.00	102.87	58.7	-	84.6	-	-
gnt	2.2	121.70	2	0.02	41.20	0.03	17.42	8.73	0.05	6.92	0.42	0.01	19.89	5.81	0.02	0.00	100.51	83.7	85.5	25.2	G9	92.9
opx	2.2	-	2	0.01	57.62	0.01	0.49	0.32	0.01	4.36	0.12	0.09	35.83	0.35	0.05	0.00	99.25	93.6	-	30.4	-	-
chr	2.2	-	2	0.00	0.13	0.11	7.94	63.93	0.30	16.59	0.40	0.08	13.00	0.04	0.02	0.00	102.54	58.3	-	84.4	-	-
gnt	3	75.20	2	0.01	41.13	0.03	15.62	11.17	0.03	6.13	0.37	0.01	22.97	2.52	0.01	0.00	100.00	87.0	87.8	32.5	G10D	93.5
olv	3	-	2	0.00	40.38	0.00	0.02	0.05	0.00	6.43	0.09	0.38	51.45	0.01	0.01	0.00	98.82	93.5	-	69.3	-	-
gnt	4.1	13.50	2	0.01	40.97	0.01	17.03	9.04	0.05	6.78	0.39	0.00	20.78	4.85	0.02	0.00	99.95	84.5	86.0	26.3	G10	92.9
gnt	4.2	29.20	2	0.00	42.55	0.01	22.81	2.07	0.01	5.17	0.27	0.01	25.26	1.44	0.02	0.00	99.63	89.7	90.1	5.7	G10D	94.8
gnt	5	17.00	2	0.01	41.00	0.17	18.11	7.66	0.05	7.13	0.42	0.01	19.12	6.58	0.03	0.00	100.28	82.6	84.7	22.2	G9	-
cpx	5	-	2	0.01	54.33	0.08	1.99	2.23	0.04	1.73	0.09	0.04	16.31	20.41	1.93	0.00	99.20	94.3	-	45.9	-	-
opx	5	-	2	0.01	57.44	0.03	0.58	0.37	0.01	4.66	0.12	0.09	35.45	0.40	0.13	0.00	99.28	93.1	-	29.9	-	-

Table 3.1 cont.

Min.	Xeno. #	Weight (mg)	Pipe #	P_2O_5	SiO_2	TiO_2	Al_2O_3	Cr_2O_3	V_2O_3	FeO	MnO	NiO	MgO	CaO	Na_2O	K_2O	Total	Mg#	Mg# Ca_corr	Cr#	Gnt Class	Ol Mg# from Gnt
gnt	6	21.60	2	0.02	41.56	0.18	19.51	5.79	0.04	7.09	0.40	0.00	20.25	5.37	0.04	0.00	100.26	83.6	85.2	16.6	G9	92.5
cpx	6	-	2	0.01	54.21	0.12	2.16	2.06	0.04	1.92	0.10	0.04	16.62	20.26	1.70	0.01	99.24	93.9	-	41.0	-	-
opx	6	-	2	0.00	57.32	0.05	0.48	0.29	0.00	4.56	0.11	0.09	35.92	0.45	0.10	0.00	99.40	93.3	-	29.2	-	-
gnt	7.1	98.90	2	0.02	40.33	0.13	14.08	12.21	0.06	7.12	0.42	0.01	19.08	6.45	0.03	0.00	99.95	82.7	84.7	36.8	G9	91.8
olv	7.1	-	2	0.01	40.26	0.01	0.02	0.04	0.00	8.06	0.11	0.38	50.56	0.03	0.02	0.00	99.49	91.8	-	59.5	-	-
chr	7.1	-	2	0.01	0.25	0.32	4.67	62.63	0.25	19.41	0.40	0.11	12.35	0.00	0.01	0.01	100.43	53.1	-	90.0	-	-
gnt	7.2	80.00	2	0.01	40.95	0.11	16.16	10.03	0.04	6.53	0.36	0.01	23.09	2.45	0.04	0.02	99.80	86.3	87.1	29.4	G10D	93.0
gnt	7.3	75.60	2	0.01	41.48	0.04	10.15	7.83	0.03	6.33	0.27	0.13	32.65	1.11	0.03	0.00	100.05	89.1	90.5	49.2	G10D	93.4
olv	7.3	-	2	0.01	40.52	0.00	0.01	0.05	0.00	6.46	0.09	0.37	51.12	0.01	0.02	0.00	98.65	93.4	-	80.9	-	-
gnt	7.4	75.50	2	0.00	41.44	0.02	18.35	7.62	0.06	6.80	0.42	0.01	19.18	6.74	0.02	0.00	100.67	83.4	85.5	21.8	G9	92.4
cpx	7.4	-	2	0.01	54.42	0.05	1.19	1.95	0.03	1.73	0.09	0.05	16.77	20.90	1.30	0.02	98.51	94.5	-	52.4	-	-
olv	7.4	-	2	0.01	40.88	0.00	0.00	0.02	0.00	7.38	0.10	0.38	50.46	0.02	0.02	0.00	99.29	92.4	-	100.0	-	-
gnt	7.5	53.60	2	0.01	41.57	0.02	18.24	8.02	0.04	6.60	0.41	0.00	20.09	5.51	0.01	0.00	100.51	84.4	86.1	22.8	G9	93.1
opx	7.5	-	2	0.00	57.09	0.00	0.48	0.32	0.01	4.16	0.11	0.10	35.39	0.36	0.03	0.01	98.06	93.8	-	30.9	-	-
gnt	7.6	49.20	2	0.00	41.48	0.01	17.47	8.81	0.05	6.76	0.42	0.00	20.16	5.19	0.02	0.00	100.38	84.2	85.8	25.3	G10	92.7
olv	7.6	-	2	0.01	41.00	0.00	0.00	0.03	0.01	7.15	0.10	0.37	50.78	0.01	0.01	0.00	99.46	92.7	-	100.0	-	-
gnt	7.7	44.40	2	0.00	42.11	0.11	22.46	2.40	0.03	6.85	0.31	0.01	21.46	5.15	0.03	0.00	100.91	84.8	86.4	6.7	G9	92.1
cpx	7.7	-	2	0.02	54.78	0.05	1.19	0.61	0.02	1.74	0.06	0.05	17.84	23.17	0.83	0.01	100.39	94.8	-	25.6	-	-
opx	7.7	-	2	0.01	57.54	0.04	0.60	0.12	0.00	4.43	0.10	0.11	35.99	0.44	0.05	0.00	99.42	93.5	-	11.9	-	-
gnt	7.8	43.90	2	0.03	41.53	0.13	18.77	6.99	0.06	6.79	0.41	0.01	19.41	6.30	0.04	0.00	100.46	83.6	85.5	20.0	G9	92.9
gnt	7.9	34.20	2	0.02	40.68	0.07	15.06	11.73	0.04	6.77	0.42	0.01	18.90	7.46	0.03	0.00	101.19	83.3	85.6	34.3	G9	91.7
opx	7.9	-	2	0.00	57.66	0.01	0.45	0.44	0.00	4.36	0.11	0.10	35.86	0.47	0.13	0.00	99.61	93.6	-	39.5	-	-
mg-ilm	8.1	19.60	2	0.01	0.13	53.04	0.68	0.98	0.70	30.80	0.28	0.13	14.08	0.03	0.04	0.00	100.91	44.9	-	49.3	-	-
mg-ilm	8.2	8.80	2	0.01	0.10	52.61	0.66	0.90	0.66	31.54	0.30	0.12	13.68	0.02	0.03	0.00	100.65	43.6	-	47.9	-	-
mg-ilm	8.3	8.30	2	0.00	0.11	53.40	0.69	1.22	0.72	29.72	0.26	0.14	14.45	0.03	0.06	0.00	100.81	46.4	-	54.3	-	-
gnt	9.1	21.90	2	0.02	42.25	0.66	20.79	2.64	0.05	7.24	0.29	0.01	21.71	4.49	0.06	0.00	100.20	84.2	-	7.8	G1	-
gnt	9.2	28.70	2	0.02	42.30	0.61	21.46	2.44	0.05	7.43	0.33	0.01	21.62	4.08	0.09	0.00	100.45	83.8	-	7.1	G1	-
gnt	9.3	31.60	2	0.02	42.35	0.34	23.19	0.72	0.03	7.53	0.32	0.00	20.77	5.06	0.06	0.00	100.40	83.1	-	2.0	G4	-
gnt	10.1	12.70	2	0.02	40.84	0.14	16.67	9.50	0.06	7.02	0.42	0.00	18.19	7.93	0.02	0.00	100.81	82.2	-	27.7	G12	-
cpx	10.1	-	2	0.02	54.52	0.02	0.73	1.22	0.02	1.74	0.09	0.05	17.76	22.72	0.75	0.03	99.65	94.8	-	52.8	-	-
gnt	10.2	9.00	2	0.02	41.28	0.24	17.42	8.63	0.05	6.17	0.35	0.00	20.49	5.75	0.05	0.00	100.46	85.5	87.3	25.0	G9	93.4
cpx	10.2	-	2	0.02	54.65	0.09	2.03	3.43	0.07	1.77	0.08	0.04	16.05	18.70	2.55	0.09	99.57	94.2	-	53.1	-	-
gnt	11.1	63.50	2	0.01	41.39	0.17	19.82	5.35	0.04	7.28	0.40	0.01	19.80	5.91	0.03	0.00	100.23	82.9	84.7	15.3	G9	92.2
cpx	11.1	-	2	0.01	54.42	0.07	1.11	1.28	0.03	1.84	0.08	0.05	17.22	21.91	1.03	0.02	99.08	94.3	-	43.5	-	-

Table 3.1 cont.

Min.	Xeno. #	Weight (mg)	Pipe #	P_2O_5	SiO_2	TiO_2	Al_2O_3	Cr_2O_3	V_2O_3	FeO	MnO	NiO	MgO	CaO	Na_2O	K_2O	Total	Mg#	Mg# Ca_corr	Cr#	Gnt Class	Ol Mg# from Gnt
gnt	11.2	17.20	2	0.03	41.44	0.17	19.82	5.46	0.03	8.08	0.45	0.01	19.43	6.10	0.03	0.00	101.04	81.1	83.0	15.6	G9	91.4
cpx	11.2	-	2	0.02	54.42	0.07	1.23	1.35	0.03	2.11	0.08	0.04	17.00	21.57	1.17	0.01	99.11	93.5	-	42.3	-	-
opx	11.2	-	2	0.00	57.19	0.04	0.56	0.25	0.01	5.21	0.13	0.09	35.11	0.43	0.07	0.00	99.08	92.3	-	23.5	-	-
gnt	12.1	12.00	2	0.02	40.63	0.06	14.63	11.90	0.07	6.85	0.43	0.01	19.72	5.28	0.02	0.00	99.61	83.7	85.4	35.3	G10D	92.3
gnt	12.2	6.90	2	0.01	41.69	0.04	17.30	8.34	0.06	6.27	0.32	0.00	21.20	4.88	0.02	0.00	100.13	85.8	87.3	24.4	G10D	92.6
gnt	12.3	6.40	2	0.03	40.92	0.06	15.69	10.54	0.07	7.60	0.45	0.01	18.80	6.32	0.01	0.00	100.52	81.5	83.5	31.1	G9	91.4
gnt	13	496.80	2	0.01	44.12	0.19	17.90	3.49	0.03	5.81	0.30	0.01	20.25	7.60	0.30	0.00	100.03	86.6	-	15.2	G12	-
cpx	13	-	2	0.01	54.68	0.14	1.79	1.43	0.04	1.57	0.08	0.04	16.87	21.43	1.48	0.02	99.58	95.0	-	34.7	-	-
opx	13	-	2	0.00	57.69	0.05	0.49	0.22	0.01	4.27	0.10	0.08	35.71	0.41	0.08	0.00	99.11	93.7	-	22.9	-	-
gnt	14.1	25.90	2	0.01	41.67	0.10	20.19	5.13	0.03	7.22	0.39	0.00	20.35	5.52	0.03	0.00	100.66	83.4	85.1	14.6	G9	92.5
cpx	14.1	-	2	0.02	54.74	0.04	1.56	1.68	0.04	1.85	0.08	0.05	16.87	21.20	1.50	0.02	99.64	94.2	-	42.0	-	-
opx	14.1	-	2	0.00	57.82	0.02	0.52	0.27	0.01	4.61	0.11	0.09	35.64	0.40	0.09	0.00	99.57	93.2	-	25.5	-	-
gnt	14.2	17.80	2	0.01	41.63	0.10	20.27	4.94	0.03	7.20	0.39	0.01	20.25	5.46	0.03	0.00	100.32	83.4	85.1	14.1	G9	92.3
cpx	14.2	-	2	0.01	54.55	0.04	1.54	1.63	0.04	1.84	0.08	0.05	16.87	21.36	1.45	0.02	99.48	94.2	-	41.4	-	-
opx	14.2	-	2	0.01	57.49	0.03	0.51	0.25	0.01	4.62	0.12	0.09	35.68	0.42	0.08	0.00	99.30	93.2	-	24.7	-	-
gnt	15.1	105.50	2	0.04	41.50	0.22	19.91	5.27	0.03	8.15	0.45	0.01	19.87	5.80	0.04	0.00	101.28	81.3	83.1	15.1	G9	91.2
cpx	15.1	-	2	0.01	54.43	0.11	1.78	1.97	0.03	2.22	0.10	0.04	16.53	21.01	1.76	0.01	100.00	93.0	-	42.6	-	-
olv	15.1	-	2	0.02	40.21	0.02	0.41	0.02	0.00	8.65	0.11	0.35	50.12	0.02	0.03	0.00	99.95	91.2	-	11.2	-	-
cpx	16.1	30.90	2	0.02	53.14	0.11	4.91	1.05	0.02	2.30	0.08	0.03	14.71	22.00	1.81	0.00	100.17	91.9	-	12.7	-	-
opx	16.1	-	2	0.00	54.81	0.03	3.48	0.49	0.00	6.98	0.16	0.07	33.32	0.25	0.04	0.00	99.65	89.5	-	8.7	-	-
olv	16.1	-	2	0.00	40.52	0.00	0.02	0.01	0.00	10.23	0.13	0.38	48.85	0.01	0.02	0.00	100.17	89.5	-	38.8	-	-
gnt	16.2	20.40	2	0.01	41.68	0.05	21.25	3.65	0.06	8.35	0.40	0.01	19.45	5.92	0.01	0.00	100.83	80.6	82.4	10.3	G9	91.0
cpx	16.2	-	2	0.02	54.52	0.01	0.46	0.32	0.02	1.90	0.07	0.06	18.21	23.89	0.22	0.02	99.71	94.5	-	31.7	-	-
gnt	16.3	7.10	2	0.04	41.30	0.16	19.93	5.19	0.04	8.36	0.45	0.01	19.47	5.80	0.03	0.00	100.77	80.6	82.4	14.9	G9	90.7
cpx	16.3	-	2	0.02	54.45	0.06	1.42	1.50	0.04	2.24	0.09	0.04	16.96	21.48	1.38	0.01	99.68	93.1	-	41.4	-	-
olv	16.3	-	2	0.01	40.33	0.01	0.05	0.02	0.00	9.17	0.12	0.35	49.91	0.02	0.01	0.00	100.02	90.7	-	35.3	-	-
gnt	17	22.70	2	0.03	42.48	0.65	21.90	1.20	0.04	6.88	0.26	0.02	22.59	4.01	0.07	0.00	100.11	85.4	-	3.5	G11	-
cpx	18.1	33.70	2	0.01	54.51	0.03	2.27	2.52	0.05	1.38	0.08	0.04	15.74	21.10	2.10	0.01	99.83	95.3	-	42.7	-	-
chr	18.1	-	2	0.01	0.05	0.17	11.99	59.88	0.26	16.02	0.43	0.05	12.80	0.01	0.01	0.00	101.67	58.8	-	77.0	-	-
cpx	18.2	19.70	2	0.01	54.45	0.18	1.58	0.66	0.03	3.56	0.13	0.07	19.40	17.76	1.18	0.03	99.03	90.7	-	21.9	-	-
cpx	19	24.40	2	0.01	53.04	0.17	3.14	1.11	0.03	2.51	0.13	0.03	17.04	21.60	0.94	0.01	99.76	92.3	-	26.5	-	-
gnt	20	1161.50	2	0.01	41.45	0.20	19.52	5.77	0.04	7.12	0.42	0.00	20.28	5.36	0.05	0.00	100.21	83.5	85.2	16.5	G9	92.8

Table 3.1 cont.

Min.	Xeno. #	Weight (mg)	Pipe #	P_2O_5	SiO_2	TiO_2	Al_2O_3	Cr_2O_3	V_2O_3	FeO	MnO	NiO	MgO	CaO	Na_2O	K_2O	Total	Mg#	Mg# Ca_corr	Cr#	Gnt Class	Ol Mg# from Gnt
mg-ilm	21.1	138.20	-	0.00	0.09	53.23	0.50	1.07	0.69	30.38	0.27	0.14	14.61	0.04	0.03	0.00	101.05	46.2	-	59.0	-	-
mg-ilm	21.2	127.30	-	0.00	0.10	53.31	0.57	0.95	0.73	30.72	0.28	0.13	14.44	0.03	0.03	0.00	101.29	45.6	-	53.0	-	-
mg-ilm	21.3	59.80	-	0.00	0.13	52.79	0.62	2.32	0.75	29.08	0.25	0.19	14.96	0.03	0.03	0.00	101.15	47.8	-	71.5	-	-
mg-ilm	22.1	14.90	-	0.01	0.15	51.32	0.94	3.81	0.72	28.66	0.26	0.22	15.53	0.04	0.04	0.01	101.71	49.1	-	73.1	-	-
mg-ilm	22.2	10.80	-	0.01	0.10	53.41	0.56	1.21	0.75	30.20	0.28	0.13	14.61	0.02	0.04	0.00	101.31	46.3	-	59.4	-	-
mg-ilm	22.3	11.60	-	0.01	0.13	53.38	0.63	0.98	0.71	29.91	0.29	0.14	14.83	0.03	0.04	0.00	101.06	46.9	-	51.0	-	-
chr	22.4	6.10	-	0.00	0.10	0.07	8.16	62.54	0.25	16.73	0.39	0.08	12.78	0.00	0.03	0.00	101.12	57.7	-	83.7	-	-
gnt	23	1865.80	3	0.03	41.89	0.35	22.22	2.05	0.03	7.40	0.37	0.01	21.29	4.23	0.08	0.00	99.93	83.7	85.0	5.8	G9	92.4
cpx	23	-	3	0.01	54.44	0.37	3.00	1.22	0.06	2.13	0.08	0.04	15.72	19.14	2.35	0.03	98.60	93.0	-	21.3	-	-
opx	23	-	3	0.00	57.28	0.12	0.56	0.15	0.01	4.64	0.11	0.10	35.54	0.35	0.10	0.00	98.96	93.2	-	14.8	-	-
rutile	23	-	3	0.00	0.02	97.61	0.03	1.62	0.88	0.11	0.01	0.00	0.02	0.01	0.03	0.00	100.35	0.0	-	0.0	-	-
gnt	24	679.50	3	0.02	41.87	0.14	19.89	5.59	0.04	7.27	0.40	0.01	20.73	4.37	0.05	0.00	100.36	83.6	84.9	15.9	G10	-
cpx	24	-	3	0.01	54.13	0.14	3.60	3.80	0.07	1.66	0.08	0.04	14.58	16.52	3.60	0.15	98.37	94.0	-	41.5	-	-
opx	24	-	3	0.01	57.53	0.03	0.63	0.39	0.01	4.61	0.12	0.09	35.28	0.34	0.18	0.00	99.22	93.2	-	29.5	-	-
gnt	25.1	166.00	3	0.03	41.63	0.15	20.82	3.89	0.03	8.39	0.43	0.00	19.91	5.23	0.03	0.00	100.56	80.9	82.5	11.2	G9	90.4
cpx	25.1	-	3	0.02	54.56	0.07	1.71	1.29	0.04	2.28	0.09	0.05	16.74	21.08	1.49	0.01	99.43	92.9	-	33.2	-	-
opx	25.1	-	3	0.01	57.36	0.04	0.52	0.13	0.00	5.33	0.12	0.10	35.06	0.42	0.09	0.00	99.19	92.1	-	14.3	-	-
olv	25.1	-	3	0.01	40.10	0.01	0.01	0.02	0.00	9.34	0.12	0.35	49.56	0.02	0.02	0.00	99.55	90.4	-	69.6	-	-
cpx	25.2	23.30	3	0.02	54.85	0.07	1.66	1.56	0.04	2.29	0.10	0.04	16.90	20.89	1.56	0.01	100.00	92.9	-	38.8	-	-
olv	25.2	-	3	0.01	40.12	0.00	0.01	0.01	0.00	9.36	0.12	0.35	49.88	0.02	0.02	0.00	99.90	90.5	-	56.1	-	-
gnt	26.1	73.80	3	0.02	41.86	0.55	22.67	0.43	0.04	7.87	0.30	0.01	21.62	4.50	0.08	0.00	99.93	83.0	84.4	1.2	G3D	-
gnt	26.2	26.30	3	0.01	41.35	0.21	23.26	0.14	0.03	12.43	0.38	0.01	19.09	3.78	0.06	0.00	100.75	73.2	-	0.4	G4	-
cpx	26.2	-	3	0.01	53.51	0.26	4.18	0.12	0.10	4.02	0.08	0.04	14.61	17.43	3.15	0.01	97.54	86.6	-	2.0	-	-
gnt	26.3	17.40	3	0.00	40.91	0.02	15.21	11.39	0.04	6.94	0.41	0.01	23.05	2.04	0.03	0.00	100.06	85.6	86.2	33.4	G10D	92.2
gnt	26.4	7.40	3	0.02	41.07	0.25	17.64	7.91	0.05	6.41	0.39	0.00	20.88	5.38	0.06	0.00	100.06	85.3	87.0	23.1	G9	93.2
gnt	26.5	7.00	3	0.02	40.58	0.16	15.45	10.49	0.06	6.81	0.39	0.01	19.77	6.23	0.06	0.01	100.04	83.8	85.8	31.3	G9	92.2
gnt	27.1	16.90	-	0.00	42.24	0.14	23.46	0.47	0.03	6.10	0.24	0.02	21.80	5.50	0.02	0.01	100.03	86.4	-	1.3	G4	-
gnt	27.2	4.20	-	0.01	42.21	0.40	23.36	0.56	0.03	6.77	0.28	0.00	22.51	3.89	0.09	0.00	100.11	85.6	-	1.6	G0	-
gnt	28.1	104.00	3	0.01	41.11	0.05	21.31	3.27	0.06	11.25	0.54	0.00	17.88	5.61	0.02	0.00	101.10	73.9	75.6	9.3	G9	84.1
cpx	28.1	-	3	0.01	54.43	0.01	0.65	0.44	0.03	3.23	0.13	0.06	17.75	23.18	0.47	0.01	100.39	90.7	-	31.1	-	-
opx	28.1	-	3	0.01	56.75	0.01	0.38	0.13	0.00	8.09	0.18	0.11	33.44	0.53	0.03	0.00	99.65	88.0	-	18.2	-	-
gnt	28.2	79.80	3	0.02	40.98	0.02	18.14	7.92	0.04	6.98	0.40	0.00	19.19	7.05	0.02	0.00	100.75	83.1	85.2	22.6	G9	91.2
opx	28.2	-	3	0.00	56.87	0.00	0.56	0.36	0.00	4.54	0.12	0.10	35.59	0.42	0.07	0.00	98.64	93.3	-	30.0	-	-

Table 3.1 cont.

Min.	Xeno. #	Weight (mg)	Pipe #	P_2O_5	SiO_2	TiO_2	Al_2O_3	Cr_2O_3	V_2O_3	FeO	MnO	NiO	MgO	CaO	Na_2O	K_2O	Total	Mg#	Mg# Ca_corr	Cr#	Gnt Class	Ol Mg# from Gnt
gnt	28.3	66.70	3	0.04	40.83	0.03	17.73	8.32	0.05	7.01	0.42	0.00	19.00	7.28	0.02	0.00	100.72	82.9	85.1	23.9	G9	90.1
cpx	28.3	-	3	0.01	53.50	0.40	1.97	1.36	0.03	3.22	0.19	0.03	18.51	19.85	0.99	0.01	100.05	91.1	-	31.7	-	-
opx	28.3	-	3	0.01	57.61	0.01	0.45	0.30	0.00	4.56	0.12	0.10	35.93	0.47	0.07	0.00	99.63	93.4	-	30.5	-	-
gnt	29	892.60	3	0.06	41.91	0.36	23.10	0.49	0.02	7.80	0.29	0.01	21.43	4.18	0.15	0.00	99.80	83.0	-	1.4	G4D	-
cpx	29	-	3	0.02	54.50	0.37	3.97	0.36	0.05	2.62	0.07	0.04	15.51	19.08	2.75	0.03	99.38	91.3	-	5.8	-	-
opx	29	-	3	0.01	56.17	0.18	1.31	0.69	0.02	5.26	0.13	0.10	33.70	1.10	0.20	0.01	98.88	91.9	-	27.0	-	-
gnt	30	73.00	3	0.02	41.98	0.24	21.87	2.83	0.03	7.98	0.38	0.01	20.86	4.73	0.05	0.00	100.97	82.3	83.8	8.0	G9	-
cpx	30	-	3	0.02	54.91	0.13	2.00	1.04	0.03	2.08	0.09	0.04	15.39	20.94	2.99	0.01	99.68	89.6	-	22.5	-	-
opx	30	-	3	0.00	56.75	0.07	2.03	0.16	0.00	5.10	0.12	0.10	34.64	0.42	0.10	0.00	99.48	92.4	-	11.9	-	-
gnt	31	805.70	3	0.01	41.96	0.22	22.36	2.27	0.02	7.18	0.32	0.01	21.41	4.66	0.05	0.00	100.49	84.2	85.6	6.4	G9	92.3
cpx	31	-	3	0.02	51.39	0.47	6.38	1.37	0.05	2.75	0.15	0.03	15.64	19.74	1.59	0.01	99.60	91.0	-	17.3	-	-
opx	31	-	3	0.00	56.09	0.15	1.04	0.42	0.01	4.91	0.11	0.10	34.62	0.53	0.12	0.00	98.10	92.6	-	18.2	-	-
Phlog	31	-	3	0.00	40.29	2.40	14.06	1.33	0.05	4.04	0.03	0.09	22.60	0.01	0.22	9.54	94.65	90.9	-	5.9	-	-
gnt	32	65.30	3	0.00	41.40	0.14	20.49	4.68	0.03	8.41	0.45	0.01	19.91	5.64	0.04	0.00	101.21	80.8	82.6	13.3	G9	87.9
cpx	32	-	3	0.00	54.12	0.08	1.83	1.64	0.05	2.39	0.10	0.05	16.76	21.13	1.78	0.02	99.94	92.6	-	37.6	-	-
opx	32	-	3	0.01	57.29	0.05	0.58	0.24	0.00	5.43	0.13	0.09	35.13	0.44	0.10	0.00	99.49	92.0	-	22.0	-	-
gnt	33.1	65.50	3	0.02	38.23	0.01	22.22	0.02	0.01	31.98	1.65	0.00	6.55	1.37	0.02	0.00	102.10	26.8	27.2	0.1	G0	-
gnt	33.2	8.90	3	0.01	41.61	0.16	20.41	4.57	0.04	7.32	0.38	0.01	20.85	4.77	0.04	0.00	100.17	83.5	85.0	13.1	G9	91.7
cpx	33.2	-	3	0.02	52.77	0.23	4.04	1.62	0.04	2.72	0.17	0.04	16.17	19.95	1.48	0.01	99.23	91.4	-	29.1	-	-
opx	33.2	-	3	0.01	56.79	0.14	1.01	0.69	0.01	5.14	0.13	0.09	34.48	0.78	0.17	0.00	99.43	92.3	-	28.8	-	-
chr	33.2	-	3	0.00	0.23	0.76	12.95	49.47	0.30	22.70	0.34	0.18	14.08	0.00	0.02	0.01	101.05	52.5	-	71.9	-	-
gnt	34.1	114.70	3	0.01	41.66	0.22	20.52	4.74	0.04	6.91	0.38	0.00	20.78	5.56	0.04	0.00	100.86	84.3	86.0	13.4	G9	91.5
opx	34.1	-	3	0.01	57.31	0.06	0.56	0.27	0.01	4.44	0.11	0.11	35.80	0.41	0.10	0.00	99.17	93.5	-	24.4	-	-
gnt	34.2	20.90	3	0.03	41.19	0.23	16.79	9.62	0.06	6.73	0.40	0.01	21.37	4.60	0.06	0.00	101.07	85.0	86.4	27.8	G10D	89.7
cpx	34.2	-	3	0.01	54.39	0.20	2.13	2.58	0.04	2.10	0.09	0.05	16.54	19.48	2.34	0.04	99.97	93.4	-	44.8	-	-
Phlog	34.2	-	3	0.00	39.43	2.61	13.96	2.56	0.04	3.52	0.05	0.09	22.12	0.01	0.25	8.92	93.57	91.8	-	11.0	-	-
gnt	35.1	43.50	3	0.00	41.87	0.21	21.95	2.83	0.03	7.77	0.40	0.00	21.14	4.78	0.05	0.00	101.05	82.9	84.3	8.0	G9	89.7
cpx	35.1	-	3	0.01	54.59	0.16	2.30	1.37	0.05	2.09	0.08	0.05	16.48	21.02	1.91	0.01	100.11	93.3	-	28.5	-	-
gnt	35.2	31.00	3	0.01	42.56	0.01	20.13	5.51	0.03	5.83	0.29	0.01	24.99	1.18	0.02	0.00	100.56	88.4	88.8	15.5	G10D	93.1
olv	35.2	-	3	0.00	40.79	0.00	0.02	0.05	0.00	6.86	0.09	0.38	51.56	0.01	0.01	0.00	99.79	93.1	-	66.4	-	-
gnt	36.1	200.30	3	0.01	39.94	0.05	16.81	9.15	0.04	6.91	0.42	0.00	20.00	5.00	0.02	0.00	98.35	83.8	85.3	26.8	G10	92.8
opx	36.1	-	3	0.00	56.12	0.01	0.49	0.34	0.00	4.32	0.11	0.10	36.05	0.31	0.05	0.00	97.90	93.7	-	32.2	-	-
gnt	36.2	148.90	3	0.01	40.47	0.19	13.86	12.70	0.05	6.20	0.41	0.01	18.57	7.86	0.04	0.00	100.37	84.2	86.7	38.1	G9	93.2

Table 3.1 cont.

Min.	Xeno. #	Weight (mg)	Pipe #	P_2O_5	SiO_2	TiO_2	Al_2O_3	Cr_2O_3	V_2O_3	FeO	MnO	NiO	MgO	CaO	Na_2O	K_2O	Total	Mg#	Mg# Ca_corr	Cr#	Gnt Class	Ol Mg# from Gnt
gnt	37.1	116.40	3	0.01	40.46	0.18	21.15	2.77	0.03	8.12	0.39	0.00	20.04	4.45	0.04	0.00	97.64	81.5	82.9	8.1	G9	91.4
cpx	37.1	-	3	0.01	53.36	0.12	1.92	1.19	0.04	2.24	0.08	0.04	16.68	19.68	1.65	0.01	97.01	93.0	-	29.3	-	-
opx	37.1	-	3	0.00	55.50	0.06	0.58	0.16	0.01	5.28	0.11	0.09	34.91	0.38	0.09	0.00	97.18	92.2	-	15.8	-	-
gnt	37.2	32.90	3	0.01	41.06	0.03	19.20	6.41	0.02	7.13	0.41	0.00	22.15	2.36	0.02	0.00	98.81	84.7	85.4	18.3	G10	92.7
opx	37.2	-	3	0.00	56.26	0.01	0.56	0.38	0.01	4.40	0.12	0.10	35.68	0.18	0.05	0.00	97.75	93.5	-	31.3	-	-
gnt	38	19.60	3	0.02	41.06	0.24	16.92	8.82	0.04	6.79	0.39	0.01	19.49	6.66	0.05	0.00	100.48	83.6	85.7	25.9	G9	92.5
gnt	39	395.30	3	0.02	41.44	0.21	22.12	1.88	0.03	8.15	0.39	0.01	20.87	4.37	0.05	0.00	99.53	82.0	83.4	5.4	G9	91.5
cpx	39	-	3	0.01	54.32	0.22	2.58	0.97	0.05	2.34	0.09	0.04	16.33	19.87	2.01	0.01	98.85	92.6	-	20.2	-	-
opx	39	-	3	0.00	57.12	0.09	0.59	0.12	0.01	5.38	0.13	0.09	35.21	0.39	0.10	0.00	99.24	92.1	-	12.0	-	-
gnt	40	124.40	3	0.03	41.14	0.34	19.81	4.99	0.03	8.61	0.46	0.01	19.23	5.91	0.05	0.00	100.60	79.9	81.7	14.5	G9	90.5
cpx	40	-	3	0.02	54.20	0.18	1.46	1.47	0.04	2.40	0.10	0.04	16.86	21.51	1.41	0.01	99.69	92.6	-	40.4	-	-
opx	40	-	3	0.00	57.09	0.11	0.53	0.25	0.01	5.63	0.14	0.09	34.81	0.43	0.08	0.00	99.16	91.7	-	23.9	-	-
gnt	41.1	104.30	4	0.01	41.01	0.18	19.73	5.34	0.04	7.19	0.39	0.01	19.73	5.67	0.03	0.00	99.34	83.0	84.8	15.4	G9	92.5
cpx	41.1	-	4	0.02	53.04	0.08	1.06	1.17	0.02	1.76	0.09	0.04	17.33	21.13	0.97	0.01	96.71	94.6	-	42.5	-	-
opx	41.1	-	4	0.00	56.53	0.04	0.46	0.24	0.01	4.72	0.12	0.09	35.34	0.45	0.06	0.00	98.06	93.0	-	25.6	-	-
gnt	41.2	65.30	4	0.01	40.19	0.06	13.41	13.65	0.07	7.12	0.47	0.01	15.94	9.66	0.02	0.00	100.61	80.0	-	40.6	G12	-
cpx	41.2	-	4	0.01	54.67	0.01	0.69	1.32	0.02	1.80	0.08	0.05	17.56	22.02	0.67	0.15	99.06	94.6	-	56.2	-	-
chr	41.2	-	4	0.01	0.09	0.63	7.73	62.83	0.27	18.58	0.41	0.08	12.46	0.03	0.02	0.00	103.13	54.5	-	84.4	-	-
gnt	41.3	49.60	4	0.03	39.20	0.23	12.32	12.58	0.05	6.20	0.32	0.00	10.90	19.25	0.02	0.00	101.11	75.8	-	40.6	G12	-
gnt	41.4	18.80	4	0.01	41.80	0.27	19.74	5.33	0.04	6.98	0.36	0.00	20.80	5.72	0.04	0.00	101.09	84.2	85.9	15.3	G9	91.2
cpx	41.4	-	4	0.00	54.74	0.09	1.36	1.34	0.03	2.09	0.10	0.05	17.58	21.62	1.31	0.07	100.37	93.7	-	39.8	-	-
gnt	42.1	71.50	4	0.01	41.74	0.05	21.92	2.77	0.02	8.13	0.51	0.00	20.27	4.61	0.03	0.00	100.06	81.6	83.0	7.8	G9	92.7
cpx	42.1	-	4	0.02	53.31	0.11	3.07	2.05	0.03	1.22	0.08	0.03	15.17	20.10	2.19	0.00	97.37	95.7	-	30.9	-	-
opx	42.1	-	4	0.00	56.02	0.03	0.73	0.29	0.00	4.77	0.12	0.07	35.31	0.24	0.05	0.00	97.65	93.0	-	21.3	-	-
chr	42.1	-	4	0.00	0.04	0.27	17.19	55.36	0.22	15.54	0.37	0.06	13.43	0.01	0.00	0.00	102.49	60.6	-	68.4	-	-
gnt	42.2	16.30	4	0.00	41.46	0.01	19.44	6.31	0.03	6.36	0.38	0.00	22.69	2.45	0.02	0.00	99.16	86.4	87.2	17.9	G10	93.6
opx	42.2	-	4	0.00	56.94	0.01	0.59	0.38	0.00	3.86	0.10	0.09	35.98	0.17	0.03	0.00	98.16	94.3	-	30.0	-	-
gnt	43.1	28.30	4	0.01	40.67	0.03	17.22	8.76	0.06	6.88	0.42	0.00	18.17	7.34	0.01	0.00	99.57	82.5	84.8	25.4	G9	92.6
opx	43.1	-	4	0.00	57.04	0.01	0.46	0.30	0.01	4.49	0.11	0.10	35.62	0.45	0.04	0.00	98.63	93.4	-	30.2	-	-
gnt	43.2	12.90	4	0.00	42.29	0.00	20.41	5.47	0.03	6.61	0.38	0.00	23.61	1.52	0.01	0.00	100.34	86.4	86.9	15.2	G10	93.4
opx	43.2	-	4	0.00	57.48	0.01	0.61	0.37	0.01	3.98	0.09	0.09	36.16	0.11	0.02	0.00	98.93	94.2	-	28.9	-	-
olv	43.2	-	4	0.00	40.66	0.01	0.03	0.04	0.00	6.56	0.09	0.35	51.87	0.01	0.01	0.00	99.62	93.4	-	47.3	-	-
gnt	44	46.20	4	0.01	41.91	0.11	22.07	2.42	0.02	8.36	0.38	0.01	20.45	4.61	0.03	0.00	100.39	81.3	82.7	6.9	G9	91.1
cpx	44	-	4	0.02	54.55	0.06	2.15	1.07	0.03	2.32	0.09	0.05	16.58	20.84	1.71	0.01	99.45	92.7	-	25.0	-	-

Table 3.1 cont.

Min.	Xeno. #	Weight (mg)	Pipe #	P_2O_5	SiO_2	TiO_2	Al_2O_3	Cr_2O_3	V_2O_3	FeO	MnO	NiO	MgO	CaO	Na_2O	K_2O	Total	Mg#	Mg# Ca_corr	Cr#	Gnt Class	Ol Mg# from Gnt
mg-ilm	45.1	120.40	4	0.01	0.12	52.25	0.71	1.68	0.69	31.01	0.28	0.14	13.53	0.03	0.02	0.01	100.47	43.7	-	61.4	-	-
mg-ilm	45.2	58.80	4	0.01	0.09	52.54	0.67	1.34	0.66	30.55	0.27	0.11	13.60	0.05	0.04	0.00	99.94	44.3	-	57.2	-	-
gnt	45.3	42.70	4	0.03	41.13	0.54	22.58	0.22	0.03	11.65	0.33	0.01	19.31	3.75	0.11	0.00	99.70	74.7	-	0.7	G4D	-
mg-ilm	45.4	40.80	4	0.00	0.12	53.31	0.64	1.07	0.64	30.93	0.29	0.12	13.61	0.03	0.03	0.01	100.79	44.0	-	52.8	-	-
mg-ilm	45.5	25.70	4	0.01	0.15	53.50	0.76	1.18	0.74	30.21	0.26	0.13	14.35	0.03	0.04	0.00	101.34	45.8	-	51.2	-	-
mg-ilm	45.6	27.60	4	0.01	0.20	53.94	0.80	1.44	0.76	28.71	0.25	0.14	14.85	0.03	0.05	0.00	101.18	48.0	-	54.7	-	-
mg-ilm	45.7	16.70	4	0.01	0.16	53.25	0.68	1.27	0.67	31.00	0.30	0.13	13.74	0.03	0.03	0.01	101.26	44.1	-	55.7	-	-
gnt	46	156.00	4	0.00	41.79	0.02	19.67	6.09	0.03	7.02	0.42	0.00	22.10	3.38	0.01	0.00	100.52	84.9	85.9	17.2	G10	92.9
gnt	47	12.80	4	0.01	41.83	0.13	22.29	1.96	0.03	8.52	0.38	0.00	20.65	4.30	0.04	0.11	100.25	81.2	82.5	5.6	G9	90.7
cpx	47	-	4	0.01	54.68	0.08	2.58	1.06	0.05	2.38	0.08	0.05	16.17	20.18	1.99	0.00	99.31	92.4	-	21.7	-	-
gnt	48.1	66.20	4	0.02	41.43	0.30	18.43	6.87	0.04	6.28	0.36	0.01	21.26	5.16	0.06	0.00	100.21	85.8	87.4	20.0	G9	93.4
spinel	48.2	55.70	4	0.01	0.25	0.14	51.73	13.17	0.06	14.50	0.15	0.39	20.08	0.00	0.01	0.00	100.50	71.2	-	14.6	-	-
mg-ilm	48.3	43.60	4	0.00	0.11	53.11	0.68	1.16	0.68	31.27	0.28	0.11	13.66	0.03	0.05	0.00	101.15	43.8	-	53.3	-	-
mg-ilm	48.4	30.90	4	0.01	0.07	53.73	0.75	1.29	0.72	29.80	0.26	0.13	14.40	0.03	0.05	0.00	101.23	46.3	-	53.5	-	-
mg-ilm	48.5	16.20	4	0.00	0.22	53.13	0.68	1.26	0.70	30.37	0.30	0.12	14.15	0.03	0.04	0.00	101.01	45.4	-	55.5	-	-
gnt	49	26.00	4	0.02	41.00	0.39	22.29	0.12	0.07	11.54	0.38	0.01	17.13	7.00	0.07	0.00	100.02	72.5	-	0.4	G3D	-
gnt	50	101.80	4	0.08	40.49	0.11	15.84	10.33	0.05	6.51	0.42	0.01	21.01	4.61	0.06	0.00	99.50	85.2	86.6	30.4	G10D	93.1
gnt	51.1	42.40	2	0.02	41.55	0.24	20.49	4.34	0.03	8.98	0.46	0.01	19.53	5.25	0.05	0.00	100.96	79.5	81.1	12.4	G9	90.4
cpx	51.1	-	2	0.02	54.52	0.15	1.65	1.52	0.04	2.47	0.10	0.05	16.54	20.47	1.54	0.01	99.07	92.3	-	38.2	-	-
gnt	51.2	41.10	2	0.01	40.98	0.10	18.43	7.12	0.05	7.18	0.43	0.00	19.41	6.17	0.03	0.00	99.91	82.8	84.7	20.6	G9	92.0
opx	51.2	-	2	0.00	57.16	0.01	0.51	0.33	0.01	4.60	0.12	0.10	35.63	0.39	0.07	0.00	98.94	93.2	-	30.0	-	-
olv	51.2	-	2	0.01	40.46	0.00	0.01	0.02	0.00	7.82	0.10	0.36	50.62	0.02	0.01	0.00	99.44	92.0	-	62.9	-	-
gnt	51.3	23.10	2	0.02	42.04	0.25	22.78	1.39	0.02	8.57	0.35	0.01	20.93	4.27	0.05	0.00	100.67	81.3	82.6	3.9	G9	90.8
cpx	51.3	-	2	0.01	54.61	0.18	2.48	0.71	0.05	2.38	0.08	0.05	16.31	20.22	1.79	0.01	98.88	92.4	-	16.2	-	-
gnt	51.4	5.10	2	0.03	42.15	0.35	22.79	1.16	0.03	9.15	0.36	0.00	20.47	4.32	0.08	0.00	100.91	79.9	81.3	3.3	G9	90.3
cpx	51.4	-	2	0.02	54.69	0.33	3.17	0.70	0.05	2.72	0.08	0.05	15.80	19.77	2.40	0.01	99.79	91.2	-	13.0	-	-

Grütter *et al.* (2004) showed that lherzolitic garnet grains plotting close to the G10/G9 divide are typically associated with cool cratonic lithospheric mantle (G9A field), whereas garnets removed towards the Ca rich side are characteristic of off-craton or sources tapping graphite-facies mantle (G9B field). This relationship has been shown (at constant Cr content) to be a function of temperature and pressure. The Ca content of garnets decreases with increasing pressure, although, the influence reduces strongly at higher pressures. However, there is a strong linear dependence on temperature, with the Ca content of the garnet decreasing with increasing temperature (i.e. Brey and Köhler 1990; Brenker and Brey 1997). The majority (37) of the lherzolitic garnets from Renard plot in the on-craton G9A field (Fig. 3.2a).

The Mg# of lherzolitic garnets ranges from 73.9 to 85.8 (mean Mg# of 82.5; $Mg\#_{Ca\_corr}$ of 84.3), harzburgitic garnets are more magnesian and range in Mg# from 83.6 to 89.7 (mean Mg# of 85.8; $Mg\#_{Ca\_corr}$ of 86.8). This is typical of worldwide peridotitic garnet diamond inclusions (Stachel and Harris, 2008) (Fig. 3.2b). $Mg\#_{Ca\text{-}corr}$ of garnet ($Mg\#_{Ca\text{-}corr}$ = Mg# + 2Ca, Ca as cations calculated on a basis of 24 oxygens, following Stachel *et al.*, 2008) is used to account for the effect of CaO on Mg/Fe partitioning between garnet and Mg-Fe silicates (O'Neill and Wood, 1979).

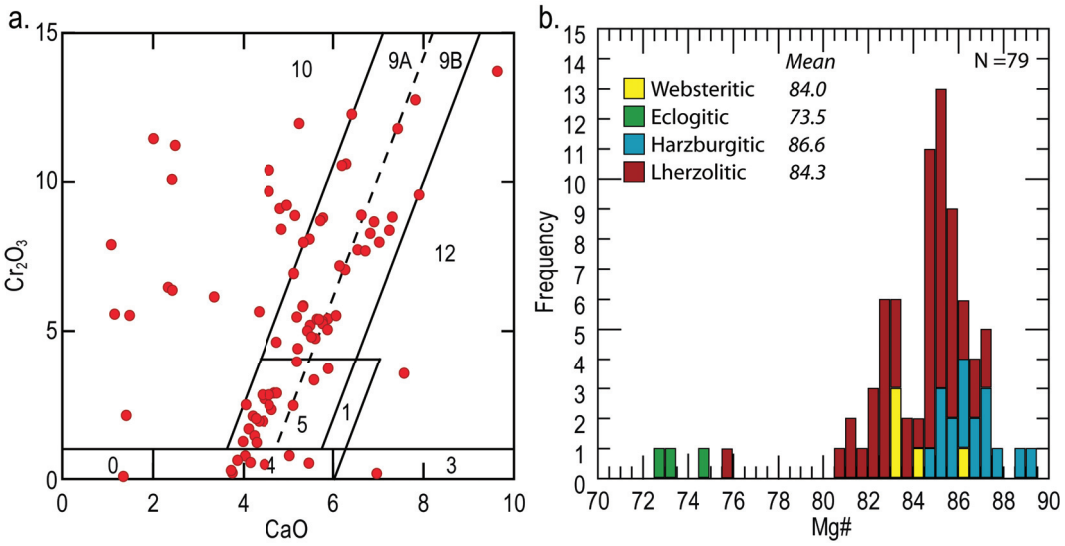

Figure 3.2. 2a. Cr_2O_3–CaO (wt%) garnet classification plot, with compositional fields of Grütter *et al.* (2004). 2b. Histogram showing molar garnet $Mg\#_{Ca\_corr}$. of peridotitic garnets and Mg# of websteritic and eclogitic parageneses.

The MgO contents (17.1, 19.1 and 19.3wt%) of the eclogitic garnets place them in the high magnesium eclogitic field. This is similar to reported values of high-Mg eclogite xenoliths from West Africa (Hills and Haggerty, 1989), the Slave craton (Aulbach *et al.*, 2003; Schmidberger *et al.*, 2007; Smart *et al.*, 2009), and West Greenland (Tappe *et al.*, 2009) (Table 3.1).

The four websteritic G4 garnets are compositionally similar to websteritic garnets from southern Africa in CaO-MgO-FeO space (Viljoen *et al.*, 2005). These garnets have higher average MgO contents (21.5 compared to 18.5wt%), lower average FeO contents (7.3 compared to 11.9wt%) and higher average Cr_2O_3 contents (0.56 compared to 0.16wt%) than the three eclogitic garnets discussed above.

3.4.1.2. Clinopyroxene

Clinopyroxene was present as two xenocrysts and in 47 microxenoliths. Based on microprobe analyses there is no evidence for compositional zoning, however a number of clinopyroxenes were partially altered. As such, where possible, only the centres of the grains were analysed, and individual analyses which showed evidence of alteration were removed.

Based on their Cr_2O_3 and Al_2O_3 concentrations, two peridotitic clinopyroxenes likely derive from spinel lherzolites and 42 fall into the "on-craton" garnet peridotite field of Ramsay (1992) (Fig. 3.3). The grains are Cr-diopsides with Cr_2O_3 contents ranging from 0.60 to 3.43wt%, with an average value of 1.46wt%, and an Mg# range from 89.6-95.7 (Table 3.1).

The remaining five clinopyroxenes plot in the eclogite, pyroxenite and phenocryst field of Ramsay (1992). Two are misclassified, since the associated garnets are lherzolitic. Of the other three, based on the associated garnets, two are websteritic and one is eclogitic. The websteritic clinopyroxenes have high Mg# of 93.8 and 91.3; the eclogitic has an Mg# of 86.6.

A distinction between eclogitic and peridotitic clinopyroxene can be made based on the Cr#. Using data from inclusions in diamond, eclogitic clinopyroxene

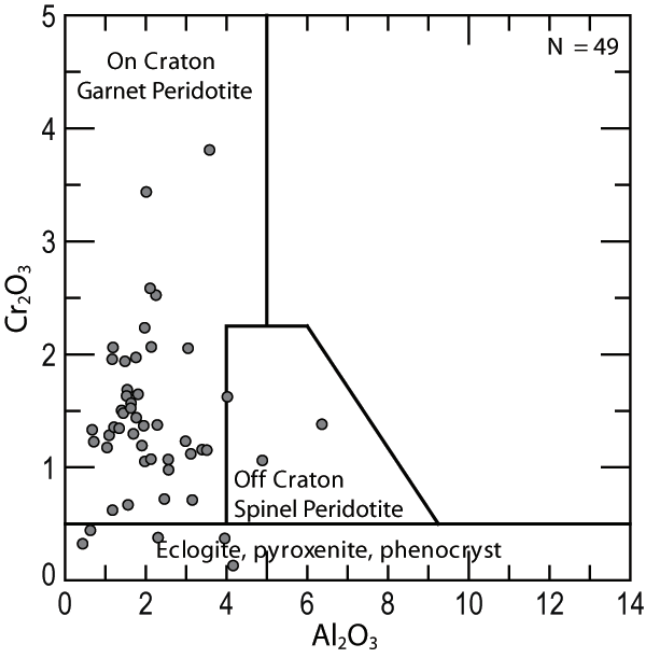

Figure 3.3. Cr_2O_3-Al_2O_3 (wt%) discrimination diagram for clinopyroxene (Ramsay, 1992).

have Cr# below ~7 to 10, peridotitic grains have higher Cr#, whilst websteritic clinopyroxene cover an intermediate range from 0.4-29 (Stachel and Harris, 2008). In our data set, the single eclogitic clinopyroxene analysed has a Cr# of 1.96 and the two websteritic clinopyroxenes have Cr# of 9.68 and 5.77.

3.4.1.3. Olivine

Olivine was analysed in nine lherzolitic and five harzburgitic microxenoliths. The lherzolitic olivines have Mg# from 89.5 to 92.4, with a mean of 91.3. The harzburgitic olivines have Mg# between 92.7 and 93.5, with a mean of 93.2. With such high forsterite (Fo) contents the harzburgitic olivines coincide with the mean composition of harzburgitic olivine inclusions in diamond (e.g. Stachel and Harris, 2008).

3.4.1.4. Orthopyroxene

Thirty-nine orthopyroxenes have been recognised, all of which occur in xenoliths. Two are websteritic and the rest are peridotitic (Table 3.1). Lherzolitic orthopyroxenes have Mg# from 88.1-93.8 (mean 92.6), harzburgitic orthopyroxenes

have Mg# from 93.2-94.3 (mean 93.8). The lherzolitic orthopyroxene grains have CaO contents of 0.1-2.0wt% and Al_2O_3 contents range between 0.4-1.0wt% with the exception of three Al_2O_3 rich grains (2.0, 3.5 and 4.4wt%) (Table 3.1). These fall within the spinel peridotite field of McDonough and Rudnick (1998).

The two websteritic orthopyroxenes have Mg# of 91.9 and 93.1, CaO contents of 1.1 and 0.4wt%, and Al_2O_3 contents of 1.3 and 0.7wt% respectively. This is within the range for the peridotitic samples.

3.4.1.5. Spinel

Nine spinel group minerals were analysed, two as xenocrysts and 7 within xenoliths. Of these, all but one are classified as Mg-chromites, with Mg# between 52.5 and 60.6 (mean 56.8) and Cr# between 68.4 and 90.0 (mean 80.5, Table 3.1). In a plot of Mg# versus Cr# (Fig. 3.4) all Mg-chromites fall in the garnet peridotite field of McDonough and Rudnick (1998). One spinel grain has an Mg# of 71.2 and a Cr# of 14.6 (Table 3.1), and represents a Cr-bearing phenocryst.

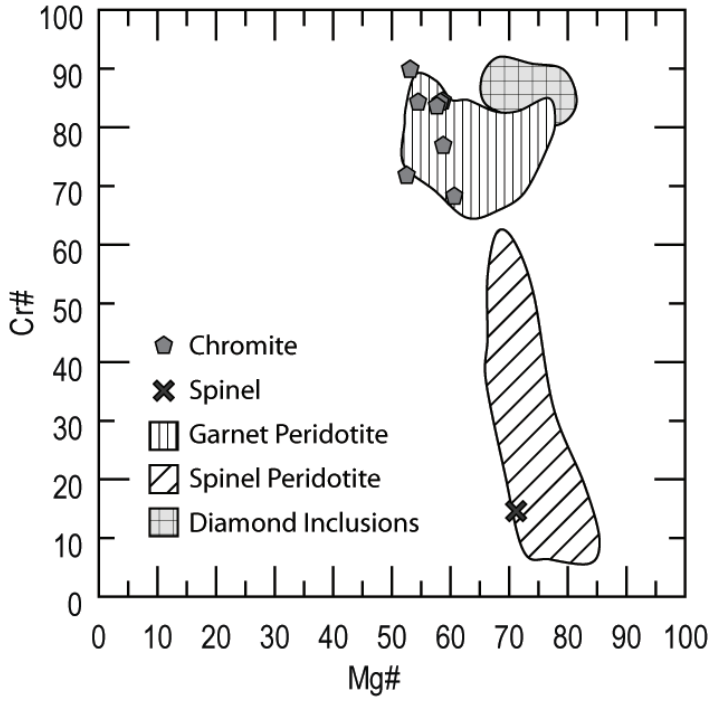

Figure 3.4. A Cr# vs Mg# discrimination diagram for spinel and chromite. Fields of McDonough and Rudnick (1998).

3.4.1.6. Mg-Ilmenite

Eighteen picro-ilmenite grains were identified in the xenocryst sample set. The ilmenites have Mg# between 43.6 and 49.1 (mean 45.7) and TiO_2 contents range between 51.3wt% and 53.9wt% (mean 53.1wt%, Table 3.1). This places the samples within the kimberlite-derived field determined by Wyatt *et al.* (2004). The Cr_2O_3 contents fall between 0.9wt% and 3.8wt% (mean 1.4wt%), again indicative of a kimberlitic origin, with non-kimberlitic ilmenites typically containing <0.5wt% Cr_2O_3 (Wyatt *et al.*, 2004).

3.4.1.7. Other Minerals

Rutile was observed as an accessory mineral in two lherzolite samples, present along veins ad crystal edges. The crystal habit suggests that the minerals are likely secondary. Phlogopite was observed in two other peridotite samples; one lherzolitic and one harzburgitic. The phlogopite has Mg# of 90.9 and 91.8, with corresponding TiO_2 contents of 2.4 and 2.6wt%.

3.5.2. Trace Elements

3.5.2.1. Garnet

3.5.2.1.1. Peridotitic Garnets

Table 3.2 lists the averaged garnet and clinopyroxene trace element data. Chondrite-normalised REE plots for garnets and clinopyroxene are shown in Figures 3.5, 3.6 and 3.7. Chondrite-normalisation ($_N$) uses the values recommended in McDonough and Sun (1995).

Considerable variability is observed in the chondrite normalised trace element patterns of the peridotitic garnets, however, a number of basic patterns types have been identified (Fig. 3.5): Type I, sinusoidal patterns, have steep positive slopes in the $LREE_N$, peaking at Nd_N, followed by negative slopes through the $MREE_N$ to minima at Ho_N or Er_N and positive slopes in the $HREE_N$ to Lu_N (Fig. 3.5a). Type II patterns can be divided into three sub-groups. Type IIa, stepped patterns, have

steep positive slopes in the $LREE_N$ from La_N to Sm_N and flat $MREE_N$ to $HREE_N$ at 5-10 times chondritic values. One sample has $MREE_N$ and $HREE_N$ at 25 times chondritic abundance (Fig. 3.5b). Type IIb represents humped patterns, with steep positive slopes through the $LREE_N$ from La_N to Sm_N, flat patterns from Sm_N to Gd_N, a negative slope down to Tb_N, and flat to slightly positive slopes from Tb_N to Lu_N (Fig. 3.5c). Type IIc patterns, again, have steep positive slopes through the $LREE_N$ from La_N to Sm_N, then negative slopes down to Ho_N followed by positive slopes up to Lu_N. The resulting REE_N patterns are sinusoidal (Fig. 3.5d). Type III sloped patterns have steeply positive slopes from Ce_N to Ho_N, with approximately flat patterns from Ho_N to Lu_N (Fig. 3.5e). For the majority of Type III samples La_N/Ce_N is greater than unity. Type IV patterns show a slight positive slope from La_N to Ce_N with a negative slope to Dy_N and then a positive slope up to Lu_N (Fig. 3.5f), resulting in a weakly sinusoidal shape. One sample has a flat Type V pattern at ~4 times chondritic values (Fig. 3.5g). Five samples have incomplete (several REE below detection) or irregular/spiky patterns. These are grouped as Type VI – unclassified (figs. 3.5h).

3.5.2.1.2. Eclogitic and websteritic garnets

The two analysed eclogitic garnets have "normal" REE_N patterns (Fig. 3.6a) commonly observed for eclogitic garnets worldwide (e.g. Stachel *et al.*, 2004). $LREE_N$ are depleted with Ce_N concentrations at ~0.1 chondritic, with an upward sloped pattern to enriched $HREE_N$ (Lu_N = ~50) (Fig. 3.6a).

The websteritic garnets have a variety of REE_N patterns ranging from "normal" to humped (Fig. 3.6b). Sample 27.1 has a similar pattern to the eclogitic garnets; depleted in $LREE_N$, and an upward sloped pattern to enriched $HREE_N$. Samples 26.1 and 29 have chondrite-normalised patterns similar to the Type III peridotitic garnets with a steep positive slope from Ce_N to Sm_N, and fairly flat positive slopes in the $MREE_N$- $HREE_N$. . Garnet 9.3 has a humped pattern similar to that observed in the Type II peridotitic garnets. The garnet has a steep positive slope through the $LREE_N$ from Ce_N to Sm_N, a slightly positive pattern from Sm_N to Tb_N with a slight negative to flat slope from Tb_N to Lu_N.

Table 3.2. Trace element data of the Renard microxenoliths and xenocrysts. Temperature determined from Ni content of garnet, using Canil (1999), pressure inferred by projecting the Ni temperature onto a determined 38mW/m^2 geotherm.

Xeno#	Min.	Ni	Zn	Y	Zr	La	Ce	Pr	Nd	Sm	Eu	Gd	Tb	Dy	Ho	Er	Tm	Yb	Lu	Temp	Pres	$^{206}/^{204}$Pb	2σ	$^{207}/^{204}$Pb	2σ
1b.1	gnt	28.44	13.99	39.45	23.90	-	-	-	0.16	0.44	0.34	2.38	0.62	5.83	1.46	4.70	0.74	5.14	0.82	952.6	44.5	-	-	-	-
1b.1	cpx	302.12	21.11	6.35	37.52	0.37	1.44	0.47	3.99	2.23	0.78	2.89	0.37	1.83	0.26	0.48	0.05	0.22	0.03	-	-	-	-	-	-
1b.2	gnt	47.70	13.79	35.30	49.88	0.07	0.06	0.05	0.60	0.96	0.50	2.66	0.69	6.00	1.41	4.62	0.68	5.00	0.79	1028.9	50.0	-	-	-	-
1b.2	cpx	248.39	14.88	5.46	42.64	1.34	5.83	1.54	10.83	3.20	0.98	2.97	0.34	1.69	0.24	0.44	0.05	0.23	0.03	-	-	14.49	0.173	14.83	0.154
2b.1	gnt	22.89	9.39	12.38	21.59	-	0.07	0.07	1.23	1.15	0.48	1.92	0.33	2.28	0.49	1.42	0.23	1.64	0.28	916.9	41.9	-	-	-	-
2b.2	gnt	41.06	14.40	17.67	3.48	-	0.05	0.01	0.11	-	0.11	0.81	0.24	2.32	0.64	2.06	0.31	2.13	0.30	-	-	-	-	-	-
2b.2	cpx	409.41	24.85	2.21	1.60	7.65	7.64	0.63	1.97	0.46	0.19	0.74	0.11	0.56	0.09	0.18	0.02	0.08	0.01	-	-	17.50	0.124	15.28	0.116
1	gnt	25.24	13.59	15.28	20.16	0.37	1.54	0.47	3.56	1.50	0.52	1.96	0.36	2.51	0.54	1.66	0.26	1.94	0.32	-	-	-	-	-	-
1	cpx	252.76	19.98	0.80	4.02	18.71	32.31	4.36	16.08	1.66	0.33	0.78	0.06	0.24	0.03	0.07	0.01	0.05	0.01	-	-	18.21	0.085	15.30	0.079
2.1	gnt	21.81	9.28	4.06	9.46	0.35	2.40	0.66	4.51	1.48	0.47	1.41	0.18	0.95	0.16	0.38	0.06	0.48	0.08	909.0	41.4	-	-	-	-
2.1	cpx	215.47	13.98	0.51	3.04	38.43	60.14	7.36	26.77	2.83	0.55	1.07	0.08	0.27	0.02	-	-	-	-	-	-	-	-	-	-
2.2	gnt	22.26	8.92	1.37	18.30	2.96	11.13	2.51	13.64	2.74	0.69	1.58	0.13	0.46	-	0.12	-	0.19	0.05	912.2	41.6	-	-	-	-
3.1	gnt	28.52	10.14	0.40	0.65	0.16	0.51	0.09	0.32	-	-	0.09	-	-	-	0.04	0.03	0.35	0.08	1000.1	47.8	-	-	-	-
3.2	gnt	37.05	8.32	1.70	2.88	1.06	7.02	1.02	3.76	0.50	0.11	0.35	0.05	0.29	0.06	0.21	0.04	0.43	0.10	-	-	-	-	-	-
4.1	gnt	26.40	8.21	0.84	2.82	0.16	1.12	0.39	2.89	0.52	0.13	0.34	0.03	0.18	0.03	0.12	0.02	0.22	0.05	940.4	43.5	-	-	-	-
4.2	gnt	33.13	7.07	0.68	3.87	0.04	0.29	0.13	1.46	0.61	0.13	0.29	0.03	0.15	0.03	0.10	0.03	0.54	0.18	979.8	46.3	-	-	-	-
5	gnt	28.17	8.81	14.79	5.85	0.36	0.31	0.07	0.53	0.52	0.25	1.66	0.33	2.35	0.57	2.05	0.30	1.81	0.24	-	-	-	-	-	-
5	gnt	19.95	12.71	20.02	14.09	-	0.03	-	0.17	0.32	0.24	1.73	0.41	3.23	0.76	2.25	0.35	2.16	0.35	-	-	-	-	-	-
5	cpx	310.91	17.46	0.28	0.10	0.48	0.70	0.12	0.62	-	0.08	0.21	0.02	0.08	0.02	-	0.02	-	0.01	-	-	-	-	-	-
6	gnt	27.62	11.11	13.35	6.44	-	0.08	-	0.32	0.38	0.15	0.98	0.23	1.98	0.48	1.64	0.25	1.80	0.30	948.1	44.1	-	-	-	-
6	cpx	248.92	15.77	1.01	1.54	0.28	0.90	0.28	1.93	0.48	0.17	0.43	0.05	0.30	0.04	0.11	0.01	0.12	0.01	-	-	-	-	-	-
7.1	gnt	35.83	8.72	2.03	2.05	0.60	2.85	0.42	2.14	0.32	0.09	0.29	0.04	0.31	0.07	0.28	0.06	0.44	0.09	993.9	47.3	-	-	-	-
7.2	gnt	36.52	8.96	6.68	40.02	0.23	1.90	0.72	5.52	1.33	0.42	1.37	0.20	1.30	0.26	0.74	0.11	0.82	0.17	997.4	47.6	-	-	-	-
7.3	gnt	42.04	10.97	4.55	16.74	0.16	1.47	0.62	4.64	1.12	0.36	1.40	0.23	1.20	0.18	0.36	0.06	0.30	0.06	1023.9	49.6	-	-	-	-
7.4	gnt	31.82	8.46	0.45	2.54	0.10	1.54	0.19	1.09	-	0.06	0.16	0.03	-	0.02	-	-	0.13	-	972.6	45.8	-	-	-	-
7.4	cpx	249.43	17.55	0.23	3.74	36.28	77.05	9.83	31.33	2.16	0.38	0.89	0.05	-	0.02	0.03	0.00	-	0.01	-	-	-	-	-	-
7.5	gnt	24.51	11.37	1.22	2.13	0.27	0.82	0.14	0.72	-	-	0.23	0.04	-	0.06	0.17	-	0.28	0.06	928.1	42.7	-	-	-	-
7.6	gnt	23.46	10.70	2.99	13.15	0.65	2.61	0.53	3.32	0.69	0.20	0.53	0.08	0.46	0.11	0.35	0.07	0.48	0.14	920.9	42.2	-	-	-	-
7.7	gnt	58.06	19.90	74.75	103.12	0.08	0.14	0.10	1.30	2.13	1.10	7.02	1.53	12.95	3.01	8.70	1.35	10.08	1.48	1088.9	54.9	-	-	-	-
7.7	cpx	332.87	19.19	3.68	8.37	4.75	11.22	1.83	9.48	2.69	0.66	2.42	0.26	1.13	0.14	0.25	0.04	0.15	0.02	-	-	-	-	-	-
7.8	gnt	23.27	9.26	5.35	14.26	0.03	0.24	0.16	1.79	0.96	0.28	1.13	0.13	1.01	0.18	0.68	0.09	0.93	0.12	919.6	42.1	-	-	-	-

Table 3.2. cont.

Xeno#	Min.	Ni	Zn	Y	Zr	La	Ce	Pr	Nd	Sm	Eu	Gd	Tb	Dy	Ho	Er	Tm	Yb	Lu	Temp	Pres	$^{206}/^{204}Pb$	2σ	$^{207}/^{204}Pb$	2σ
7.9	gnt	56.33	21.42	5.47	17.21	0.35	3.54	1.16	8.98	2.86	0.63	1.46	0.15	1.01	0.19	0.63	0.12	1.21	0.24	1082.5	54.2	-	-	-	-
9.1	gnt	75.53	16.81	19.04	43.99	0.06	0.32	0.13	1.19	0.94	0.40	1.85	0.33	3.09	0.72	2.25	0.35	2.98	0.41	-	-	-	-	-	-
9.2	gnt	40.89	14.31	26.20	44.27	0.02	0.11	0.07	0.56	0.61	0.30	1.91	0.44	3.99	0.97	2.96	0.45	3.26	0.50	-	-	-	-	-	-
9.3	gnt	41.34	15.13	5.60	26.31	-	0.12	0.07	0.78	0.44	0.25	1.06	0.21	1.08	0.22	0.62	0.08	0.42	0.05	-	-	-	-	-	-
10.1	gnt	28.63	11.06	5.45	2.86	0.55	1.20	0.25	1.11	0.54	0.12	0.69	0.12	0.98	0.20	0.65	0.10	0.95	0.16	-	-	-	-	-	-
10.1	cpx	274.30	18.97	0.18	0.33	4.58	5.72	0.55	1.68	0.32	0.06	0.16	-	-	0.03	0.05	-	-	0.01	-	-	17.80	0.165	15.32	0.189
10.2	gnt	32.32	10.39	8.05	16.47	0.09	0.59	0.23	2.13	0.90	0.31	1.19	0.20	1.44	0.30	0.81	0.15	1.04	0.19	975.4	45.9	-	-	-	-
10.2	cpx	224.78	15.52	0.63	3.98	5.64	14.68	2.58	10.40	0.99	0.17	0.61	0.05	0.20	0.03	-	-	0.04	-	-	-	-	-	-	-
11.1	gnt	28.48	10.96	10.80	8.77	-	0.06	-	0.35	0.62	0.20	0.83	0.19	1.84	0.40	1.30	0.21	1.48	0.22	952.7	44.5	-	-	-	-
11.1	cpx	273.07	17.06	0.60	1.18	0.79	1.69	0.30	1.30	0.29	0.14	0.28	0.05	0.22	0.01	-	0.01	0.03	-	-	-	-	-	-	-
11.2	gnt	25.26	12.67	14.49	15.15	0.11	0.46	0.14	1.07	0.97	0.36	1.11	0.32	2.47	0.55	1.52	0.24	1.68	0.26	933.1	43.0	-	-	-	-
11.2	cpx	257.67	17.40	0.94	2.67	13.17	19.79	2.34	8.44	1.12	0.28	0.71	0.07	0.33	0.05	-	0.01	0.08	-	-	-	-	-	-	-
12.1	gnt	32.45	12.11	1.98	27.54	0.35	2.22	0.61	3.79	0.71	0.17	0.33	0.07	0.34	0.08	0.27	0.04	0.25	0.07	976.1	46.0	-	-	-	-
12.2	gnt	59.01	20.83	2.19	1.42	0.34	1.32	0.23	1.24	0.28	0.06	-	0.03	0.29	0.07	0.33	0.06	0.76	0.13	1092.4	55.1	-	-	-	-
12.3	gnt	31.44	11.56	2.30	11.75	0.16	1.14	0.28	2.05	0.53	0.13	0.30	0.06	0.25	0.11	0.25	0.05	0.32	0.08	970.5	45.6	-	-	-	-
13	gnt	18.92	11.54	18.92	13.09	0.20	0.15	0.04	0.34	0.58	0.24	1.59	0.34	3.21	0.71	2.25	0.34	2.44	0.33	887.0	40.0	-	-	-	-
13	cpx	193.67	15.92	1.90	4.25	1.60	3.68	0.72	4.24	1.17	0.39	1.04	0.13	0.60	0.08	0.16	0.02	0.08	0.01	-	-	-	-	-	-
14.1	gnt	25.68	9.47	10.37	3.36	0.04	0.10	0.04	0.32	-	0.14	0.68	0.14	1.52	0.32	1.45	0.21	1.49	0.23	935.8	43.3	-	-	-	-
14.1	cpx	249.68	15.61	0.70	0.66	1.49	3.12	0.51	2.18	0.40	0.08	0.25	0.05	0.18	0.03	0.08	-	0.07	0.01	-	-	-	-	-	-
14.2	gnt	28.66	9.93	10.89	3.71	0.12	0.12	0.05	0.28	0.56	0.13	0.73	0.17	1.51	0.41	1.33	0.23	1.58	0.28	954.3	44.6	-	-	-	-
14.2	cpx	246.70	15.48	1.29	4.39	5.37	9.80	1.52	6.47	1.15	0.25	0.68	0.07	0.44	0.07	0.11	0.02	0.12	-	-	-	16.38	0.163	15.00	0.122
15.1	gnt	42.61	16.97	25.68	43.92	0.19	1.07	0.38	3.71	2.49	1.00	3.65	0.66	4.75	1.03	3.02	0.46	3.60	0.59	1026.4	49.7	-	-	-	-
15.1	cpx	270.64	17.01	1.38	8.70	14.14	30.27	4.31	17.37	2.47	0.59	1.32	0.12	0.40	0.06	0.12	0.02	0.09	0.03	-	-	-	-	-	-
16.1	cpx	8591.39	405.95	3.17	3.06	1.70	1.45	0.09	0.35	-	0.08	1.99	0.04	2.31	0.08	0.78	0.05	1.68	1.21	-	-	-	-	-	-
16.2	gnt	27.14	10.16	9.53	0.27	0.80	0.38	0.05	0.31	-	0.08	0.27	0.12	1.21	0.35	1.10	0.21	1.29	0.22	945.1	44.0	-	-	-	-
16.2	cpx	330.72	18.60	0.22	0.11	0.39	0.64	0.08	0.27	-	0.04	0.24	-	0.07	-	-	-	-	-	-	-	-	-	-	-
16.3	gnt	26.88	10.76	10.93	13.31	0.06	0.32	0.10	0.72	-	0.17	1.14	0.18	1.85	0.37	1.29	0.21	1.47	0.28	943.5	43.8	-	-	-	-
16.3	cpx	253.20	19.33	0.79	3.11	8.02	11.75	1.38	5.46	0.76	0.28	0.46	0.06	0.19	0.02	-	-	-	-	-	-	18.03	0.119	15.45	0.125
17	gnt	78.90	15.83	26.35	64.84	0.03	0.26	0.07	0.98	0.92	0.53	2.49	0.54	4.50	1.05	3.08	0.45	3.29	0.52	-	-	-	-	-	-
18.1	cpx	206.18	11.60	0.22	1.76	1.68	2.51	0.37	1.65	0.26	0.06	0.20	0.02	0.07	0.01	-	-	0.01	0.02	-	-	-	-	-	-
18.2	cpx	378.89	27.38	1.92	1.97	1.60	4.56	0.82	4.33	0.98	0.29	0.79	0.09	0.55	0.10	0.14	-	0.13	0.01	-	-	-	-	-	-
19	cpx	317.41	19.76	0.36	0.25	2.36	2.82	0.29	1.05	-	0.09	0.27	0.02	0.10	0.03	-	-	0.09	-	-	-	16.92	0.352	15.37	0.288

Table 3.2. cont.

Xeno#	Min.	Ni	Zn	Y	Zr	La	Ce	Pr	Nd	Sm	Eu	Gd	Tb	Dy	Ho	Er	Tm	Yb	Lu	Temp	Pres	$^{206}/^{204}$Pb	2σ	$^{207}/^{204}$Pb	2σ
20	gnt	21.01	10.31	11.37	16.55	-	-	0.04	0.83	0.87	0.33	1.52	0.27	2.08	0.45	1.45	0.23	1.73	0.30	903.0	41.0	-	-	-	-
23	gnt	24.65	13.08	38.55	51.25	-	0.04	0.04	0.63	1.00	0.56	3.11	0.71	6.20	1.48	4.76	0.74	5.06	0.81	928.9	42.8	-	-	-	-
23	cpx	230.66	18.72	6.50	52.58	1.65	6.58	1.89	13.50	4.11	1.20	3.73	0.42	2.02	0.28	0.53	0.05	0.25	0.03	-	-	15.72	0.213	14.79	0.158
24	cpx	167.40	14.81	2.09	10.94	0.50	1.00	0.20	1.41	0.72	0.30	1.13	0.14	0.62	0.08	0.15	0.02	0.08	0.01	-	-	-	-	-	-
25.1	gnt	23.65	12.27	13.00	6.49	-	0.16	0.04	0.39	-	0.16	0.84	0.21	1.83	0.50	1.58	0.26	2.01	0.31	919.7	42.1	-	-	-	-
25.1	cpx	228.93	20.24	1.35	3.13	13.84	19.75	2.27	7.89	1.05	0.27	0.76	0.07	0.36	0.06	0.11	0.02	0.08	0.01	-	-	18.17	0.100	15.50	0.132
25.2	cpx	211.93	18.99	1.14	4.17	19.43	27.83	3.29	11.74	1.42	0.32	0.86	0.07	0.31	0.05	0.09	0.01	0.06	0.01	-	-	18.79	0.069	15.62	0.069
26.1	gnt	43.67	19.70	17.41	34.37	-	0.15	0.07	0.83	0.76	0.41	1.78	0.37	2.97	0.67	2.06	0.31	2.21	0.34	-	-	-	-	-	-
26.2	gnt	21.63	35.64	32.80	11.04	0.01	0.02	0.01	0.05	-	0.10	1.09	0.35	4.20	1.25	4.67	0.88	6.79	1.17	-	-	-	-	-	-
26.3	gnt	45.31	13.60	0.63	4.21	0.09	1.12	0.60	6.09	1.14	0.24	0.52	0.04	0.15	0.03	0.08	0.04	0.43	0.17	1038.4	50.5	-	-	-	-
26.4	gnt	33.06	10.36	9.08	15.11	0.09	0.69	0.23	2.24	1.06	0.29	1.44	0.24	1.71	0.34	1.06	0.17	1.23	0.20	979.4	46.2	-	-	-	-
26.5	gnt	41.28	12.15	5.74	11.32	0.14	1.22	0.39	3.34	1.10	0.33	1.06	0.13	0.95	0.22	0.72	0.11	0.89	0.21	1020.4	49.3	-	-	-	-
27.1	gnt	85.83	15.43	38.76	16.42	0.06	0.16	0.04	0.49	0.55	0.24	1.21	0.42	4.37	1.41	5.76	1.06	8.73	1.58	-	-	-	-	-	-
27.2	gnt	19.27	12.63	37.91	41.94	-	0.07	0.05	0.82	1.39	0.67	3.63	0.84	6.45	1.58	4.52	0.70	5.08	0.79	-	-	-	-	-	-
28.1	gnt	90.54	46.16	18.43	5.41	0.15	0.23	0.14	0.86	1.15	0.20	0.94	0.22	2.91	0.77	2.67	0.40	3.22	0.60	-	-	-	-	-	-
28.1	cpx	4424.70	408.24	2.16	8.81	16.72	21.02	2.26	8.94	3.22	0.57	1.69	0.18	1.05	0.23	0.49	0.19	0.74	0.27	-	-	-	-	-	-
28.2	gnt	69.59	27.07	1.87	2.57	0.21	1.02	0.27	1.18	0.73	0.20	0.70	0.09	0.48	0.13	0.39	0.15	0.92	0.22	1128.3	58.4	-	-	-	-
28.3	gnt	131.39	54.77	6.77	122.58	5.32	32.54	7.63	47.33	12.24	2.30	5.88	0.65	2.13	0.36	0.68	0.17	1.62	0.28	1286.7	-	-	-	-	-
29	gnt	31.14	19.22	25.90	30.98	-	0.19	0.08	0.99	1.13	0.49	2.45	0.49	3.92	0.95	3.06	0.48	3.30	0.53	-	-	-	-	-	-
29	cpx	236.57	23.65	5.17	27.94	13.91	25.69	3.93	20.24	5.04	1.23	3.25	0.32	1.50	0.21	0.43	0.04	0.23	0.02	-	-	-	-	-	-
30	gnt	30.12	11.16	17.24	7.45	0.14	0.18	0.04	0.25	0.40	0.21	1.34	0.30	2.71	0.75	2.21	0.37	2.57	0.40	962.8	45.1	-	-	-	-
30	cpx	297.52	18.15	2.44	4.42	6.18	7.08	0.59	2.72	0.89	0.34	1.11	0.13	0.73	0.11	0.21	0.03	0.15	0.03	-	-	-	-	-	-
31	gnt	34.99	9.59	25.54	18.79	0.06	0.06	0.04	0.30	0.46	0.29	1.67	0.44	4.00	1.04	3.35	0.54	4.06	0.67	983.7	46.7	-	-	-	-
31	cpx	331.44	16.53	4.10	29.00	1.25	3.12	0.64	5.08	2.08	0.68	2.25	0.26	1.28	0.18	0.37	0.04	0.21	0.03	-	-	17.98	0.171	15.16	0.151
32	gnt	171.82	47.58	80.75	23.58	0.56	0.82	0.11	0.83	1.22	0.58	5.00	1.03	11.56	3.24	10.10	1.62	12.06	1.84	1348.0	-	-	-	-	-
32	cpx	261.35	18.46	2.88	4.55	2.22	3.46	0.49	2.57	0.88	0.30	1.01	0.15	0.80	0.11	0.20	0.03	0.16	0.03	-	-	-	-	-	-
33.1	gnt	0.58	66.18	1077.21	11.33	0.36	0.36	0.08	0.86	2.88	0.08	18.23	8.38	115.62	42.10	188.40	37.26	300.49	49.29	-	-	-	-	-	-
33.2	gnt	43.83	13.33	0.57	3.23	0.03	0.24	0.11	0.94	0.44	0.07	-	0.03	0.32	0.03	0.11	0.04	0.29	0.07	-	-	-	-	-	-
33.2	gnt	29.48	8.87	22.78	4.56	-	0.06	-	-	0.64	0.19	1.43	0.36	3.02	0.82	2.78	0.40	2.85	0.55	-	-	-	-	-	-
33.2	cpx	247.71	54.28	1.93	2.31	8.89	12.50	1.46	5.20	0.64	0.25	0.78	0.09	0.46	0.07	0.14	0.03	-	0.01	-	-	-	-	-	-
34.1	gnt	73.34	22.98	59.49	28.19	0.14	0.63	0.15	1.50	1.43	0.82	4.32	1.04	9.04	2.27	7.97	1.32	9.43	1.62	1139.9	59.5	-	-	-	-
34.2	gnt	281.06	89.49	13.68	56.21	3.17	13.17	3.24	21.10	5.68	1.47	4.33	0.80	3.24	0.52	1.17	0.41	1.77	0.37	1530.1	-	-	-	-	-
34.2	cpx	255.16	17.12	3.60	18.17	4.24	11.72	2.00	9.80	2.26	0.72	2.16	0.26	1.05	0.16	0.33	0.04	0.17	0.03	-	-	-	-	-	-

Table 3.2. cont.

Xeno#	Min.	Ni	Zn	Y	Zr	La	Ce	Pr	Nd	Sm	Eu	Gd	Tb	Dy	Ho	Er	Tm	Yb	Lu	Temp	Pres	$^{206}/^{204}$Pb	2σ	$^{207}/^{204}$Pb	2σ
35.1	gnt	116.53	55.72	76.63	39.87	0.79	1.39	0.28	2.58	2.44	1.15	5.13	1.40	11.11	2.91	9.14	1.68	11.88	1.88	1254.1	73.3	-	-	-	-
35.1	cpx	261.44	19.61	1.55	6.80	15.09	26.95	3.13	11.19	1.46	0.45	1.00	0.10	0.39	0.06	0.12	0.02	0.12	0.02	-	-	-	-	-	-
35.2	gnt	57.80	12.80	0.72	0.34	0.15	0.24	-	0.13	-	-	-	-	-	-	0.16	0.06	0.67	0.17	1087.9	54.7	-	-	-	-
36.1	gnt	22.09	8.14	5.89	17.45	0.28	2.40	0.51	2.79	0.73	0.21	0.79	0.13	1.02	0.18	0.69	0.09	0.87	0.20	911.2	41.6	-	-	-	-
36.2	gnt	31.53	10.52	8.19	18.22	0.19	1.44	0.44	2.65	0.74	0.26	1.25	0.21	1.57	0.33	1.09	0.18	1.32	0.23	971.0	45.7	-	-	-	-
37.1	gnt	23.16	9.60	15.47	7.36	1.10	-	-	0.31	-	0.16	0.81	0.21	2.00	0.51	1.92	0.32	2.36	0.36	918.8	42.2	-	-	-	-
37.1	cpx	934.35	76.62	1.62	2.55	2.33	2.11	0.25	1.19	0.51	0.18	0.51	0.08	0.43	0.06	0.23	0.02	-	0.03	-	-	-	-	-	-
37.2	gnt	22.53	9.26	0.71	1.98	0.37	1.10	0.17	0.55	-	0.04	0.22	-	-	0.05	0.16	0.03	0.26	0.10	914.4	41.9	-	-	-	-
38	gnt	33.43	9.85	9.15	31.89	0.09	0.76	0.38	4.19	2.94	0.93	3.41	0.32	2.08	0.39	0.97	0.14	0.99	0.16	981.4	46.3	-	-	-	-
39	gnt	25.91	15.51	36.75	10.14	-	-	0.05	0.36	-	0.27	1.96	0.54	5.33	1.36	4.66	0.73	5.30	0.81	937.2	43.3	-	-	-	-
39	cpx	247.22	20.53	5.51	12.17	17.72	30.49	4.02	15.93	2.57	0.74	2.37	0.28	1.48	0.24	0.48	0.04	0.24	0.03	-	-	18.48	0.107	15.46	0.099
40	gnt	30.03	9.84	11.86	16.11	0.28	0.63	0.18	1.43	0.84	0.36	1.67	0.29	2.16	0.45	1.38	0.20	1.48	0.23	960.9	44.8	-	-	-	-
41.1	gnt	23.29	7.82	8.36	10.47	-	0.62	0.12	0.80	0.51	0.27	1.09	0.21	1.34	0.33	0.86	0.16	1.07	0.20	919.8	42.2	-	-	-	-
41.1	cpx	278.38	16.80	0.55	1.13	1.03	3.00	0.79	4.08	0.65	0.22	0.31	0.04	0.14	0.03	-	0.01	0.08	0.01	-	-	17.69	0.261	14.97	0.172
41.2	gnt	23.16	8.36	1.30	3.05	0.84	1.92	0.23	0.89	-	0.05	0.33	-	0.17	0.03	0.18	0.03	0.39	0.06	-	-	-	-	-	-
41.2	cpx	258.60	15.37	0.09	0.99	7.35	5.51	0.34	0.78	-	0.03	0.12	-	0.08	-	-	0.01	-	0.01	-	-	16.72	0.284	15.21	0.167
41.3	cpx	62.64	12.43	6.48	6.59	1.11	3.22	0.46	2.14	0.55	0.18	0.63	0.11	0.99	0.24	0.86	0.17	1.54	0.31	-	-	-	-	-	-
41.4	gnt	91.34	27.15	9.29	42.61	0.10	0.76	0.34	3.94	2.74	0.91	2.97	0.40	2.07	0.33	0.86	0.12	1.13	0.17	-	-	-	-	-	-
41.4	cpx	304.64	19.80	0.33	2.29	2.08	8.98	1.97	12.50	1.97	0.35	0.70	0.04	0.15	0.02	0.06	0.02	0.11	0.02	-	-	-	-	-	-
42.1	gnt	9.76	9.15	2.10	2.40	0.47	0.29	0.04	-	0.35	0.07	0.32	0.04	0.32	0.08	0.21	0.05	0.23	0.05	793.6	34.4	-	-	-	-
42.1	cpx	172.98	11.21	0.34	2.87	0.50	1.08	0.18	0.94	0.47	0.09	0.25	-	0.10	0.03	0.03	0.02	0.03	0.01	-	-	-	-	-	-
42.2	gnt	22.04	7.40	0.67	3.19	0.66	2.53	0.35	1.37	0.35	0.08	0.17	-	0.19	0.05	0.11	-	0.22	0.05	910.9	41.6	-	-	-	-
43.1	gnt	23.44	7.86	1.58	4.61	0.94	4.80	0.95	3.28	-	0.05	0.39	0.04	0.27	0.05	0.23	0.04	0.31	0.07	920.6	42.3	-	-	-	-
43.2	gnt	20.74	8.47	0.28	0.47	0.21	0.94	0.13	0.51	-	-	0.18	0.01	0.09	-	-	-	0.12	0.02	901.2	40.9	-	-	-	-
44	gnt	26.99	12.96	14.24	2.78	-	-	-	-	-	0.09	0.70	0.21	2.04	0.53	1.70	0.26	2.19	0.29	944.1	43.8	-	-	-	-
44	cpx	289.78	19.16	1.89	3.10	16.60	22.72	2.60	8.96	1.32	0.39	0.66	0.13	0.48	0.07	0.18	-	0.13	-	-	-	-	-	-	-
46	gnt	23.51	10.90	2.06	1.73	0.49	1.75	0.30	1.07	-	0.08	0.11	0.02	0.27	0.10	0.34	0.10	1.15	0.28	921.3	42.3	-	-	-	-
47	gnt	31.33	13.02	21.38	5.56	0.08	0.09	0.01	-	-	0.15	1.31	0.30	2.63	0.77	2.79	0.42	3.12	0.53	969.2	45.4	-	-	-	-
47	cpx	296.86	20.31	2.57	2.93	0.82	0.37	0.07	0.40	0.46	0.19	0.86	0.14	0.59	0.12	0.24	0.02	0.16	0.02	-	-	-	-	-	-
48.1	gnt	32.43	10.09	14.81	76.84	0.08	0.47	0.25	2.72	1.95	0.63	2.17	0.33	2.56	0.67	2.04	0.32	2.38	0.39	976.0	45.9	-	-	-	-
49	gnt	65.12	24.21	38.10	23.55	0.04	0.35	0.14	1.38	0.87	0.39	2.03	0.50	5.36	1.51	5.32	0.93	6.66	1.06	-	-	-	-	-	-
50	gnt	30.51	10.81	7.71	52.50	0.62	2.96	0.99	10.23	3.25	0.91	2.84	0.35	1.82	0.30	0.78	0.10	0.83	0.14	962.8	45.1	-	-	-	-

Table 3.2. cont.

Xeno#	Min.	Ni	Zn	Y	Zr	La	Ce	Pr	Nd	Sm	Eu	Gd	Tb	Dy	Ho	Er	Tm	Yb	Lu	Temp	Pres	$^{206}/^{204}$Pb	2σ	$^{207}/^{204}$Pb	2σ
51.1	gnt	23.95	10.89	16.10	16.37	0.09	0.26	0.11	0.63	-	0.30	1.11	0.26	2.41	0.61	1.64	0.26	1.95	0.33	923.7	42.5	-	-	-	-
51.1	cpx	243.73	17.19	1.59	6.35	13.55	19.55	2.34	8.94	1.52	0.35	0.98	0.09	0.48	0.07	0.15	0.02	0.08	-	-	-	18.24	0.060	15.22	0.074
51.2	gnt	24.14	9.18	1.09	1.90	0.23	0.94	0.21	1.13	0.56	0.11	0.32	0.03	0.20	0.05	0.19	0.04	0.46	0.09	925.6	42.6	-	-	-	-
51.3	gnt	29.94	11.83	31.06	16.31	0.02	-	0.01	0.28	0.28	0.25	1.29	0.42	3.96	1.11	3.94	0.66	4.69	0.80	961.9	45.1	-	-	-	-
51.3	cpx	257.89	17.78	4.59	8.21	0.49	0.71	0.15	1.43	0.89	0.41	1.44	0.18	1.04	0.17	0.36	0.04	0.20	-	-	-	-	-	-	-
51.4	gnt	25.94	12.24	24.83	24.49	-	0.04	-	0.40	-	0.28	1.84	0.42	3.51	0.86	2.82	0.44	3.19	0.49	937.5	43.4	-	-	-	-
51.4	cpx	253.08	18.05	4.20	26.32	1.05	3.37	0.84	5.62	1.77	0.55	2.01	0.27	1.20	0.17	0.37	0.04	0.16	0.03	-	-	14.50	0.224	14.66	0.214

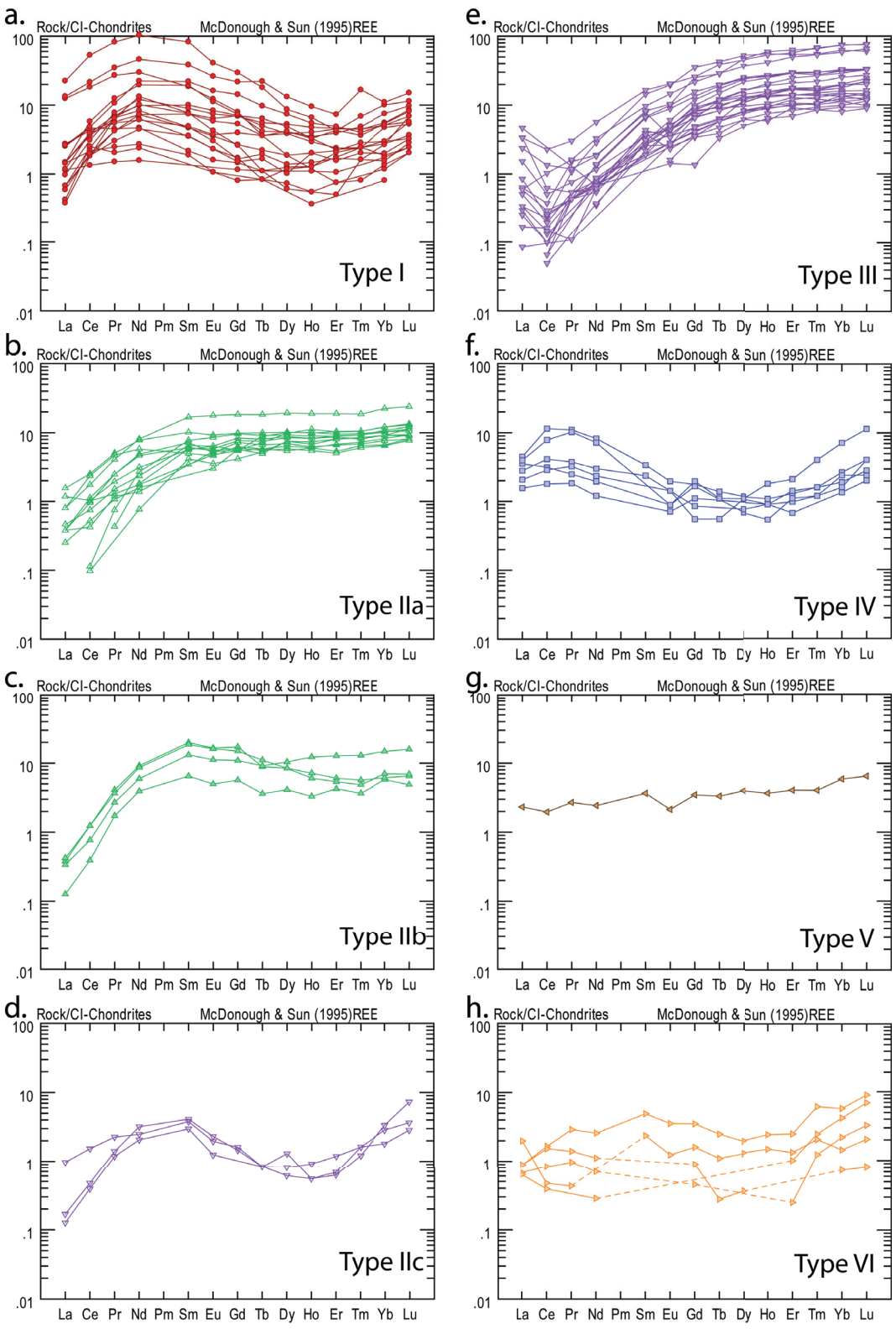

Figure 3.5. Peridotitic garnet chondrite normalised (McDonough and Sun, 1995) REE plots separated into trace element types.

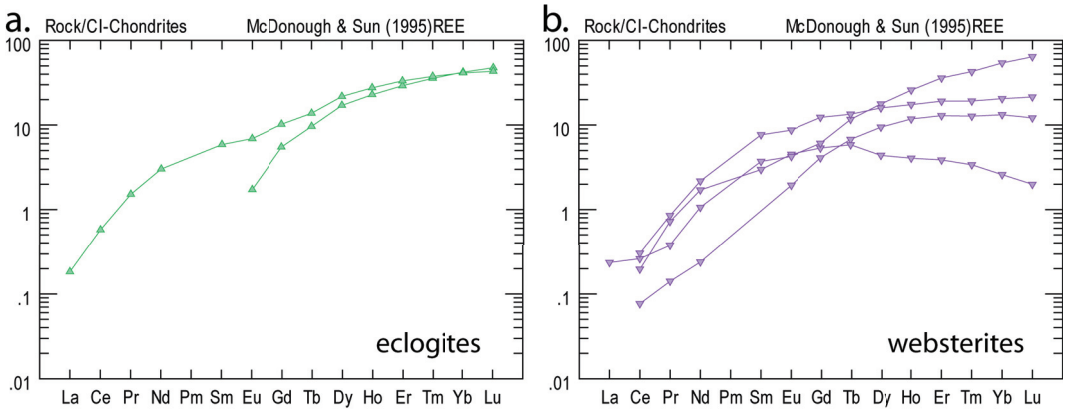

Figure 3.6. Eclogitic and websteritic garnet chondrite normalised (McDonough and Sun, 1995) REE plots.

3.5.2.2. Clinopyroxene

3.5.2.2.1. Peridotitic clinopyroxene

The trace element patterns for the clinopyroxenes (Fig. 3.7) are all $LREE_N$ enriched and $HREE_N$ depleted. The clinopyroxenes can be classified into types A and B. Type A clinopyroxenes are the most enriched in $LREE_N$ with strong negatively sloped patterns down to the $HREE_N$ (Fig. 3.7a). Type B clinopyroxenes are less enriched in $LREE_N$ and less depleted in $HREE_N$ than Type A. A number of clinopyroxenes display humped patterns with maxima at Sm_N (Fig. 3.7b). This pattern only occurs in clinopyroxene associated with Type III garnets. Four clinopyroxenes display spiky and irregular patterns and are not discussed further.

3.5.2.2.2. Websteritic clinopyroxene

Websteritic clinopyroxenes are similar to the Type A peridotitic samples, with $LREE_N$ enrichment and $HREE_N$ depletion (Fig. 3.7c).

3.5.3. Clinopyroxene Pb Isotope Compositions

The measured clinopyroxene Pb isotopic compositions define a large range of values for both $^{206}Pb/^{204}Pb$ (~13.5 - 19) and $^{207}Pb/^{204}Pb$ (~14.5 – 15.5) ratios. No correction for the *in situ* decay of U was applied to these Pb isotope data as the

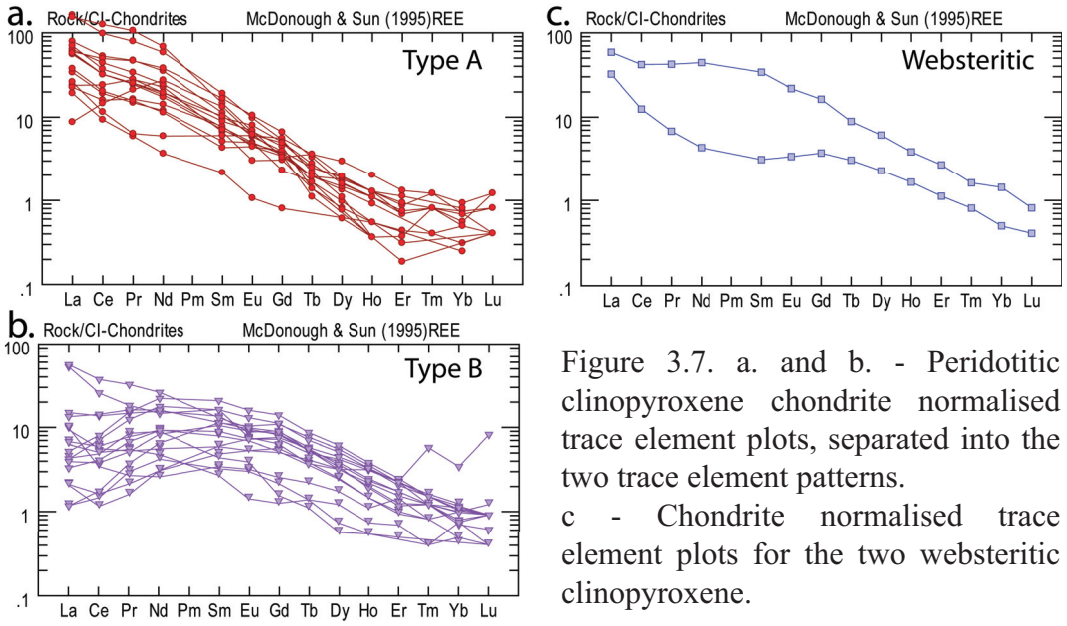

Figure 3.7. a. and b. - Peridotitic clinopyroxene chondrite normalised trace element plots, separated into the two trace element patterns.
c - Chondrite normalised trace element plots for the two websteritic clinopyroxene.

clinopyroxene U/Pb ratio is extremely small (0.01-0.11; mean 0.04), thus the age corrections are smaller than the analytical precision. From Fig. 3.8 it is apparent that two main data clusters exist: the radiogenic Pb isotope cluster ($^{206}Pb/^{204}Pb$ ratios higher than 17.2) contains Type-B clinopyroxenes showing a strong enrichment in Pb (0.35-0.67 ppm; mean 0.48) and depletion in the LREE (Fig. 3.8 inset). In contrast, 'unradiogenic' Type-A clinopyroxenes have very low Pb contents (<0.2ppm) and their REE patterns are typical of clinopyroxenes in equilibrium with Type III garnet.

We note that the 'radiogenic' clinopyroxenes partially overlap (Fig. 3.8) the field for bulk-rock Pb isotope compositions of other Late Neoproterozoic ultramafic alkaline intrusives from northern Quebec and Labrador (Fig. 3.1) (Tappe *et al.*, 2007; 2008). This, in combination with the enriched trace element signatures, suggests a secondary origin for the Pb of the 'radiogenic' Renard clinopyroxenes. The clinopyroxenes may have formed from melts, which could be related to the Late Neoproterozoic kimberlite magmatism at Renard. Alternatively, these clinopyroxenes may have had a primary origin but were overprinted by such kimberlitic melts.

A linear regression through the entire data set yields an apparent isochron age of 2357 (+190-210) Ma. Based on the reasoning above, this must be interpreted as an errorchron, and the age has no geological meaning. Rather, the linear relationship

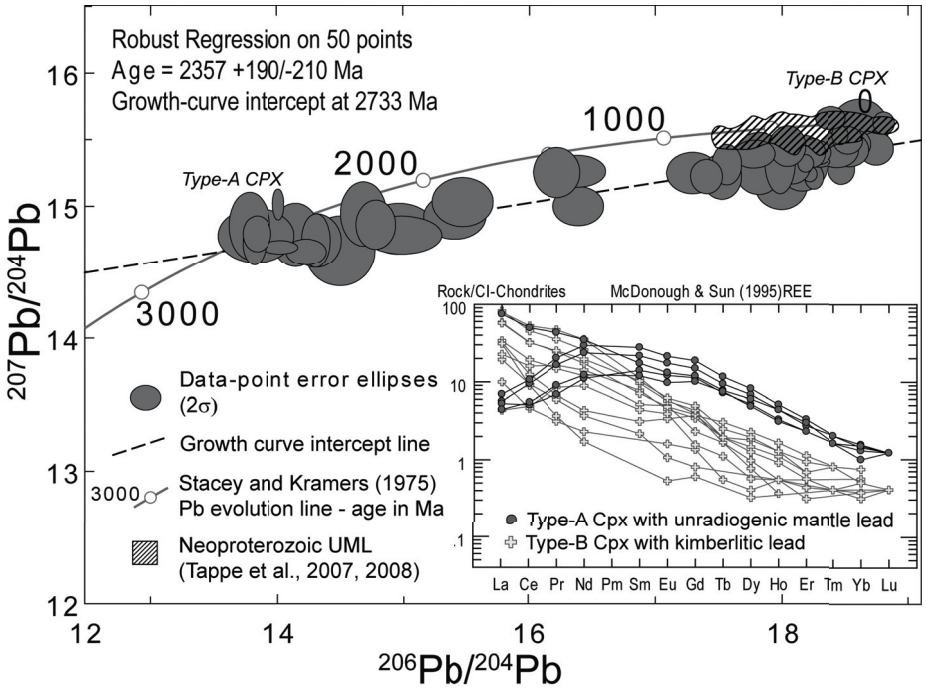

Figure 3.8. Common lead analyses showing both the isochron age and the model age using the Stacey and Kramers (1975) lead evolution age. Torngat and Aillik Bay alkaline magma data (Tappe *et al.*, 2007; Tappe *et al.*, 2008) superimposed on the common lead plot to act as a proxy for the isotopic lead composition of the Renard kimberlites magmas. Inset of chondrite normalised (McDonough and Sun, 1995) trace element patterns for the unradiogenic mantle clinopyroxenes, and those which are more radiogenic due to kimberlitic lead.

in Pb-Pb isotope space suggests mixing between two main sources of common Pb. A mixing origin is strongly indicated by a plot of $^{206}Pb/^{204}Pb$ versus 1/Pb which shows a significant correlation (R^2=0.879). Importantly, clinopyroxenes that fall at the unradiogenic end of the mixing trend intercept the Stacey and Kramers (1975) terrestrial Pb evolution curve at ca. 2733 Ma (Fig. 3.8). This suggests that the unradiogenic Pb analysed in the equilibrated clinopyroxenes originated from a source (protolith or melt) of Late Archean age (see Discussion section).

3.5.4. Geothermobarometry

For thermobarometric calculations, accurate analyses and confirmation of equilibrium conditions between minerals in each sample were established through a number of filters: oxide and cation totals were checked for garnet, olivine,

orthopyroxene and clinopyroxene and only values within narrow limits were accepted (following Nimis and Grütter (2010): oxide totals: 98.5-101.5wt%; cation totals: pyroxene ≥3.990 apfu per 6 oxygens; olivine ≥2.990 apfu per 4 oxygens; garnet compositions were limited to Cr_2O_3 >1wt% or Cr_2O_3<1wt% and $Mg/(Mg+Fe)_{mol}$>0.6). Equilibrium between clinopyroxene-orthopyroxene and pyroxene-garnet within individual microxenoliths was verified following Nimis and Grütter (2010): calculated temperature differences between enstatite in clinopyroxene (Nimis and Taylor, 2000) and Ca in orthopyroxene (Brey and Köhler, 1990) based thermometry, and between enstatite in clinopyroxene (Nimis and Taylor, 2000) and Mg-Fe exchange based thermometry using orthopyroxene-garnet pairs (Nimis and Grütter 2010), were constrained to acceptable limits derived from uncertainties of the calibrations. For application of the single crystal clinopyroxene geothermobarometer of Nimis and Taylor (2000), an additional set of tests was applied to establish: (1) Derivation from the garnet stability field. (2) Overlap with the compositional range for which the thermobarometer was originally calibrated (see Grütter, 2009 for details).

Evidence of major-element disequilibrium within some of the samples was observed: Two samples indicate orthopyroxene disequilibrium, one sample shows disequilibrium between clinopyroxene and garnet, whilst five samples show disequilibrium of clinopyroxene with garnet and orthopyroxene (Fig. D3).

An additional problem encountered in our study is considerable disagreement (8 to 27kbar) between the Cr-in-clinopyroxene barometer (Nimis and Taylor, 2000) and the Al exchange between garnet-orthopyroxene based barometer (Nickel and Green, 1985; Brey and Köhler, 1990). The authors have found that 20 of 28 clinopyroxenes, in which a comparison to other barometers is possible and that pass the pressure temperature filters, plot off the derived geotherm to lower pressures. Grütter (2009) has shown that Cr-in-clinopyroxene barometry may under-estimate pressure for garnet-spinel peridotites, as clinopyroxenes with low modal garnet/spinel have elevated Al-Tschermaks (Grütter, 2009). The elevated Cr/Al ratio of depleted cratonic peridotites increases the stability of spinel deep into the garnet stability field (Webb and Wood, 1986; Klemme, 2004). Five of the samples studied

here contain garnet and spinel, up to a pressure of 50kbar (Fig. 3.9). Therefore, as so many of the data do not contribute to resolving the actual conductive geotherm the authors have chosen not to use the P_{NT} barometry data.

Current single clinopyroxene thermobarometry techniques permit calculation of pressure for garnet-facies grains only (Grütter, 2009). Xenoliths with low modal garnet/spinel have elevated clinopyroxene Al+Cr+Na, which results in pressure estimates that are substantially under-estimated (Grütter, 2009).

After equilibrium was ensured, several thermobarometer combinations were used to calculate the equilibrium P-T conditions of the samples. For rocks in which garnet and orthopyroxene were observed, the Fe-Mg exchange thermometers of Harley (1984) in combination with the Al-in-orthopyroxene barometer of Brey and Köhler (1990) and the Nimis and Grütter (2010) Fe-Mg exchange thermometer in combination with the Al-in-orthopyroxene barometer of Nickel and Green (1985) were utilised. In samples where clinopyroxene is present the thermometers of Taylor (1998) were used in combination with the Nickel and Green (1985) barometer. Finally, as 28 single garnet xenocrysts were present in the sample set, the Ni-in-garnet thermometer of Canil (1999), projected onto the determined geotherm, was employed.

The thermobarometer combinations depict, within error, a "cold" 38mW/m^2 model geotherm (Pollack and Chapman, 1977) at the time of kimberlite emplacement. Maximum pressure of origin reaches 60kbar which corresponds to a depth of ~190km (Fig. 3.9). Similarly, the Cr-in-garnet P^{38} barometer (Grütter *et al.*, 2006) also yields minimum (presence of spinel not established) pressures up to 60kbar. The implied thickness of the lithosphere beneath Renard of ~ 190km at 632Ma agrees well with the results of a regional geophysical study on the present state of the Superior SCLM by Mareschal *et al.* (2000). Combining lithosphere thickness and geothermal gradient indicates a large "diamond window" extending from ca. 130-190km depth during the Late Neoproterozoic.

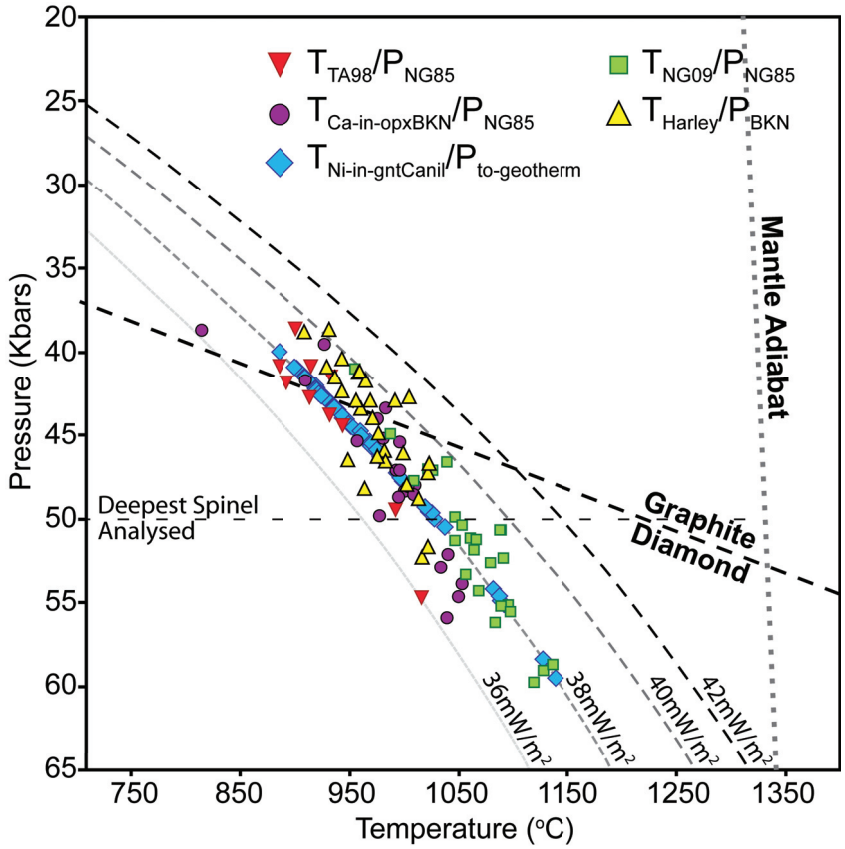

Figure 3.9. Pressure-temperature graph showing the results of five thermobarometer combinations. T_{NT}/P_{NT} – Nimis and Taylor (2000) thermobarometer; $T_{Ca\text{-}in\text{-}opxBKN}$ – Brey and Kohler (1990) thermometer; P_{NG85} – Nickel and Green (1985) barometer; $T_{Ni\text{-}in\text{-}gnt}$ – Canil (1999) thermometer; $P_{to\text{-}geotherm}$ – pressure calculated to the reference 38mW/m^2 geotherm of Pollack and Chapman (1977); T_{TA98} – Taylor (1998) thermometer; T_{NG09} – Nimis and Grütter (2010) thermometer; T_{Harley} – Harley (1984) Thermometer; P_{BKN} – Brey and Kohler (1990) barometer. Reference geotherms by Pollack and Chapman (1977) and terminate in a mantle adiabat with Tp=1300 °C.

3.6. Discussion

3.6.1. Composition of the Eastern Superior SCLM

Based on xenoliths/xenocrysts studied, the lithospheric mantle beneath the Renard kimberlite cluster is composed predominantly of garnet lherzolite. Out of 113 samples only three are eclogitic and four websteritic. Using the Ni-in-Garnet thermometer (Canil, 1999) the peridotitic xenoliths were placed in a "stratigraphic" context. One eclogitic xenolith and two websteritic xenoliths could also be placed

"stratigraphically", using the Ravna (2000) thermometer, as both garnet and unaltered clinopyroxene cores were present. All the temperatures were converted to pressures and depths assuming a 38mW/m^2 reference geotherm (Chapman and Pollack, 1977) determined by thermobarometry (Fig. 3.10).

The kimberlites sampled, predominantly (79%), from a depth of ~130-160km (40-50kbar). One reason for the large proportion of xenoliths/xenocrysts from this depth may be due to a change in the ascent velocity of the kimberlite magma. Brey *et al.* (1991) showed that during ascent, the maximum solubility of CO_2 in a kimberlitic like melt decreases by at least 8wt% between 160 and 130 km depth; the release of large amounts of CO_2 fluid may trigger rapid upward transport of the kimberlitic magma through the overlying lithosphere. Eventually this fluid is likely lost from the ascending kimberlite magma; hence a correlation in depth between preferred xenolith sampling and intense fluid exsolution should exist. From this horizon (~130-160km) the majority (68%) of samples are lherzolitic. With greater depth the abundance of xenoliths decreases whilst the ratio of harzburgitic to lherzolitic samples increases.

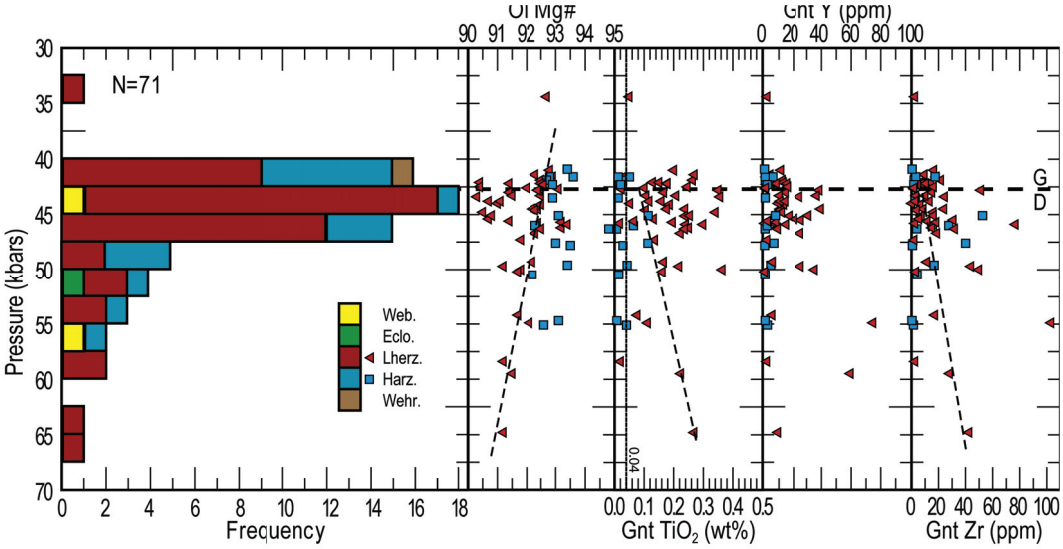

Figure 3.10. Lithospheric "stratigraphy" beneath Renard based on this sample set. Plots show lithology, Ol Mg#, gnt TiO_2, Y and Zr versus pressure. Pressure determined for peridotitic garnets using the $T_{Ni\text{-}in\text{-}gnt}$ (Canil, 1999) projected on to a 38mW/m^2 geotherm and for eclogitic/websteritic garnets using the Krogh-Ravna (2000) thermometer projected onto the geotherm. Garnets below 0.04wt% TiO_2 are assumed to represent truly depleted and least metasomatised compositions (Stachel and Harris, 2008). Dashed lines show trends of Ol Mg#, Gnt TiO_2 and Gnt Zr with depth.

Whilst olivine in equilibrium with harzburgitic garnets generally have higher Fo contents as compared to lherzolitic olivine, due to a significant temperature and Ca# dependence, the Mg# of the garnet is not a particularly useful indicator of bulk Mg# or depletion (O'Neill and Wood, 1979). However, the high modal proportion (60-90%) of olivine in peridotite (e.g. McDonough, 1990; Pearson *et al.*, 2004 and references therein) allows its composition to be used as a measure of enrichment/ depletion. The low abundance of olivine in this sample set means it is not possible to determine the variation, if any, of the Fo_{oliv} content with depth. However, it is possible, using an inversion of the olivine-garnet Mg-Fe exchange geothermometer of O'Niell and Wood (1979) with the garnet composition and $T_{Ni\text{-}in\text{-}gnt}$ (Canil, 1999) to determine the Fo_{oliv} coexisting with the xenocryst garnet. A depth estimate can then be derived by projecting the temperature onto the paleogeotherm (Fig. 3.10).

The $Mg\#_{oliv}$ calculated for 11 microxenoliths agree to within ±0.7% with analysed olivine compositions, one other is observed with a difference of 1.3% ($Mg\#_{oliv}$ 93.4 calculated vs. 94.8 observed). $Mg\#_{oliv}$ inverted from 42 garnet xenocryst compositions fall within the range 91.0 to 94.3, including nine from harzburgitic garnet in the range 93.7 to 94.3. The majority plot in the pressure range of 40-47kbar and show a large spread in Fo_{oliv} content. However, a general decrease in the mean Fo_{oliv} with depth is observed, approaching $Fo_{89\text{-}90}$ towards the base of the lithosphere (Fig. 3.10). This is the composition of olivine expected for asthenospheric peridotites, assuming that their compositions are near that of primitive mantle (McDonough and Sun, 1995). This observed trend is consistent with most other cratonic lithosphere sections (Gaul et al, 2000).

The Y, Zr and TiO_2 contents of the garnets versus depth were also plotted (Fig. 3.10). The removal of large melt fractions during the, assumed, initial depletion event invariably associated with the creation of cratonic peridotites should have largely removed TiO_2 from the residue. Consequently, TiO_2 contents in garnet from cratonic peridotites exceeding 0.04wt% provide evidence for strong depletion followed by metasomatic re-enrichment (Stachel and Harris, 2008). High levels of Y and Zr in garnets are indicators of modification of the lower lithosphere by metasomatic

melts derived from the asthenosphere (Griffin *et al.*, 1999b). Similar to the Fo_{oliv} composition, a range of Y, Zr and TiO_2 values are observed in the pressure range of 40-47kbar. However, there is an increase in Zr and TiO_2 from 47kbar to the base of the lithosphere at ~60kbar (Fig. 3.10). This trend likely reflects more extensive melt-related metasomatism toward the base of the lithospheric mantle. This same metasomatic event also appears to have lowered the Fo_{oliv} of these xenoliths, and created the trend toward more enriched Fe-rich compositions with depth.

Scully *et al.* (2004) observed areas within the Superior craton that showed layering on both a large (mantle) and small (few km) scale. Based on the Renard sample set, evidence for gross compositional layering of the lithospheric mantle is absent; however enrichment towards the base of the lithosphere is observed.

Whilst eclogite is only a minor constituent, the high sodium content (≥0.07wt% Na_2O) of the garnets is considered an indication of a high pressure origin, as was shown for eclogitic diamond inclusions (Gurney, 1984; Gurney *et al.*, 1993). Despite an overall broad correlation between depth of origin and Na in eclogitic garnet, a clear cut minimum Na concentration for garnet from diamond stable conditions is hampered by a strong dependence of eclogitic garnet composition on bulk rock chemistry (e.g. Grütter & Quadling, 1999). For example, there is an observation of decreasing Na in increasingly Mg-rich (and Ca-poor) inclusion garnets (Stachel and Harris, 2008). Therefore, $Na_2O > 0.07$wt% for Mg-rich garnets has more meaning for high diamond potential than for low-Mg garnets. The three eclogitic garnets in this study have very high Mg contents, and as such the Na_2O contents predict a high pressure origin and as a consequence higher diamond potential.

3.6.2. Metasomatic History of the Eastern Superior SCLM

The major element composition of mantle minerals chiefly reflects primary processes related to the formation of SCLM. Trace element abundances and patterns can, however, be used to decipher the processes that occurred after formation of the SCLM prior to the time of kimberlite eruption.

3.6.2.1. Peridotitic Garnets

Peridotitic garnets display a range of chondrite normalised rare earth element patterns, indicating a number of possible metasomatising agents (Fig. 3.5). Griffin and co-authors (Griffin and Ryan, 1995; Griffin *et al.*, 1999b) used an Y-Zr discrimination diagram on garnet samples derived largely from the Kaapvaal craton to distinguish between two principal metasomatising agents. From a field for depleted garnets with low Y and Zr two trends emerge, one of increasing Zr with subtle to no increase in Y up to 100 ppm Zr, and, a second, characterised by a pronounced positive correlation between Y and Zr. The first trend is attributed to low-temperature fluid (or phlogopite) metasomatism and the second to melt metasomatism (Griffin and Ryan, 1995; Griffin *et al.*, 1999b) (Fig. 3.11).

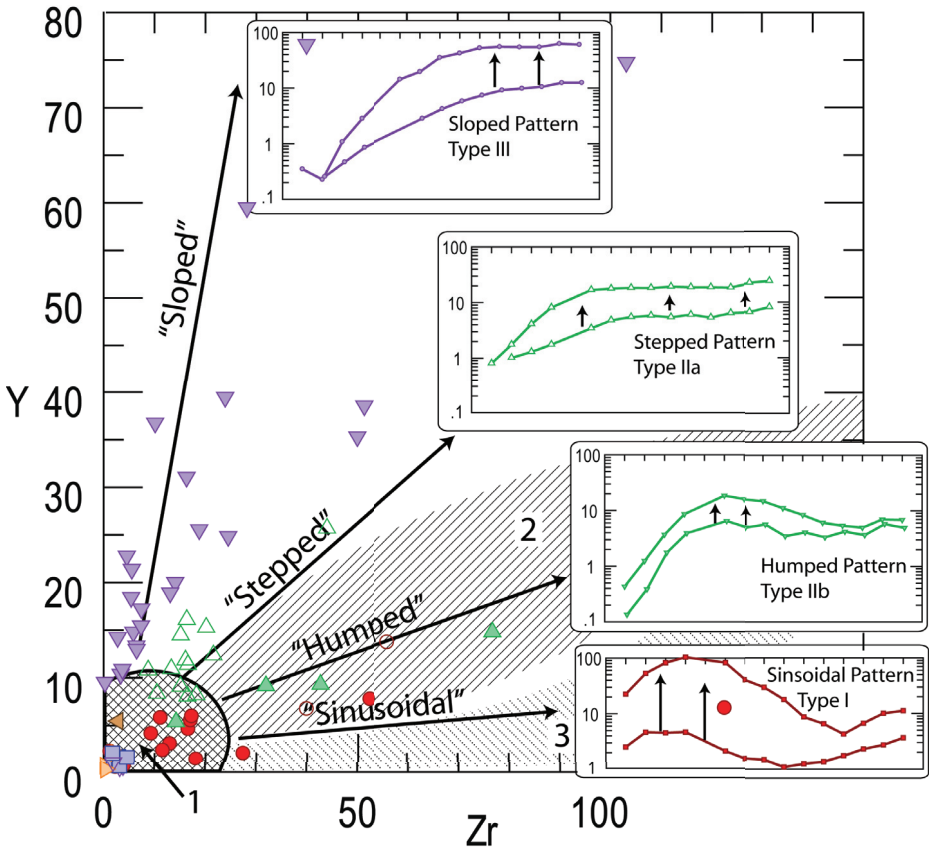

Figure 3.11. Y-Zr discrimination diagram showing the observed trends. As the points fall further along the trend line (away from the depleted field), the trace element patterns become more extreme. Numbered shaded regions represent fields and trends of Griffin *et al.*, (1999): 1-depleted field; 2-melt metasomatism trend; 3-fluid metasomatism trend.

The Renard peridotitic garnets fall along three trends on an Y-Zr discrimination diagram (Fig. 3.11): Garnets with sinusoidal Type I REE_N fall along the trend for fluid metasomatism; along this trend sinuosity increases with higher Zr concentration. Garnets with humped Type IIb REE_N patterns follow the melt metasomatism trend of Griffin *et al.* (1999b) (Fig. 3.11); with increasing Y and Zr concentrations the characteristic "hump" for these garnets at Sm_N-Gd_N becomes more pronounced. Garnets with stepped Type IIa REE_N patterns fall along the same trend, but with a slightly steeper positive slope (i.e. with lower Zr/Y); increasing degree of metasomatic re-enrichment is associated with overall increasing HREE concentrations. Garnets with sloped Type III REE_N patterns fall along a third trend not observed in the sample set of Griffin and others (Griffin and Ryan, 1995; Griffin *et al.*, 1999b). These samples plot along a trend of increasing Y with little to no associated increase in Zr; along this trend increasing Y concentrations correlate with overall HREE enrichment. The remaining garnets with other types of REE_N patterns fall in the depleted low-Y, low-Zr field of Griffin *et al.* (1999b) (Fig. 3.11).

3.6.2.2. Melt Compositions from Modelled Peridotitic Garnet

Using the partition coefficients (D) in Table 2 of Zack *et al.* (1997) ($D^{GAR/L}$ and $D^{CPX/L}$. For $D^{CPX/L}$ Zack *et al.* (1997) used values from Hart and Dunn (1993) unless otherwise stated) the trace element characteristics of the metasomatising agents are determined (Fig. 3.12). These D values, obtained on natural garnet pyroxenites from Kakanui, were selected as these rocks are similar in composition to our samples. In addition the 920°C data set of Zack *et al.* (1997) is more applicable to many natural crystallisation conditions than experimental data sets at 1400°C, with no significant difference observed between the $D^{GNT/CPX}$ of Zack *et al.* (1997) and other experimental and natural partitioning data from the literature (e.g. Hauri *et al.* 1994; Eggins *et al.* 1998; Glaser *et al.* 1999; Green *et al.* 2000).

For garnets with sinusoidal REE_N patterns, the metasomatising agent is highly fractionated (Fig. 3.12a). Mantle melts with $LREE_N/HREE_N$ >10,000 have not been observed in nature and, therefore, the likely agent is a CHO fluid (e.g. Stachel *et al.*, 2004). Garnets which fall within the depleted field (trace element types IIc, IV,

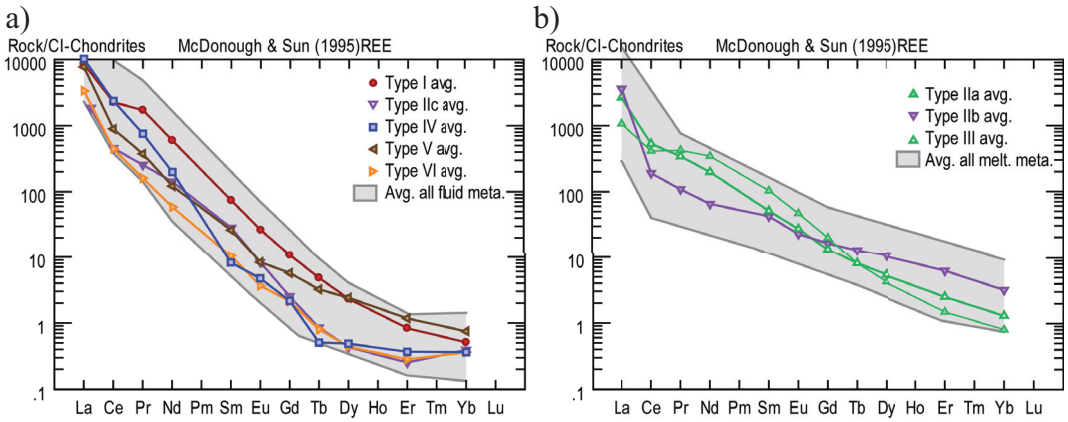

Figure 3.12. Chondrite normalised trace element patterns of the associated metasomatising agent separated into the different garnet trace element groups.

V and VI) have similar, highly fractionated REE_N patterns (fig. 3.12a), implying that their source rocks were infiltrated by highly fractionated fluids as well, but at a lower fluid/rock ratio, due to the low Zr. This interpretation is consistent with the observation that both lherzolitic and harzburgitic garnets have been affected by this style of metasomatism. Due to the high solidus temperature of harzburgite, the percolation of silicate and carbonate melts along grain boundaries is effectively prevented, at the temperatures and pressures of diamond formation (Nielson and Wilshire, 1993; Stachel and Harris, 1997; Stachel *et al.*, 2004). As such only fluids are able to penetrate and metasomatise harzburgitic sources.

The REE_N patterns of the agent associated with Type III (sloped REE_N) garnets is much less fractionated (Fig. 3.12b) and more typical of low volume silicate mantle melts. The chondrite normalised REE patterns of these garnets show an inflection of the pattern at Ce in a number of the samples. This may be an artefact of very low, and hence imprecise, La concentrations within the garnets. It may also be a consequence of a second stage of metasomatic overprint via a fluid with extreme LREE-HREE fractionation. Navon and Stolper (1987) and Bodinier *et al.* (1990) suggested that chromatographic effects of melt/fluid percolation within a peridotite matrix could create such extreme fractionation.

The metasomatic agent associated with the humped patterns (Type IIb) is similar to that associated with Type III garnets, although with elevated LREE/HREE

(e.g. higher Nd/Yb), and likely also a mantle derived melt (Fig. 3.12b). Garnets with stepped REE_N patterns (Type IIa) are associated with model melts that are intermediate from the metasomatic agent for Type IIb garnets and Type III garnets – being less enriched in LREE than Type IIa and more than Type III garnets, and more enriched in HREE than Type IIa and less enriched than Type III garnets (Fig. 3.12b).

The above separation into various types of metasomatic agents should be viewed as being gradational. This is exemplified by two Type I garnets (shown as open circles in Fig. 3.11) which show a transition from the fluid- to the melt-metasomatic trend in Zr-Y space.

3.6.2.3. Evolution of the Lithospheric Mantle

Pre-metasomatic garnet in equilibrium with highly depleted SCLM would have a steep positive slope from $LREE_N$ to $HREE_N$ (fig. 3.13a e.g. Stachel and Harris, 2008). Garnet from cratonic peridotites displaying pre-metasomatic patterns has never been observed, not even in harzburgites/dunites with ultra-depleted major element chemistry (Banas *et al.*, 2009; Smith *et al.*, 2009). The subsequent metasomatic processes are extremely effective at reversing the original melt depletion trends in trace element space (Burgess and Harte, 1999). This is in agreement with the universal principle of a two-stage evolution of lithospheric mantle, primary depletion followed by secondary re-enrichment (Frey and Green, 1974).

For Renard, the most depleted sample displays a mildly sinusoidal REE_N pattern (Fig. 3.13a), indicating that LREE and moderate MREE enrichment must have occurred. During further metasomatic re-enrichment, through a highly fractionated fluid, the garnets will be further enriched in LREE and to a lesser degree MREE. This, combined with rapidly increasing partition coefficients within the LREE, further increases the sinuosity of the REE_N patterns. For sinusoidal garnets, the $HREE_N$ largely retain the positive slope inherited from the original melt depletion of their source (Stachel *et al.*, 1998), consistent with only minimal HREE re-enrichment.

The sloped (Type III) garnets document the starting point of an entirely different evolutionary trend. We suggest that the melt affecting their sources also is “parental”

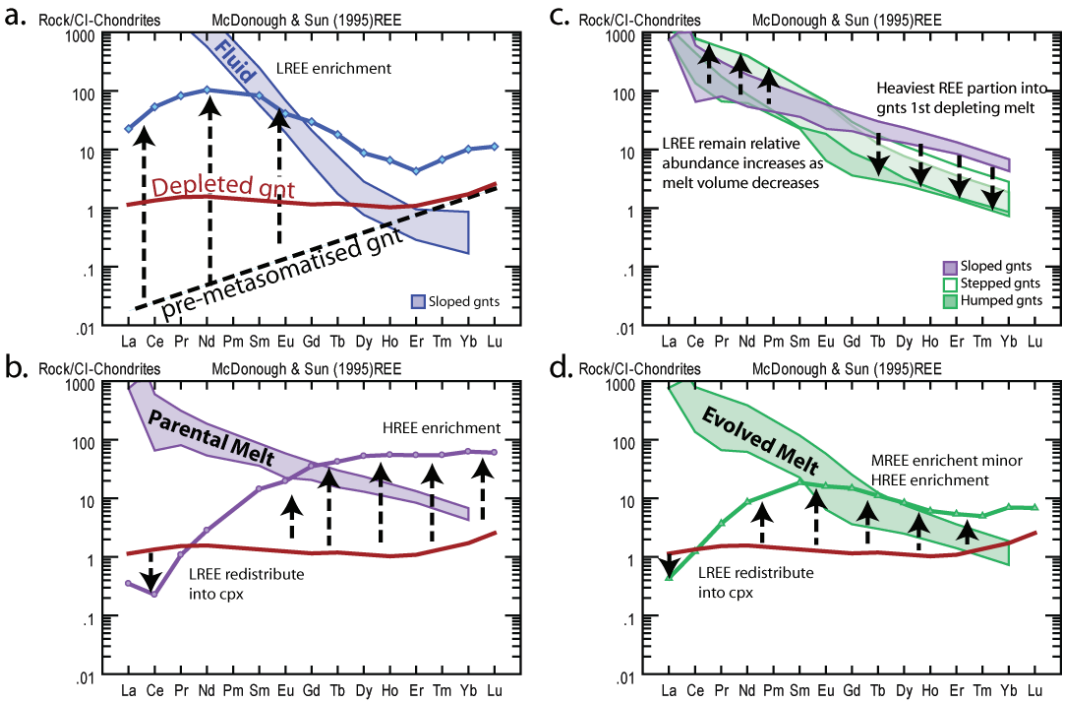

Figure 3.13. a and b) Model showing different metasomatising agents and how they are reflected in the trace element patterns of garnets. c and d) Evolution of the "parental" metasomatic melt during continued wall rock interaction and the reflection of this fractionation process in garnet REE_N. Follows the Two stage evolution model of Frey and Green (1974).

to the more fractionated metasomatic agents seen for garnets with Type IIa and Type IIb REE_N patterns and intermediate Zr/Y. Due to the strong preference of the garnet structure for HREE relative to LREE, interaction with a metasomatic agent with a fairly steep negative slope from $LREE_N$ to $HREE_N$ will still result mainly in HREE enrichment with little effect on LREE (Fig. 3.13b).

As the "parental" metasomatic melt percolates upward through the lithospheric mantle it continuously interacts with wall rock garnet, which preferentially extracts HREE and Y from the melt but leaves the strictly incompatible LREE and Zr behind; this process results in gradually increasing LREE/HREE and Zr/Y in the proposed metasomatic agent. Wall rocks interacting with this increasingly fractionated metasomatic agent (Fig. 3.13c) will be characterised by garnets with stepped (Type IIa) REE_N and upon further interaction, humped (Type IIb) REE_N patterns (Fig. 3.13d).

Previous research suggests that there is a transition from melt metasomatism (typical for the lherzolitic sources), to metasomatism by CHO fluids (Stachel *et al.*, 2004). Stachel *et al.* (2004) viewed melt and fluid metasomatism as a compositional continuum, with residual CHO fluids resulting from primary silicate or carbonate melts progressively refining by interaction with lithospheric host rocks. The observed metasomatism beneath Renard may thus represent a compositional continuum from melt metasomatism which evolves as it passes through the lithospheric mantle, to fluid metasomatism.

Using Ni-in-garnet temperatures (Canil, 1994; 1999) projected on the local paleo-geotherm (Fig. 3.9) it is possible to add a depth constraint to the styles of metasomatism (Fig. 3.14). Fluid metasomatism is focused on a lithospheric section bracketing the graphite diamond transition, characterised by temperatures between ~900-1100°C (with only one sample showing T_{Ni} greater – ~1300°C). Based on how far a garnet is removed from the depleted field of the Y-Zr plot as a measure for the intensity of metasomatism, the most intense fluid metasomatism appears to be restricted to $T_{Ni} \leq 1000$°C. Fewer garnets exhibit fluid metasomatism than melt

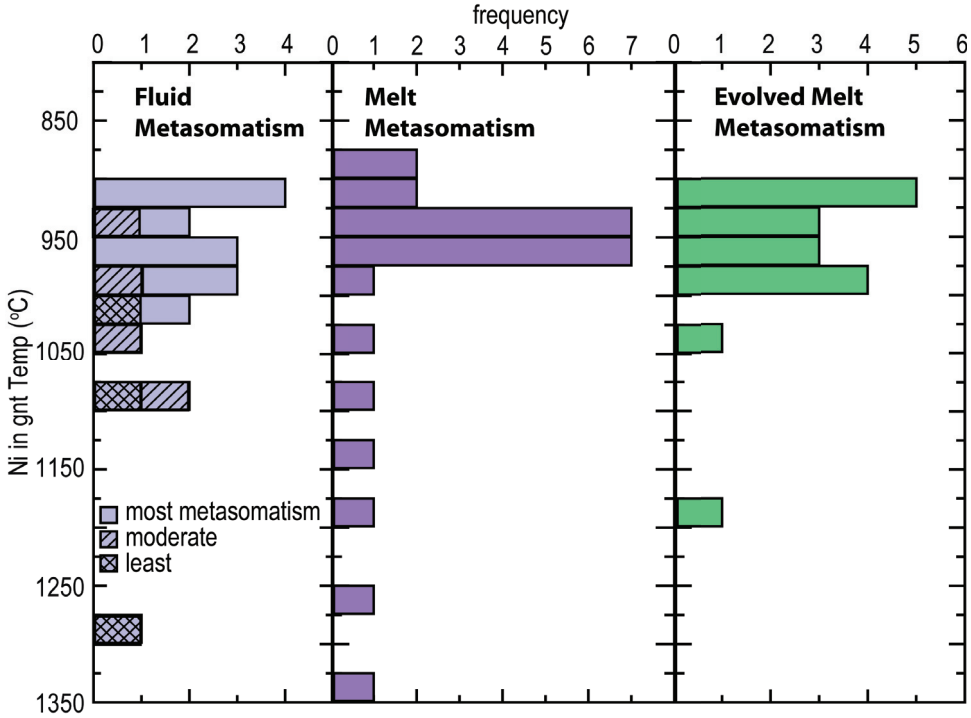

Figure 3.14. Model showing the depth of the garnets affected by the different metasomatising agents.

metasomatism. Melt metasomatism is observed at lithospheric depths represented by T_{Ni} between ~875-1350°C and hence pervasive throughout the entire lithosphere section represented by garnet xenocrysts (Fig. 3.14). The observation that fluid metasomatism affects the lithospheric mantle at shallower depths than the more pervasive melt metasomatism is consistent with the interpretation that there is a transition from melt to fluid metasomatism (Stachel *et al.*, 2004).

3.6.2.4. Peridotitic Clinopyroxenes

$D^{GNT/CPX}$ ratios can be used as a test for the attainment of chemical equilibrium based on the knowledge that the Kakanui garnet pyroxenite xenoliths (Zack *et al.* 1997) are well equilibrated. The trace element partition coefficients between the Renard clinopyroxene and garnet compare well with the $D^{GNT/CPX}$ values of Zack *et al.* (1997), indicating good equilibration (Fig. 3.15).

Two distinct trace element patterns (A, B) were observed for the clinopyroxenes (Fig. 3.7). Type B clinopyroxenes (Fig. 3.7b) only occur with Type III, IIa and IIb garnets. Applying the partition coefficients of Zack *et al.* (1997) gives a metasomatic agent trace element pattern which matches that calculated from coexisting garnets

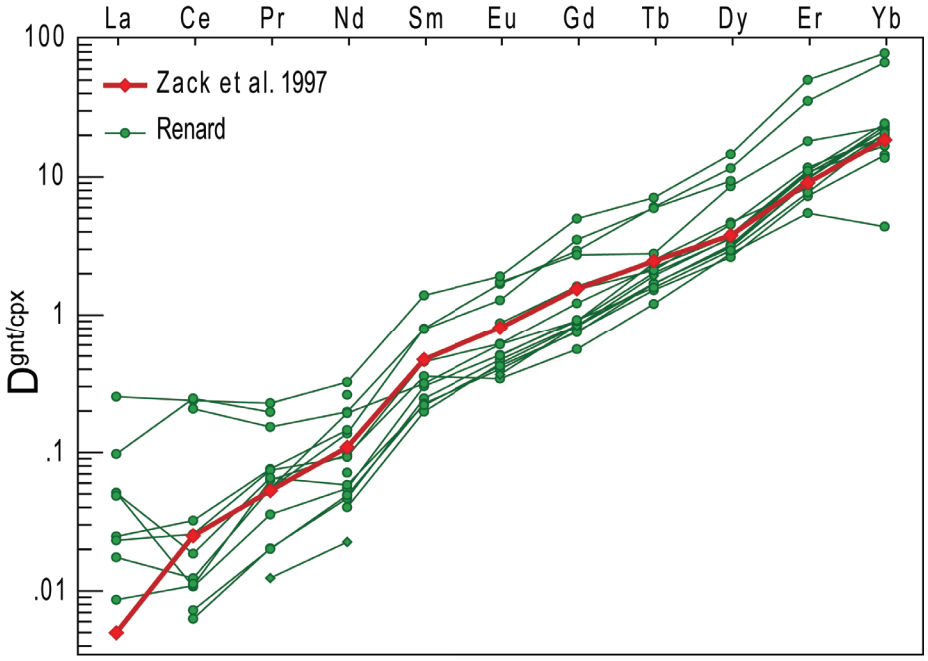

Figure 3.15. Trace element partitioning between coexisting garnet and Type B clinopyroxene compared to published D-values of Zack *et al.* (1997).

(Fig. 3.13). This indicates the garnet and clinopyroxenes underwent the same low volume mantle melt metasomatism. This is consistent with the findings of Stachel and Harris (1997) for garnet and cpx inclusions in diamonds from Akwatia (Ghana).

The second, Type A, clinopyroxene pattern (Fig. 3.7a), when using the Zack *et al.* (1997) partition coefficients, does not give a trace element pattern comparable to any of those determined from the garnets. However, these clinopyroxenes appear to have interacted with a kimberlite melt. If the partition coefficients for an alkaline melt of Foley and Jenner (2004) are used, then the trace element pattern of the metasomatising melt is similar to that of a kimberlite. These clinopyroxenes were either formed (i.e. the grains are megacrysts) or metasomatised by kimberlitic-like melts passing through the lithospheric mantle. Both the Type A and Type B temperatures (Nimis and Taylor, 2000) show a similar range: Type B 782-1018^{o}C; Type A 790-1026^{o}C. No evidence of zoning within the Type A clinopyroxenes was observed, which suggests that they formed, or were metasomatised 100's Ma prior to their eruption, giving the major and trace elements time to re-equilibrate.

Approximately 400Ma before the eruption of the Renard kimberlites the Grenville Orogeny occurred to the south (~1.3-0.9Ma; e.g. Rivers, 1997 and references therein) (Fig. 3.1). This continent-continent collision created major uplift and magmatism (e.g. Rivers, 1997 and references therein) and has been linked to the Abitibi Dyke swarm (e.g. Ranalli and Ernst, 1986) and the failed Keweenawan rift event (e.g. Gordon and Hempton, 1986). Melts related to this orogeny may have been responsible for the formation/metasomatism of the Type A clinopyroxenes. More precise estimates on the exact timing, and therefore event, cannot be determined.

3.6.3. Lead Isotopic Constraints on the Eastern Superior SCLM Formation

As discussed in the previous sections, the SCLM section sampled by the Renard kimberlites has experienced metasomatic overprinting to variable degrees. However, our mineral chemical data suggest that major and trace-element equilibrium has been largely preserved. A prime example is the peridotitic garnet-clinopyroxene

assemblage with sloped REE_N (Type III) patterns for garnets and humped REE_N (Type B) patterns for clinopyroxene suggestive of full chemical equilibration. Some of these well equilibrated clinopyroxenes fall onto the Stacey and Kramers (1975) terrestrial Pb evolution curve with an intercept at ca. 2733 Ma.

The two-stage Pb evolution model of Stacey and Kramers (1975) is consistent with both the accepted age of the earth, moon and meteorites, and the assumed values for primordial lead, as well as permitting various primary curves to have developed in different parts of the earth at different times (Rickard, 1978). Although a number of Pb evolution models exist (e.g., the Plumbotectonics model of Doe and Zartman, 1979), the Stacey-Kramers model is essentially the simplest approximation to a multi-stage model for lead isotopic evolution and the most frequently employed (cf., Bickford *et al.*, 2005; Schmidberger *et al.*, 2007; Tappe *et al.*, 2007). This model is particularly suited to the Pb isotope evolution of the Superior Province, as many of the galenas utilised for calibration of the growth curve came from cratonic areas of eastern Canada. Furthermore, it has been noted by a number of authors (e.g. Rickard, 1978) that a model growth curve is only as precise as the original ages that were used for its calibration. We note that in the original work by Stacey and Kramers (1975) the difference between the accepted age and the newly derived two-stage model age did not exceed 100Ma. We further note that the Stacey-Kramers model is the best estimate of terrestrial Pb isotopic composition through time, until models more regionally specific to certain cratons are developed (e.g. Jahn *et al.*, 1980).

Minerals with negligibly low U/Pb ratios retained the initial common Pb isotopic composition of the medium they last equilibrated with, i.e. a melt or a protolith, and thus may retain important Pb-Pb model age and tracer isotopic information on the origin of the precursor(s). In studies of crustal evolution, feldspars are typically used for Pb-Pb studies (Connelly and Thrane, 2005). For mantle environments, clinopyroxene has been demonstrated to be the most feasible mineral for Pb-Pb isotope studies as it has ultra-low U/Pb ratios (Jacob and Foley, 1999; Schmidberger *et al.*, 2007).

Depending on the origin of the clinopyroxenes two interpretations of the Pb-Pb clinopyroxene data obtained in this study are feasible. The first interpretation is that the grains shown to be in equilibrium with the garnets are primary, and preserved the isotopic composition of Pb that was inherited from a Late Archean source (the 2733Ma growth curve intercept in the Stacey-Kramers model). Most models for the formation of cratonic mantle argue for a polybaric origin of the SCLM by melt depletion in subduction zone settings (Stachel *et al.*, 1998; Walter, 1999). If the protolith(s) for the Renard SCLM section was such an oceanic lithospheric section, then the ~2700Ma model age obtained here suggests an origin of the eastern Superior SCLM by Late Archean subduction. Alternatively, if the clinopyroxene (and by inference the equilibrated garnet) were introduced subsequently to SCLM stabilisation, then the ~2700Ma model age would represent a minimum age of SCLM formation. Late Archean subduction in the eastern Superior Province is recorded by the collision of the Abitibi-Opatica oceanic plateau with the composite Superior superterrane accompanied by ca. 2.7Ga arc volcanism. During this so-called Shebandowanian orogeny a major portion of the crust in the eastern Superior Province was generated (Percival and western Superior NATMAP working group, 2004). Our new Pb-Pb clinopyroxene data suggest that the thick cratonic mantle lithosphere sampled by the Renard kimberlites was either formed during this subduction cycle or had garnet and clinopyroxene introduced at that time.

Numerous Re-Os isotopic studies on mantle peridotites show that cratonic lithospheric mantle and overlying continental crust have remained coupled since their formation (Pearson, 1999). For the Superior Province, precise radiometric age determinations show that the major portion of the igneous crust formed during the Late Archean between 3.1-2.6Ga, with a major magmatic pulse at ca. 2.7Ga (Card, 1990). The coincidence of this latter age with the here obtained minimum model age of ~2700Ma for SCLM formation points to coupling between the crust-mantle system of the Superior craton, as observed for most other cratons worldwide (Grütter *et al.*, 1999).

3.7. Conclusions

A portion of the SCLM beneath the Renard kimberlite cluster retained ultra-low U/Pb since the Late Archean as indicated by a Pb-Pb clinopyroxene model age of ca. 2.7Ga. At this time a major period of crustal formation was taking place throughout the Superior province. Within the southern Superior Craton a number of elongated belts were accreted together in a series of convergent-plate margins. The limited age determinations of the crustal units of the Opanica, through which the Renard kimberlites are extruded, indicate that underlying mantle and crust have remained coupled since their formation.

Since its formation, a number of metasomatic events modified the lithospheric mantle underlying the eastern Superior Craton. The most pervasive metasomatism is related to melt infiltration and affected garnets over the entire sampling depth. An unfractionated "parental" melt with sloped chondrite normalised trace element pattern metasomatised the lithosphere. As the melt moved upward through the lithospheric mantle it gradually evolved towards higher LREE/HREE and Zr/Y via equilibrium fractionation and imparted stepped and humped REE_N patterns on the lithospheric peridotitic garnets. Less pervasive metasomatism through a highly fractionated further refined fluid predominantly affected the lithospheric mantle between 125 and 170km depth and is reflected in garnets with sinusoidal REE_N patterns.

Two main trace element patters have been observed for the clinopyroxenes. Based on a similar range of determined clinopyroxene temperatures (Nimis and Taylor, 2000) the authors suggest the metasomatism related to the Type A pyroxenes likely occured 100's Ma prior to the eruption of the Renard kimberlites, allowing time for major elements to be re-equilibrated. This metasomatic event may relate to the Grenville Orogeny, which occured ~400Ma (e.g. Rivers, 1997) prior to kimberlite emplacement.

The lithospheric mantle had very favourable conditions for diamond formation at the time of kimberlite emplacement (~0.6Ga). Geothermobarometry suggests

a minimum cratonic thickness of ~190km, which, combined with a syneruptive paleogeotherm of 38mW/m^2, results in a diamond window of ~60km thickness. Based on the comparatively limited samples studied, the majority of the lithospheric mantle comprises of peridotite, with only minor eclogitic and websteritic portions. The peridotitic portion is strongly dominated by lherzolite (71%), with minor harzburgitic (24%) and rare wehrlitic (5%) subpopulations. Whilst eclogite is only a minor constituent, the high sodium content (>0.07wt% Na_2O) of the garnets is considered an indication of a high pressure origin (Gurney, 1984; Gurney *et al.*, 1993). This implies that both depleted harzburgite and eclogite may be the mantle sources of diamonds at Renard. From these analyses there is no evidence for gross compositional layering of the lithospheric mantle beneath Renard at time of kimberlite emplacement. This is in contrast to previous studies of the Superior Craton (Scully *et al.*, 2004) where layering on both a large and small scale was postulated.

References

Aulbach, S., Griffin, W.L., Pearson, N.J., O'Reilly, S.Y., Kivi, K. and Doyle, B.J., 2003. Origins of eclogites beneath the central Slave Craton, 8th International Kimberlite Conference, Victoria (BC, Canada), pp. 5 p. (CD, not paginated).

Banas, A., Stachel, T., Phillips, D., Shimizu, N., Viljoen, K.S. and Harris, J.W., 2009. Ancient metasomatism recorded by ultra-depleted garnet inclusions in diamonds from DeBeers Pool, South Africa. Lithos, 112(Supplement 2): 736-746.

Bickford, M.E., Mock, T.D., Steinhart, W.E., Collerson, K.D. and Lewry, J.F., 2005. Origin of the Archean Sask craton and its extent within the Trans-Hudson orogen: evidence from Pb and Nd isotopic compositions of basement rocks and post-orogenic intrusions. Canadian Journal of Earth Sciences, 42(4): 659-684.

Birkett, T.C., McCandless, T.E. and Hood, C.T., 2004. Petrology of the Renard igneous bodies: host rocks for diamond in the northern Otish Mountains region, Quebec. Lithos, 76(1-4): 475-490.

Bodinier, J.L., Vasseur, G., Vernieres, J., Dupuy, C. and Fabries, J., 1990. Mechanisms of Mantle Metasomatism: Geochemical Evidence from the Lherz Orogenic Peridotite 10.1093/petrology/31.3.597. Journal of Petrology, 31(3): 597-628.

Boyd, F.R. and Gurney, J.J., 1986. Diamonds and the African Lithosphere. Science, 232(4749): 472-477.

Brenker, F.E. and Brey, G.P., 1997. Reconstruction of the exhumation path of the Alpe Arami garnet-peridotite body from depths exceeding 160 km. Journal of Metamorphic Geology, 15: 581-592.

Brey, G., Kogarko, L. and Ryabchikov, I.D., 1991. Carbon dioxide in kimberlitic melts. Neues Jahrbuch für Mineralogie, Monatshefte, 4: 159-168.

Brey, G.P. and Köhler, T., 1990. Geothermobarometry in four-phase lherzolites II. New thermobarometers, and practical assessment of existing thermobarometers. Journal of Petrology, 31: 1353-1378.

Brey GP, Köhler TP, Nickel KG (1990) Geothermobarometry in Four-phase Lherzolites I. Experimental Results from 10 to 60 kb. J Petrol 31(6):1313-1352

Burgess, S.R. and Harte, B., 1999. Tracing lithospheric evolution trough the analysis of heterogeneous G9/G10 garnets in peridotite xenoliths, I: Major element chemistry. In: J.J. Gurney, J.L. Gurney, M.D. Pascoe and S.H. Richardson (Editors), The J.B. Dawson Volume, Proceedings of the VIIth International Kimberlite Conference. Red Roof Design, Cape Town, pp. 66-80.

Canil, D., 1994. An Experimental Calibration of the Nickel in Garnet Geothermometer with Applications. Contributions to Mineralogy and Petrology, 117(4): 410-420.

Canil, D., 1999. The Ni-in-garnet geothermometer: calibration at natural abundances. Contributions to Mineralogy and Petrology, 136(3): 240-246.

Canil, D., Schulze, D.J., Hall, D., Hearn, B.C. and Milliken, S.M., 2003. Lithospheric roots beneath western Laurentia: the geochemical signal in mantle garnets. Canadian Journal of Earth Sciences, 40: 1027-1051.

Card, K.D., 1990. A review of the Superior Province of the Canadian Shield, a product of Archean accretion. Precambrian Research, 48(1-2): 99-156.

Chapman, D.S. and Pollack, H.N., 1977. Regional geotherms and lithospheric thickness. Geology, 5(5): 265-268.

Connelly, J.N. and Thrane, K., 2005. Rapid determination of Pb isotopes to define Precambrian allochthonous domains: an example from West Greenland. Geology, 33: 953-956.

Doe, B.R. and Zartman, R.E., 1979. Plumbotectonics: the Phanerozoic. In: H.L. Barnes (Editor), Geochemistry of Hydrothermal Ore Deposits. Wiley: 22-70.

Eggins S.M., Rudnick R.L. and McDonough W.F., 1998. The composition of peridotites and their minerals: A laser-ablation ICP-MS study. Earth and Planetary Science Letters 154(1-4):53-71

Farrow, D., 2011. NI 43-101 Technical Report - Updated Preliminary Economic: 2010 Mineral Resource Update for the Renard Diamond Project, GeoStrat Consulting Services Inc.

Fitzgerald, C.E., Hetman, C.M., Lepine, I.M., Skelton, D.S. and McCandless, T.E., 2008. The internal geology and emplacement history of the Renard 2 kimberlite, Superior Province, Canada. Extended Abstract - 9th International Kimberlite Conference, Frankfurt, 2008.

Foley, S.F. and Jenner, G.A., 2004. Trace element partitioning in lamproitic magmas - the Gaussberg olivine leucitite. Lithos, 75: 19-38.

Frey, F.A. and Green, D.H., 1974. The mineralogy, geochemistry and origin of lherzolite inclusions in Victorian basanites. Geochimica Et Cosmochimica Acta, 38: 1023-1059.

Gaul, O.F. , Griffn, W.L., O'Reilly, S.Y. and Pearson, N.J., 2000. Mapping olivine composition in the lithospheric mantle. Earth and Planetary Science Letters 182: 223-235.

Girard, R., 2001. Caracterisation de l'intrusion Kimberlitique du lac Beaver, Monts Otish—Petrographie et Mineralogy. Ressources Naturelles Quebec, Government Province Quebec, Canada, MB 2001-08: 23.

Glaser S.M., Foley S.F. and Gunther D. 1999. Trace element compositions of minerals in garnet and spinel peridotite xenoliths from the Vitim volcanic field, Transbaikalia, eastern Siberia. Lithos 48(1-4):263-285

Gordon M.B. and Hempton M.R., 1986. Collison-induced rifting: The Grenville Orogeny and the Keweenawan Rift of North America. Tectonophysics 127(1-2):1-25

Green T.H., Blundy J.D., Adam J. and Yaxley G.M., 2000. SIMS determination of trace element partition coefficients between garnet, clinopyroxene and hydrous basaltic liquids at 2-7.5 GPa and 1080-1200oC. Lithos 53:165-187

Griffin, W.L., Doyle, B.J., Ryan, C.G., Pearson, N.J., O'Reilly, S.Y., Davies, R., Kivi, K., VanAchterbergh, E. and Natapov, L.M., 1999a. Layered mantle lithosphere in the Lac de Gras area, Slave Craton: Composition, structure and origin. Journal of Petrology, 40(5): 705-727.

Griffin, W.L., O'Reilly, S.Y. and Ryan, C.G., 1999b. The composition and origin of subcontinental lithospheric mantle. In: Y. Fei, C.M. Bertka and B.O. Mysen (Editors), Mantle Petrology: Field Observations and High Pressure Experimentation: A tribute to Francis R. (Joe) Boyd. Special Publication. The Geochemical Society, Houston: 13–45.

Griffin, W.L. and Ryan, C.G., 1995. Trace-Elements in Indicator Minerals - Area Selection and Target Evaluation in Diamond Exploration. Journal of Geochemical Exploration, 53(1-3): 311-337.

Grütter, H., Latti, D. and Menzies, A., 2006. Cr-saturation arrays in concentrate garnet compositions from kimberlite and their use in mantle barometry. Journal of Petrology, 47(4): 801-820.

Grütter, H.S., 2009. Pyroxene xenocryst geotherms: Techniques and application. Lithos, 112: 1167-1178.

Grütter, H.S., Apter, D.B. and Kong, J., 1999. Crust-mantle coupling: evidence from mantle-derived xenocrystic garnets. In: J.J. Gurney, J.L. Gurney, M.D. Pascoe and S.H. Richardson (Editors), The J.B. Dawson Volume, Proceedings of the VIIth International Kimberlite Conference. Red Roof Design, Cape Town, pp. 307-313.

Grütter, H.S., Gurney, J.J., Menzies, A.H. and Winter, F., 2004. An updated classification scheme for mantle-derived garnet, for use by diamond explorers. Lithos, 77(1-4): 841-857.

Grütter, H.S. and Quadling, K.E., 1999. Can sodium in garnet be used to monitor eclogitic diamond potential? In: J.L.G. J.J. Gurney, M.D. Pascoe and S.H. Richardson (Editor), J.B. Dawson volume, Proceedings of the 7th International Kimberlite Conference. Red Roof Design, Cape Town, pp. 314-320.

Gurney, J.J., 1984. A correlation between garnets and diamonds in kimberlites, Publications of the Geology Department & Extension Service, University of Western Australia: 143-166.

Gurney, J.J., Helmstaedt, H. and Moore, R.O., 1993. A Review of the Use and Application of Mantle Mineral Geochemistry in Diamond Exploration. Pure and Applied Chemistry, 65(12): 2423-2442.

Harley, S.L., 1984. An experimental study of the partitioning of iron and magnesium between garnet and orthopyroxene. Contributions to Mineralogy and Petrology, 86: 359-373.

Hart, S.R. and Dunn, T., 1993. Experimental cpx/melt partitioning of 24 trace elements. Contributions to Mineralogy and Petrology 113(1):1-8

Harte, B. and Kirkley, M.B., 1997. Partitioning of trace elements between clinopyroxene and garnet: data from mantle eclogites. Chemical Geology, 136(1-2): 1-24.

Hauri E.H., Wagner T.P., and Grove T.L., 1994. Experimental and natural partitioning of Th, U, Pb and other trace elements between garnet, clinopyroxene and basaltic melts. Chemical Geology 117(1-4):149-166

Hills, D.V. and Haggerty, S.E., 1989. Petrochemistry of Eclogites From the Koidu Kimberlite Complex, Sierra-Leone. Contributions to Mineralogy and Petrology, 103(4): 397-422.

Hoffman, P.F., 1988. United Plates of America, the Birth of a Craton - Early Proterozoic Assembly and Growth of Laurentia. Annual Review of Earth and Planetary Sciences, 16: 543-603.

Jahn, B.M., Vidal, P. and Tilton, G.R., 1980. Archean Mantle Heterogeneity - Evidence from Chemical and Isotopic Abundances in Archean Igneous Rocks. Philosophical Transactions of the Royal Society of London Series a-Mathematical Physical and Engineering Sciences, 297(1431): 353-364.

Klemme, S., 2004. The influence of Cr on the garnet-spinel transition in the Earth's mantle: experiments in the system MgO-Cr2O3-SiO2 and thermodynamic modelling. Lithos, 77(1-4): 639-646.

Kopylova, M.G. and Russell, J.K., 2000. Chemical stratification of cratonic lithosphere: constraints from the Northern Slave craton, Canada. Earth and Planetary Science Letters, 181(1-2): 71-87.

Letendre, J.P.L., L'Heureux, M., Nowicki, T.E. and Creaser, R.A., 2003. The Wemindji kimberlites: exploration and geology, Proceedings of the 8th International Kimberlite Conference, Victoria, B.C., pp. 71.

Longerich, H.P., Fryer, B.J. and Strong, D.F., 1987. Determination of Lead Isotope Ratios by Inductively Coupled Plasma-Mass Spectrometry (Icp-Ms). Spectrochimica Acta Part B-Atomic Spectroscopy, 42(1-2): 39-48.

MacKenzie, J.M. and Canil, D., 1999. Composition and thermal evolution of cratonic mantle beneath the central Archean Slave Province, NWT, Canada. Contributions to Mineralogy and Petrology, 134(4): 313-324.

Mareschal, J.C., Jaupart, C., Gariepy, C., Cheng, L.Z., Guillou-Frottier, L., Bienfait, G. and Lapointe, R., 2000. Heat flow and deep thermal structure near the southeastern edge of the Canadian Shield. Canadian Journal of Earth Sciences, 37: 399-414.

McDonough, W.F., 1990. Constraints on the Composition of the Continental Lithospheric Mantle. Earth and Planetary Science Letters, 101(1): 1-18.

McDonough, W.F. and Rudnick, R.L., 1998. Mineralogy and composition of the upper mantle. Reviews in Mineralogy, 37: 139-164.

McDonough, W.F. and Sun, S.-S., 1995. The composition of the Earth. Chemical Geology, 120: 223-253.

Menzies, A., Westerlund, K., Grutter, H., Gurney, J., Carlson, J., Fung, A. and Nowicki, T., 2004. Peridotitic mantle xenoliths from kimberlites on the Ekati Diamond Mine property, NWT, Canada: major element compositions and implications for the lithosphere beneath the central Slave craton. Lithos, 77(1-4): 395-412.

Moorhead, J., Beaumier, M., Girard, R. and Heaman, L.M., 2003. Distribution, structural controls and ages of kimberlite fields in the Superior Province of Quebec. Proceedings of the 8th International Kimberlite Conference, Victoria, B.C.: 128.

Moorhead, J., Girard, R. and Heaman, L.M., 2002. Caractérisation des Kimberlites au Québec. Ministère des Ressources Naturelles du Québec, Government Province Quebec, Canada, DV 2002-10: 36.

Navon, O. and Stolper, E., 1987. Geochemical Consequences of Melt Percolation: The Upper Mantle as a Chromatographic Column. The Journal of Geology, 95(3): 285-307.

Nickel, K.G. and Green, D.H., 1985. Empirical Geothermobarometry for Garnet Peridotites and Implications for the Nature of the Lithosphere, Kimberlites and Diamonds. Earth and Planetary Science Letters, 73(1): 158-170.

Nielson, J.E. and Wilshire, H.G., 1993. Magma transport and metasomatism in the mantle: A critical review of current models. American Mineralogist, 78(11-12): 1117-1134.

Nimis, P. and Grütter , H., 2010. Internally consistent geothermometers for garnet peridotites and pyroxenites. Contributions to Mineralogy and Petrology, 159(3): 411-427.

Nimis, P. and Taylor, W.R., 2000. Single clinopyroxene thermobarometry for garnet peridotites. Part I. Calibration and testing of a Cr-in-Cpx barometer and an enstatite-in-Cpx thermometer. Contributions to Mineralogy and Petrology, 139(5): 541-554.

O'Neill, H.S.C. and Wood, B.J., 1979. An experimental study of the iron-magnesium partitioning between garnet and olivine and its calibration as a geothermometer. Contributions to Mineralogy and Petrology, 70: 59-70.

Pearson, D.G., 1999. The age of continental roots. Lithos, 48(1-4): 171-194.

Pearson, D.G., Canil, D. and Shirey, S.B., 2004. Mantle samples included in volcanic rocks: xenoliths and diamonds. In: R.W. Carlson (Editor), Treatise on Geochemistry. Volume 2: The Mantle and Core. Elsevier-Pergamon, Oxford: 171-275.

Percival, J.A., 2007. Geology and metallogeny of the Superior Province, Canada in, Mineral deposits of Canada: 471 a synthesis of major deposit-types, district metallogeny, the evolution of geological provinces, and exploration 472 methods. In: W.D. Goodfellow (Editor), Geological Association of Canada, Mineral Deposits Division, Special 473 Publication no. 5: 903-928.

Percival, J.A., Stern, R.A., Skulski, T., Card, K.D., Mortensen, J.K. and Begin, N.J., 1994. Minto Block, Superior Province - Missing Link in Deciphering Assembly of the Craton at 2.7 Ga. Geology, 22(9): 839-842.

Percival, J.A. and western Superior NATMAP working group, 2004. Orogenic framework for the Superior Province: Dissection of the "Kenoran Orogeny", The LITHOPROBE Celebratory Conference: From Parameters to Processes - Revealing the Evolution of a Continent, Toronto.

Pollack, H.N. and Chapman, D.S., 1977. On the regional variation of heat flow, geotherms, and lithospheric thickness. Tectonophysics, 38: 279-296.

Ramsay, R.R., 1992. Geochemistry of Diamond Indicator Minerals. PhD Thesis, University of Western Australia, Perth.

Ranalli G. and Ernst R. 1986. The Abitibi dyke swarm: a consequence of Superior-Grenville interaction? Tectonophysics 121(2-4):357-363

Ravna, E.K., 2000. The garnet-clinopyroxene Fe2+-Mg geothermometer: an updated calibration. Journal of Metamorphic Geology, 18(2): 211-219.

Reed, W.P., 1992. 614, Trace elements in glass matrix (3 mm wafer), 615, trace elements in a glass matrix (1vmm wafer).

Rickard, D.T., 1978. The Svecokarelian anomalous lead line. GFF, 100(1): 19-30.

Rivers T. 1997. Lithotectonic elements of the Grenville Province: review and tectonic implications. Precambrian Research 86:117-154

Rosman, K.J.R. and Taylor, P.D.P., 1999. Isotopic compositions of the elements 1997. Journal of Analytical Atomic Spectrometry, 14(1): 5n-24n.

Schmidberger, S.S., Simonetti, A., Heaman, L.M., Creaser, R.A. and Whiteford, S., 2007. Lu-Hf, *in situ* Sr and Pb isotope and trace element systematics for mantle eclogites from the Diavik diamond mine: Evidence for Paleoproterozoic subduction beneath the Slave craton, Canada. Earth and Planetary Science Letters, 254(1-2): 55-68.

Scully, K.R., Canil, D. and Schulze, D.J., 2004. The lithospheric mantle of the Archean Superior Province as imaged by garnet xenocryst geochemistry. Chemical Geology, 207(3-4): 189-221.

Simonetti, A., Heaman, L.M., Hartlaub, R.P., Creaser, R.A., MacHattie, T.G. and Bohm, C., 2005. U-Pb zircon dating by laser ablation-MC-ICP-MS using a new multiple ion counting Faraday collector array. Journal of Analytical Atomic Spectrometry, 20(8): 677-686.

Smart, K.A., Heaman, L.M., Chacko, T., Simonetti, A., Kopylova, M.G., Mah, D. and Daniels, D., 2009. The origin of high-MgO diamond eclogites from the Jericho Kimberlite, Canada. Earth and Planetary Science Letters, 284(3-4): 527-537.

Smith, C.B., Pearson, D.G., Bulanova, G.P., Beard, A.D., Carlson, R.W., Wittig, N., Sims, K., Chimuka, L. and Muchemwa, E., 2009. Extremely depleted lithospheric mantle and diamonds beneath the southern Zimbabwe Craton. Lithos, 112: 1120-1132.

Stacey, J.S. and Kramers, J.D., 1975. Approximation of Terrestrial Lead Isotope Evolution by a 2-Stage Model. Earth and Planetary Science Letters, 26(2): 207-221.

Stachel, T., Aulbach, S., Brey, G.P., Harris, J.W., Leost, I., Tappert, R. and Viljoen, K.S., 2004. The trace element composition of silicate inclusions in diamonds: a review. Lithos, 77(1-4): 1-19.

Stachel, T. and Harris, J.W., 1997. Diamond precipitation and mantle metasomatism - evidence from the trace element chemistry of silicate inclusions in diamonds from Akwatia, Ghana. Contributions to Mineralogy and Petrology, 129(2-3): 143-154.

Stachel, T. and Harris, J.W., 2008. The origin of cratonic diamonds -- Constraints from mineral inclusions. Ore Geology Reviews, 34: 5-32.

Stachel, T., Harris, J.W., Tappert, R. and Brey, G.P., 2003. Peridotitic diamonds from the Slave and the Kaapvaal cratons - similarities and differences based on a preliminary data set. Lithos, 71(2-4): 489-503.

Stachel, T., Viljoen, K.S., Brey, G. and Harris, J.W., 1998. Metasomatic processes in lherzolitic and harzburgitic domains of diamondiferous lithospheric mantle: REE in garnets from xenoliths and inclusions in diamonds. Earth and Planetary Science Letters, 159(1-2): 1-12.

Tappe, S., Foley, S.F., Jenner, G.A., Heaman, L.M., Kjarsgaard, B.A., Romer, R.L., Stracke, A., Joyce, N. and Hoefs, J., 2006. Genesis of Ultramafic Lamprophyres and Carbonatites at Aillik Bay, Labrador: a Consequence of Incipient Lithospheric Thinning beneath the North Atlantic Craton. Journal of Petrology, 47(7): 1261-1315.

Tappe, S., Foley, S.F., Kjarsgaard, B.A., Romer, R.L., Heaman, L.M., Stracke, A. and Jenner, G.A., 2008. Between carbonatite and lamproite - Diamondiferous Torngat ultramafic lamprophyres formed by carbonate-fluxed melting of cratonic MARID-type metasomes. Geochimica Et Cosmochimica Acta, 72(13): 3258-3286.

Tappe, S., Foley, S.F., Stracke, A., Romer, R.L., Kjarsgaard, B.A., Heaman, L.M. and Joyce, N., 2007. Craton reactivation on the Labrador Sea margins: 40Ar/39Ar age and Sr–Nd–Hf–Pb isotope constraints from alkaline and carbonatite intrusives. Earth and Planetary Science Letters, 256(3-4): 433-454.

Tappe, S., Heaman, L.M., Smart, K.A., Muehlenbachs, K. and Simonetti, A., 2009. First Results From Greenland Eclogite Xenoliths: Evidence for an Ultra-depleted Non- peridotitic Component Within the North Atlantic Craton Mantle Lithosphere. American Geophysical Union, Spring Meeting 2009, abstract #MA72A-03.

Tappert, R., Stachel, T., Harris, J.W., Muehlenbachs, K., Ludwig, T. and Brey, G., 2005. Diamonds from the Jagersfontein (South Africa):messengers from the sublithospheric mantle. Contributions to Mineralogy and Petrology, 150(5): 505-522.

Taylor, W.R., 1998. An experimental test of some geothermometer and geobarometer formulations for upper mantle peridotites with application to the thermobarometry of fertile Iherzolite and garnet websterite. Neues Jahrbuch Fur Mineralogie-Abhandlungen, 172(2-3): 381-408.

van Achterbergh, E., Ryan, C.G., Jackson, S.E. and Griffin, W.L., 2001. Laser-ablation-ICPMS in the earth sciences — Appendix 3 data reduction software for LA–ICP–MS. In: P. Sylvester (Editor), Mineralogical Association of Canada Short Course: 239-243.

Viljoen, K.S., Schulze, D.J. and Quadling, A.G., 2005. Contrasting Group I and Group II Eclogite Xenolith Petrogenesis: Petrological, Trace Element and Isotopic Evidence from Eclogite, Garnet-Websterite and Alkremite Xenoliths in the Kaalvallei Kimberlite, South Africa. Journal of Petrology, 46(10): 2059-2090.

Walter, M.J., 1999. Melting residues of fertile peridotite and the origin of cratonic lithosphere. In: Y. Fei, C.M. Bertka and B.O. Mysen (Editors), Mantle Petrology: Field Observations and High Pressure Experimentation: A tribute to Francis R. (Joe) Boyd. Special Publication. The Geochemical Society, Houston: 225-239.

Webb, S.A.C. and Wood, B.J., 1986. Spinel-pyroxene-garnet relationships and their dependence on Cr/Al ratio. Contributions to Mineralogy and Petrology, 92(4): 471-480.

Wyatt, B.A., Baumgartner, M., Anckar, E. and Grutter, H., 2004. Compositional classification of “kimberlitic” and “non-kimberlitic” ilmenite. Lithos, 77(1-4): 819-840.

Zack, T., Foley, S.F. and Jenner, G.A., 1997. A consistent partition coefficient set for clinopyroxene, amphibole and garnet from laser ablation microprobe analysis of garnet pyroxenites from Kakanui, New Zealand. Neues Jahrbuch Fur Mineralogie-Abhandlungen, 172(1): 23-41.

CHAPTER 4

DIAMONDS AND THEIR MINERAL INCLUSIONS FROM THE RENARD KIMBERLITES IN QUEBEC

The content of this chapter, in modified form, is being prepared for publication as: Lucy Hunt, Thomas Stachel, Tom E. McCandless, John Armstrong and Karlis Muehlenbachs: Diamonds from the Renard Kimberlites in Quebec

4.1. Introduction

The Superior Craton of Eastern Canada is the largest known continuous region of Archean crust in the world. Whilst the crustal evolution is well understood, little is known about the underlying sub-continental lithospheric mantle (SCLM). Mantle derived xenoliths and xenocrysts provide information on the formation and history of the lithospheric mantle, but may not be representative of the SCLM at the time of diamond formation, due to a complex subsequent history (Stachel *et al.*, 1998b; Griffin *et al.*, 1999). The study of diamonds and the mineral inclusions within them provides an alternative means of directly sampling the Earth's upper mantle. During the growth of diamonds, syngenetic mineral inclusions can be trapped and enclosed within them (Harris, 1968). As diamonds are chemically inert inclusions are protected from chemical alteration, preserving their original mantle signature during their mantle residence and transport to the surface. Inclusions, therefore, provide the only pristine information on the cratonic mantle at the time of diamond formation.

Our study of diamonds from the Renard kimberlites complements previous work on mantle xenoliths/xenocrysts and diamonds from the Superior Craton (e.g. Sage *et al.* (1996) , Scully (2000), Armstrong *et al.* (2004), Griffin *et al.* (2004), Scully *et al.* (2004), Stachel *et al.* (2006), Hunt *et al.* (in press)) and provide new information on the SCLM. A comprehensive study on the carbon isotopic composition of the diamonds was performed to identify the possible diamond forming agents. Inclusion and nitrogen based thermometry was used to constrain the physical conditions

of diamond formation and mantle residence. The composition of syngenetic and epigenetic mineral inclusions provided information on the composition and evolution of the SCLM during and after diamond growth.

4.2. Geological Background

The Renard bodies are located within a 2km^2 area in the northern Otish Mountains of Quebec (Fig. 4.1), 820km north of Montreal. Ashton Mining of Canada (now Stornoway Diamond Corporation) and its joint venture partner Soquem Inc. discovered the pipes in 2001. The initial discovery identified ten kimberlite pipes. Later work determined that Renard 5 and 6 joined at depth, and consequently the name Renard 65 was introduced (Fig. D1). Of these nine pipes, four are of particular economic interest due to high diamond grades: Renard 2, 3, 4 and 9.

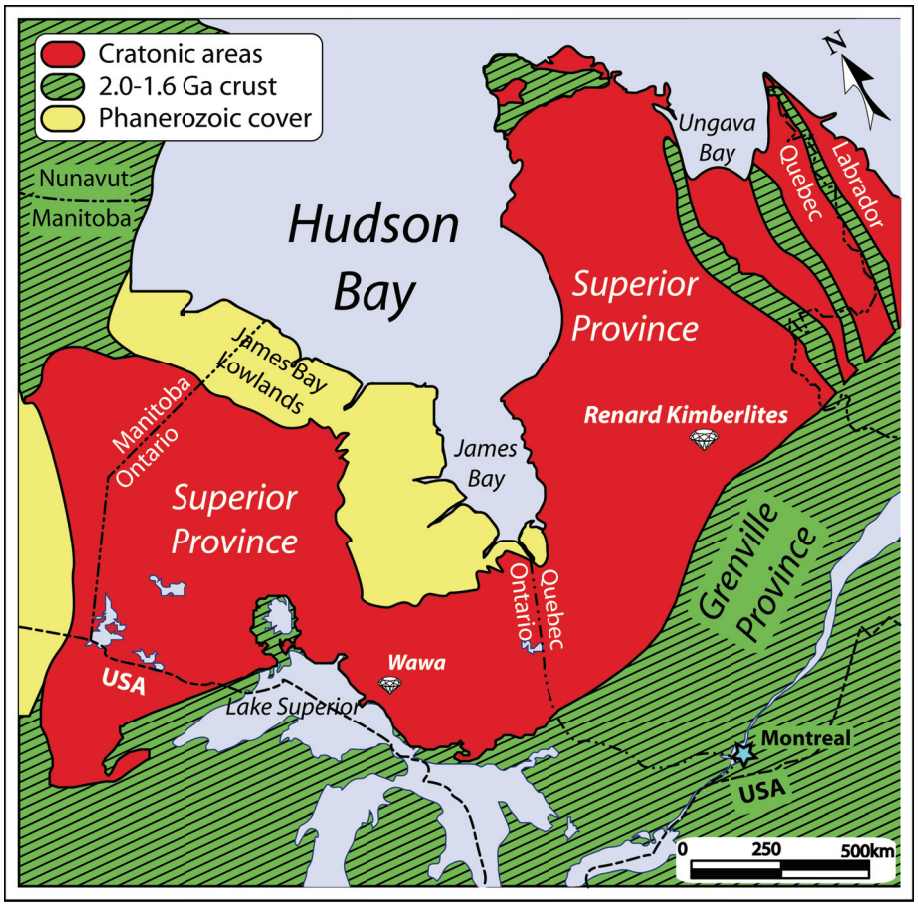

Figure 4.1. Simplified geological map of the Superior Province and adjacent areas showing the location of the Renard Kimberlites (redrawn using information from: Hoffman, 1988; Card, 1990; Percival *et al.*, 1992).

The Renard kimberlites classify as Group I (Birkett *et al.*, 2004; Fitzgerald *et al.*, 2008) and are part of the Otish kimberlitic volcanic event. Emplacement has been dated to the Neoproterozoic (631.6±3.5 Ma Birkett *et al.*, 2004: 640.5±2.8Ma Fitzgerald *et al.*, 2008). This is broadly coeval with the conversion from subduction magmatism to rifting in northern Laurentia (Birkett *et al.*, 2004). The kimberlites are emplaced into Archean granitic and gneissic host rocks of the Opinaca Subprovince (Percival, 2007). Xenoliths and xenocrysts from the kimberlites also indicate a late Archean age for the formation of the SCLM beneath Renard (Hunt *et al.*, in press).

4.3. Samples

Our study is based on a subset of 56 diamonds, strongly biased toward inclusion bearing stones, from mini-bulk samples from five of the nine Renard kimberlite pipes: Four from Renard 1; 15 from Renard 2; eight from Renard 3; 17 from Renard 4; and 12 from Renard 65. The diamonds were selected from the +0.85mm to +3.35mm square mesh sieve size fractions, and range in weight from 1.5-152.8mg (table 4.1).

All the diamonds were visually studied and classified based on their physical characteristics. Inclusions were recovered from 33 of the diamonds and analysed with an electron microprobe. All diamonds were analysed for their carbon isotopic composition and their nitrogen content and aggregation state.

4.4. Analytical Techniques

4.4.1. Inclusions

Inclusions were identified, where possible, with the aid of a stereomicroscope, prior to diamond breakage. At this time, the inclusions were evaluated for possible alteration through fractures connecting to the diamond surface. Mineral inclusions were then released from the diamonds using a steel breaker. The recovered inclusions were mounted in brass pips using Araldite® epoxy resin and polished. After several steps using increasingly finer polishing media, they were finished using 0.05μm alumina suspension on a polishing wheel.

The minor and major element composition of inclusions were measured by wavelength-dispersion spectrometry (WDS) on a JEOL JXA-8900 Superprobe at the University of Alberta. Silicate, oxide and metal standards were used and analyses were conducted with an accelerating voltage of 20kV and a beam current of 20nA. Peak counting times for each element were 30-60 seconds with half the time on each background. Where possible three spots were measured on each sample and averaged, in cases where the grains were determined to be homogeneous. For averaged analyses, detection limits are ≤0.01wt% for all oxides with the exception of Na_2O (≤0.02wt%) and P_2O_5 (≤0.03wt%).

$Mg\#_{Ca\text{-}corr.}$ ($Mg\#_{Ca\text{-}corr.}$ = Mg# + 2Ca, Ca as cations calculated on a basis of 24 oxygens, following Stachel *et al.*, 2008) is given for garnet inclusions to account for the effect of CaO on Mg/Fe partitioning between garnet and Mg-Fe silicates (O'Neill and Wood, 1979).

4.4.2. Nitrogen Content and Aggregation State

The concentration and aggregation state of nitrogen impurities within the diamonds was determined by FTIR spectrometry using a Thermo-Nicolet Nexus 470 FTIR spectrometer coupled with a Nicolet Continuum infrared microscope. The spectra were collected for 200 seconds in transmittance mode for a range in wave number from 650 to 4000cm^{-1}. An aperture of 100μm was used, and the spectral resolution was 4cm^{-1}.

A Type II diamond standard was analysed, baseline corrected and converted to absorption coefficient (absorbance of a sample of 1cm thickness) through normalisation of the absorbance at 1995cm^{-1} to 11.94cm^{-1}. The sample spectra were also baselined and then, through a combined subtraction and normalisation procedure involving the Type II diamond spectrum, converted to absorption coefficient. Sample spectra were de-convoluted into the A, B and D components based on software provided by David Fisher (Research Laboratories of the Diamond Trading Company, Maidenhead, UK). Concentrations of nitrogen (atomic ppm) were calculated using

absorption coefficient values at 1282cm^{-1} using the factors derived by Boyd *et al.* (1994) for the A-centre and Boyd *et al.* (1995) for the B-centres.

Analyses were performed on fragments of broken diamonds. Multiple analyses on each diamond were completed in order to detect variations in the nitrogen content and aggregation state within individual stones. The detection limits depend strongly on the quality of the fragments, but are generally in the range 5–15 at. ppm, with relative errors for concentration and aggregation state for each measurement being at the level of ~5–10%.

4.4.3. Carbon Isotopic Composition

The carbon isotopic composition of the diamonds was determined using a Finnigan MAT 252 dual inlet mass spectrometer at the University of Alberta. Inclusion and graphite free diamond fragments (0.3–2mg) were combusted (at 980°C) in a sealed and evacuated quartz glass tube for ~12 hours with ~1.0-2.0g of CuO as an oxygen source. The results are reported relative to the V-PDB standard (Coplen *et al.*, 1983). Instrumental precision is in the order of ±0.02‰.

4.5. Results

4.5.1. Diamond Characteristics

4.5.1.1. Morphology

The morphologies of the diamonds include primary octahedra and secondary resorbed rounded dodecahedral shapes. Pseudohemimorphic stones, showing differential resorption, indicating the diamond protruded from a xenolith during kimberlite ascent, are also present. Diamonds which show a herringbone line, defining the compositional plane of a twin, are identified as macles. Samples comprising irregular intergrowth of two or more stones with no prominent twin line are classified as aggregates. Diamond fragments and other types of irregular stones are categorised according to their residual features.

The diamonds are predominantly rounded dodecahedra (50%) with a further 14% remaining as primary octahedra. Macles and aggregates each comprise 16% of the sample set. The remainder of the diamonds are pseudohemimorphic (4%) (Table 4.1). Assuming similar classification criteria, morphological differences observed in this research vary slightly from larger populations of Renard diamonds classified by Stornoway Diamond Corp.. An unbiased selection of 97 unbroken stones from Renard 2, in the same size range, consist of 7% octahedra, 45% dodecahedra, 7% twins and 41% aggregates (McCandless pers. comms). In contrast to 15 stones from Renard 2 analysed for this research, comprising 7% octahedra, 47% dodecahedra, 27% macles and 20% aggregates.

4.5.1.2. Colour

The 56 Renard diamonds examined are colourless or exhibit either yellow or brown to pink-brown colouration of varying intensity. Yellow colouration is produced by nitrogen impurities giving rise to N3 and N2 centres within diamond (Collins, 1982). Brown and pink colouration is caused by plastic deformation and is attributed to the formation of defects in the diamond lattice due to strain (Harris, 1987).

The majority of the diamonds have a pale/very pale yellow (38%) or a pale/very pale brown colour (23%). A further 2% have a stronger yellow colour, 9% have a stronger brown colour and 2% have a pink brown colour. The remaining 27% are colourless (Table 4.1). No correlation is observed between morphology and colour.

4.5.1.3. Surface Features

The surface features observed on the 56 diamonds relate to the morphology of the diamond, with specific features associated with dodecahedral faces, and others seen only on octahedral faces. Due to the predominance of dodecahedral diamonds, surface features related to resorption of primary octahedral growth layers are dominant.

Terracing and hillocks on dodecahedral faces are the most abundant surface features – observed on 36% and 50% of the diamonds respectively. Trigons are present on all octahedra and are common (45%) on residual octahedral faces. Plastic

Table 4.1. Table of the Renard diamond characteristics, including morphology, colour and main surface features (n=56).

Diamond	Pipe #	Weight (mg)	Morphology	Colour	Surface Features								
					trigons	stacked g.l.	hillocks	terr.	def. lines	herringbone twin	tetra.	green spots	microdisks
12026	1	7	d.oct.	v.p.y.	x	x							
12027	1	4	imp.oct.	clls.	x	x							
12029	1	24	d.oct.	v.p.br.		x							
12031	1	8	p.rsb.oct.mac.	v.p.y.	x		x		x	x			
12036a	2	17	dodec.agg.(2)mac.	v.p.y.			x		x	x			
12036b	2	10	dodec.agg.(2)mac.	v.p.y.	x		x						
12040	2	2	agg.(2)dodec.resoct.	clls.	x		x	x					
12041	2	119	irr.flt.dodec.	v.p.y.							x		
12042	2	11	dodec.resoct.	v.p.y.	x		x		x				
13527	2	3	dodec.frag.	clls.			x		x			x	
13528a	2	6	oct.agg.(2)	clls.		x							
13528b	2	7	irr.elon.dodrsp.	v.p.y.			x		x				
13803a	2	4	oct.cl.frag.	clls.									
13803b	2	3	irr.elon.dodrsp.resoct.	p.y.	x								
13803c	2	7	tri.agg.(2)mac.	p.br.		x				x	x		
13804a	2	2	oct.agg.(3)	clls.	x	x							
13804b	2	4	dodec.	p.br.				x	x				
13805a	2	12	d.dodec.	br.			x	x	x				
13805b	2	16	flt.dodec.mac.	v.p.br.			x		x	x			
13530a	3	47	dodec.	v.p.y.			x	x	x				
13530b	3	16	flt.oct.agg.(2)	clls.	x	x							
13530c	3	16	flt.dodec.mac.	clls.			x	x	x	x			
13531a	3	6	irr.dodrsp.	p.y.					x				
13531b	3	51	flt.tri.dodec.resoct.	p.y.	x		x		x				
13532a	3	4	flt.dodec.	p.br.	x		x	x	x				
13532b	3	21	dodec.	v.p.y.			x	x	x			x	
13533	3	9	dodec.mac.resoct.	clls.			x		x	x			
13520	4	9	dodec.frag.	br.			x		x	x			
13521a	4	4	d.dodec.	v.p.br.			x						
13521b	4	3	d.dodec.	clls.			x		x				

Table 4.1. cont.

Diamond	Pipe #	Weight (mg)	Morphology	Colour	Surface Features								
					trigons	stacked g.l.	hillocks	terr.	def. lines	herringbone twin	tetra.	green spots	microdisks
13521c	4	7	dodec.frag.	v.p.y.	x		x	x					
13523	4	17	pseudo.	v.p.br.	x			x	x		x		
13524	4	2	flt.dodec.	v.p.y.			x	x					
13536	4	5	pseudo.	v.p.y.	x	x		x					
13537	4	3	oct.frag.	clls.	x			x					
13538	4	14	irr.agg.(2+)dodec.resoct.	p.br.	x			x					
13539a	4	3	dodec.frag.	p.y.	x			x				x	
13539b	4	3	flt.elon.oct.	p.br.		x							
13540	4	3	irr.dodec.frag.	p.br.	x			x					
13544	4	4	oct.	y.			x					x	
13545	4	6	dodec.mac.frag.	p.y.			x			x			
13547a	4	8	dodec.frag.	p.y.	x			x	x				
13547b	4	29	d.dodec.resoct.	clls.	x			x					
13548	4	30	oct.mac.	p.br.	x	x			x				
12001	65	2	dodec.	br.			x		x				x
12003	65	12	dodec.frag.	p.br.			x		x			x	
12004	65	4	dodec.	pk.br.			x		x			x	
12006a	65	4	dodec.	br.			x	x	x			x	
12006b	65	153	dodec.	br.			x	x	x		x	x	
12011	65	8	dodec.frag.	clls.								x	
12012	65	3	dodec.agg.(2)frag.	v.p.y.			x					x	
12013	65	5	oct.agg.(2)frag.dodrsp.	v.p.br.	x	x							
12014	65	6	flt.dodec.mac.	v.p.y.	x				x			x	
12016a	65	3	flt.irr.agg.(2)dodrsp.resoct.	clls.			x						
12016b	65	3	flt.oct.agg.(2)	clls.	x							x	
12018	65	4	flt.dodec.	p.y.				x				x	

mac.-macle
irr. - irregular
oct. - octahedra
dodec. - dodecahedra

br. - brown
y. - yellow
pk. - pink
clls. - colourless

p. - pale
v.p. - very pale

tri. - triangular
frag. - fragment
cl. - cleavage
d. - distorted

imp. - imperfect
rsb. - resorbed
p.rsb. - partially resorbed

agg.(#) - aggregate (no. of stones in agg.)
resoct. - minor residual octahedra remains

flt. - flattened
elon. - elongate
dodrsp. - dodecahedral resorption features

stacked g.l. - stacked growth layers
terr. - terracing
def.lines - deformation lines
tetra. - tetragons

deformation lines are observed on 46% of the diamonds and are commonly associated with brown colouration. Other surface features observed include: stacked growth layers with both shield and serrate laminae; tetragons on {100} fracture faces; and, observed in only one case, a microdisk pattern (Table 4.1).

Dark green spots were recognised on 23% of the samples and are particularly abundant in pipes 65, where 75% of the stones have one or more green spots. These spots result from defects in the diamond lattice caused by alpha particle irradiation, and as they have very low penetration depth, indicate prolonged contact with radioactive minerals (Meyer *et al.*, 1965; Harris, 1987).

One diamond (also from pipe 65) exhibits elongate green depressions on its faces (Fig. 4.2). The outside of the diamond is irregular, which may represent a partially resorbed coat. The depressions are interpreted as voids left by mineral inclusions which formed within the diamond coat and have subsequently been removed. The green colouration is interpreted as forming from processes similar to those which produced the green spots. If the inclusions were enriched in radioactive elements, as would be the case for minerals such as zircon or apatite, then the green colouration would form during prolonged contact of the diamond with the inclusions.

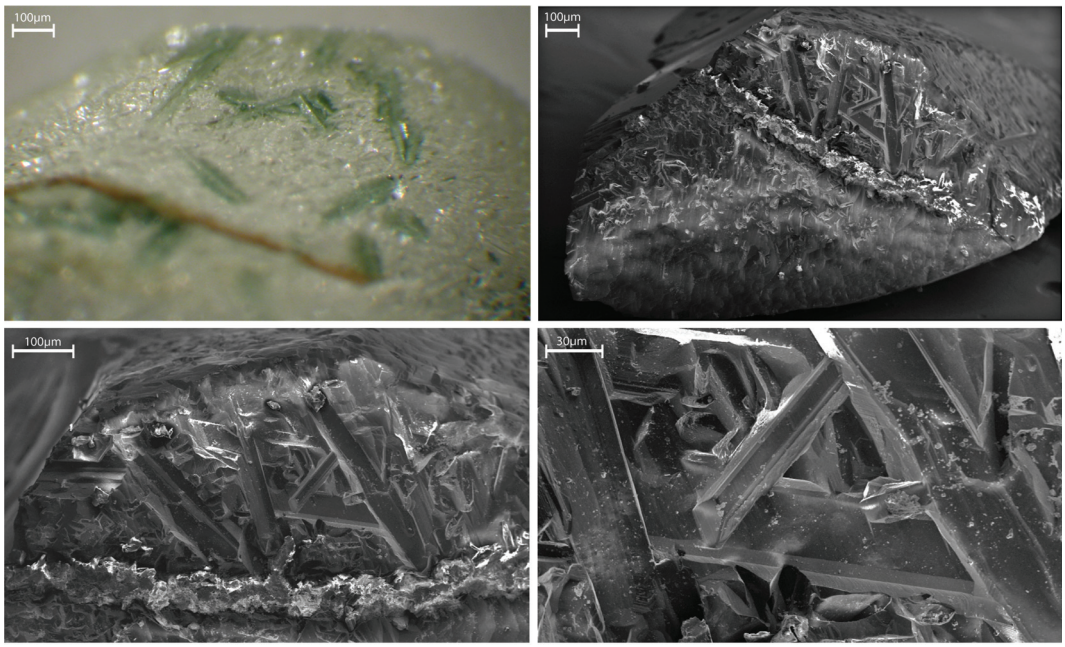

Figure 4.2. Photo and SEM figures of elongate green depressions observed on stone 12011.

4.5.2. Inclusions in Diamond

4.5.2.1. Syngenetic Inclusions

4.5.2.1.1. Olivine

Olivine is the dominant mineral inclusion within the Renard suite. Sixty-three olivine inclusions were recovered from 16 diamonds. The olivines have Mg-numbers (Mg#) ranging from 92.1 to 94.3 with a mean of 92.7 (Fig. 4.3, Table 4.2), with variations within individual stones (ΔFo) up to 0.4-0.5 (e.g. 12036b ΔFo 0.37, 13547b Δ Fo 0.45 and 13805a ΔFo 0.45). The mean falls between the worldwide mean of lherzolitic and harzburgitic diamond inclusion olivines (92.1 and 93.2, respectively: e.g. Stachel and Harris, 2008), and coincides with the mean of samples of unknown, likely mixed, parageneses (Stachel and Harris, 2008). This was confirmed statistically with a student t-test, by comparing the olivine inclusions with all three groupings in the database of Stachel and Harris (2008). The test indicated that, with

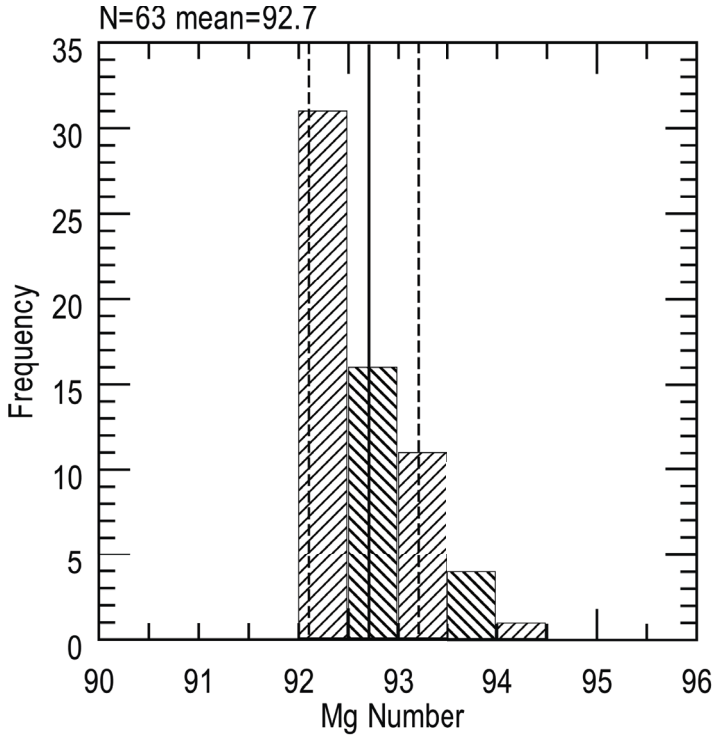

Figure 4.3. Renard inclusion olivine Mg#, solid line represents mean (92.7). Dashed lines represent mean worldwide lherzolitic (92.1) and harzburgitic (93.2) Mg# for olivine inclusions (Stachel and Harris, 2008), as well as the mean Mg# (93.2) for Renard xenolithic harzburgitic olivine (Hunt et al., in press).

a 99% confidence, the olivines were not purely harzburgitic or lherzolitic However, the test accepted with a 99% confidence limit that Renard olivine inclusions were the same as worldwide olivine inclusions from mixed, mostly unknown, parageneses. No clear paragensis can, therefore, be defined, although the range does encompass the composition of harzburgitic olivines in microxenoliths from the Renard kimberlites (92.7-93.5, mean 93.2: Hunt *et al.*, in press).

Two olivines from one diamond (13539a) have CaO contents of 0.05wt% indicating a high likelihood that they crystallised in equilibrium with clinopyroxene. The remainder all have CaO contents ≤0.04wt% CaO, which may be suggestive of a harzburgitic paragenesis. Precipitation of lherzolitic olivine along a "cool" geothermal gradient and in the uppermost part of the diamond stability field could, however, equally explain CaO contents as low as 0.01wt% (Stachel *et al.*, 2009).

4.5.2.1.2. Orthopyroxene

Five orthopyroxenes were recovered from three diamonds: two from 13521c; one from 13532a; and two from 13538. All have Al_2O_3 contents between 0.4-0.7wt%, and CaO contents from 0.1-0.8wt%. Two orthopyroxenes from diamond 13521c have Mg# of 94.6, two orthopyroxenes from diamond 13538 have Mg# of 93.6, and the orthopyroxene from diamond 13532a has an Mg# of 93.0 (Table 4.2). Using the CaO vs. Mg# discrimination diagram of Stachel and Harris (2008), orthopyroxenes from diamonds 13538 and 13532a fall within the region occupied by both harzburgitic and lherzolitic inclusions. The inclusions from stone 13521c, however, fall in the compositional space for harzburgitic inclusions only. This agrees with orthopyroxenes in microxenoliths from the Renard kimberlites, which have Mg# from 93.2-94.3 (mean 93.8) for the harzburgitic paragenesis and Mg# from 88.1-93.8 (mean 92.6) for the lherzolitic paragenesis (Hunt *et al.*, in press).

4.5.2.1.3. Garnet

Two garnet inclusions were recovered from two stones: 12013 and 13523. The garnets are chrome pyropes, with concentrations of 3.1 and 3.8wt% CaO, 8.7

Table 4.2. Table of the syngenetic inclusion electron microprobe data.

Mineral	Olv	Olv	Gnt	Olv	Olv	SiO_2	SiO_2	Olv	SiO_2	Chr	Chr	Chr	Chr	Olv	SiO_2
Sample	12001-2	12001-1	12013-1	12013-2	12013-6	12014-2	12014-4	12016a-3	12018-3	12031-2	12031-3	12031-113	12031-111	12036a-2	12036a-6
Paragen.	p			p(H)		?		p	?			p		p	
Assem.	olv			olv, gnt		SiO_2		olv	SiO_2			chr		olv,SiO_2	
TiO_2	≤0.00	≤0.00	0.03	≤0.00	≤0.00	≤0.00	≤0.00	≤0.00	≤0.00	0.03	0.03	0.02	0.04	0.01	0.16
Al_2O_3	≤0.00	0.01	16.57	0.03	0.03	0.02	0.04	0.01	0.19	7.27	7.72	7.70	7.55	0.01	1.42
P_2O_5	0.01	≤0.00	≤0.00	0.01	0.01	≤0.00	≤0.00	0.01	≤0.00	≤0.00	≤0.00	0.01	≤0.00	≤0.00	≤0.00
Na_2O	0.02	0.01	0.01	0.01	0.01	0.01	0.01	0.01	0.02	0.02	0.02	0.01	0.01	0.02	0.05
NiO	0.34	0.36	0.01	0.33	0.33	≤0.00	≤0.00	0.35	≤0.00	0.10	0.09	0.11	0.10	0.35	0.01
Cr_2O_3	0.03	0.07	8.68	0.07	0.07	≤0.00	≤0.00	0.05	≤0.00	63.52	63.56	65.30	64.51	0.06	≤0.00
SiO_2	40.29	41.31	41.17	40.61	40.38	101.56	101.24	40.23	100.38	0.24	0.18	0.26	0.23	40.49	98.25
CaO	0.02	0.04	3.06	0.03	0.03	0.01	≤0.00	0.03	≤0.00	≤0.00	≤0.00	≤0.00	≤0.00	0.03	0.05
MgO	50.55	50.40	23.21	51.47	52.20	≤0.00	0.01	53.09	0.01	14.82	14.67	14.97	15.20	50.41	0.11
FeO	7.55	7.74	6.34	7.41	7.33	1.13	1.20	7.77	0.01	13.72	14.01	14.14	14.02	7.10	0.11
K_2O	≤0.00	≤0.00	≤0.00	≤0.00	≤0.00	≤0.00	≤0.00	≤0.00	≤0.00	≤0.00	≤0.00	≤0.00	≤0.00	≤0.00	0.31
MnO	0.11	0.12	0.35	0.14	0.14	0.03	0.03	0.12	≤0.00	0.39	0.41	0.38	0.36	0.11	0.01
V_2O_3	≤0.00	≤0.00	0.05	≤0.00	≤0.00	≤0.00	≤0.00	0.01	≤0.00	0.21	0.23	0.22	0.22	0.01	≤0.00
Total	98.93	100.05	99.46	100.10	100.53	102.75	102.54	101.68	100.62	100.31	100.93	103.13	102.24	98.58	100.47
Mg#	92.27	92.07	86.71	92.53	92.69			92.42		65.83	65.12	65.35	65.89	92.68	

Mineral	SiO_2	Olv	Olv	SiO_2	Olv	Olv	SiO_2	Olv	Olv	Olv	Olv	Olv	SiO_2	Olv	Olv
Sample	12036a-8	12036a-12	12036a-19	12036a-20	12036b-1	12036b-3	12036b-4	12036b-6	12036b-7	12036b-114	12036b-116	12036b-117	12036b-121	12035b-115	12035b-118
Paragen.	p								p					p	
Assem.	olv,SiO_2								olv, SiO_2					olv	
TiO_2	≤0.00	≤0.00	≤0.00	0.01	≤0.00	0.01	≤0.00	≤0.00	≤0.00	≤0.00	≤0.00	0.01	≤0.00	≤0.00	0.01
Al_2O_3	0.03	0.02	0.03	0.01	0.01	0.02	0.02	0.27	0.10	0.40	0.02	0.01	0.01	0.05	0.02
P_2O_5	≤0.00	≤0.00	≤0.00	≤0.00	0.01	≤0.00	≤0.00	0.01	0.01	≤0.00	0.01	0.01	≤0.00	0.01	≤0.00
Na_2O	0.02	0.02	0.02	≤0.00	0.01	0.02	≤0.00	0.01	0.02	0.02	0.02	0.01	≤0.00	0.02	0.02
NiO	≤0.00	0.35	0.35	≤0.00	0.34	0.35	≤0.00	0.34	0.35	0.33	0.32	0.36	≤0.00	0.34	0.33
Cr_2O_3	≤0.00	0.06	0.06	≤0.00	0.06	0.06	≤0.00	0.05	0.06	0.04	0.05	0.06	0.01	0.06	0.06
SiO_2	101.18	40.78	40.24	99.10	41.10	40.63	100.32	40.19	40.91	40.03	38.71	40.08	100.59	39.97	41.82
CaO	≤0.00	0.03	0.03	≤0.00	0.03	0.03	≤0.00	0.03	0.04	0.03	0.04	0.03	0.01	0.04	0.03
MgO	≤0.00	50.71	49.92	≤0.00	50.90	50.50	≤0.00	51.17	50.90	50.41	53.24	51.58	0.01	51.86	50.57
FeO	0.01	7.28	7.25	0.01	7.26	7.15	1.07	7.54	7.05	7.16	7.25	7.35	≤0.00	7.24	7.31
K_2O	≤0.00	≤0.00	≤0.00	≤0.00	≤0.00	≤0.00	≤0.00	≤0.00	≤0.00	≤0.00	≤0.00	≤0.00	≤0.00	≤0.00	≤0.00
MnO	0.01	0.11	0.10	0.01	0.11	0.10	0.01	0.16	0.10	0.10	0.10	0.13	0.01	0.11	0.11
V_2O_3	≤0.00	≤0.00	≤0.00	≤0.00	0.01	≤0.00	≤0.00	≤0.00	0.01	≤0.00	≤0.00	≤0.00	≤0.00	≤0.00	≤0.00
Total	101.24	99.37	98.01	99.12	99.84	98.86	101.43	99.77	99.55	98.51	99.76	99.61	100.62	99.69	100.29
Mg#		92.55	92.47		92.59	92.64		92.36	92.79	92.62	92.90	92.60		92.74	92.50

Table 4.2. cont.

Mineral	Olv	Olv	Olv	Olv	Olv	Chr	SiO_2	Opx	SiO2	Opx	Olv	Olv	Garnet	Olv	Chr
Sample	12041-1	12041-2	12041-3a	12041-5	12041-6	13520-9	13521b-1	13521c-1	13521c-3	13521c-4	13523-6	13523-7	13523-8	13530a-110	13530a-110b
Paragen.			p			p	?		p			p(H)		p	
Assem.			olv			chr	SiO_2		opx, SiO_2			olv, gnt		olv, chr	
TiO_2	≤0.00	≤0.00	≤0.00	≤0.00	≤0.00	0.04	≤0.00	0.01	≤0.00	0.01	≤0.00	≤0.00	0.06	0.01	0.13
Al_2O_3	0.02	0.05	0.02	0.04	0.01	6.50	0.01	0.72	0.02	0.71	0.02	0.05	16.11	0.01	7.90
P_2O_5	0.01	0.01	≤0.00	0.01	≤0.00	0.01	≤0.00	≤0.00	≤0.00	0.01	0.01	0.01	0.01	≤0.00	≤0.00
Na_2O	0.03	0.01	0.01	0.03	0.01	0.02	0.01	0.04	0.01	0.03	0.02	0.02	0.03	0.02	0.03
NiO	0.36	0.37	0.36	0.36	0.34	0.09	0.01	0.11	≤0.00	0.11	0.35	0.35	0.01	0.34	0.07
Cr_2O_3	0.07	0.06	0.06	0.06	0.06	65.28	≤0.00	0.51	≤0.00	0.54	0.04	0.05	10.15	0.06	65.73
SiO_2	40.58	40.08	40.37	41.32	38.72	0.22	100.89	58.12	96.22	57.44	41.09	41.18	41.66	41.24	0.10
CaO	0.04	0.04	0.03	0.04	0.03	≤0.00	0.01	0.11	≤0.00	0.12	0.02	0.02	3.81	0.02	≤0.00
MgO	51.23	50.89	50.72	50.07	50.78	14.53	≤0.00	36.16	0.01	36.56	50.93	50.59	22.27	52.41	14.44
FeO	7.59	7.60	7.66	7.43	7.64	14.12	≤0.00	3.68	≤0.00	3.73	7.11	7.03	5.87	5.65	13.39
K_2O	≤0.00	≤0.00	≤0.00	≤0.00	≤0.00	≤0.00	≤0.00	≤0.00	≤0.00	≤0.00	0.01	0.01	≤0.00	≤0.00	≤0.00
MnO	0.11	0.11	0.10	0.11	0.12	0.37	0.01	0.10	0.01	0.10	0.09	0.11	0.31	0.08	0.37
V_2O_3	≤0.00	≤0.00	≤0.00	0.01	≤0.00	0.17	≤0.00	0.01	≤0.00	0.01	≤0.00	≤0.00	0.03	≤0.00	0.15
Total	100.03	99.24	99.34	99.45	97.71	101.36	100.94	99.56	96.27	99.36	99.67	99.39	100.32	99.84	102.33
Mg#	92.33	92.27	92.19	92.32	92.22	64.71		94.60		94.59	92.74	92.77	87.12	94.29	65.78

Mineral	Olv	Olv	Olv	Chr	Chr	Chr	Chr	Chr	Chr	Chr	Chr	Chr	Chr	Chr	Cpx
Sample	13530b-113	13530b-114	13530b-115	13530b-115	13530c-1	13530c-2	13530c-3	13530c-3	13530c-4	13530c-5	13530c-6	13530c-112	13530c-113	13530c-114	13532a-1
Paragen.		p							p						p(L)
Assem.		olv, chr							chr						cpx, opx
TiO_2	0.01	≤0.00	0.01	0.13	0.13	0.12	0.13	0.13	0.14	0.12	0.12	0.14	0.13	0.14	0.16
Al_2O_3	0.01	0.17	0.05	7.49	7.87	7.98	7.79	7.61	7.80	7.68	7.76	7.71	7.86	7.71	0.05
P_2O_5	0.01	0.01	0.01	0.01	0.01	≤0.00	≤0.00	≤0.00	≤0.00	≤0.00	≤0.00	≤0.00	0.01	0.01	≤0.00
Na_2O	0.02	0.02	0.02	0.02	0.02	0.01	≤0.00	0.03	0.02	0.01	≤0.00	0.01	0.01	0.01	0.18
NiO	0.31	0.31	0.32	0.09	0.10	0.09	0.10	0.09	0.10	0.09	0.09	0.09	0.09	0.10	0.01
Cr_2O_3	0.10	0.09	0.09	65.64	64.64	63.74	64.48	64.18	64.62	64.41	64.52	65.77	65.97	65.48	0.19
SiO_2	40.92	41.04	41.06	0.21	0.20	0.22	0.19	0.23	0.21	0.19	0.22	0.21	0.21	0.20	54.32
CaO	0.02	0.02	0.02	≤0.00	0.01	≤0.00	0.01	0.01	0.01	0.01	≤0.00	≤0.00	0.01	≤0.00	25.09
MgO	51.61	51.43	51.92	14.81	15.71	15.82	16.11	15.45	15.84	15.31	15.47	15.68	15.19	15.66	17.07
FeO	6.03	6.17	6.09	12.66	12.21	12.14	12.26	12.40	12.24	12.14	12.37	12.66	12.73	12.62	1.63
K_2O	≤0.00	≤0.00	≤0.00	≤0.00	≤0.00	≤0.00	≤0.00	≤0.00	≤0.00	≤0.00	≤0.00	≤0.00	≤0.00	≤0.00	0.03
MnO	0.08	0.08	0.09	0.36	0.36	0.35	0.38	0.32	0.37	0.36	0.33	0.34	0.35	0.35	0.07
V_2O_3	≤0.00	≤0.00	≤0.00	0.15	0.15	0.16	0.16	0.16	0.17	0.18	0.17	0.17	0.15	0.16	0.01
Total	99.13	99.36	99.65	101.58	101.41	100.64	101.60	100.58	101.52	100.49	101.07	102.78	102.73	102.44	98.80
Mg#	93.85	93.69	93.83	67.58	69.64	69.91	70.07	68.96	69.75	69.21	69.04	68.82	68.02	68.86	94.93

Table 4.2. cont.

Mineral	Opx	Chr	Chr	Chr	Chr	Chr	Chr	Chr	SiO_2	SiO_2	Olv	Olv	Opx	Opx	Olv
Sample	13532a-3	13533-1	13533-2	13533-3a	13533-3b	13533-3c	13533-4a	13533-4b	13533-7	13533-8	13533-111	13537-2	13538-1	13538-4	13539a-1
Paragen.	p(L)	p										p	p		p
Assem.	cpx, opx	chr, olv, SiO_2										olv	opx		olv
TiO_2	0.02	0.05	0.06	0.06	0.05	0.05	0.05	0.05	≤0.00	0.00	0.01	0.01	0.01	0.01	≤0.00
Al_2O_3	0.39	6.76	6.56	6.48	6.50	6.48	6.47	6.60	0.06	0.02	0.02	0.01	0.45	0.50	0.01
P_2O_5	0.01	0.01	0.01	0.01	0.00	0.01	≤0.00	0.01	≤0.00	≤0.00	0.01	0.01	0.01	0.00	0.01
Na_2O	0.14	0.03	0.02	0.01	0.01	0.01	0.03	0.01	0.01	0.01	0.02	0.02	0.05	0.04	0.01
NiO	0.11	0.10	0.10	0.10	0.10	0.10	0.08	0.10	≤0.00	≤0.00	0.33	0.34	0.11	0.10	0.36
Cr_2O_3	0.33	65.80	65.35	66.30	66.37	66.37	66.31	65.88	≤0.00	0.01	0.06	0.06	0.30	0.38	0.05
SiO_2	58.38	0.21	0.25	0.28	0.21	0.27	0.27	0.28	102.21	99.78	40.90	41.80	56.79	54.74	41.32
CaO	0.81	0.01	0.01	0.01	0.00	0.01	≤0.00	0.00	≤0.00	0.00	0.02	0.03	0.42	0.53	0.05
MgO	35.29	14.67	14.91	14.78	14.87	14.58	14.07	14.85	0.01	0.01	50.80	49.84	36.31	36.48	51.54
FeO	4.75	14.04	13.97	14.17	14.16	14.16	14.15	14.07	0.01	0.00	7.24	7.38	4.46	4.45	7.68
K_2O	≤0.00	≤0.00	≤0.00	≤0.00	0.00	≤0.00	0.00	≤0.00	≤0.00	0.00	0.00	0.00	≤0.00	≤0.00	0.00
MnO	0.14	0.38	0.35	0.37	0.38	0.37	0.38	0.37	0.01	≤0.00	0.11	0.14	0.11	0.11	0.11
V_2O_3	0.00	0.18	0.17	0.19	0.17	0.17	0.18	0.18	≤0.00	≤0.00	≤0.00	0.00	0.00	0.01	≤0.00
Total	100.36	102.23	101.76	102.73	102.83	102.59	102.00	102.40	102.30	99.84	99.52	99.62	99.01	97.36	101.14
Mg#	92.98	65.07	65.55	65.04	65.18	64.73	63.93	65.29			92.60	92.33	93.56	93.60	92.29

Table 4.2. cont.

Mineral	Olv	Olv	SiO_2	SiO_2	Cpx	Olv	Olv	Olv	Olv	Olv	Olv	Olv	Olv	Olv	Olv
Sample	13539a-4	13539a-5	13539b-1	13539b-2	13544-1a	13547b-1	13547b-2	13547b-3	13547b-3	13547b-4	13547b-5	13547b-6a	13547b-7	13547b-9	13547b-10
Paragen.	p		?		p(L)					p					
Assem.	olv		SiO_2		cpx					olv					
TiO_2	0.01	≤0.00	0.00	0.00	1.62	0.00	≤0.00	0.00	0.00	0.00	≤0.00	0.00	0.00	0.01	0.00
Al_2O_3	0.02	0.01	0.21	0.06	0.86	0.10	0.01	0.00	0.00	0.01	0.01	0.00	0.02	0.01	0.02
P_2O_5	0.01	0.01	0.00	0.00	0.02	≤0.00	0.01	0.00	0.00	≤0.00	≤0.00	0.01	0.01	≤0.00	0.00
Na_2O	0.01	0.01	0.01	0.00	1.10	0.01	0.01	0.01	0.02	0.02	0.01	0.01	0.02	0.01	0.01
NiO	0.33	0.36	0.00	0.00	0.02	0.37	0.36	0.36	0.36	0.36	0.35	0.36	0.36	0.37	0.35
Cr_2O_3	0.05	0.05	0.00	0.00	0.02	0.03	0.07	0.03	0.03	0.07	0.06	0.04	0.07	0.04	0.06
SiO_2	42.70	39.24	99.36	101.89	52.13	40.43	41.22	41.45	41.58	40.83	40.64	40.44	40.95	40.84	40.91
CaO	0.05	0.04	0.00	0.01	22.82	0.02	0.04	0.03	0.02	0.04	0.04	0.02	0.04	0.02	0.04
MgO	51.01	51.11	0.01	0.00	14.27	51.33	50.99	50.86	52.17	50.30	52.36	51.11	50.95	50.53	51.21
FeO	7.54	7.60	1.19	1.12	6.07	7.69	7.77	7.75	7.71	7.73	7.63	7.68	7.77	7.66	7.62
K_2O	≤0.00	≤0.00	0.04	0.01	≤0.00	≤0.00	≤0.00	≤0.00	≤0.00	≤0.00	0.00	≤0.00	≤0.00	≤0.00	≤0.00
MnO	0.11	0.11	0.04	0.02	0.13	0.11	0.10	0.11	0.11	0.11	0.11	0.11	0.10	0.11	0.11
V_2O_3	≤0.00	0.01	0.00	0.00	0.03	≤0.00	≤0.00	≤0.00	0.00	0.00	≤0.00	≤0.00	0.00	≤0.00	0.01
Total	101.84	98.54	100.87	103.10	99.09	100.11	100.58	100.61	102.00	99.48	101.23	99.79	100.29	99.60	100.35
Mg#	92.34	92.30			80.72	92.25	92.13	92.12	92.34	92.07	92.44	92.23	92.12	92.16	92.30

Table 4.2. cont.

Mineral	Olv	Olv	Olv	Olv	Olv	Olv	Chr	SiO_2	Olv	Olv	Olv	Olv	Olv	Olv	Olv
Sample	13547b-11	13547b-13	13547b-14	13547b-15	13547b-16	13547b-112a	13803b-1	13803c-3	13804b-1	13804b-2	13805a-1	13805a-2	13805a-3	13805a-4	13805a-5
Paragen.			p				p	?	p				p		
Assem.			olv				chr	SiO_2	olv				olv		
TiO_2	0.01	0.00	0.01	≤0.00	0.01	≤0.00	0.04	≤0.00	0.01	≤0.00	≤0.00	0.01	≤0.00	≤0.00	≤0.00
Al_2O_3	0.01	0.02	0.02	0.01	0.01	0.00	5.79	0.07	0.03	0.03	0.02	0.02	0.01	0.04	0.03
P_2O_5	≤0.00	0.01	0.01	0.01	0.01	0.01	0.01	≤0.00	0.01	≤0.00	0.01	0.01	≤0.00	0.01	≤0.00
Na_2O	0.02	0.00	0.01	0.01	0.02	0.00	0.01	0.01	0.02	0.02	0.02	0.02	0.02	0.02	0.02
NiO	0.34	0.37	0.33	0.36	0.36	0.36	0.10	≤0.00	0.35	0.36	0.33	0.32	0.33	0.33	0.33
Cr_2O_3	0.07	0.08	0.07	0.06	0.07	0.03	65.81	0.01	0.08	0.06	0.03	0.01	0.02	0.04	0.03
SiO_2	40.80	40.90	40.89	39.28	41.27	39.77	0.11	100.56	40.57	40.92	41.57	40.42	41.07	40.82	40.67
CaO	0.04	0.04	0.03	0.04	0.04	0.03	≤0.00	≤0.00	0.02	0.03	0.01	0.01	0.01	0.01	≤0.00
MgO	50.70	51.23	51.60	51.79	51.43	51.73	13.87	≤0.00	51.43	50.60	50.64	50.78	51.49	51.19	51.94
FeO	7.64	7.74	7.50	7.75	7.66	7.65	15.29	1.20	7.32	7.30	6.68	6.56	6.43	6.68	6.37
K_2O	≤0.00	≤0.00	0.01	≤0.00	≤0.00	≤0.00	≤0.00	≤0.00	≤0.00	≤0.00	0.00	0.00	≤0.00	≤0.00	0.01
MnO	0.11	0.12	0.11	0.11	0.11	0.12	0.40	0.03	0.11	0.10	0.11	0.11	0.09	0.09	0.10
V_2O_3	≤0.00	0.00	0.00	≤0.00	0.01	0.01	0.23	0.01	0.01	0.01	0.00	0.00	≤0.00	0.00	≤0.00
Total	99.75	100.49	100.57	99.42	101.00	99.70	101.67	101.90	99.94	99.42	99.44	98.25	99.48	99.24	99.50
Mg#	92.21	92.19	92.46	92.26	92.29	92.34	61.79		92.61	92.52	93.11	93.24	93.45	93.18	93.56

Mineral	Olv	Olv	Olv	Olv	Olv	Olv	Olv
Sample	13805a-6	13805a-7	13805a-9b	13805a-10	13805a-12	13805a-13	13805a-15
Paragen.				p			
Assem.				olv			
TiO_2	≤0.00	0.01	≤0.00	0.00	0.00	≤0.00	0.01
Al_2O_3	0.01	0.01	0.03	0.01	0.02	≤0.00	≤0.00
P_2O_5	0.01	0.02	≤0.00	≤0.00	0.01	0.01	0.01
Na_2O	0.01	0.01	0.02	0.02	0.01	0.02	0.01
NiO	0.32	0.33	0.31	0.31	0.31	0.32	0.34
Cr_2O_3	0.02	0.03	0.03	0.04	0.03	0.03	0.04
SiO_2	41.00	41.06	42.40	40.70	41.43	40.92	40.18
CaO	0.01	0.01	0.01	0.01	0.02	0.01	0.02
MgO	51.36	51.14	49.80	51.45	53.43	50.64	51.14
FeO	6.54	6.56	6.64	6.77	6.64	6.68	6.71
K_2O	≤0.00	≤0.00	≤0.00	≤0.00	≤0.00	≤0.00	≤0.00
MnO	0.10	0.10	0.09	0.10	0.10	0.09	0.09
V_2O_3	0.01	≤0.00	≤0.00	0.00	≤0.00	0.01	≤0.00
Total	99.40	99.26	99.32	99.41	101.99	98.71	98.55
Mg#	93.33	93.29	93.04	93.13	93.49	93.11	93.14

Mineral	Pyrrhotitite	Pyrrhotitite
Sample	12006b-7	12006b-6
Paragen.	e	e
Assem.	FeS	FeS
Cr	0.01	≤0.00
Mn	0.00	0.00
Fe	61.92	61.85
Ti	0.00	0.00
P	0.00	0.00
Ni	0.16	0.06
V	0.00	0.00
Co	0.06	0.05
Cu	0.01	0.02
Zn	0.00	0.00
As	0.03	0.03
Mo	0.59	0.59
S	37.24	37.80
Total	100.03	100.37

Paragen. - parageesis; Assem. - assemblage; olv - olivine; chr - chromite; SiO_2 - coesite; Gnt - garnet; Opx - orthopyroxene; p - peridotitic; e - eclogitic

and 10.2wt% Cr_2O_3, 23.2 and 22.3wt% MgO and 6.3 and 5.9wt% FeO, respectively. Compositionally the garnets classify as type G10 in the classification scheme of Grütter *et al.* (2004), i.e. they derive from deeper diamond facies harzburgitic sources. The $Mg\#_{Ca\_corr}$ of the two garnets is 87.7 and 88.3 (Table 4.2). This falls within the range found for harzburgitic garnet xenocrysts from the Renard kimberlites ($Mg\#_{Ca\_corr}$ 84.9 to 90.5 with a mean of 86.9; Hunt *et al.*, in press) and is typical for harzburgitic inclusions worldwide (Stachel and Harris, 2008).

4.5.2.1.4. Clinopyroxene

One clinopyroxene inclusion (from diamond 13532a) was recovered together with an orthopyroxene indicating a lherzolitic or websteritic paragenesis. High Mg# of both the orthopyroxene (93.0) and clinopyroxene (94.9) suggest a peridotitic paragenesis. The Cr_2O_3 content of the clinopyroxene is very low (0.19wt%) being more typical of an eclogitic paragenesis (Table 4.2). However, a very high Cr# (100*Cr/[Cr+Al]) of 79.2 clearly testifies to a lherzolitic origin, with low Cr and Al contents being a reflection of unusually low alkalis, allowing for only very low kosmochlor and jadeite components.

4.5.2.1.5. Spinel

Twenty-five spinel group inclusions were recovered from seven diamonds: 12031, 13520, 13530a, 13530b, 13530c, 13803b and 13533. They all classify as Mg-chromites with Mg# between 61.8 and 70.1 (mean 66.8) and Cr# between 84.3 and 88.4 (mean 85.8) (Table 4.2). This is normal for Mg-chromite inclusions in diamonds from worldwide sources (Stachel and Harris, 2008).

4.5.2.1.6. Sulphides

Two sulphides were recovered from one diamond (12006b). The inclusions are almost pure iron sulphide (Fe: 61.8 and 62.0wt%; S: 37.8 and 37.0wt%, respectively) (Table 4.2). A Ni and Cu rich rim was identified in element maps (Fig. 4.4) but due to very small thickness and relief along the grain edge a fully quantitative analysis could not be achieved. From the features observed along the grain edge, it is assumed

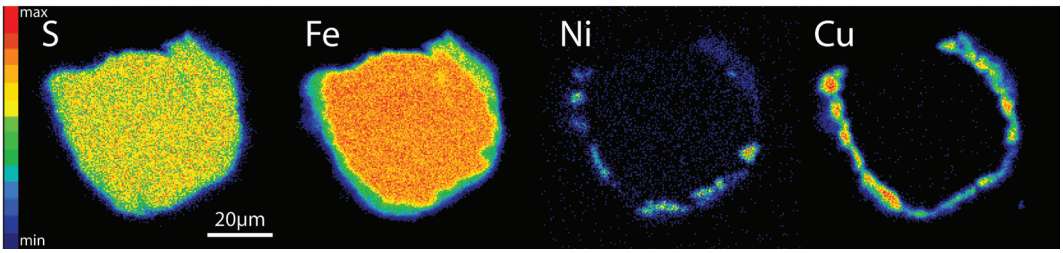

Figure 4.4. Microprobe element maps of a zoned sulphide inclusion from diamond 12006b.

that the inclusions initially precipitated as Mss (monosulphide solid solutions) but subsequently exsolved into pyrrhotite (FeS) within the core and chalcopyrite ($CuFeS_2$) and pentlandite ($[Fe,Ni]_9S_8$) forming the rim.

Bulanova *et al.* (1996), building on work by Yefimova *et al.* (1983), suggested that the Ni content of sulphides may be used to assign paragenesis, with peridotitic sulphide inclusions having high (22-36wt%) and eclogitic inclusions low (<12wt%) Ni contents. With a bulk Ni content of ~0.1 and 0.2wt%, the two sulphides recovered here are clearly eclogitic.

There are large differences in thermal expansion between diamond and Mss (e.g. Birch *et al.*, 1942; Clark, 1966). On cooling, during kimberlite ascent and emplacement, this causes the Mss to increase in volume more than the host diamond, creating a halo of cracks around the inclusion, as was observed within this stone. Cooling also causes the Mss to undergo exsolution into different phases, including pyrrhotite, pentlandite, chalcopyrite and pyrite (Harris, 1992; Taylor and Liu, 2009). Taylor and Liu (2009) showed that Cu and Ni often concentrate around the edges and in the expansion cracks, similar to what is seen for the sulphides analysed here.

4.5.2.1.7. SiO_2

Fifteen SiO_2 inclusions were recovered from nine Renard diamonds. Coesite inclusions have been observed as minor phases at other localities (e.g. Kopylova *et al.,* 1997, Sobolev *et al.*, 1998, Stachel *et al.*, 1998a), however, such a high abundance at one locality is very unusual. The inclusions were identified prior to breakage of their diamond hosts, and imposed cubo-octahedral morphologies were clearly observed

after breakage, indicating syngenetic origins. Based on an empirical test (e.g. Schertl *et al.*, 2004 and references therein) the observed blue cathodoluminescence colour was taken to indicate that the SiO_2 inclusions, structurally, are coesite. Coesite is associated with olivine in three diamonds and with orthopyroxene in one diamond.

4.5.2.2. Epigenetic Inclusions

4.5.2.2.1. Carbonate

Twenty-seven calcite inclusions with 100*Ca/(Ca+Mg ranging from 97.0 to 100.0) were recovered from seven diamonds.

Carbonate inclusions have previously been discovered at other localities. Calcite inclusions were reported by Meyer and McCallum (1986) and Leung (1984), magnesite was described by Harris *et al.* (2004), Phillips and Harris (1995) and Wang *et al.* (1996), siderite was found by Stachel *et al.* (2000) and dolomite by Stachel *et al.* (1998), although carbonates were never encountered in such high abundance.

Typically, calcite inclusions in diamond have an epigenetic origin, as in a peridotitic environment, magnesite rather than calcite is expected as the stable carbonate phase at the conditions of diamond formation (Wyllie and Huang, 1976; Wyllie, 1978). Although no fractures were observed in the host diamonds, connecting the inclusion to the surface, such features may have been obscured due to strong relief on diamond surfaces causing poor transparency.

4.5.2.2.2. Phlogopite

Three phlogopite inclusions were collected from one diamond and a fourth was recovered touching with clinopyroxene, from a second diamond. Although phlogopite has been found as rare syngenetic inclusions in diamond (e.g. Sobolev *et al.*, 2009 and references therein), unequivocally establishing a primary or secondary origin for phlogopite inclusions is, however, extremely difficult.

The phlogopite compositions were compared to phlogopite analysed from the Renard kimberlites (data from Birkett *et al.*, 2004; Patterson *et al.*, 2009). The

inclusions plot in a line of decreasing Al and Ti, identified as a late stage crystallisation trend by Birkett *et al.* (2004). Whilst the bulk of Renard kimberlitic phlogopite falls in the FeO_T-Al_2O_3 and TiO_2-Al_2O_3 space identified as the kimberlite field by Mitchell (1997) and Mitchell *et al.* (1999) a number also fall along this late stage trend. Based on the similarities between the phlogopite inclusions and kimberlitic phlogopite from Renard an epigenetic origin is suggested.

4.5.2.2.3. Clinopyroxene

Two clinopyroxenes (one touching with phlogopite as discussed above) were recovered from one diamond and are thought to be epigenetic. Both clinopyroxenes showed large internal chemical heterogeneity and, overall, are compositionally similar to late stage kimberlitic clinopyroxene observed in the Renard kimberlites (Patterson *et al.* 2009).

4.5.2.2.4. Amphibole

Three inclusions of amphibole were irecovered from two diamonds. The inclusions showed internal heterogeneity, and appeared altered in back scattered electron (BSE) images, indicating an epigenetic origin. The first amphibole has concentrations of 5.1wt% CaO, 6.1wt% Na_2O, 1.3wt% TiO_2, 2.3wt% K_2O, 22.44wt% MgO and 2.8wt% FeO. Using the programme WinAmphcal (Yavuz, 2007), the inclusion was identified as potassium-richterite. The two other amphiboles have concentrations of 2.0-2.4wt% CaO, 6.5-6.3wt% Na_2O, 1.3-1.2wt% TiO_2, 1.7-1.8wt% K_2O, 20.2-19.9wt% MgO and 5.7-5.5wt% FeO, respectively. The ferric/ferrous iron proportions were not measured and for this composition the final classification is dependent on the ferric iron content of the amphiboles. However, the most likely is that the inclusions fall in the richterite group, being the most typical kimberlitic amphibole composition (WinAmphcal: Yavuz, 2007).

4.5.2.2.5. Altered sulphides

Seven altered sulphide inclusions were observed in four diamonds. Accurate determinations of composition were not possible due to the alteration so identification

was made based on element maps. The remnant sulphides were predominantly composed of Fe, Ni and S (Fig. 4.5).

Melt/fluid infiltration along grain boundaries and fractures is evident, with the remaining sulphide exhibiting exsolution textures (Fig. 4.4). The majority of the cavity occupied by the original sulphide inclusion is now filled with calcite and, minor apatite, chromite, magnesite, dolomite, spinel and titanite (Fig. 4.5). This indicates open system behaviour.

4.5.2.2.6. Djerfisherite bearing inclusion

A polymineralic inclusion containing djerfisherite (K-rich sulphide), calcite, dolomite and apatite was identified (Fig. 4.5). The majority of the inclusion was calcite, with well formed apatite, a single crystal of djerfisherite and a single crystal of dolomite. The apatite and dolomite exhibit euhedral crystal shapes, whilst the djerfisherite has a subhedral crystal form, with slightly irregular grain edges.

Due to the crystal habit, the djerfisherite is presumed to be secondary; however, djerfisherite has also been identified as inclusions in the outer growth zones of diamond (Bulanova *et al.*, 1980). Therefore, the possibility that primary djerfisherite formed in the mantle and has subsequently been altered, as was observed for other sulphide inclusions from this study, cannot be completely dismissed.

The djerfisherite grain contains 41.9wt% Fe, 11.1wt% Ni, 30.0wt% S, 9.8wt% K and 1.1wt% Cl which is in agreement with other mantle derived examples of Ni

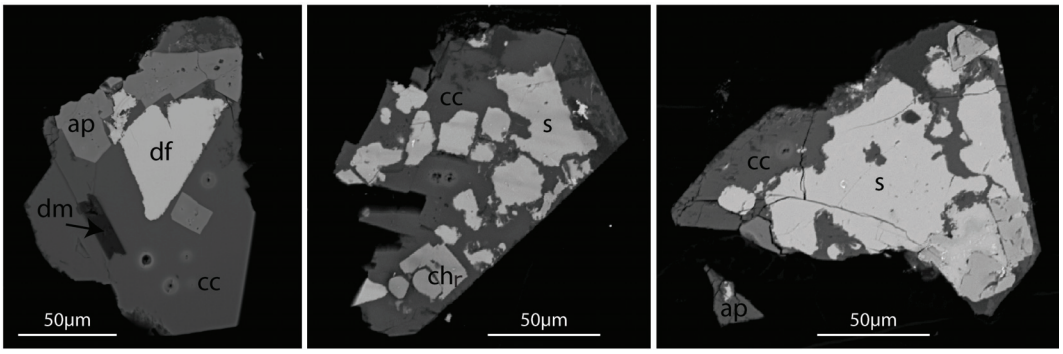

Figure 4.5. Back-scattered electron (BSE) images of polymineralic inclusions. df = djerfisherite, s = sulphide (typically pyrrhotite), cc = calcite, dm = dolomite, ap = apatite, chr = chromite.

rich and Cu poor djerfisherite from peridotite xenoliths (e.g. Clarke *et al.*, 1977; Boyd *et al.*, 1979; Clarke *et al.* 1994; Takechi *et al.* 2000; Henderson *et al.* 1999; Sharygin *et al.* 2007) and inclusions in diamond (Bulanova *et al.*, 1980. This contrasts with occurrences of djerfisherite in sulphide deposits and alkaline rocks which are rich in Cu (Dawson *et al.*, 1992;1995; Henderson *et al.*, 1999; Mitchell 1997).

4.5.3. Nitrogen Concentration and Aggregation State

Due to the fact that it has an ionic radius that is similar to carbon, nitrogen is the main substitutional impurity in diamond. The concentrations of nitrogen within diamond vary broadly, from below detection to 5500 at. ppm (Sellschop *et al.*, 1979), but rarely exceed 1400 at. ppm (Stachel *et al.*, 2009). Diamonds with eclogitic inclusions typically have higher nitrogen contents (median: 378 at. ppm) compared to peridotitic samples (median: 72 at. ppm) (c.f. Deines *et al.*, 1989; Stachel, 2007).

Diamonds without measurable nitrogen are classified as Type II, whilst those with detectable nitrogen contents are classified as Type I. Type I diamonds may be further subdivided based on the aggregation state of the nitrogen (Evans *et al.*, 1981). Initially, nitrogen substitutes into the diamond lattice as single atoms. Diamonds with nitrogen in single substitution are classified as Type Ib and are rare in nature. This is due to the high ambient temperatures in the Earth's mantle which cause the singly substituted nitrogen to rapidly aggregate into pairs of nitrogen (A centre) (e.g. Taylor *et al.*, 1996). Diamonds which contain >90% of their nitrogen in the A centre are classified as Type IaA. During continued mantle residence the nitrogen pairs may aggregate into rings of four atoms surrounding a vacancy (B centre) (Davies, 1976; Evans *et al.*, 1981). Diamonds which contain >90% of their nitrogen in B centres are classified as Type IaB. Type IaAB diamonds contain nitrogen in both aggregation states (10-90% of nitrogen in B centres). Many of these diamonds have an absorbance peak at ~1370cm^{-1} associated with platelets (Evans *et al.*, 1981; Woods, 1986).

Renard diamonds have nitrogen contents ranging from below the detection limit to 1619 at. ppm with an average of 146 at. ppm (Table 4.1, Fig. 4.5), falling between

the worldwide average for peridotitic and eclogitic diamonds. The diamonds show a range in aggregation from 0-70% B, up to type IaAB (intermediate aggregation), with no diamonds having fully aggregated nitrogen type IaB). At least two analyses per stone were carried out, and variations within single diamond crystals average ~60 at. ppm but are as high as ~900 at. ppm. Possible variations with growth from core to rim could not be assessed as nitrogen was measured on cleavage fragments after breakage.

Of the 56 diamonds analysed five classify as Type II with both analyses of the stones containing no detectable nitrogen (Table 4.1). A further two diamonds contain no nitrogen in one fragment and low but measurable nitrogen (9 and 39 at. ppm) in the second. Type II diamonds are only observed in pipes 2 and 4, and all five samples weigh less than 7.8mg (<1.2mm wide). The percentage of Type II diamonds is less than that observed worldwide, where Type II diamonds comprise 20% of all samples bearing lithospheric mineral inclusions (Stachel, 2007).

The remaining 51 diamonds contain measurable nitrogen in all fragments (classifying as Type Ia) at varying stages of aggregation (Table 4.3). Four stones classify as Type IaA, with nitrogen concentrations between 3 and 1324 at. ppm. The majority of the diamonds (25) are Type IaAB, a further 20 have mixed aggregation states within the same stone. Diamond fragments with Type IaAB aggregation have nitrogen concentrations ranging from 8 to 1619 at. ppm. Type IaA and IaAB stones are found in all pipes sampled for this study.

The time needed for the transition from the A-centre (pairs of nitrogen) to the B-centre (rings of four nitrogen surrounding a vacancy) depends on the absolute nitrogen concentration and time-averaged mantle residence temperatures. Assuming geologically reasonable residence times, the aggregation state of nitrogen in diamonds may thus be used as a geothermometer (Evans and Harris, 1989; Taylor *et al.*, 1990).

The exact residence time for the diamonds is not known. Based on the Neoproterozoic eruption ages of the kimberlites (Birkett *et al.*, 2004; Fitzgerald *et al.*, 2008) and late Archean cratonic formation age (Hunt *et al.*, in press) a mantle

residence time of 2Ga has been assumed. It has been shown that mantle residence temperatures are fairly insensitive to the approximated residence time (Evans and Harris, 1989; Leahy and Taylor, 1997). This is demonstrated in Table 4.1, where a difference of 2Ga in age (3Ga compared to 1Ga) gives a maximum temperature difference of ~30°C. In the case of unaggregated Type IaA diamonds, following Leahy and Taylor (1997), a maximum mantle residence temperature was calculated assuming the amount of B-defect is present at half the detection limit (~0.5%).

Nitrogen based time averaged mantle residence temperatures (Leahy and Taylor, 1997) give a range from ~1040-1230°C, with the majority of the samples falling between 1100-1200°C (Table 4.3, Fig. 4.6). Type IaA diamonds give a cooler range of temperatures (~1040-1180°C), compared to the type IaAB diamonds which approximately span the entire temperature range (1065-1230°C). The diamonds from all pipes, with the exception of pipe 4, have a bimodal distribution in nitrogen

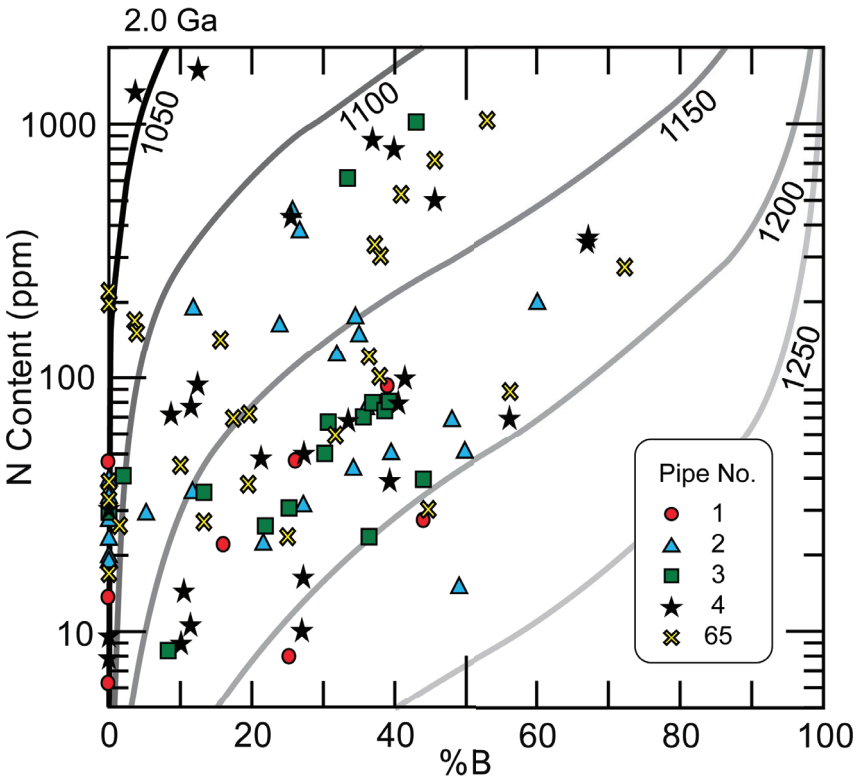

Figure 4.6. Time averaged mantle storage temperatures determined from nitrogen content and aggregation state. Nitrogen aggregation (%B) is expressed as the relative proportion of nitrogen in the B centre. Isotherms based on 2Ga mantle residence times are calculated after Leahy and Taylor (1997) and Taylor *et al.* (1990).

Table 4.3. The carbon isotopic composition, inclusion thermometry and nitrogen content and aggregation state of the diamonds. Nitrogen mantle residence temperatures have been determined after Leahy and Taylor (1997). For unaggregated Type IaA diamonds, a maximum mantle residence temperature was calculated assuming 0.05% B-defect (following Leahy and Taylor, 1997).

Pipe No.	Diamond	N Content (ppm)	%B	Type	T [Nitrogen, 3Ga]	T [Nitrogen, 2Ga]	T [Nitrogen, 1Ga]	Inclusion temp	Carbon $\delta^{13}C$
1	12026	46.1	0.0	IaA	1062	1071	1086	-	-
1	12026	46.6	26.2	IaAB	1162	1172	1190	-	-2.712
1	12027	6.2	0.0	IaA	1107	1117	1133	-	-
1	12027	7.9	25.3	IaAB	1207	1218	1237	-	-2.860
1	12029	21.8	16.1	IaAB	1165	1176	1194	-	-
1	12029	92.0	39.1	IaAB	1160	1170	1188	-	-4.429
1	12031	27.2	44.1	IaAB	1197	1208	1226	-	-
1	12031	13.5	0.0	IaA	1089	1099	1115	-	-4.025
2	12036a	28.7	5.2	IaA	1128	1138	1155	-	-
2	12036a	30.9	27.2	IaAB	1174	1184	1203	-	-3.431
2	12036b	27.1	0.0	IaA	1073	1083	1098	-	-
2	12036b	49.6	39.5	IaAB	1176	1186	1205	-	-4.493
2	12040	19.5	0.0	IaA	1081	1090	1106	-	-
2	12040	18.7	0.0	IaA	1082	1091	1107	-	-3.841
2	12041	18.6	0.0	IaA	1082	1091	1107	-	-
2	12041	34.9	11.7	IaAB	1145	1155	1172	-	-3.500
2	12042	185.7	11.8	IaAB	1104	1114	1131	-	-
2	12042	159.7	23.9	IaAB	1128	1138	1155	-	-3.636
2	13527	0.0	0.0	II	-	-	-	-	-
2	13527	0.0	0.0	II	-	-	-	-	-3.459
2	13528a	74.5	36.0	IaAB	1162	1172	1190	-	-
2	13528a	121.7	31.9	IaAB	1145	1155	1173	-	-3.893
2	13528b	0.0	0.0	II	-	-	-	-	-
2	13528b	0.0	0.0	II	-	-	-	-	-3.381
2	13803a	43.0	34.2	IaAB	1174	1184	1203	-	-
2	13803a	66.9	48.0	IaAB	1177	1188	1206	-	-4.351
2	13803b	50.2	49.8	IaAB	1186	1197	1216	-	-
2	13803b	22.8	0.0	IaA	1077	1086	1102	-	-4.011

Table 4.3. cont.

Pipe No.	Diamond	N Content (ppm)	%B	Type	T [Nitrogen, 3Ga]	T [Nitrogen, 2Ga]	T [Nitrogen, 1Ga]	Inclusion temp	Carbon $\delta^{13}C$
2	13803c	0.0	0.0	II	-	-	-	-	-
2	13803c	39.0	0.0	IaA	1065	1074	1090	-	-3.342
2	13804a	0.0	0.0	II	-	-	-	-	-
2	13804a	33.3	0.0	IaA	1069	1078	1094	-	-
2	13804a	21.8	21.6	IaAB	1175	1185	1204	-	-3.314
2	13804b	194.2	60.1	IaAB	1162	1173	1191	-	-
2	13804b	14.7	49.0	IaAB	1219	1230	1249	-	-3.738
2	13805a	171.9	34.5	IaAB	1139	1149	1167	-	-
2	13805a	145.9	35.0	IaAB	1144	1154	1171	-	-3.366
2	13805b	373.1	26.7	IaAB	1112	1121	1138	-	-
2	13805b	449.1	25.7	IaAB	1106	1116	1132	-	-3.847
3	13530a	74.1	38.6	IaAB	1165	1175	1193	-	-
3	13530a	70.0	35.6	IaAB	1163	1173	1191	-	-3.063
3	13530b	29.5	0.0	IaA	1072	1081	1096	-	-
3	13530b	23.6	36.4	IaAB	1192	1203	1222	-	-3.527
3	13530c	8.4	8.3	IaA	1171	1181	1200	-	-
3	13530c	26.0	21.9	IaAB	1171	1181	1200	-	-3.890
3	13531a	1018.0	43.0	IaAB	1105	1115	1131	-	-
3	13531a	613.4	33.4	IaAB	1107	1117	1134	-	-5.412
3	13531b	35.3	13.3	IaAB	1148	1158	1176	-	-
3	13531b	41.0	2.0	IaA	1095	1105	1121	-	-4.377
3	13532a	30.6	25.2	IaAB	1171	1182	1200	1122	-
3	13532a	50.3	30.2	IaAB	1165	1175	1194	-	-3.713
3	13532b	80.4	39.2	IaAB	1163	1174	1192	-	-
3	13532b	79.7	36.9	IaAB	1161	1171	1189	-	-3.371
3	13533	66.7	30.7	IaAB	1158	1169	1187	-	-
3	13533	39.8	44.0	IaAB	1186	1197	1216	-	-4.466
4	13520	38.9	39.3	IaAB	1182	1193	1211	-	-
4	13520	14.3	10.5	IaAB	1164	1174	1192	-	-4.353
4	13521a	0.0	0.0	II	-	-	-	-	-
4	13521a	0.0	0.0	II	-	-	-	-	-3.095

Table 4.3. cont.

Pipe No.	Diamond	N Content (ppm)	%B	Type	T [Nitrogen, 3Ga]	T [Nitrogen, 2Ga]	T [Nitrogen, 1Ga]	Inclusion temp	Carbon $\delta^{13}C$
4	13521b	1619.3	12.5	IaAB	1057	1066	1081	-	-
4	13521b	1323.8	3.7	IaA	1033	1042	1057	-	-4.077
4	13521c	69.0	56.2	IaAB	1185	1196	1214	-	-
4	13521c	16.2	27.2	IaAB	1191	1201	1220	-	-3.083
4	13523	49.8	27.3	IaAB	1162	1172	1190	1177	-
4	13523	47.8	21.3	IaAB	1154	1165	1183	1170	-3.653
4	13524	0.0	0.0	II	-	-	-	-	-
4	13524	0.0	0.0	II	-	-	-	-	-3.388
4	13536	3.1	0.0	IaA	1124	1133	1151	-	-
4	13536	10.0	27.0	IaAB	1203	1214	1233	-	-2.094
4	13537	8.9	10.1	IaAB	1175	1185	1204	-	-
4	13537	0.0	0.0	II	-	-	-	-	-3.506
4	13538	7.8	0.0	IaA	1102	1111	1128	-	-
4	13538	30.2	0.0	IaA	1071	1080	1096	-	-3.529
4	13539a	9.5	0.0	IaA	1097	1107	1123	-	-
4	13539a	10.5	11.4	IaAB	1174	1185	1203	-	-3.656
4	13539b	93.4	12.4	IaAB	1122	1132	1149	-	-
4	13539b	76.4	11.5	IaAB	1125	1135	1152	-	-2.864
4	13540	500.2	45.6	IaAB	1124	1134	1151	-	-
4	13540	428.9	25.5	IaAB	1107	1116	1133	-	-3.493
4	13544	98.9	41.4	IaAB	1160	1171	1189	-	-
4	13544	71.2	8.7	IaA	1119	1129	1146	-	-5.346
4	13545	67.1	33.5	IaAB	1162	1172	1190	-	-
4	13545	78.8	40.5	IaAB	1165	1175	1194	-	-3.158
4	13547a	0.0	0.0	II	-	-	-	-	-
4	13547a	0.0	0.0	II	-	-	-	-	-4.081
4	13547b	355.4	67.2	IaAB	1155	1165	1183	-	-
4	13547b	339.5	67.0	IaAB	1156	1166	1184	-	-3.944
4	13548	793.2	39.9	IaAB	1108	1118	1134	-	-
4	13548	861.8	36.9	IaAB	1103	1113	1129	-	-3.282

Table 4.3. cont.

Pipe No.	Diamond	N Content (ppm)	%B	Type	T [Nitrogen, 3Ga]	T [Nitrogen, 2Ga]	T [Nitrogen, 1Ga]	Inclusion temp	Carbon $\delta^{13}C$
65	12001	335.7	37.2	IaAB	1126	1136	1153	-	-
65	12001	303.5	38.0	IaAB	1129	1139	1156	-	-1.192
65	12003	16.9	0.0	IaA	1084	1093	1109	-	-
65	12003	23.6	25.0	IaAB	1178	1188	1207	-	-3.950
65	12004	220.5	0.0	IaA	1028	1037	1051	-	-
65	12004	197.1	0.0	IaA	1031	1039	1054	-	-2.822
65	12006a	151.5	3.9	IaA	1082	1091	1107	-	-
65	12006a	169.0	3.6	IaA	1077	1086	1102	-	-3.089
65	12006b	142.0	15.6	IaAB	1118	1128	1145	-	-
65	12006b	1030.8	53.1	IaAB	1114	1124	1141	-	-
65	12006b	720.2	45.6	IaAB	1116	1125	1142	-	-3.644
65	12011	88.4	56.3	IaAB	1179	1189	1208	-	-
65	12011	529.8	40.9	IaAB	1118	1128	1145	-	-3.006
65	12012	27.0	13.3	IaAB	1155	1165	1183	-	-
65	12012	26.1	1.5	IaA	1100	1110	1126	-	-3.280
65	12013	272.6	72.3	IaAB	1168	1178	1196	1140	-
65	12013	30.2	44.7	IaAB	1195	1205	1224	1110	-
65	12013	33.0	0.0	IaA	1069	1078	1094	-	-3.376
65	12014	121.6	36.4	IaAB	1150	1160	1178	-	-
65	12014	45.1	10.0	IaA	1134	1144	1161	-	-3.478
65	12016a	69.1	17.4	IaAB	1139	1149	1166	-	-
65	12016a	101.1	37.9	IaAB	1156	1166	1184	-	-4.695
65	12016b	71.9	19.6	IaAB	1142	1152	1169	-	-
65	12016b	38.8	0.0	IaA	1065	1074	1090		-4.534
65	12018	59.3	31.7	IaAB	1163	1173	1191	-	-
65	12018	38.0	19.5	IaAB	1157	1168	1186	-	-2.685

averaged mantle residence temperatures: A mode at ~1075-1100°C (primarily composed of Type IaA stones, assuming 0.5% B component, following Leahy and Taylor, 1997); and a second mode at ~1150-1200°C (predominantly composed of Type IaAB stones). Pipe 4 likely sampled different diamond horizons, with only one large mode at 1150-1175°C. Type IaA diamonds are relatively less abundant in this pipe, and plot at higher average temperatures, due to very low nitrogen contents, than those observed in other pipes. However, these are maximum temperature estimates, as 0.5% aggregation is assumed.

4.5.4. Carbon Isotopic Composition

Worldwide data show diamonds to have a broad range in stable carbon isotopic composition ($\delta^{13}C$) from −41‰ (De Stefano *et al.*, 2009) to +5‰ (Cartigny, 2005). Peridotitic diamonds are mainly restricted to $\delta^{13}C$ values between −10 and −2‰ whereas eclogitic diamonds have isotopic compositions from −38.5 (Cartigny et al., 2004) to +2.9‰ (Davies et al., 2003).

The Renard diamonds have a small range in $\delta^{13}C$ of -5.4‰ to -1.2‰ relative to V-PDB. All but four of the diamonds, however, fall within an even narrower range between -4.6‰ and -2.6‰ (Table 4.3, Fig. 4.7). The distribution of $\delta^{13}C$ has a well defined mode at -3.25‰ (class -3.5 to -3.0‰), which agrees well with carbon isotopic data for octahedral diamonds from Wawa (Stachel *et al.*, 2006) - a conglomerate hosted diamond deposit in the Superior Craton, ~1000km SW of Renard (Fig. 4.7). Diamonds at Crystal have a similar range in $\delta^{13}C$ from -5.5 to -1.1‰, with a well defined mode at -3.25‰ (Fig. 4.7). This is confirmed statistically using a student t-test. The test confirms, with a 95% confidence, that the mean observed for the Renard diamonds agrees with that determined for the diamonds from the Crystal showing at Wawa.

There is no correlation observed between the physical characteristics (colour, surface features, morphology) and the $\delta^{13}C$. No significant differences in carbon isotopic composition were observed among diamonds from the five studied pipes

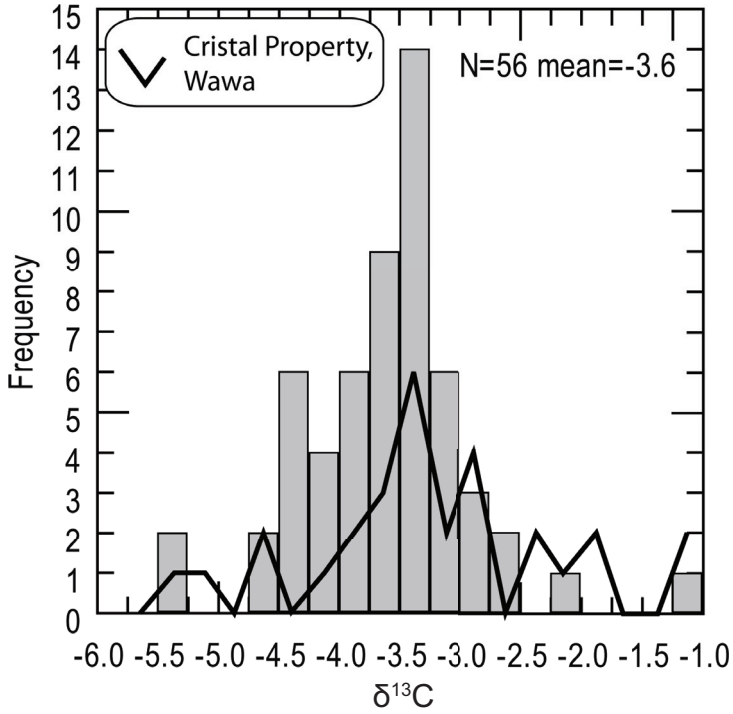

Figure 4.7. Histogram of carbon isotopic compositions of the diamonds. Black line represents comparison data from Wawa (Crystal showing) (Stachel *et al.*, 2006).

nor among different inclusion assemblages. The latter observation includes the coesite bearing diamonds, and the single, eclogitic diamond containing two Ni poor sulphide inclusions, with a $\delta^{13}C$ of -3.6‰.

4.5.5. Inclusion Thermometry

Three diamonds contained minerals for which thermometry estimates were possible. The coexistence of garnet and olivine within two diamonds allowed for the calculation of equilibrium temperatures based on Fe-Mg exchange (O'Neill and Wood, 1979). Both diamonds 12013 and 13523 contained a garnet inclusion and two olivine inclusions, and as such two estimates of temperature could be determined using the two olivines. At the time at which the minerals were enclosed, diamond 12013 resided at temperatures of 1110 and 1140°C. Diamond 13523 gave equilibrium temperatures of 1170 and 1180°C. A third diamond (13532a) contained a single clinopyroxene and a single orthopyroxene. The Ca-in-orthopyroxene thermometer

(Brey and Kohler, 1990) gave an equilibrium temperature of 1120°C. No other thermometers could be utilised due to the composition of the clinopyroxene, which fell outside the calibated compositions for other thermometers and barometers.

4.6. Discussion

4.6.1. Diamondiferous SCLM

Based on this inclusion study the diamondiferous lithospheric mantle beneath Renard appears to be strongly dominated by peridotite, with only one of 33 inclusion bearing diamonds having an eclogitic origin. This agrees with the xenolith/xenocryst record (Hunt *et al.*, in press) which is predominantly peridotitic, with only a minor (3%) eclogitic portion. Of the 32 diamonds with peridotitic inclusions, three are of harburgitic paragenesis (two diamonds contain harzburgitic garnets, and a further contains a low Ca orthopyroxene of likely harzburgitic origin) and one diamond is of lherzolitic origin (containing both an orthopyroxene and high Cr# clinopyroxene). A more specific parageneis cannot be determind for the remainder of the inclusion bearing diamonds.

The majority (79%) of Renard micro-xenoliths were sampled from a depth range of ~130-160km, with the deepest samples coming from ~190km (Hunt *et al.*, in press). Projecting the results of inclusion thermometry (1110-1180°C) on the xenolith based Neoproterozoic model geotherm of 38mW/m^2 (Hunt *et al.*, in press), the diamonds derive from a depth range of ~175-200km, i.e. from near the base of the lithosphere. Projecting the nitrogen thermometry data (1040-1230°C) onto the same geotherm gives a similar depth range of 160-210km (majority derived from 170-205km; average 190km). This implies that the majority of diamonds, for which either inclusion or nitrogen based temperatures are available, appear to derive from greater depths than the bulk of the xenolith record. This may indicate selective sampling of diamond/xenoliths at different depths or may simply reflect minor lithospheric cooling/transient heating events between, likely Archean, diamond formation and a Neoproterozoic geotherm, determined at the time of kimberlite emplacement.

4.6.2. Diamond Formation and Residence

4.6.2.1. Diamond Source Carbon

The carbon isotopic data ($\delta^{13}C$ -5.4‰ to -1.2‰: Fig. 4.7) are consistent with the predominantly peridotitic suite defined via inclusions. The mode of -3.25‰ agrees with previous work from the Superior (Wawa: Stachel *et al.*, 2006) (Fig. 4.7). This mode is not observed in other cratonic regions (database of Stachel and Harris 2008), and may suggest distinct carbon isotopic sources for diamonds from the Superior craton. A student t-test confirms that for worldwide peridotitic damonds, the $\delta^{13}C$ mode is not statistically similar to that of the Renard diamonds, at a 95% confidence limit. The small range in $\delta^{13}C$ also implies an excess of diamond forming melts/fluids.

It is generally accepted that peridotitic suite diamond formation occurs during redox reactions between either a reduced (e.g. Taylor, 1988) or an oxidized (e.g. Luth, 1993) fluid/melt and the host peridotite. Stachel *et al.,* (2009) showed that for diamonds with peridotitic inclusions, co-variations in nitrogen content and $\delta^{13}C$ exist. Nitrogen contents exceeding 1500 at. ppm are limited to $\delta^{13}C$ values between -5.5 and -5.0‰, whereas maximum nitrogen contents drop off rapidly towards both lower and higher $\delta^{13}C$ (Stachel *et al.,* 2009).

Stachel *et al.,* (2009) showed that a dataset of worldwide inclusion bearing peridotitic diamonds are consistent with having crystallised, in a closed system, by Raleigh fractionation from fluids/melts that are either reducing or oxidising. Using the same methods and fractionation factors of Polyakov and Kharlashina (1995) for a carbonatitic fluid/melt, Richet *et al.*, (1977) for a methane bearing fluid/melt and Chacko *et al.,* (1991) for a CO_2 melt/fluid, possible diamond forming fluids/melts for the Type IaAB Renard diamonds were modelled (Fig. 4.8). Only Type IaAB were selected, based on the assumption that they grew uninterupted over a similar time period, as one population. However, Type IaA and Type II diamonds also fit with the following model. As was concluded by Stachel *et al.,* (2009), there are indications that precipitation of Renard diamonds is compatible with crystallization

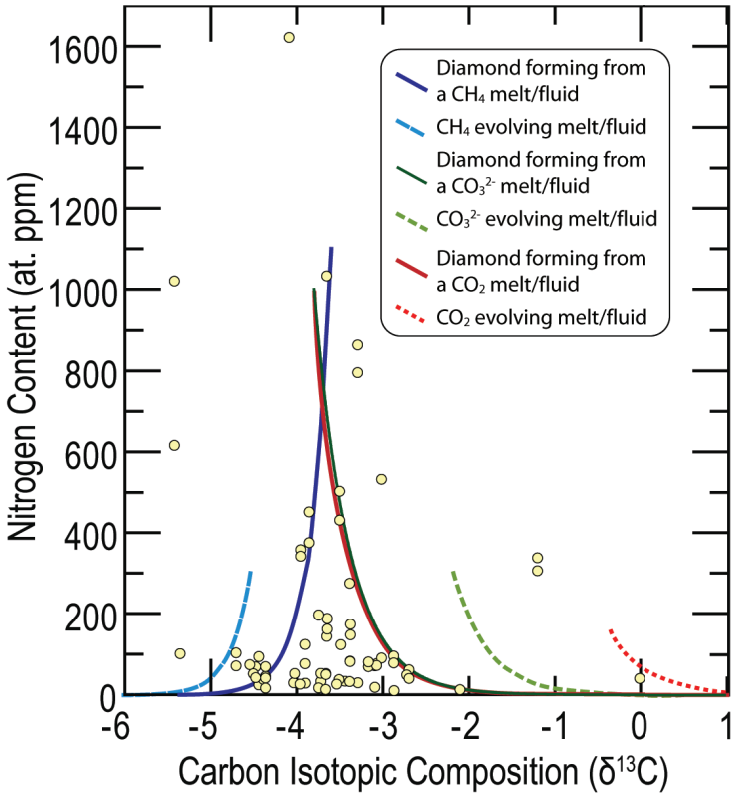

Figure 4.8. Carbon isotopic composition and nitrogen content of Type IaAB diamonds.

The bulk of the data can be modelled assuming precipitation of diamond from a reduced CH_4 melt/fluid and/or an oxidised CO_3^{2-} of CO_2 melt/fluid. Points that plot off the bounding curves may result from multiple diamond forming melts/fluids with variable initial nitrogen contents and or $\delta^{13}C$ (Stachel *et al.,* 2009).

The model parameters used are:

CH_4: N_0 = 220 at. ppm; KD = 5; $\delta^{13}C$ = -4.54‰
CO_3^{2-}: N_0 = 200 at. ppm; KD = 5; $\delta^{13}C$ = -2.18‰
CO_2: N_0 = 200 at. ppm; KD = 10; $\delta^{13}C$ = -1‰

from reducing CH_4 ($\delta^{13}C$ of crystallising diamond decreases) fluids/melts and/or oxidising CO_3^{2-} and CO_2 ($\delta^{13}C$ of crystallising diamond increases) fluids/melts. CO_2 is buffered by carbonation reactions in olivine bearing rocks at high pressure (Wyllie and Huang, 1976), therefore, it is not likely to be a significant diamond forming agent in the majority of diamond forming lithospheric mantle. However, as will be discussed below, the coesite inclusions found within the Renard diamonds could form through such carbonation reactions, and as such, free CO_2 could exist within localised regions of the mantle.

The proposed modelled melts/fluids are consistent with those expected in the SCLM. The model proposed here requires an initial carbon isotopic composition ($\delta^{13}C_0$) of −4.5‰ for diamonds crystallising from a CH_4 fluid/melt, which is within a typical mantle isotopic carbon range (-5‰ ±1 e.g. Cartigny, 2005). Methane related diamond formation may well occur from fluids/melts of fairly constant initial composition ($\delta^{13}C_0$~−5.5‰; Stachel *et al.,* 2009). For diamonds crystallising from CO_3^{2-}/CO_2 an initial $\delta^{13}C_0$ of –2.2‰ is required. This is consistent with subducted marine carbonates ($\delta^{13}C_0$ of 0±5‰; Schidlowski *et al.,* 1983) which have undergone progressive devolatilisation during subduction, driving their isotopic composition towards lower and hence more mantle-like $\delta^{13}C$ values (Schidlowski *et al.,* 1983).

4.6.2.2. Paleothermometry: From Nitrogen and Inclusions

The diamond nitrogen paleothermometry agree with worldwide peridotitic diamond data (database of Stachel and Harris, 2008). Of the 835 peridotitic diamonds plotted from the database, 73% have nitrogen residence temperatures between 1100-1200°C (mean of 1155°C) (Fig. 4.9). The Renard diamonds therefore grew in an environment typical for peridotitic diamonds from other cratonic regions, with the kimberlite sampling the entire depth of cratonic lithospheric mantle. The temperatures calculated from mineral pair thermometry agree within error to the nitrogen mantle

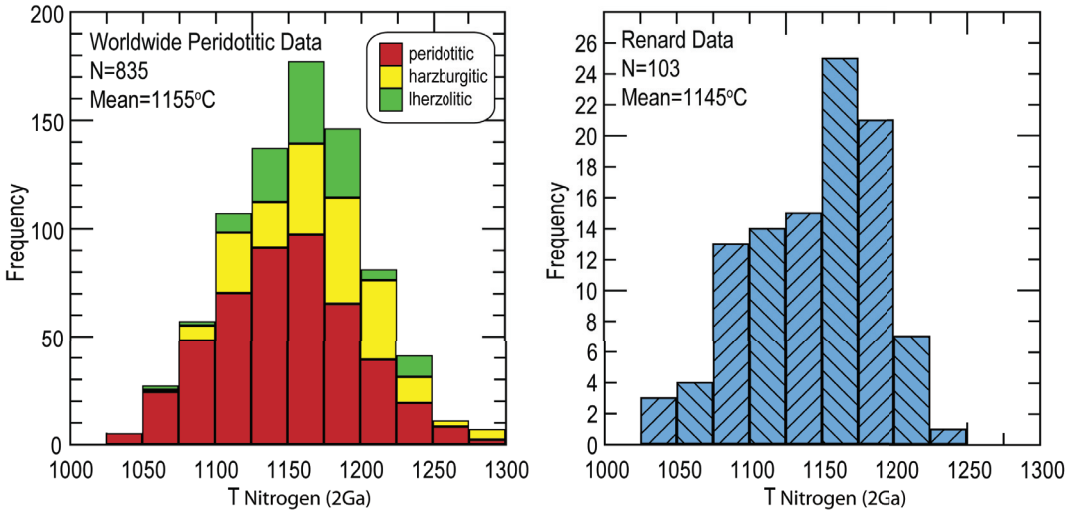

Figure 4.9. Histogram of time averaged mantle residence temperatures separated into pipe number compared to world wide lherzolitic, harzburgitic and "unspecified" peridotitic data (database of Stachel and Harris, 2008).

residence temperatures of the associated diamond (Table 4.3). The overall good agreement suggests that nitrogen aggregation provides a robust geothermometer. Furthermore the assumed age of 2Ga for diamond mantle residence appears realistic.

Time averaged temperatures do not distinguish between storage at constant temperature and, for example, formation in a very hot environment, in which the nitrogen aggregates very quickly, and subsequent storage for longer periods of time in a cool lithosphere. The agreement with inclusion thermometry, uniform $\delta^{13}C$, and the relatively good co-variation in nitrogen concentration and aggregation state of the majority of these diamonds is consistent with one main stage of diamond growth.

However, co-variation in nitrogen content and aggregation state is absent within some of the Renard diamonds (13 of the 56 diamonds). This gives apparent differences in temperature from separate fragments of individual stones of up to 127°C (Fig. 4.10), which is considered outside of error. Absolute errors on %B and nitrogen content, give maximum temperature differences of up to 20°C (Fig. 4.10), however, the quality of the spectra collected is not always equal, with some requiring more base line correction. This is not quantifiable, but can increase the error on the determined paleo-temperature. As such, only diamonds with spectra which required minimal baseline correction, and as such the associated error was small, were considered for this interpretation.

The large difference in aggregation state and determined nitrogen temperatures within individual diamonds likely relates to at least two distinct growth events and provides evidence for multiple diamond formation events. The growth events either occurred over an extended time period (billions of years) or during relaxation back to a local geotherm following a thermal perturbation. Within the diamond, the most aggregated analysis must be from the centre of the stone which has resided for the longest time period and/or at higher mantle temperatures, the less aggregated analysis, from the outer growth zones of the stone, is due to shorter residence times in the mantle and/or cooler mantle conditions during diamond growth.

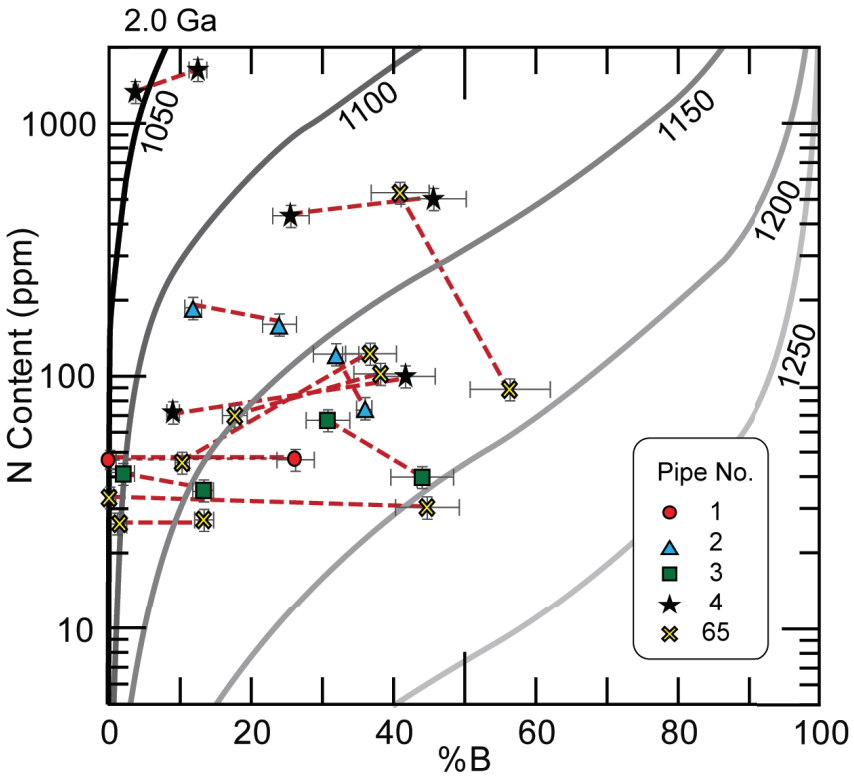

Figure 4.10. Time averaged mantle storage temperatures determined from nitrogen content and aggregation state. Isotherms based on 2Ga mantle residence times are calculated after Leahy and Taylor (1997) and Taylor *et al.* (1990). For good spectra error bars for %B at ± 5, errors of N content are less than the symbol size on the logorithmic scale (~10% below 500ppm, 5% above 500ppm). Dashed tie lines represent analyses from the same stone in which the determined residence temperature difference from the two analyses is greater than the error shown.

4.6.3. SCLM Modification

4.6.3.1. SiO_2 Inclusion Paragenesis

Microprobe analyses of the Renard diamond inclusions show a dominantly peridotitic suite, consisting of abundant olivine and chromite, and lesser amounts of clinopyroxene, orthopyroxene and garnet. Only one diamond is of likely eclogitic origin, containing two sulphide inclusions of low Ni content. A coesite inclusion assemblage was also identified (Table 4.2). Coesite is associated with olivine in three diamonds and with orthopyroxene in one diamond. The “coexistence” of olivine and SiO_2 in single diamonds reflects trapping of inclusions during different stages of diamond growth in an environment in which the chemical conditions were

changing. This agrees with multiple diamond growth events as was suggested for the mixed nitrogen content and aggregation states within individual stones. This is also observed in the olivine inclusion population. Within individual stones the olivine Fo content varies up to 0.4-0.5 e.g. in stones 12036b (ΔFo 0.37), 13547b (Δ Fo 0.45) and 13805a (ΔFo 0.45), suggesting a relative depletion or, more likely, enrichment in the environment in which the diamonds were growing.

The presence of abundant coesite inclusions at Renard is unusual: worldwide, coesite forms only ~1% of observed inclusions and the majority of these coesites are eclogitic (74%) (Stachel and Harris, 2008). Other localities where coesite is relatively abundant are the Argyle lamproite, Western Australia (Jaques *et al.*, 1989; Sobolev *et al.*, 1989), and the Guaniamo kimberlites, Venezuela (Sobolev *et al.*, 1998).

The low $\delta^{13}C$ values of the Guaniamo diamonds (as low as -28.7‰, with most diamonds in the range -10‰ to -20‰: Sobolev *et al.*, 1998; Kaminsky *et al.*, 2000) and the high $\delta^{18}O_{V\text{-}SMOW}$ of the coesite inclusions (10.2-16.9‰: Schulze *et al.*, 2003) has been used to suggest that a subducted crustal component may have contributed to their genesis. The abundance of coesite is used to propose a silica rich growth environment, consistent with little or no partial melting of the basaltic/eclogitic material in the oceanic slab during and following subduction.

An alternative hypothesis involves extreme carbonation of peridotitic sources, which has the ability to create free SiO_2 (Wyllie and Huang, 1976). In a peridotite all olivine must be carbonated before free SiO_2 is stable. Assuming a typical lherzolitic assemblage of forsterite, orthopyroxene and clinopyroxene, at high enough pressures and with an excess of CO_2, calcic magnesite and SiO_2 can be formed by progressive carbonation of clinopyroxene, orthopyroxene and finally olivine:

1) $2Mg_2SiO_4 + CaMgSi_2O_6 + 2CO_2 = CaMg(CO_3)_2 + 2Mg_2Si_2O_6$ (lherzolite: Wyllie et al., 1983)

2) $2Mg_2SiO_4 + 2CO_2 = 2MgCO_3 + Mg_2Si_2O_6$ (harzburgite: Wyllie et al., 1983)

3) $Mg_2Si_2O_6 + 2CO_2 = 2MgCO_3 + 2SiO_2$ (Wyllie and Huang, 1976)

Such carbonation involves the addition of >30wt% of CO_2 to the peridotite (Schrauder and Navon, 1993). This extreme CO_2 influx could only occur within localised regions of the lithosphere, for example as fully carbonated metasomatic veins or as blocks of subducted carbonaceous sediment (Schrauder and Navon, 1993).

Due to a paucity of eclogitic inclusions at Renard, or a highly negative carbon isotopic signature, we propose the second hypothesis as the mechanism for coesite growth. Source carbonation may explain the presence of peridotitic olivine and orthopyroxene with coesite within single diamonds. Olivine and orthopyroxene would need to be occluded prior to complete elimination during source carbonation, whilst coesite would only form after completion of all the successive reactions (Fig. D2). This is consisitent with the peridotitic chemistry of both the olivine and orthopyroxene. If coesite was included first, in an eclogitic environment subsequently metasomatised to an olivine websterite, then the chemistry of the olivine and orthopyroxene inclusions should be very different: e.g., websteritic orthopyroxene inclusions worldwide have average Mg# of 83.9 ± 3.98 (1σ) (Stachel and Harris, 2009). Average Mg# of websteritic olivine inclusions have not been determined, however the Mg# of olivine has been shown to be similar to or slightly lower than that of orthopyroxene, due to a relative Fe-Mg partition coefficient of ~1 that is independent of P and T (von Seckendorff and O'Neill, 1993). These Mg# are markedly lower than the observed values of 92.4-92.9 for olivine inclusions and 94.6 for orthopyroxene included with coesite. This clearly precludes formation of these diamonds in compositionally evolving coesite eclogites.

4.6.3.2. Epigenetic Inclusions

The presence of highly altered sulphide inclusions partially replaced by carbonate has not been observed in previous diamond inclusion studies. Whilst carbonatitic and sulphide bearing diamond-forming media both exist in the upper mantle, experimental data indicate that melting relations of carbonate–silicate and sulphide melts at P–T conditions of diamond stability are characterised by complete immiscibility (e.g. Litvin and Butvina, 2004; Litvin *et al.*, 2005; Shushkanova and Litvin, 2005; 2008).

For Renard diamonds, the immiscibility between sulphide and carbonate/ silicate melts, and the lack of Fe in the carbonate (identified primarily as calcite) suggest that a two stage open system process, rather than simple replacement of iron sulphide through carbonate, occurred. The first stage is the partial removal of primary sulphide inclusions, and the second stage is the deposition of carbonate. Jugo *et al.* (2005) showed that sulphur solubility in basaltic melts is strongly dependent on sulphur speciation, which, in turn is controlled by oxygen fugacity. Whilst sulphide has negligible solubility, sulphate ($[SO_4]^{2-}$) has a high solubility. It is, therefore, conceivable that an oxidising melt/fluid entered the diamond, through fractures, and oxidised and dissolved pre-existing sulphide as sulphate. After partial inclusion removal the "void" was then filled predominantly by calcite. At the high pressures required for diamond stability, calcite is not a stable phase in peridotite: reacting with orthopyroxene to form magnesite and diopside. The carbonate could, therefore, not have been in equilibrium with the peridotite, and likely precipitated at lower pressures/temperatures, possibly during kimberlite ascent.

Evidence for the involvement of alkali rich melts in processes surrounding the alteration of inclusions is derived from the observation of djerfisherite. Djerfisherite in mantle xenoliths (e.g. Clarke *et al.*, 1977; Clarke *et al.* 1994; Takechi *et al.* 2000; Henderson *et al.* 1999; Sharygin *et al.* 2007) and as rare inclusions in diamonds (Bulanova *et al.*, 1980) is believed to be the product of reactions between evolved kimberlitic melt/fluid, rich in K and Cl, and primary sulphides (typically pyrrhotite) (e.g. Bulanova *et al.*, 1980; Sharygin *et al.*, 2007). Supporting evidence for infiltration of diamond by an evolved, K and Cl rich melt/fluid comes from the presence of other epigenetic inclusions, including phlogopite and apatite.

4.7. Conclusions

Syngenetic inclusions in 33 diamonds from Renard indicate a predominantly peridotitic assemblage, typical for inclusions worldwide (2:1 peridotitic to eclogitic: e.g. Stachel and Harris, 2008). Only one likely eclogitic inclusion, a low Ni sulphide, was analysed. Abundant SiO_2 inclusions are not interpreted to form part

of an eclogitic suite. The absence of a distinctive, strongly negative carbon isotopic signature in the diamonds, and the presence of peridotitic inclusions with coesite within the same stone, removes the requirement of a crustal origin and instead, we suggest that free SiO_2 formed in peridotitic sources during progressive carbonation reactions. Extreme source carbonation occurred during diamond growth, as SiO_2 inclusions are present together with peridotitic olivine and orthopyroxene in four diamonds; this indicates multiple stages of diamond growth in a changing chemical environment. A changing growth environment is also observed in the data from the olivine inclusion population. Within individual stones the olivine Fo content varies up to ~0.5, suggesting a relative depletion or, more likely, enrichment in the environment in which the diamonds were growing.

The Renard diamonds have a narrow range in $\delta^{13}C$ from -5.4 to -1.2‰, with all but four of the diamonds having isotopic compositions between -4.6‰ and -2.6‰. The narrow range suggests an excess of diamond forming melts/fluids. A similar mode towards slightly ^{13}C enriched isotopic compositions, as compared to typical mantle values, was previously observed on the Superior Craton for a largely harzburgitic diamond suite from the Crystal showing at Wawa. The carbon isotopic distribution, therefore, is consistent with the observed predominantly peridotitic inclusion suite at Renard. Based in the $\delta^{13}C$ ratios and nitrogen contents of the diamonds they are interpreted to have formed from reducing (CH_4) melts/fluids and/or oxidising (CO_3^{-2} and CO_2) melts/fluids.

Using the nitrogen content and aggregation state in diamond, the majority of the time averaged mantle temperatures of he diamonds are between 1100 and 1200°C. The paleothermometry agrees with mineral inclusion thermometry (1110-1180°C) indicating that the age of 2Ga for diamond mantle residence is realistic. Multiple growth stages are again observed, with large differences in aggregation state and determined nitrogen temperatures within individual diamonds. The growth events either occurred over an extended time period (billions of years) or during relaxation back to a local geotherm following a thermal perturbation.

In conclusion, Renard diamonds are almost exclusively peridotitic, and grew from multiple events in a chemically changing environment from both reducing and oxidising agents, and were subsequently stored at typical cratonic conditions. Evidence for younger inclusion modification driven by infiltration of alkali rich melts, as shown by the presence of djerfisherite, apatite and phlogopite.

References

Armstrong, K.A., Nowicki, T.E. and Read, G.H., 2004. Kimberlite AT-56: a mantle sample from the north central Superior craton, Canada. Lithos, 77(1-4): 695-704.

Birch, F., Schairer, J.F. and Spicer, H.C. (Editors), 1942. Handbook of physical constants. Geological Society of America Special Papers Number 36. The Geological Society of America, Baltimore, 325 pp.

Birkett, T.C., McCandless, T.E. and Hood, C.T., 2004. Petrology of the Renard igneous bodies: host rocks for diamond in the northern Otish Mountains region, Quebec. Lithos, 76(1-4): 475-490.

Boyd, S.R., Kiflawi, I. and Woods, G.S., 1994. The Relationship between Infrared-Absorption and the A Defect Concentration in Diamond. Philosophical Magazine B-Physics of Condensed Matter Statistical Mechanics Electronic Optical and Magnetic Properties, 69(6): 1149-1153.

Boyd, S.R., Kiflawi, I. and Woods, G.S., 1995. Infrared-Absorption by the B-Nitrogen Aggregate in Diamond. Philosophical Magazine B-Physics of Condensed Matter Statistical Mechanics Electronic Optical and Magnetic Properties, 72(3): 351-361.

Broecker, W.S. and Oversby, V.M., 1971. Chemical equilibrium in the Earth. McGraw-Hill, New York, 318 pp.

Bulanova, G.P., Shestakova, O.E. and Leskova, N.V., 1980. Djerphisherite from Sulfide Inclusions in Diamonds. Doklady Akademii Nauk Sssr, 255(2): 430-433.

Card, K.D., 1990. A review of the Superior Province of the Canadian Shield, a product of Archean accretion. Precambrian Research, 48(1-2): 99-156.

Cartigny, P., 2005. Stable isotopes and the origin of diamond. Elements, 1(2): 79-84.

Cartigny, P., Harris, J.W. and Javoy, M., 2001. Diamond genesis, mantle fractionations and mantle nitrogen content: a study of delta C-13-N concentrations in diamonds. Earth and Planetary Science Letters, 185(1-2): 85-98.

Cartigny, P., Stachel, T., Harris, J.W., Javoy, M., 2004. Constraining diamond metasomatic growth using C- and N-stable isotopes: examples from Namibia. Lithos 77 (1–4), 359–373.

Chacko, T., Mayeda, T.K., Clayton, R.N. and Goldsmith, J.R., 1991. Oxygen and carbon isotope fractionations between CO2 and calcite. Geochimica Et Cosmochimica Acta, 55(10): 2867-2882.

Clark, S.P. (Editor), 1966. Handbook of Physical Constants, Revised Edition. The Geological Society of America, Inc. Memoir 97. The Geological Society of America, New York, 587 pp.

Collins, A.T., 1982. Colour centres in diamond. Journal of Gemmology, 18(37-75).

Coplen, T.B., Kendall, C. and Hopple, J., 1983. Comparison of Stable Isotope Reference Samples. Nature, 302(5905): 236-238.

Davies, G., 1976. The A nitrogen aggregate in diamond-its symmetry and possible structure. Journal of Physics C-Solid State Physics, 9(19): L537.

Davies, R.M., Griffin, W.L., O'Reilly, S.Y., Andrew, A.S., 2003. Unusual mineral inclusions and carbon isotopes of alluvial diamonds from Bingara, eastern Australia. Lithos 69 (1–2), 51–66.

De Stefano, A., Kopylova, M.G., Cartigny, P. and Afanasiev, V., 2009. Diamonds and eclogites of the Jericho kimberlite (Northern Canada). Contributions to Mineralogy and Petrology, 158(3): 295-315.

Deines, P., Harris, J.W., Spear, P.M. and Gurney, J.J., 1989. Nitrogen and ^{13}C content of Finsch and Premier diamonds and their implications. Geochimica Et Cosmochimica Acta, 53(6): 1367-1378.

Evans, T., Qi, Z. and Maguire, J., 1981. The Stages of Nitrogen Aggregation in Diamond. Journal of Physics C-Solid State Physics, 14(12): L379-L384.

Fitzgerald, C.E., Hetman, C.M., Lepine, I.M., Skelton, D.S. and McCandless, T.E., 2008. The internal geology and emplacement history of the Renard 2 kimberlite, Superior Province, Canada. Extended Abstract - 9th International Kimberlite Conference, Frankfurt, 2008.

Griffin, W.L., O'Reilly, S.Y., Doyle, B.J., Pearson, N.J., Coopersmith, H., Kivi, K., Malkovets, V. and Pokhilenko, N., 2004. Lithosphere mapping beneath the north American plate. Lithos, 77(1-4): 873-922.

Griffin, W.L., Shee, S.R., Ryan, C.G., Win, T.T. and Wyatt, B.A., 1999. Harzburgite to lherzolite and back again: metasomatic processes in ultramafic xenoliths from the Wesselton kimberlite, Kimberley, South Africa. Contributions to Mineralogy and Petrology, 134(2-3): 232-250.

Grütter, H.S., Gurney, J.J., Menzies, A.H. and Winter, F., 2004. An updated classification scheme for mantle-derived garnet, for use by diamond explorers. Lithos, 77(1-4): 841-857.

Harris, J.W., 1968. Recognition of Diamond Inclusions .1. Syngenetic Mineral Inclusions. Industrial Diamond Review, 28(334): 402-&.

Harris, J.W., 1987. Recent physical, chemical, and isotopic research of diamonds. In: P.H. Nixon (Editor), Mantle Xenoliths. John Wiley and Sons.

Hoffman, P.F., 1988. United Plates of America, the Birth of a Craton - Early Proterozoic Assembly and Growth of Laurentia. Annual Review of Earth and Planetary Sciences, 16: 543-603.

Hunt, L., Stachel, T., Armstrong, J., McCandless, T.E., Grütter, H., Simonetti, A. and Tappe, S. (Submitted) Mantle-derived microxenoliths and xenocrysts from the Renard kimberlites, Quebec: A record of mantle lithosphere formation and modification beneath the Eastern Superior Craton. Joural of Petrology.

Jugo, P.J., Luth, R.W. and Richards, J.P., 2005. Experimental data on the speciation of sulfur as a function of oxygen fugacity in basaltic melts. Geochimica Et Cosmochimica Acta, 69(2): 497-503.

Kaminsky, F.V., Zakharchenko, F.V., Griffin, W.L., Channer, D.M.D. and Khachatryan-Blinova, G.K., 2000. Diamond from the Guaniamo area, Venezuela. Canadian Mineralogist, 38(1347-1370).

Kopylova, M.G., Gurney, J.J. and Daniels, L.R.M., 1997. Mineral inclusions in diamonds from the River Ranch kimberlite, Zimbabwe. Contributions to Mineralogy and Petrology, 129(4): 366-384.

Leahy, K. and Taylor, W.R., 1997. The influence of the Glennie domain deep structure on the diamonds in Saskatchewan kimberlites. Geologiya I Geofizika, 38(2): 451-460.

Litvin, Y.A. and Butvina, V.G., 2004. Diamond-forming media in the system eclogite-carbonatite-sulfide-carbon: Experiments at 6.0-8.5 GPa. Petrology, 12(4): 377-387.

Litvin, Y.A., Shushkanova, A.V. and Zharikov, V.A., 2005. Immiscibility of sulfide-silicate melts in the mantle: Role in the syngenesis of diamond and inclusions (based on experiments at 7.0 GPa). Doklady Earth Sciences, 403(5): 719-722.

Luth, R.W., 1993. Diamonds, Eclogites, and the Oxidation-State of the Earths Mantle. Science, 261(5117): 66-68.

Meyer, H.O.A., Milledge, H.J. and Nave, E., 1965. Natural Irradiation Damage in Ivory Coast Diamonds. Nature, 206(4982): 392.

O'Neill, H.S.C. and Wood, B.J., 1979. An experimental study of the iron-magnesium partitioning between garnet and olivine and its calibration as a geothermometer. Contributions to Mineralogy and Petrology, 70: 59-70.

Percival, J.A., 2007. Geology and metallogeny of the Superior Province, Canada in, Mineral deposits of Canada: 471 a synthesis of major deposit-types, district metallogeny, the evolution of geological provinces, and exploration 472 methods. In: W.D. Goodfellow (Editor), Geological Association of Canada, Mineral Deposits Division, Special 473 Publication no. 5: 903-928.

Percival, J.A., Mortensen, J.K., Stern, R.A., Card, K.D. and Begin, N.J., 1992. Giant granulite terranes of northeastern Superior Province: the Ashuanipi complex and Minto block. Canadian Journal of Earth Sciences, 29: 2287-2308.

Polyakov, V.B. and Kharlashina, N.N., 1995. The Use of Heat-Capacity Data to Calculate Carbon-Isotope Fractionation between Graphite, Diamond, and Carbon-Dioxide - a New Approach. Geochimica Et Cosmochimica Acta, 59(12): 2561-2572.

Rayleigh, J.W.S., 1896. Theoretical considerations respecting the separation of gases by diffusion and similar processes. Philosophical Magazine, 42: 493-498.

Richet, P., Bottinga, Y. and Javoy, M., 1977. Review of Hydrogen, Carbon, Nitrogen, Oxygen, Sulfur, and Chlorine Stable Isotope Fractionation among Gaseous Molecules. Annual Review of Earth and Planetary Sciences, 5: 65-110.

Sage, R.P., Lightfoot, P.C. and Doherty, W., 1996. Bimodal cyclical Archean basalts and rhyolites from the Michipicoten (Wawa) greenstone belt, Ontario: Geochemical evidence for magma contributions from the asthenospheric mantle and ancient continental lithosphere near the southern margin of the Superior Province. Precambrian Research, 76(3-4): 119-153.

Schertl, H.P., Neuser, R.D., Sobolev, N.V. and Shatsky, V.S., 2004. UHP-metamorphic rocks from Dora Maira/Western Alps and Kokchetav/Kazakhstan: new insights using cathodoluminescence petrography. European Journal of Mineralogy, 16(1): 49-57.

Schidlowski, M., Hayes, J.M. and Kaplan, I.R., 1983. Isotopic inferences of ancient biochemitries; carbon, sulfur, hydrogen, and nitrogen. In: J.W. Schopf (Editor), Earth's earliest biosphere; its origin and evolution. Princeton University Press, Princeton, NJ, pp. 149-186.

Schrauder, M. and Navon, O., 1993. Solid Carbon-Dioxide in a Natural Diamond. Nature, 365(6441): 42-44.

Schulze, D.J., Harte, B., Valley, J.W., Brenan, J.M. and Channer, D.M.D.R., 2003. Extreme crustal oxygen isotope signatures preserved in coesite in diamond. Nature, 423(6935): 68-70.

Scully, K.R., 2000. Kimberlites of the Attawapiskat area, James Bay Lowlands, Northern Ontario, Ontario Geological Survey.

Scully, K.R., Canil, D. and Schulze, D.J., 2004. The lithospheric mantle of the Archean Superior Province as imaged by garnet xenocryst geochemistry. Chemical Geology, 207(3-4): 189-221.

Sharygin, V.V., Golovin, A.V., Pokhilenko, N.P. and Kamenetsky, V.S., 2007. Djerfisherite in the Udachnaya-East pipe kimberlites (Sakha-Yakutia, Russia): paragenesis, composition and origin. European Journal of Mineralogy, 19(1): 51-63.

Shushkanova, A.V. and Litvin, Y.A., 2005. Phase relations in diamond-forming carbonate-silicate-sulfide systems on melting. Russian Geology and Geophysics, 46(12): 1317-1326.

Shushkanova, A.V. and Litvin, Y.A., 2008. Diamond formation in sulfide pyrrhotite-carbon melts: Experiments at 6.0-7.1 GPa and application to natural conditions. Geochemistry International, 46(1): 37-47.

Sobolev, N.V., Yefimova, E.S., Channer, D.M.D., Anderson, P.F.N. and Barron, K.M., 1998. Unusual upper mantle beneath Guaniamo, Guyana shield, Venezuela: Evidence from diamond inclusions. Geology, 26(11): 971-974.

Stachel, T., 2007. Diamond. Mineralogical Association of Canada Short Course Series, 37: 1-22.

Stachel, T., Banas, A., Muehlenbachs, K., Kurszlaukis, S. and Walker, E.C., 2006. Archean diamonds from Wawa (Canada): samples from deep cratonic roots predating cratonization of the Superior Province. Contributions to Mineralogy and Petrology, 151(6): 737-750.

Stachel, T. and Harris, J.W., 2008. The origin of cratonic diamonds -- Constraints from mineral inclusions. Ore Geology Reviews, 34: 5-32.

Stachel, T., Harris, J.W. and Brey, G.P., 1998a. Rare and unusual mineral inclusions in diamonds from Mwadui, Tanzania. Contributions to Mineralogy and Petrology, 132(1): 34-47.

Stachel, T., Harris, J.W. and Muehlenbachs, K., 2009. Sources of carbon in inclusion bearing diamonds. Lithos, 112: 625-637.

Stachel, T., Viljoen, K.S., Brey, G. and Harris, J.W., 1998b. Metasomatic processes in lherzolitic and harzburgitic domains of diamondiferous lithospheric mantle: REE in garnets from xenoliths and inclusions in diamonds. Earth and Planetary Science Letters, 159(1-2): 1-12.

Taylor, L.A. and Liu, Y., 2009. Sulfide inclusions in diamonds: not monosulfide solid solution. Russian Geology and Geophysics, 50(12): 1201-1211.

Taylor, W.R., 1988. Measurement of reduced peridotite-C-O-H solidus and implications for redox melting of the mantle. Nature, 332(6162): 349-352.

Taylor, W.R., Canil, D. and Milledge, H.J., 1996. Kinetics of Ib to IaA nitrogen aggregation in diamond. Geochimica Et Cosmochimica Acta, 60(23): 4725-4733.

Thomassot, E., Cartigny, P., Harris, J.W. and (Fanus) Viljoen, K.S., 2007. Methane-related diamond crystallization in the Earth's mantle: Stable isotope evidences from a single diamond-bearing xenolith. Earth and Planetary Science Letters, 257(3-4): 362-371.

Woods, G.S., 1986. Platelets and the Infrared-Absorption of Type-Ia Diamonds. Proceedings of the Royal Society of London Series a-Mathematical Physical and Engineering Sciences, 407(1832): 219-238.

Wyllie, P.J. and Huang, W.L., 1976. Carbonation and Melting Reactions in System Cao-MgO-SiO_2-CO_2 at Mantle Pressures with Geophysical and Petrological Applications. Contributions to Mineralogy and Petrology, 54(2): 79-107.

Wyllie, P.J., Huang, W.L., Otto, J. and Byrnes, A.P., 1983. Carbonation of peridotites and decarbonation of siliceous dolomites represented in the system CaO-MgO-SiO_2-CO_2 to 30 kbar. Tectonophysics, 100(1-3): 359-388.

Yavuz, F., 2007. WinAmphcal: A Windows program for the IMA-04 amphibole classification. Geochemistry Geophysics Geosystems, 8(1): Q01004.

CHAPTER 5

CONCLUSIONS

Extensive studies have focused on understanding the chemical composition of diamond bearing SCLM. This has predominantly been through the characterisation of mantle derived xenoliths and xenocrysts (Boyd, 1989; Schulze, 1989; Griffin *et al.*, 2003b) and inclusions in diamonds (e.g. Meyer, 1987; Gurney, 1989; Harris, 1992; Stachel *et al.*, 2004; Stachel and Harris, 2008). The combined studies have shown that diamondiferous SCLM is dominated by peridotite with only a minor eclogitic component (e.g. Schulze, 1989). However, from an economic viewpoint, diamond eclogite is far more prospective in terms of diamond potential, with *in situ* grades of 1000 to 20000 cpt (carats per tonne), as compared to diamond peridotite, with *in situ* grades of 5 to 550 cpt (Grütter pers. comm.).

Research has shown that macrodiamonds require specific pressures and temperatures to form and remain stable with respect to graphite, and has led to the assumption that primary diamond deposits reside in thick ancient lithospheric mantle keels older than 1.5Ga, with low paleogeothermal gradients (e.g. Richardson *et al.*, 1984; Boyd *et al.*, 1985; Boyd and Gurney, 1986; Haggerty, 1986). More specifically, Archean diamond inclusion ages (e.g. Richardson *et al.*, 1984; Richardson *et al.*, 1993; Pearson *et al.*, 1999; Shirey *et al.*, 2003; Shirey *et al.*, 2004), have been used by Janse (1994) to suggest kimberlite diamond deposits are found within Archean cratonic regions. Both Janse's rule (1994), and the empirical rule proposed by Clifford (Clifford, 1966), are the views which have guided diamond exploration for the past four decades

This thesis builds on our understanding of a typical Archean cratonic region, as well as challenging the beliefs which have historically guided diamond exploration. The Renard kimberlites are located on the Superior craton, and, whilst the SCLM is poorly constrained, is a typical region for diamond exploration. In contrast, the Carolina kimberlite is located within poorly understood Proterozoic terrane which, according to the aforesaid beliefs, should not be a target for primary diamond deposits.

5.1 The Amazon Craton beneath the Carolina Kimberlite

With its setting in a Proterozoic (≤1.8Ga) basement province (e.g. Tassinari and Macambira, 1999) without any indications for an Archean crustal prehistory, the diamond bearing Carolina kimberlite occurs in a seemingly unconventional tectonic setting. Geochronological studies have focused on understanding the crustal ages in the region, with little work having been carried out to establish the age of the underlying lithospheric mantle. A Paleoproterozoic age may be inferred from the observation that crust and mantle in cratonic areas have generally remained coupled since their formation (Pearson, 1999). Whilst not conclusive, evidence that the underlying lithospheric mantle has a similar age as the basement rocks of the area comes through the study of garnet xenocrysts. The Carolina xenocrysts are typical for diamond-poor to barren circum-cratonic source regions, being derived predominantly from an exclusively lherzolitic peridotitic source (87%). The complete absence of harzburgitic garnet xenocrysts is unusual for a diamondiferous kimberlite, but it is consistent with a post Archean setting (c.f. Griffin *et al.*, 1999; Griffin *et al.*, 2003a; Hood and McCandless, 2003).

The absence of G10 garnet xenocrysts indicates that Carolina diamonds are unlikely to be derived from harzburgitic sources, but it rather points to a lherzolitic and/or eclogitic diamond population. Thirteen percent of the garnets belong to the eclogitic suite, being more abundant in core (28%) compared to surficial samples (9%). They also derive from distinct sources, with 96% of the garnets from core having higher sodium contents, as opposed to only 28% of concentrate garnets. High sodium (>0.07wt% Na_2O) in garnet is considered an indication of a high pressure origin and possibly a characteristic of diamond facies eclogites (Gurney, 1984b; Gurney *et al.*, 1993). This, combined with high nitrogen contents and, in part, highly negative carbon isotopic values of the diamonds themselves, suggests an eclogitic source region for, at least a portion of the Carolina diamonds.

An eclogitic, or lherzolitic, diamond source is also consistent with the younger Proterozoic age of the region. It has been shown that harzburgitic diamonds are

typically Archean in age, whilst lherzolitic or eclogitic diamonds can be younger (e.g. Pearson and Shirey, 1999; Shirey *et al.*, 2002; Shirey *et al.*, 2004; Stachel and Harris, 2008). For example, a synthesis of data from the Zimbabwe-Kaapvaal craton (Shirey *et al.* 2002) suggests that Middle Archean mantle depletion events initiated craton formation and created early harzburgitic diamond. Later Proterozoic tectonic and magmatic events subsequently added new lherzolitic and eclogitic diamonds.

Mantle storage of the diamonds occurred at temperatures that are otherwise typical for cratonic geotherms (1100-1150^{o}C). Platelet degradation amongst the majority of Carolina diamonds is evidence for thermal perturbations and/or strain affecting the diamond source regions prior to kimberlite emplacement. The number of transient heating events that affected the diamond source regions and their timing cannot be constrained from the nitrogen data. However, any heating events must have been short lived or occurred shortly before eruption of the kimberlite else the aggregation state of the diamonds would be higher. What can be determined, through evaluating platelet degradation in conjunction with nitrogen based mantle residence temperatures, is that strong platelet degradation occurs with high residence temperatures and, by inference, with great depths of origin. This is consistent with the heat source for platelet degradation being upwelling asthenospheric melts, and/or with increased strain with depth.

The most obvious change to the diamond source region occurred after the eruption of the Carolina kimberlite, dated here at ~230Ma. Using the single mineral geothermobarometer of Nimis and Taylor (2000), a typical cratonic model geotherm (~38 mW/m^2) is calculated for clinopyroxene xenocrysts derived directly from the Carolina kimberlite. Clinopyroxenes sourced from nearby garimpeiro diggings, derived from both local and regional sources, fall along a hotter 44mW/m^2 model geotherm, which is far less prospective. It is proposed that after eruption of the Triassic Carolina kimberlite a large scale heating event affected the underlying diamondiferous lithospheric mantle, which created the change in geothermal gradient. The heating event may relate to the intense plume activity which affected the Amazon Craton throughout the Cretaceous.

The heating event is also evidenced by the garnet xenocrysts. Garnets derived from the kimberlite plot predominantly in the G9A field of Grütter *et al.* (2004); indicative of a cool cratonic geotherm. Whilst xenocrysts taken from surficial samples show a shift to more Ca rich values (G9B field); typical of more off-craton kimberlites and a hotter geotherm. Similar observations have previously been made e.g. for the São Francisco Craton, where extreme heating of the deep lithospheric mantle occurred in a time window between 95-85Ma (Read *et al.*, 2004).

This study emphasises that Proterozoic, or circum-cratonic tectonic settings, which traditionally may have been ignored, may still host economically viable diamond deposits. It has provided new information on the origin and composition of deep (>140 km) and apparently stable Proterozoic cratonic keels. Most importantly, we have shown that whilst Clifford's Rule (1966) is still a very useful guide to finding new diamond deposits, more unconventional settings should also be considered.

5.2 The Superior Craton beneath the Renard Kimberlites

Similar to the Amazon craton, the majority of the crustal geology of the Superior craton has been well characterised, whilst the underlying SCLM is poorly understood. There is only limited age dating of the crustal units of the Opanica, through which the Renard kimberlites are extruded. However, an age of ~2.7Ga is well constrained by adjacent sub-province boundaries. Assuming that underlying mantle and crust have remained coupled since their formation, an Archean age for the SCLM would be expected. This research confirms a coupled crust mantle history, with the SCLM beneath the Renard kimberlite cluster forming during the Late Archean, as indicated by a Pb-Pb clinopyroxene model age of ca. 2.7 Ga. This was a time of major crustal formation throughout the Superior province.

A number of independent geothermobarometer combinations depict a "cold" 38mW/m^2 model geotherm (Pollack and Chapman, 1977) at the time of kimberlite emplacement (~0.6Ga). The majority (79%) of Renard microxenoliths were sampled from a depth range of ~130-160km, with the maximum pressure of origin reaching 60kbar (~190km).

Using the nitrogen content and aggregation state of the diamond, time averaged mantle temperatures can be determined assuming an approximate age of mantle residence. Based on the Neoproterozoic eruption ages of the kimberlites (Birkett *et al.*, 2004; Fitzgerald *et al.*, 2008) and late Archean cratonic formation, a residence time of 2Ga has been assumed. Mantle residence temperatures from 1040-1230^{o}C were determined, with the majority falling between 1100 and 1200^{o}C; which is in agreement with limited mineral inclusion thermometry (1110-1180^{o}C). These thermometry data are typical of worldwide diamond deposits (database of Stachel and Harris, 2008).

Projecting the results of inclusion thermometry (1110-1180^{o}C) onto an assumed 38mW/m^{2} model geotherm, indicates that the diamonds derive from a depth range of ~175-200km, i.e. from near the base of the lithosphere. Projecting the nitrogen thermometry data (1040-1230^{o}C) onto the same geotherm gives a similar depth range of 160-210km for time-integrated diamond residence. Combining lithosphere thickness and geothermal gradient indicates a large "diamond window" extending from ca. 130 to 210km during the Late Neoproterozoic, of which the kimberlite sampled the entire depth. The high diamond grade (e.g. Farrow, 2011) of the Renard kimberlites is not surprising, due to the very favourable conditions for diamond formation.

Based on the xenocrysts, xenoliths and inclusions studied, the majority of the lithospheric mantle comprises peridotite, with only minor eclogitic and websteritic portions. The xenoliths and xenocrysts show that the peridotitic portion is strongly dominated by lherzolite (71%), with minor harzburgitic (24%) and rare wehrlitic (5%) subpopulations. Worldwide peridotite is the dominant inclusion assemblage, however, the proportion of peridotite to eclogite is much higher (2:1 peridotitic to eclogitic: e.g. Stachel and Harris, 2008), making the paucity of eclogitic diamond inclusions unusual.

The Renard diamonds have a small range in $\delta^{13}C$ from -5.4 to -1.2‰, with all but four of the diamonds having isotopic compositions between -4.6‰ and -2.6‰.

The carbon isotopic distribution, therefore, is consistent with a predominantly peridotitic inclusion suite at Renard. The mode of -3.25‰ agrees with previous work from the Superior Craton for a largely harzburgitic diamond suite from the Cristal showing at Wawa (Stachel *et al.*, 2006). This isotopic composition, compared to other cratonic regions, is slightly ^{13}C enriched, and suggests possible distinct carbon isotopic sources for diamonds from the Superior.

Abundant coesite diamond inclusions were identified, which is unusual, as worldwide coesite forms only ~1% of observed inclusions (Stachel and Harris, 2008). Whilst the majority (74%) of SiO_2 inclusions in other localities are thought to be part of an eclogitic suite (e.g. Schulze *et al.*, 2003), at Renard, we suggest that due the lack of other eclogitic indicators (e.g. inclusions, highly negative $\delta^{13}C$) free SiO_2 formed in peridotitic sources during progressive carbonation reactions (Wyllie and Huang, 1976). Such carbonation involves the addition of >30wt% of CO_2 to the peridotite (Schrauder and Navon, 1993), which could only occur within localised regions of the lithosphere, such as along veins or as blocks of subducted carbonaceous sediment (Schrauder and Navon, 1993). These carbonation reactions occurred during diamond growth, as SiO_2 inclusions are present together with olivine in three diamonds. Olivine must have been included prior to complete elimination during source carbonation.

Since its formation, a number of metasomatic events have modified the lithospheric mantle underlying the eastern Superior Craton. The most pervasive is from melt infiltration, affecting garnets from the entire depth range sampled. An initial "parental" metasomatising agent imparted a sloped chondrite normalised trace element pattern on Cr-pyrope garnets. As the melt migrated upward through the lithospheric mantle it gradually evolved towards higher LREE/HREE and Zr/Y and imparted stepped and humped REE_N patterns. Less pervasive fluid metasomatism predominantly affected the shallower lithospheric mantle between 125 and 170km depth and is reflected in garnets with sinusoidal REE_N patterns. Similar to findings elsewhere (e.g. Malkovets *et al.*, 2007), it may have been the interaction of these enrichment events with previously depleted regions in the subcratonic lithospheric

mantle that promoted diamond formation. Based on this subset of diamonds, the $\delta^{13}C$ and the nitrogen content indicate they likely formed from a reducing (CH_4) and/or oxidising (CO_3^{-2} or CO_2) melt(s)/fluid(s); the same fluids could also be responsible for the metasomatism trends observed in silicate minerals.

The SCLM of the Superior craton beneath Renard is typical for cratonic lithosphere worldwide. It provided very favourable diamond forming conditions, with, at the time of kimberlite emplacement, a "cold" geothermal gradient and a thick lithosphere, producing a large diamond window.

References

Birkett, T.C., McCandless, T.E. and Hood, C.T., 2004. Petrology of the Renard igneous bodies: host rocks for diamond in the northern Otish Mountains region, Quebec. Lithos, 76(1-4): 475-490.

Boyd, F.R., 1989. Compositional distinction between oceanic and cratonic lithosphere. Earth and Planetary Science Letters, 96(1-2): 15-26.

Boyd, F.R. and Gurney, J.J., 1986. Diamonds and the African Lithosphere. Science, 232(4749): 472-477.

Boyd, F.R., Gurney, J.J. and Richardson, S.H., 1985. Evidence for a 150-200-Km Thick Archean Lithosphere from Diamond Inclusion Thermobarometry. Nature, 315(6018): 387-389.

Clifford, T.N., 1966. Tectono-metallogenic units and metallogenic provinces of Africa. Earth and Planetary Science Letters, 1(6): 421-434.

Farrow, D., 2011. NI 43-101 Technical Report - Updated Preliminary Economic: 2010 Mineral Resource Update for the Renard Diamond Project, GeoStrat Consulting Services Inc.

Fitzgerald, C.E., Hetman, C.M., Lepine, I.M., Skelton, D.S. and McCandless, T.E., 2008. The internal geology and emplacement history of the Renard 2 kimberlite, Superior Province, Canada. Extended Abstract - 9th International Kimberlite Conference, Frankfurt, 2008.

Griffin, W.L., O'Reilly, S.Y., Abe, N., Aulbach, S., Davies, R.M., Pearson, N.J.,

Doyle, B.J. and Kivi, K., 2003a. The origin and evolution of Archean lithospheric mantle. Precambrian Research, 127(1-3): 19-41.

Griffin, W.L., O'Reilly, S.Y., Natapov, L.M. and Ryan, C.G., 2003b. The evolution of lithospheric mantle beneath the Kalahari Craton and its margins. Lithos, 71(2-4): 215-241.

Griffin, W.L., O'Reilly, S.Y. and Ryan, C.G., 1999. The composition and origin of subcontinental lithospheric mantle. In: Y. Fei, C.M. Bertka and B.O. Mysen (Editors), Mantle Petrology: Field Observations and High Pressure Experimentation: A tribute to Francis R. (Joe) Boyd. Special Publication. The Geochemical Society, Houston: 13–45.

Grütter, H.S., Gurney, J.J., Menzies, A.H. and Winter, F., 2004. An updated classification scheme for mantle-derived garnet, for use by diamond explorers. Lithos, 77(1-4): 841-857.

Gurney, J.J., 1984a. A correlation between garnets and diamonds in kimberlites, Publications of the Geology Department & Extension Service, University of Western Australia: 143-166.

Gurney, J.J., 1984b. A correlation between garnets and diamonds in kimberlites, University of Western Australia, Geology Department and Extension Service: 143-166.

Gurney, J.J., 1989. Diamonds. In: J. Ross (Editor), Kimberlites and related rocks. Geological Society of America Special Publication No. 14. Blackwell, Scientific, Oxford, Carlton: 935-965.

Gurney, J.J., Helmstaedt, H. and Moore, R.O., 1993. A Review of the Use and Application of Mantle Mineral Geochemistry in Diamond Exploration. Pure and Applied Chemistry, 65(12): 2423-2442.

Haggerty, S.E., 1986. Diamond Genesis in a Multiply-Constrained Model. Nature, 320(6057): 34-37.

Harris, J.W., 1992. Diamond geology. In: J.E. Field (Editor), The properties of natural and synthetic diamond. Academic Press, London, pp. 345-393.

Hood, C. and McCandless, T., 2003. Systematic variations in xenocryst mineral composition at the province scale, Buffalo Hills kimberlites, Alberta, Canada, 8th International Kimberlite Conference, Victoria (BC), Canada: 3.

Janse, A.J.A., 1994. Is Clifford's rule still valid? Affirmative examples from around the world. In: H.O.A. Meyer and O.H. Leonardos (Editors), Diamonds: Characterization, Genesis and Exploration. CPRM — Special Publication Jan/94, Brasilia, pp. 215–235.

Malkovets, V.G., Griffin, W.L., O'Reilly, S.Y. and Wood, B.J., 2007. Diamond, subcalcic garnet, and mantle metasomatism: Kimberlite sampling patterns define the link. Geology, 35(4): 339-342.

Meyer, H.O.A., 1987. Inclusions in diamond. In: P.H. Nixon (Editor), Mantle xenoliths. John Wiley New York: 501-522.

Nimis, P. and Taylor, W.R., 2000. Single clinopyroxene thermobarometry for garnet peridotites. Part I. Calibration and testing of a Cr-in-Cpx barometer and an enstatite-in-Cpx thermometer. Contributions to Mineralogy and Petrology, 139(5): 541-554.

Pearson, D.G., 1999. Evolution of cratonic lithospheric mantle: an isotopic perspective. In: Y. Fei, C.M. Bertka and B.O. Mysen (Editors), Mantle Petrology Field Observations and High-Pressure Experimentation. A Tribute to Francis, R. (Joe) Boyd, The Geochemical Society Special Publications, Houston, TX: 57-78.

Pearson, D.G. and Shirey, S.B., 1999. Isotopic dating of diamonds. In: J. Ruiz and D.D. Lambert (Editors), Applications of radiogenic isotopes to ore deposit research. Economic Geology special publication: SEG Reviews in Economic Geology: 143-171.

Pearson, D.G., Shirey, S.B., Bulanova, G.P., Carlson, R.W. and Milledge, H.J., 1999. Re-Os isotope measurements of single sulfide inclusions in a Siberian diamond and its nitrogen aggregation systematics. Geochimica Et Cosmochimica Acta, 63(5): 703-711.

Pollack, H.N. and Chapman, D.S., 1977. On the regional variation of heat flow, geotherms, and lithospheric thickness. Tectonophysics, 38: 279-296.

Read, G., Grutter, H., Winter, S., Luckman, N., Gaunt, F. and Thomsen, F., 2004. Stratigraphic relations, kimberlite emplacement and lithospheric thermal evolution, Quiricó Basin, Minas Gerais State, Brazil. Lithos, 77(1-4): 803-818.

Richardson, S.H., Gurney, J.J., Erlank, A.J. and Harris, J.W., 1984. Origin of diamonds in old enriched mantle. 310(5974): 198-202.

Richardson, S.H., Harris, J.W. and Gurney, J.J., 1993. Three generations of diamonds from old continental mantle. 366(6452): 256-258.

Schrauder, M. and Navon, O., 1993. Solid Carbon-Dioxide in a Natural Diamond. Nature, 365(6441): 42-44.

Schulze, D.J., Harte, B., Valley, J.W., Brenan, J.M. and Channer, D.M.D.R., 2003. Extreme crustal oxygen isotope signatures preserved in coesite in diamond. Nature, 423(6935): 68-70.

Shirey, S.B., Harris, J.W., Richardson, S.H., Fouch, M., James, D.E., Cartigny, P., Deines, P. and Viljoen, F., 2003. Regional patterns in the paragenesis and age of inclusions in diamond, diamond composition, and the lithospheric seismic structure of Southern Africa. Lithos, 71: 243-258.

Shirey, S.B., Harris, J.W., Richardson, S.H., Fouch, M.J., James, D.E., Cartigny, P., Deines, P. and Viljoen, F., 2002. Diamond Genesis, Seismic Structure, and Evolution of the Kaapvaal-Zimbabwe Craton 10.1126/science.1072384. Science, 297(5587): 1683-1686.

Shirey, S.B., Richardson, S.H. and Harris, J.W., 2004. Integrated models of diamond formation and craton evolution. Lithos, 77(1-4): 923-944.

Stachel, T., Aulbach, S., Brey, G.P., Harris, J.W., Leost, I., Tappert, R. and Viljoen, K.S., 2004. The trace element composition of silicate inclusions in diamonds: a review. Lithos, 77(1-4): 1-19.

Stachel, T., Banas, A., Muehlenbachs, K., Kurszlaukis, S. and Walker, E.C., 2006. Archean diamonds from Wawa (Canada): samples from deep cratonic roots predating cratonization of the Superior Province. Contributions to Mineralogy and Petrology, 151(6): 737-750.

Stachel, T. and Harris, J.W., 2008. The origin of cratonic diamonds -- Constraints from mineral inclusions. Ore Geology Reviews, 34: 5-32.

Tassinari, C.C.G. and Macambira, M.J.B., 1999. Geochronological provinces of the Amazonian Craton. Episodes, 22: 174–182.

Wyllie, P.J. and Huang, W.L., 1976. Carbonation and Melting Reactions in System Cao-MgO-SiO_2-CO_2 at Mantle Pressures with Geophysical and Petrological Applications. Contributions to Mineralogy and Petrology, 54(2): 79-107.

Appendix A

ANALYTICAL METHODS

Appendix A

Sample Preparation

Diamond Crushing

The diamond samples are crushed in a steel breaker to release any inclusions present: The diamonds are aligned in the breaker to ensure, where possible, that the stone breaks along a cleavage plane. This prevents the stone from being powdered, allowing larger cleavage fragments to be later analysed for nitrogen content and aggregation, and finally combusted to determine carbon isotopic composition determination. The diamond fragments are continually cleaved until the inclusion is released.

Mounting of Material

Mounting of Inclusions

Any inclusions recovered are characterised visually. Special attention is paid to confirm a clear imposed morphology is present, and to ensure that the inclusion does not look at all altered. They are mounted in small (6mm diameter) brass pips. The pips are adhered to double sided carbon tape, to ensure a seal along the base. The inclusions are dropped into the centre of each pip, onto the carbon tape.

The inclusions are then mounted using Araldite® epoxy resin. The resin is composed of 5 parts Araldite® D and 1 part Hardener, which is thoroughly mixed in an aluminium dish. When filling the pips with resin, a 10ml syringe is used, and a needle placed on the end. The resin is then slowly dripped onto the sides of the pip, and left to run down, ensuring that no air bubbles are trapped around the inclusions. The inclusions are then placed on a hot plate at ~60^{o}C overnight. Any residual Araldite® epoxy resin is left in the aluminium dish and also placed on the hotplate. This can then be checked in the morning to ensure the epoxy has set.

Mounting of Xenocrysts and Xenoliths

Grease is thinly smeared across the base of a large (1 inch diameter) plastic holder. The small xenoliths and xenocrysts selected for analysis are then placed in rows along the base, held in place by the grease. A small piece of copper wire (~1mm diameter) is set at the top of the rows and is used as both a guide when probing, and to ensure constant coat thickness. The copper should go a pink colour when carbon coated, and the colour should not vary from one grain mount to the next, else the coat thickness has varied.

The same Araldite® epoxy resin is used to mount the xenocrysts/xenoliths. The epoxy should be slowly dripped onto each grain to ensure that no air pockets are trapped around the minerals.

Polishing of Grain Mounts and Inclusion Pips

After the grain mounts and pips have hardened the samples are polished on a polishing wheel. Progressively finer and finer sand paper is used, and eventually silk paper and a 0.05μm alumina oxide suspension. For diamond inclusios, polishing is also achieved by hand, using figure of eight motions on fixed sand paper.

Appendix A

Electron-Probe Microanalysis (EPMA)

For this research the electron microprobe was used, primarily, for quantitative WDS (wavelength dispersion spectrometry) analysis of the concentrations of major- and minor-elements for both diamond inclusions and xenocrysts. The microprobe was also used for backscattered electron and secondary electron imagery, and to construct X-Ray elemental maps.

The analyses are carried out on the JEOL JXA-8900 Superprobe. The instrument contains five wavelength dispersion spectrometers, and an energy dispersion spectrometer.

Sample Preparation

Prior to analysis of the polished sample it is cleaned for ~5 minutes in an ultrasonic bath using petrol ether to remove any surface contamination. To ensure electrical conductivity the samples are then coated with a thin film of carbon by combusting graphite rods in a high vacuum chamber.

Analytical Technique

Quantitative WDS analyses are performed with an accelerating voltage of 20kV and a beam current of 20nA and a 1μ beam diameter. Peak and background counts (seconds) are given in Table A.1., for silicate and oxide analysis, and Table A.3., for sulphide analysis. Typically, counts for each element are collected for 30-60 seconds (peak) and for half the time on each background. The spectrometer settings are summarised in Tables A.1. and A.3. Standards used for calibration are listed in Table A.2., for silicate analysis, and A.4., for sulphide analysis. Data reduction is performed using the CITZAF correction (Armstrong, 1995). The instrument calibration was deemed successful when the composition of secondary standards was reproduced within the error margins defined by the counting statistics. The standards, and well characterised grains from previous analyses, were also run at regular intervals during any session to ensure there is no instrument drift.

PET crystal Channel 1			TAP crystal Channel 2			PETH crystal Channel 3			TAP crystal Channel 4			LIFH crystal Channel 5		
Element	Peak	BG	Element	Peak	BG	Element	Peak	BG	Element	Peak	BG	Element	Peak	BG
Cr	40	20	Al	60	30	P	50	25	Mg	50	25	Ni	40	20
Ti	50	25	Si	60	30	K	60	30	Na	60	30	Fe	30	15
Ca	40	20										Mn	30	15
												V	30	15
Meas. time		260	Meas. time		210	Meas. time		220	Meas. time		165	Meas. time		245
Spec. move		52	Spec. move		32	Spec. move		36	Spec. move		28	Spec. move		64
Total time		**312**	Total time		**242**	Total time		**256**	Total time		**193**	Total time		**309**

Table A.1. JEOL JXA-8900 Superprobe spectrometer setup for silicate/oxide analysis.

Standards: **Bgd positions:**

Element	X-ray	Standard	Locality	Source	Reference	BG neg.	BG pos.
Na	Ka	Albite	Casedero, CA, USA	U of A collection		0	3
P	Ka	Apatite	Durango, Mexico	Smithsonian Inst.	Jarosewich, 2002	-1.8	1.5
Cr	Ka	Chromite		U of A collection		2.5	2.5
Si	Ka	Diopside	Wakefield, QB	U of A collection		0	2
Ca	Ka	Diopside	Wakefield, QB	U of A collection		-2	2
Fe	Ka	Fayalite	Rockport, MA	Smithsonian Inst.	Jarosewich, 2002	2.5	2.5
Mg	Ka	Fo93		U of A collection		0	3
Mn	Ka	Mn2O3	synthetic			0	1.5
Ni	Ka	Nickel	synthetic	U of A collection		-1.5	1.5
K	Ka	Orthoclase		U of A collection		-1.7	1.7
Al	Ka	Pyrope	Kakanui, New Zealand	Smithsonian Inst.	Jarosewich, 2002	-2.6	2
Ti	Ka	Rutile		U of A collection		2	2
V	Ka	V metal		U of A collection		-3	3

Table A.2. Standards used for silicate/oxide analysis, with the position of the background measurement relative to the peak position.

PET crystal Channel 1			TAP crystal Channel 2			PETH crystal Channel 3			TAP crystal Channel 4			LIFH crystal Channel 5		
Element	Peak	BG	Element	Peak	BG	Element	Peak	BG	Element	Peak	BG	Element	Peak	BG
S	30	15	Mg	50	25				Mn	100	50	Co	40	20
Cr	40	20	Si	80	40							Ni	40	20
			As	80	40							Cu	40	20
												Zn	40	20
												Fe	20	10
Meas. time		140	Meas. time		315	Meas. time			Meas. time		200	Meas. time		360
Spec. move		36	Spec. move		40	Spec. move			Spec. move		20	Spec. move		84
Total time		**176**	Total time		**355**	Total time			Total time		**220**	Total time		**444**

Table A.3. JEOL JXA-8900 Superprobe spectrometer setup for sulphide analysis.

Standards:						Bgd positions:	
Element	X-ray	Standard	Locality	Source	Reference	BG neg.	BG pos.
As	La	Arsenopyrite		U of A collection		0	3
Cr	Ka	Chromite		U of A collection		2.5	2.5
Co	Ka	Cobalt	Synthetic	U of A collection		-3	3
Cu	Ka	Copper	Synthetic	U of A collection		-2	2
Si	Ka	Diopside	Wakefield, QB	U of A collection		0	2
Mg	Ka	Fo93		U of A collection		0	3
Mn	Ka	Mn2O3	synthetic			-2	2
Ni	Ka	Ni	synthetic	U of A collection		-1.5	1.5
S	Ka	Pyrite	Black Angel, Greenland	U of A collection		-1.7	1.7
Fe	Ka	Pyrite	Black Angel, Greenland	U of A collection		2.5	2.5
Zn	Ka	Sphalerite		U of A collection		-2	2

Table A.4. Standards used for sulphide analysis, with the position of the background measurement relative to the peak position.

Appendix A

In-Situ Trace Element Analysis

Trace element analysis is carried out at the University of Alberta's Isotope Facility, on minerals prepared in grain mounts. Data is collected by laser ablation ICP-MS, using a New Wave Research Nd:YAG UV213 laser system coupled to a Perkin Elmer Elan 6000 Quadrupole ICP-MS.

Laser ablation runs are carried out in a mixed high purity He:Ar atmosphere, with a laser diameter of 160μm. Individual analyses consist of an ~20 second measurement of background levels followed by ~50 seconds of ion signal acquisition. During ablation a fluence (energy density) of ~10J/cm^2 and a 5Hz repetition rate is used. Data acquisition and processing/reduction is conducted using the GLITTER® (van Achterbergh *et al.*, 2001) laser ablation software.

The NIST 612 standard is used as the external calibration standard. Each analysis is normalised to the calcium contents, determined by electron microprobe analysis. This acts as an internal standard for monitoring instrumental drift. Analytical precision at the 2σ level ranges between 7 and 40% (relative), but is generally better than 10%. Relative uncertainties >10% are typical for elements present in ultra low abundances (e.g., <<1ppm; U, Th in garnet and HREEs in clinopyroxene).

Analytical accuracy of the trace element concentrations is verified by repeated analysis of two megacrystic garnet standards (PN1, PN2, Tappert *et al.* 2005). These grains have been well characterised compositionally by various analytical techniques (INAA, SIMS, LA-ICPMS) in several laboratories world-wide (e.g. Canil *et al.*, 2003; Tappert *et al.*, 2005). Repeated measurements of the same grains on different days yielded an external reproducibility (relative standard deviation) well within the 2σ precision.

Where possible, multiple spots were studied per grain, and a minimum of six grains per xenolith were analysed. After checking for homogeneity only average results per xenocryst/xenolith are reported here.

Appendix A

Pb-Pb Clinopyroxene Dating Procedure

In-situ Pb isotope data are obtained using a New Wave Research Nd:YAG UP213 laser system coupled to a NuPlasma MC-ICP-MS instrument at the University of Alberta Radiogenic Isotope Facility. Grains which showed little to no alteration were selected for analysis, and the minerals are prepared in grain mounts. The low abundance of Pb (<1ppm) present in the clinopyroxene grains investigated precluded the use of Faraday detectors for the acquisition of the Pb ion signals during the in-situ analyses (e.g. Schmidberger *et al.*, 2007). Thus, a new protocol was developed using the Faraday–multiple ion counter (IC) (n=3) collector block (Table A.5). The latter was developed and used extensively for the purposes of U-Pb geochronology (e.g. Schmidberger *et al.*, 2005; Schultz *et al.*, 2007). A detailed description of the collector configuration array, laser and ICP-MS instrument configurations are provided in Simonetti *et al.* (2005). In brief, the sample-out line from the laser ablation cell is 'y'-connected to the sample-out line from the desolvating nebuliser system (DSN-100 from Nu instruments) to allow for simultaneous aspiration of a dilute Tl solution (NIST SRM 997 standard in 2% HNO_3). The latter is used to monitor and correct for instrumental mass bias of the measured Pb isotope ratios (Longerich *et al.*, 1987).

Prior to the start of ablation, a 30 second on-peak baseline measurement is conducted in order to correct for the background ^{207}Pb, ^{206}Pb and ^{204}Hg and ^{204}Pb ion signals. Following the start of laser ablation, the acquisition sequence consists of a two-step peak-jumping routine; in the first sequence the isotopes simultaneously measured are ^{207}Pb, ^{206}Pb, ^{205}Tl, ^{204}Pb, and ^{203}Tl. The second sequence consists solely of measuring the $^{202}Hg/^{204}Hg$ ratio. The purpose of the acquisition sequence is to primarily ensure the removal of any ^{204}Hg produced during the ablation process using a $^{204}Hg/^{202}Hg$ ratio of 0.22988 (Rosman and Taylor, 1999). Data acquisition consists of 8 cycles of 10 second and 5 second integration intervals for sequences 1 and 2 (with 3 second magnet settling time) respectively, resulting in a total ablation time of ~3 minutes. Thus, in order to minimize the volume of sample consumed,

clinopyroxene grains are ablated in raster mode using a 320µm by 320µm area, with a scan speed of 160µm/s, a 20Hz repetition rate, and ~15J/cm^2 fluence.

Accuracy and external reproducibility is verified at the start of each session through multiple ablations of the NIST SRM 614 international glass standard. This standard was chosen as its certified Pb concentration (2.32ppm: Reed, 1992) is close to that expected of the clinopyroxene grains investigated here. Repeated measurements (n=4) of the NIST SRM 614 standard, ablated using the same analytical settings as for the clinopyroxene grains, indicate that the 'per session' external reproducibility (2σ, %RSD – relative standard deviation) for $^{206}Pb/^{204}Pb$ and $^{207}Pb/^{204}Pb$ ratios is better than 1% (for 6 sessions). The Pb/Pb ratios obtained here are also within 1% of the accepted values for NIST SRM 614.

Age calculations are performed using the Isoplot version 3.00 software (Ludwig, 2003). Error ellipses are at the 2σ level of uncertainty.

Table A.5. Configuration of the collector block for Pb-Pb analysis (Simonetti *et al.*, 2005).

EX-H	H6	H5	H4	H3	H2	H1	AX	L1	L2	IC0	IC1	L3	IC2	EX-L
Far.	Far.	Far.	Far.	Far.	Far.	Far.	Far.	Far.	Far.	I.C.	I.C.	Far.	I.C.	Far.
^{238}U	^{235}U	-	-	-	-	-	-	-	-	^{207}Pb	^{206}Pb	^{205}Tl	^{204}Pb	^{203}Tl
											^{204}Hg		^{202}Hg	
													^{204}Hg	

Appendix A

Fourier Transform Infrared (FTIR) Spectrometry

FTIR spectrometry is used to determine the concentration and aggregation state of nitrogen impurities within the diamonds (Fig. A.1.). The analyses are carried out at the University of Alberta, using a Thermo-Nicolet Nexus 470 FTIR spectrometer coupled with a Nicolet Continuum infrared microscope. The spectra are collected in transmittance mode, through an aperture of 100μm for 200 seconds and for a range of wave number from 650 to 4000cm^{-1}. The spectral resolution is 4cm^{-1}. The system is purged with a dry nitrogen-oxygen mix to maintain a stable environment, and background measurements are taken at regular intervals.

Analyses are performed on fragments of broken diamonds which are cleaned in an ultrasonic bath of petrol ether. The fragments are mounted on the edge of a glass slide, held in place with double sided carbon tape. Several fragments can be arranged along the side of the slide and analysed sequentially. Multiple analyses on each diamond are performed in order to detect variations in the nitrogen content and aggregation state within individual stones.

The sample spectra collected are background and baseline corrected. The spectra are then normalised to a thickness of 1cm and de-convoluted into the A, B and D components based on software provided by David Fisher (Research Laboratories of the Diamond Trading Company, Maidenhead, UK) (Figs. A.2., A.3. and A.4.). The normalisation is accomplished by analysing a nitrogen free Type II diamond plate standard. The standard is baseline corrected and converted to absorption coefficient (absorbance of a sample of 1cm thickness) through normalisation of the absorbance at 1995cm^{-1} to 11.94cm^{-1}. This gives the conversion factor for the unknown sample. Concentrations of nitrogen (atomic ppm) are calculated using absorption coefficient values at 1282cm^{-1} using the factors derived by Boyd *et al.* (1994) for the A-centre and Boyd *et al.* (1995) for the B-centres.

The detection limits depend strongly on the quality of the fragments, but are generally in the range 5–15 at. ppm.

Diamond Nitrogen Classification

Type II: Diamonds without detectable nitrogen (fig. A.1.a.)

Type IIa: Nitrogen free diamonds (Nitrogen below DL.)

Type IIb: Diamonds with boron as the main impurity

Type I: Diamonds with detectable nitrogen

Type Ia: Diamonds that contain aggregated nitrogen

Type IaA: Diamonds with nitrogen ≥90% in A-centres (Figs. A.1.b and A.2.)

Type IaB: Diamonds with nitrogen ≥90% in B-centres (Figs. A.1.c and A.4.)

Type IaAB: Diamonds with nitrogen (≥10% and ≤90%) in A-centres and (≥10% and ≤90%) in B-centres (Figs. A.1.d and A.3.)

Type Ib: Diamonds with singly substituted nitrogen

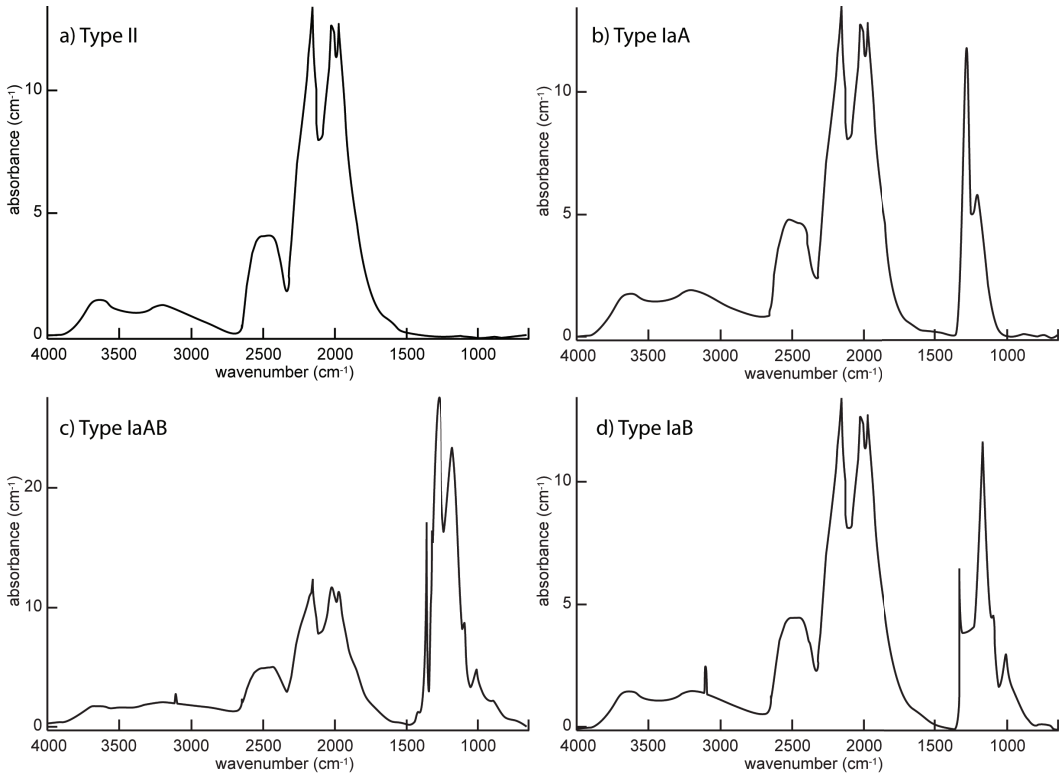

Figure A.1. Absorbance versus wave number for representative FTIR spectra. a) Nitrogen free Type II diamond spectra. b) Type IaA diamond spectra: Characteristic A-centre absorbance at 1282cm^{-1} c) Type IaAB diamond spectra: Absorbance peak at 1370cm^{-1} is due to platelet formation. d) Type IaB diamond spectra: Characteristics B-centre absorbance at 1185cm^{-1}.

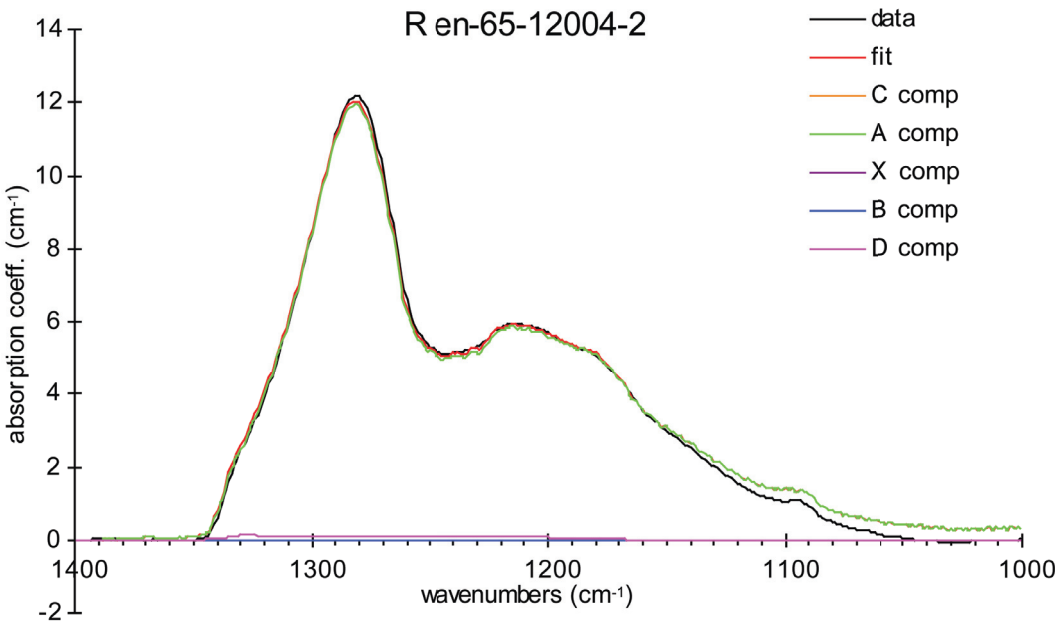

type Ib	μ(1130cm^{-1})	0.00 cm^{-1}	[N_C]	0.0 ppm	
type IaA	μ(1282cm^{-1})	11.94 cm^{-1}	[N_A]	197.1 ppm	
N^+	μ(1332cm^{-1})	0.00 cm^{-1}	[N^+]	0.0 ppm	
type IaB	μ(1282cm^{-1})	0.00 cm^{-1}	[N_B]	0.0 ppm	fit range
D	μ(1282cm^{-1})	0.09 cm^{-1}	[N_T]	197.1 ppm	1001 to 1399

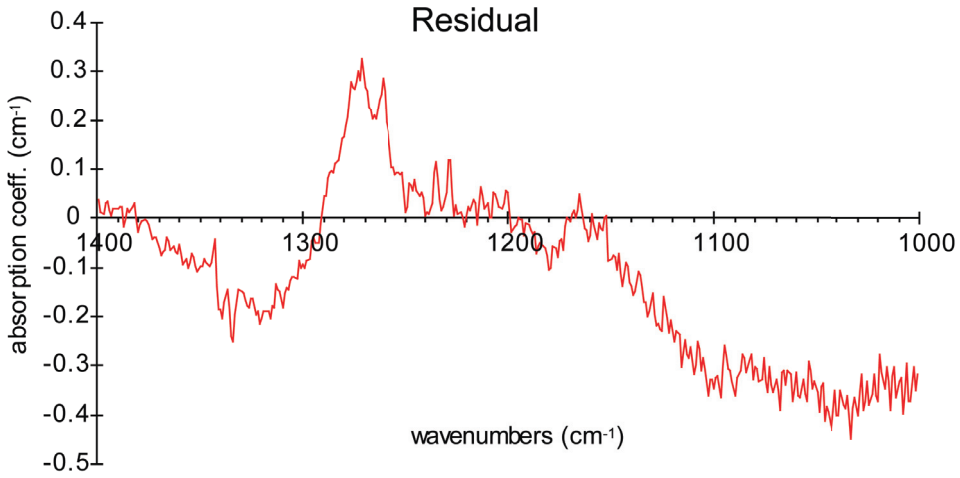

Figure A.2. Deconvoluted spectrum of a Type IaA diamond using software provided by David Fisher (Research Laboratories of the Diamond Trading Company, Maidenhead, UK).

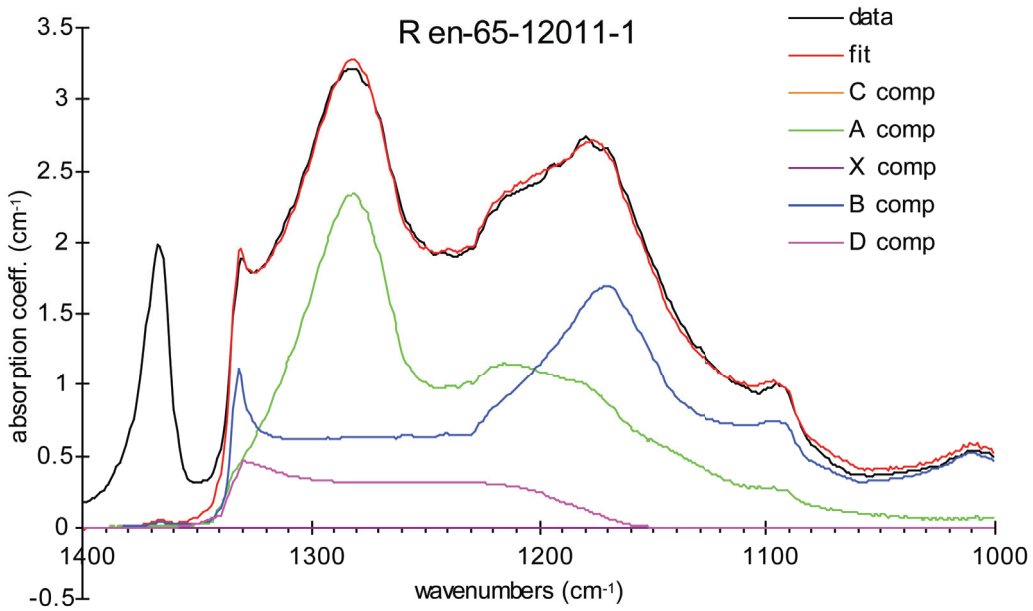

type Ib	μ(1130cm^{-1})	0.00 cm^{-1}	[N_C]	0.0 ppm	
type IaA	μ(1282cm^{-1})	2.34 cm^{-1}	[N_A]	38.6 ppm	
N^+	μ(1332cm^{-1})	0.00 cm^{-1}	[N^+]	0.0 ppm	
type IaB	μ(1282cm^{-1})	0.63 cm^{-1}	[N_B]	49.8 ppm	fit range
D	μ(1282cm^{-1})	0.31 cm^{-1}	[N_T]	88.4 ppm	1001 to 1399

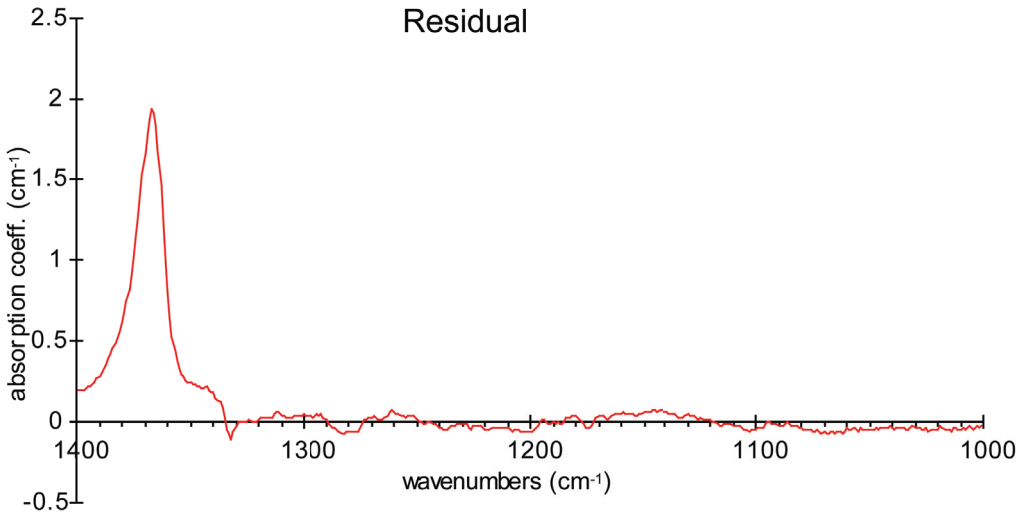

Figure A.3. Deconvoluted spectrum of a Type IaAB diamond using software provided by David Fisher (Research Laboratories of the Diamond Trading Company, Maidenhead, UK).

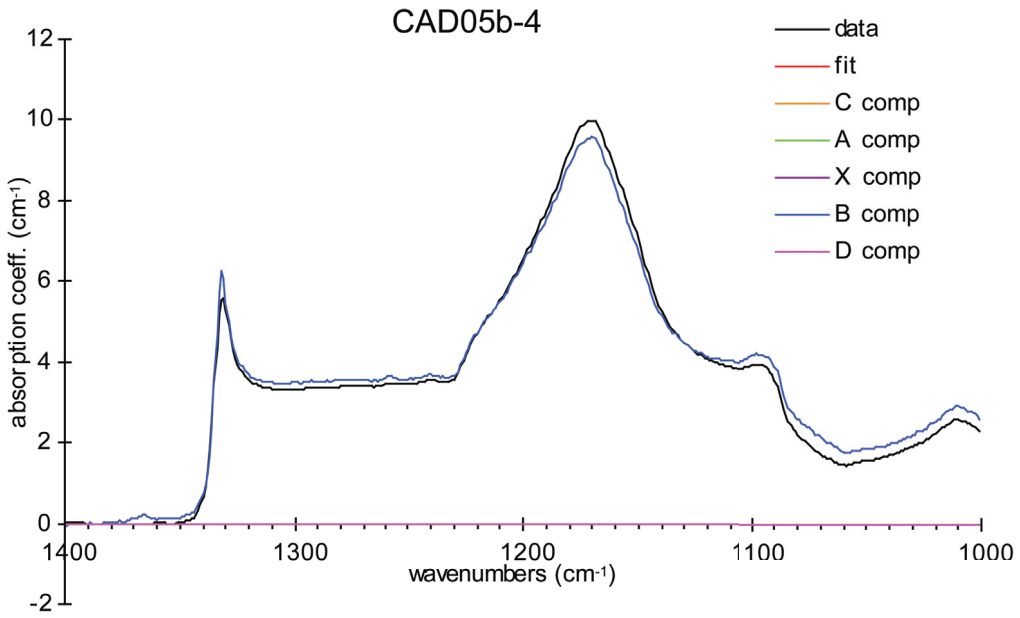

type Ib	μ(1130cm^{-1})	0.00 cm^{-1}	[N_C]	0.0 ppm	
type IaA	μ(1282cm^{-1})	0.00 cm^{-1}	[N_A]	0.0 ppm	
N^+	μ(1332cm^{-1})	0.00 cm^{-1}	[N^+]	0.0 ppm	
type IaB	μ(1282cm^{-1})	3.54 cm^{-1}	[N_B]	280.7 ppm	fit range
D	μ(1282cm^{-1})	0.00 cm^{-1}	[N_T]	280.7 ppm	1001 to 1399

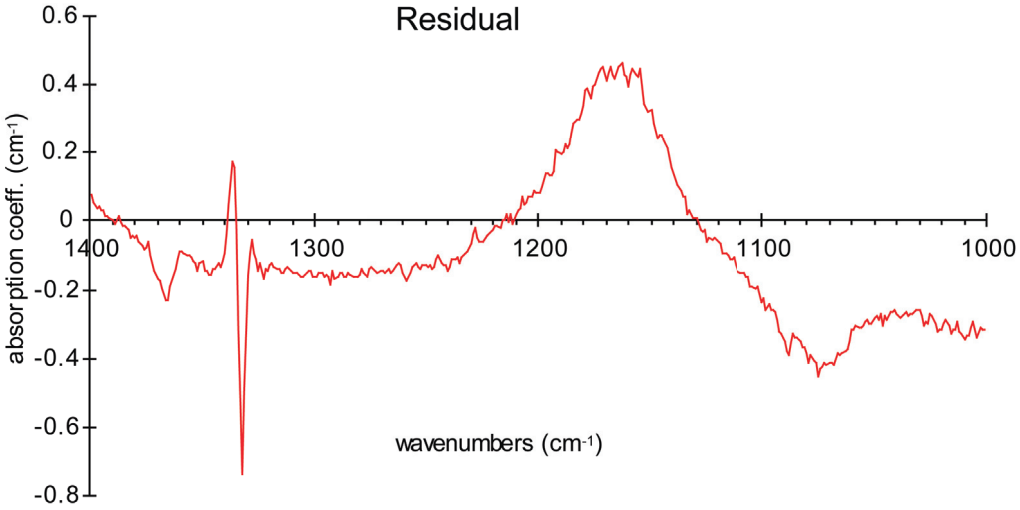

Figure A.4. Deconvoluted spectrum of a Type IaB diamond using software provided by David Fisher (Research Laboratories of the Diamond Trading Company, Maidenhead, UK).

Appendix A

Carbon Stable Isotope Analysis

The stable isotopic composition was determined at the University of Alberta Stable isotope lab facility.

Diamond fragments (0.6-2mm) are weighed out for analysis: Preferably one large fragment, or a few larger fragments are selected. The fragments should be inclusion and graphite free, and cleaned in an ultrasonic bath of petrol ether if necessary. The fragments were placed in a ~25cm long silica tube which had been previously sealed at one end with an oxyacetylene blow torch. Copper oxide (1-2g) is then added to the tube to act as an oxygen source.

The tube is placed on a vacuum line and evacuated for several hours. It is then sealed with an oxyacetylene blow torch. In order to convert the diamond fragment into CO_2 gas, the tubes are placed in an oven set to 980^{o}C. The silica tubes are heated overnight, and afterwards slowly cooled. The tubes are visually inspected to ensure the diamond fragment has combusted, and the integrity of the tube has remained.

The sealed glass tube is placed back onto the vacuum line, and broken. The sample gas is then extracted under vacuum using nitrogen traps. During the extraction the sample gas volume is measured to ensure there has been complete combustion of the diamond sample. The extracted gas sample is collected in a glass sample tube for subsequent analysis on a Finnigan MAT 252 gas flow mass spectrometer. The results are reported relative to the V-PDB standard (Coplen *et al.*, 1983). Instrumental precision is in the order of ±0.02‰.

References

Armstrong, J.T., 1995. Citzaf - a Package of Correction Programs for the Quantitative Electron Microbeam X-Ray-Analysis of Thick Polished Materials, Thin-Films,

Boyd, S.R., Kiflawi, I. and Woods, G.S., 1994. The Relationship between Infrared-Absorption and the A Defect Concentration in Diamond. Philosophical Magazine B-Physics of Condensed Matter Statistical Mechanics Electronic Optical and Magnetic Properties, 69(6): 1149-1153.

Boyd, S.R., Kiflawi, I. and Woods, G.S., 1995. Infrared-Absorption by the B-Nitrogen Aggregate in Diamond. Philosophical Magazine B-Physics of Condensed Matter Statistical Mechanics Electronic Optical and Magnetic Properties, 72(3): 351-361.

Canil, D., Schulze, D.J., Hall, D., Hearn, B.C. and Milliken, S.M., 2003. Lithospheric roots beneath western Laurentia: the geochemical signal in mantle garnets. Canadian Journal of Earth Sciences, 40: 1027-1051.

Coplen, T.B., Kendall, C. and Hopple, J., 1983. Comparison of Stable Isotope Reference Samples. Nature, 302(5905): 236-238.

Jarosewich, E., 2002. Smithsonian Microbeam Standards. Journal of Research of the National Institute of Standards and Technology, 107(6): 681-685.

Longerich, H.P., Fryer, B.J. and Strong, D.F., 1987. Determination of Lead Isotope Ratios by Inductively Coupled Plasma-Mass Spectrometry (Icp-Ms). Spectrochimica Acta Part B-Atomic Spectroscopy, 42(1-2): 39-48.

Ludwig, K.R., 2003. Isoplot/Ex version 3.0; a geochronological toolkit for Microsoft Excel; Berkeley Geochronology Center Special Publication No. 1a; Berkeley, California.

Reed, W.P., 1992. 614, Trace elements in glass matrix (3 mm wafer), 615, trace elements in a glass matrix (1vmm wafer).

Rosman, K.J.R. and Taylor, P.D.P., 1999. Isotopic compositions of the elements 1997. Journal of Analytical Atomic Spectrometry, 14(1): 5n-24n.

Schmidberger, S.S., Heaman, L.M., Simonetti, A. and Whiteford, S., 2005. In-situ Pb and Sr and Lu-Hf isotope systematics of mantle eclogites from the Diavik diamond mine, NWT, Canada. Geochimica Et Cosmochimica Acta, 69(10): A287-A287.

Schmidberger, S.S., Simonetti, A., Heaman, L.M., Creaser, R.A. and Whiteford, S., 2007. Lu-Hf, in-situ Sr and Pb isotope and trace element systematics for mantle eclogites from the Diavik diamond mine: Evidence for Paleoproterozoic subduction beneath the Slave craton, Canada. Earth and Planetary Science Letters, 254(1-2): 55-68.

Schultz, M.F.J., Chacko, T., Heaman, L.M., Sandeman, H.A., Simonetti, A. and Creaser, R.A., 2007. Queen Maud block: A newly recognized paleoproterozoic (2.4-2.5 Ga) terrane in northwest Laurentia. Geology, 35(8): 707-710.

Simonetti, A., Heaman, L.M., Hartlaub, R.P., Creaser, R.A., MacHattie, T.G. and Bohm, C., 2005. U-Pb zircon dating by laser ablation-MC-ICP-MS using a new multiple ion counting Faraday collector array. Journal of Analytical Atomic Spectrometry, 20(8): 677-686.

Tappert, R., Stachel, T., Harris, J.W., Muehlenbachs, K., Ludwig, T. and Brey, G., 2005. Diamonds from the Jagersfontein (South Africa):messengers from the sublithospheric mantle. Contributions to Mineralogy and Petrology, 150(5): 505-522.

van Achterbergh, E., Ryan, C.G., Jackson, S.E. and Griffin, W.L., 2001. Laser-ablation-ICPMS in the earth sciences — Appendix 3 data reduction software for LA–ICP–MS. In: P. Sylvester (Editor), Mineralogical Association of Canada Short Course, pp. 239-243.

Appendix B

ADDITIONAL DATA

Appendix B

Carolina Clinopyroxene Data

Table B.1. Clinopyroxene electron microprobe data separated into minerals derived from concentrate and core, indicated in the loc. (location) column.

Grain	loc.	TiO_2	SiO_2	K_2O	Na_2O	FeO	Cr_2O_3	Al_2O_3	CaO	MgO	MnO	NiO	Total
cad6-1	conc	0.13	53.22	0.01	1.95	2.87	1.42	2.89	19.88	16.29	0.11	0.04	98.90
cad6-2	conc	0.10	53.55	0.00	1.85	2.71	1.85	1.92	20.43	16.41	0.12	0.04	99.03
cad6-3	conc	0.32	52.82	0.00	1.76	3.09	1.02	2.69	20.92	15.98	0.09	0.05	98.78
cad6-4	conc	0.27	52.75	0.01	1.82	3.71	1.03	2.57	20.36	16.11	0.10	0.03	98.82
cad6-5	conc	0.25	53.18	0.00	1.96	2.97	1.24	2.98	20.26	15.84	0.10	0.05	98.89
cad6-6	conc	0.23	53.39	0.01	1.58	3.04	1.84	1.28	20.61	16.48	0.13	0.05	98.67
cad6-7	conc	0.27	53.14	0.00	2.42	3.19	1.07	3.31	19.67	15.55	0.09	0.04	98.80
cad6-8	conc	0.08	53.05	0.01	2.17	2.58	2.21	2.77	19.97	15.93	0.10	0.05	98.96
cad6-9	conc	0.25	53.05	0.00	1.84	3.10	1.10	2.80	20.57	15.90	0.09	0.04	98.82
cad6-10	conc	0.22	53.17	0.01	1.56	4.61	0.58	1.89	20.68	15.98	0.14	0.03	98.91
cad6-11	conc	0.11	53.65	0.01	2.47	2.99	1.41	3.00	19.30	15.36	0.13	0.04	98.53
cad6-12	conc	0.27	53.03	0.00	2.08	2.82	1.13	3.17	20.96	15.17	0.07	0.03	98.81
cad6-13	conc	0.32	53.04	0.00	1.88	2.91	0.93	3.10	21.10	15.39	0.09	0.04	98.87
cad6-14	conc	0.17	53.26	0.00	1.46	3.81	1.50	1.29	20.94	16.14	0.15	0.04	98.82
cad6-15	conc	0.24	53.38	0.01	1.70	2.99	2.09	1.29	20.61	16.38	0.13	0.05	98.91
cad6-16	conc	0.11	53.17	0.00	1.66	2.59	1.36	2.47	21.30	15.90	0.09	0.04	98.77
cad6-17	conc	0.34	53.34	0.00	2.15	3.04	1.12	3.19	19.95	15.81	0.09	0.05	99.12
cad6-18	conc	0.20	53.32	0.00	1.91	3.25	0.91	3.24	20.74	15.31	0.10	0.04	99.07
cad6-19	conc	0.23	53.24	0.00	1.72	3.16	1.00	2.69	20.87	15.90	0.09	0.04	99.00
cad6-20	conc	0.18	53.24	0.01	1.61	3.92	0.98	2.21	21.22	15.70	0.12	0.03	99.26
cad6-21	conc	0.21	55.69	0.00	0.15	5.33	0.79	1.61	1.09	33.66	0.16	0.12	98.80
cad6-22	conc	0.20	53.51	0.01	2.02	2.95	1.12	3.06	20.09	15.76	0.08	0.03	98.88
cad6-23	conc	0.20	53.24	0.01	2.26	3.02	1.49	3.04	19.50	15.51	0.09	0.06	98.49
cad6-24	conc	0.10	53.57	0.02	1.73	2.46	1.88	2.27	20.46	16.57	0.10	0.05	99.25
cad6-25	conc	0.29	53.46	0.00	2.06	2.94	1.19	2.96	20.48	15.57	0.08	0.05	99.14
cad6-26	conc	0.15	53.27	0.00	1.84	2.84	1.49	2.59	20.68	16.10	0.08	0.05	99.14
cad6-27	conc	0.16	53.63	0.01	1.89	3.22	1.26	2.67	20.50	15.81	0.10	0.04	99.32
cad6-28	conc	0.09	54.08	0.01	1.69	2.64	1.62	2.18	20.38	16.59	0.10	0.05	99.47
cad6-29	conc	0.38	53.42	0.02	1.49	2.73	1.57	2.38	20.21	17.10	0.11	0.05	99.51
cad6-30	conc	0.11	53.69	0.00	1.30	3.41	1.34	0.73	22.38	16.14	0.12	0.03	99.29
cad6-31	conc	0.13	52.72	0.02	1.52	2.96	1.18	2.45	21.84	15.84	0.10	0.04	98.83
cad6-32	conc	0.30	53.74	0.00	2.45	3.15	1.05	3.52	19.40	15.36	0.09	0.04	99.16
cad6-33	conc	0.55	52.37	0.00	2.29	2.01	1.37	5.11	21.27	14.19	0.08	0.03	99.32
cad6-34	conc	0.34	52.89	0.00	2.32	2.83	1.15	4.14	20.82	14.59	0.07	0.04	99.24
cad6-35	conc	0.29	53.36	0.00	2.09	2.99	1.31	3.09	20.22	15.78	0.10	0.05	99.32
cad6-36	conc	0.20	53.52	0.00	1.17	3.49	0.90	1.41	22.16	16.26	0.12	0.04	99.30
cad6-37	conc	0.31	53.48	0.01	2.11	3.26	0.90	3.06	20.14	15.66	0.10	0.04	99.13
cad6-38	conc	0.23	53.62	0.00	1.77	3.52	1.08	2.41	21.18	15.67	0.08	0.04	99.66
cad6-39	conc	0.03	53.77	0.00	1.61	2.46	1.71	2.26	20.94	16.33	0.11	0.03	99.32
cad6-40	conc	0.16	53.46	0.00	2.14	2.99	1.23	3.06	20.35	15.67	0.11	0.04	99.24
cad6-41	conc	0.31	53.45	0.01	1.91	2.81	1.05	2.77	20.56	15.91	0.09	0.05	99.01
cad6-42	conc	0.20	53.66	0.00	1.89	2.51	1.87	2.70	20.27	16.21	0.11	0.05	99.51
cad6-43	conc	0.24	53.58	0.01	1.71	3.06	1.03	2.91	19.97	16.75	0.10	0.06	99.46

Appendix B

Carolina Clinopyroxene Data

cont.

Grain	loc.	TiO_2	SiO_2	K_2O	Na_2O	FeO	Cr_2O_3	Al_2O_3	CaO	MgO	MnO	NiO	Total
cad6-44	conc	0.21	53.87	0.00	1.91	3.10	0.93	2.73	20.35	15.95	0.10	0.04	99.24
cad6-45	conc	0.15	53.55	0.00	1.47	3.52	1.24	1.93	21.64	15.72	0.12	0.04	99.41
cad6-46	conc	0.29	53.48	0.01	2.11	2.84	2.18	2.79	19.74	15.96	0.12	0.05	99.60
cad6-47	conc	0.12	53.90	0.01	1.83	2.76	1.33	2.25	20.85	16.30	0.11	0.05	99.54
cad6-48	conc	0.22	53.41	0.00	2.10	3.06	1.15	2.91	20.68	15.67	0.10	0.03	99.39
cad6-49	conc	0.17	53.62	0.00	2.15	2.78	1.50	2.73	20.37	15.89	0.09	0.04	99.40
cad6-50	conc	0.11	55.99	0.00	0.12	5.12	0.74	1.63	1.64	33.71	0.14	0.12	99.33
cad6-51	conc	0.24	53.97	0.01	2.34	3.26	1.10	3.16	19.46	15.70	0.12	0.05	99.46
cad6-52	conc	0.14	53.89	0.00	1.80	2.78	1.03	2.53	21.26	16.05	0.10	0.04	99.64
cad6-53	conc	0.18	53.73	0.00	1.87	3.30	1.03	2.64	20.66	16.06	0.11	0.04	99.67
cad6-54	conc	0.17	54.05	0.01	1.99	2.69	1.25	2.54	20.57	16.08	0.10	0.04	99.53
cad6-55	conc	0.23	53.89	0.00	1.87	2.92	1.02	2.85	20.64	16.16	0.10	0.05	99.79
cad6-56	conc	0.28	53.56	0.00	1.42	3.69	0.95	1.88	20.89	16.47	0.13	0.04	99.37
cad6-57	conc	0.08	53.85	0.00	2.01	2.78	1.71	2.67	19.99	16.20	0.10	0.05	99.49
cad6-58	conc	0.10	53.50	0.01	1.70	3.26	1.50	1.84	20.68	16.38	0.12	0.04	99.17
cad6-59	conc	0.22	53.66	0.00	1.87	2.75	1.42	2.74	20.40	16.12	0.09	0.05	99.39
cad6-60	conc	0.36	53.50	0.00	2.21	3.01	1.13	3.02	19.90	15.89	0.10	0.05	99.26
cad6-61	conc	0.08	53.96	0.01	1.92	2.77	1.66	2.31	20.17	16.30	0.12	0.04	99.41
cad6-62	conc	0.19	53.86	0.00	1.91	2.90	1.51	2.56	20.94	15.88	0.11	0.03	99.94
cad6-63	conc	0.09	53.76	0.01	2.06	2.73	2.00	2.60	19.95	15.95	0.10	0.05	99.34
cad6-64	conc	0.30	53.39	0.00	1.54	3.39	1.42	2.19	20.39	16.51	0.12	0.04	99.37
cad6-65	conc	0.26	54.00	0.00	1.47	2.78	1.72	1.37	21.42	16.47	0.10	0.04	99.68
cad6-66	conc	0.24	54.20	0.01	1.77	3.26	0.94	2.92	18.49	17.41	0.12	0.06	99.45
cad6-67	conc	0.18	53.82	0.00	2.11	3.27	1.26	2.99	20.22	15.63	0.13	0.03	99.66
cad6-68	conc	0.15	54.20	0.00	2.15	2.57	2.20	2.68	18.69	16.06	0.09	0.05	98.87
cad6-69	conc	0.22	54.23	0.01	2.12	2.59	2.39	2.70	18.34	16.36	0.09	0.04	99.13
cad6-70	conc	0.31	54.16	0.00	2.08	2.87	1.21	2.95	18.94	16.07	0.08	0.04	98.76
cad6-72	conc	0.07	53.48	0.01	1.24	1.76	1.00	3.48	21.59	16.11	0.09	0.04	98.90
cad6-73	conc	0.16	54.13	0.00	1.75	3.75	1.23	2.34	19.30	16.06	0.11	0.04	98.91
cad6-74	conc	0.26	54.38	0.00	1.97	2.64	1.37	2.95	18.80	16.59	0.10	0.05	99.14
cad6-75	conc	0.17	53.62	0.02	1.48	2.84	1.14	2.66	20.18	16.39	0.09	0.04	98.68
cad6-76	conc	0.23	54.16	0.01	1.92	2.63	1.34	2.80	19.14	16.51	0.08	0.06	98.92
cad6-77	conc	0.22	54.32	0.01	1.93	3.12	1.36	2.31	19.65	15.86	0.08	0.05	98.95
cad6-78	conc	0.24	54.29	0.00	1.84	2.41	1.28	2.92	20.05	15.77	0.08	0.05	98.99
cad6-79	conc	0.17	54.52	0.01	1.99	3.47	1.49	2.66	18.53	16.28	0.11	0.04	99.29
cad6-80	conc	0.12	54.38	0.01	1.98	2.62	1.78	2.72	18.51	16.31	0.11	0.04	98.63
cad6-81	conc	0.18	54.16	0.00	1.86	2.48	1.72	2.52	19.94	15.90	0.07	0.04	98.91
cad6-82	conc	0.20	54.34	0.01	2.20	2.58	2.38	2.90	18.11	16.33	0.10	0.04	99.24
cad6-83	conc	0.19	54.06	0.01	1.83	2.85	1.30	2.82	19.95	15.70	0.08	0.04	98.85
cad6-84	conc	0.11	54.75	0.01	2.20	2.93	1.62	2.43	19.02	16.14	0.10	0.04	99.39
cad6-85	conc	0.19	54.11	0.00	1.73	3.08	1.23	2.36	19.96	16.18	0.09	0.04	99.00
cad6-86	conc	0.12	54.56	0.01	2.00	2.79	1.33	2.90	18.73	16.54	0.09	0.05	99.16
cad6-87	conc	0.13	54.32	0.00	1.88	2.86	1.31	2.86	18.62	16.57	0.08	0.05	98.72
cad6-89	conc	0.25	54.24	0.00	1.90	2.83	1.21	2.87	19.11	16.29	0.08	0.04	98.88
cad6-90	conc	0.15	54.90	0.00	1.99	2.66	1.62	2.59	18.77	16.42	0.09	0.04	99.29
cad6-91	conc	0.30	54.33	0.01	1.97	3.02	1.12	3.10	18.36	16.46	0.10	0.05	98.85
cad6-92	conc	0.32	54.15	0.00	2.22	2.41	0.87	3.64	19.52	15.38	0.05	0.04	98.68

Appendix B

Carolina Clinopyroxene Data

cont.

Grain	loc.	TiO_2	SiO_2	K_2O	Na_2O	FeO	Cr_2O_3	Al_2O_3	CaO	MgO	MnO	NiO	Total
cad6-93	conc	0.33	54.07	0.03	1.14	2.97	1.22	2.36	18.03	18.44	0.11	0.07	98.80
cad6-94	conc	0.40	54.15	0.02	1.27	3.12	1.12	2.46	18.25	18.00	0.11	0.05	98.98
cad6-95	conc	0.34	54.30	0.00	2.12	3.05	1.11	3.09	18.92	16.05	0.07	0.05	99.16
cad6-96	conc	0.09	54.47	0.01	2.21	2.42	2.07	2.77	18.63	16.07	0.09	0.03	98.88
cad6-97	conc	0.09	54.42	0.01	1.76	3.20	1.61	1.89	18.98	16.60	0.10	0.04	98.76
cad8-2	conc	0.23	53.89	0.00	2.83	3.27	1.30	4.05	19.66	15.07	0.10	0.04	100.50
cad8-8	conc	0.26	54.28	0.00	2.57	3.20	1.05	3.79	20.12	15.70	0.09	0.03	101.14
cad8-10	conc	0.07	53.47	0.00	1.02	2.38	1.42	1.89	22.96	16.91	0.08	0.06	100.28
cad8-11	conc	0.27	53.35	0.00	1.80	3.32	0.67	2.78	21.04	15.94	0.10	0.04	99.34
cad8-12	conc	0.32	53.19	0.00	2.25	2.76	1.27	3.78	21.45	14.85	0.06	0.03	100.04
cad8-15	conc	0.09	53.06	0.00	2.44	2.52	2.30	3.07	19.54	15.56	0.09	0.05	98.77
cad8-16	conc	0.13	53.61	0.01	1.67	3.13	1.52	2.14	21.39	16.14	0.09	0.04	99.94
cad8-17	conc	0.24	53.99	0.00	3.06	3.15	1.15	4.56	18.54	14.61	0.09	0.04	99.51
cad8-19	conc	0.24	53.56	0.01	2.03	2.58	1.58	2.76	21.25	15.47	0.07	0.04	99.65
cad8-21	conc	0.15	53.16	0.00	1.70	2.70	1.18	2.53	21.99	15.56	0.07	0.04	99.15
cad8-22	conc	0.06	54.16	0.01	2.19	2.58	2.22	2.87	19.89	15.96	0.08	0.04	100.10
cad C1-1	core	0.02	54.07	0.04	1.22	2.85	0.95	1.37	20.83	17.58	0.08	0.05	99.11
cad-C1-2	core	0.26	53.63	0.00	1.04	3.08	1.35	1.00	20.97	17.43	0.09	0.05	98.94
cad-C1-3	core	0.28	54.11	0.02	1.59	3.27	1.28	1.56	19.41	17.36	0.09	0.04	99.05
cad-C1-4	core	0.12	54.01	0.02	2.24	2.95	2.23	2.08	18.96	16.11	0.10	0.04	98.92
cad-C1-5	core	0.28	53.99	0.04	1.76	3.39	1.19	1.86	19.18	17.02	0.07	0.05	98.86
cad-C1-6	core	0.16	53.58	0.02	2.00	2.45	1.59	2.18	19.93	16.18	0.08	0.04	98.29
cad-C1-7	core	0.17	54.08	0.02	1.99	2.53	1.70	2.20	19.90	16.15	0.07	0.05	98.89
cad-C1-8	core	0.18	54.48	0.02	1.56	3.48	1.13	1.25	19.97	16.95	0.12	0.05	99.26
cad-C1-9	core	0.17	54.37	0.03	2.00	2.45	1.59	2.25	19.88	16.15	0.08	0.04	99.07
cad-C1-10	core	0.27	53.87	0.03	1.59	3.35	1.31	1.61	19.51	17.18	0.11	0.05	98.91
cad-C1-11	core	0.22	53.77	0.01	1.41	3.39	1.87	0.87	20.46	16.59	0.09	0.06	98.76
cad-C1-12	core	0.14	54.37	0.02	1.88	3.06	1.09	2.17	19.32	16.66	0.12	0.05	98.93
cad-C1-13	core	0.15	53.95	0.02	2.00	2.86	2.95	0.99	19.42	16.41	0.10	0.04	98.94
cad-C1-14	core	0.33	53.92	0.02	1.53	3.14	1.82	1.16	19.26	17.59	0.09	0.05	98.95
cad-C1-15	core	0.22	54.16	0.02	2.22	2.62	1.92	2.25	18.83	16.51	0.12	0.05	98.99
cad-C1-16	core	0.16	54.08	0.01	2.02	3.25	2.29	1.31	19.00	16.43	0.10	0.04	98.75
cad-C1-17	core	0.24	54.06	0.02	2.12	3.11	1.56	2.20	18.32	16.97	0.10	0.06	98.82
cad-C2-5	core	0.12	54.57	0.02	1.47	2.38	1.25	1.69	21.02	16.69	0.08	0.05	99.41
cad-C2-6	core	0.10	54.53	0.01	1.92	2.97	1.35	2.04	19.46	16.55	0.07	0.04	99.09
cad-C2-7	core	0.15	54.03	0.08	1.32	3.41	1.91	0.69	20.04	17.03	0.11	0.05	98.86
cad-C2-1	core	0.11	54.38	0.03	1.46	2.33	1.23	1.74	21.21	16.78	0.05	0.05	99.41
cad-C2-2	core	0.11	55.11	0.04	1.50	2.35	1.20	1.78	20.92	16.79	0.07	0.04	99.95
cad-C2-3	core	0.16	54.34	0.02	1.85	2.97	1.49	1.90	19.76	16.35	0.09	0.04	99.04
cad-C2-4	core	0.11	55.09	0.01	1.60	2.84	1.40	1.54	20.66	16.87	0.08	0.04	100.29

Appendix B

Carolina Clinopyroxene Data

Figure B.1. Discrimination diagrams of Carolina clinopyroxene electron microprobe data (derived from core and concentrate) to distinguish the correct grain compositions to use for the Nimis and Taylor (2000) geothermobarometer.

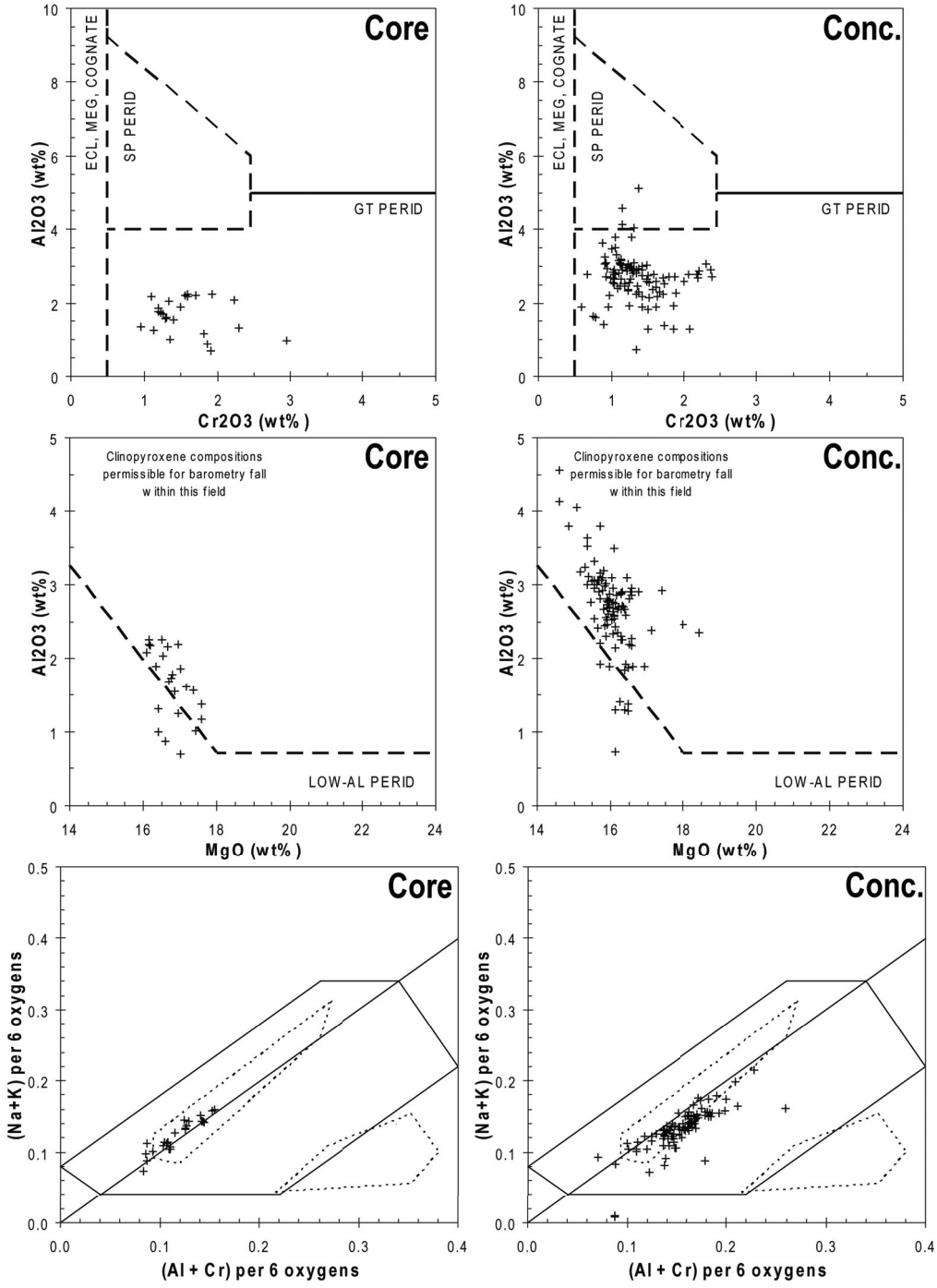

Appendix B

Carolina Clinopyroxene Data

Figure B.2. Nimis and Taylor (2000) geothermobarometer diagrams for Carolina clinopyroxenes derived from core and from concentrate

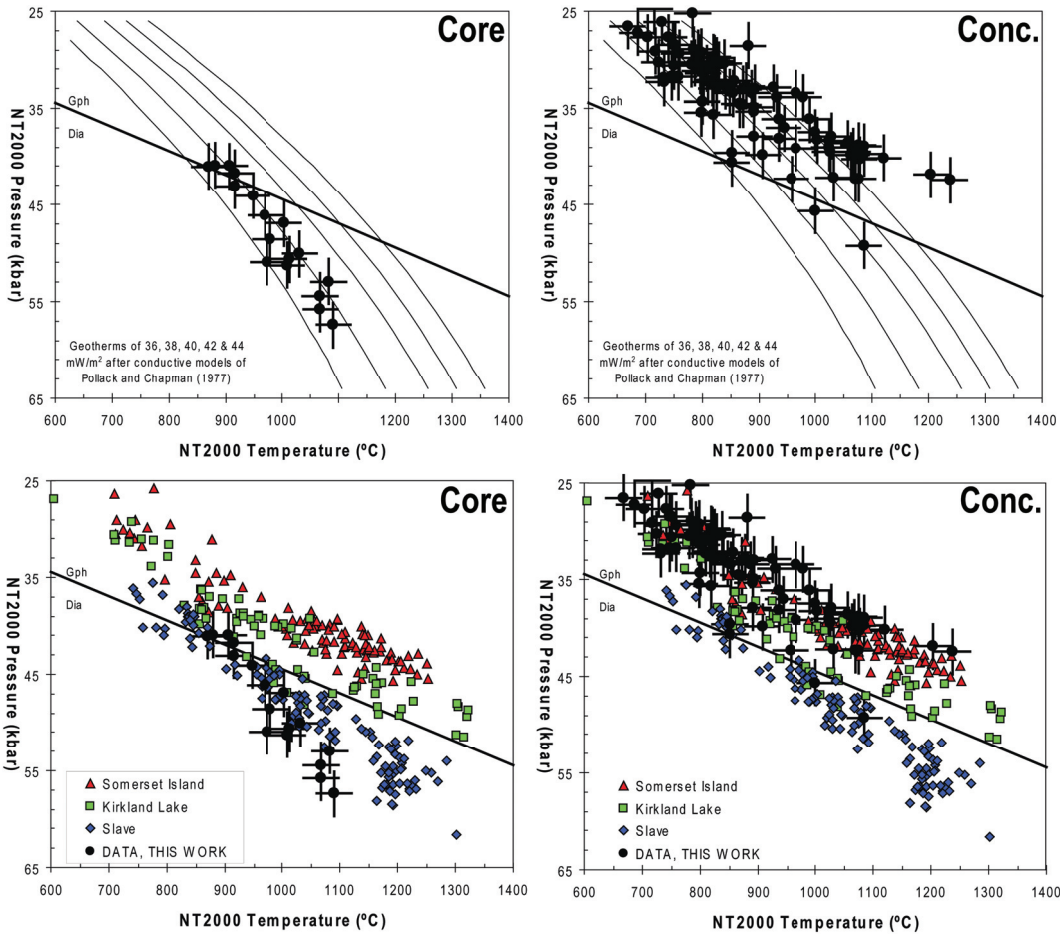

Appendix B

Carolina Garnet Data

Table B.2. Carolina garnet electron microprobe data separated into minerals derived from concentrate and core, indicated in the loc. (location) column.

Grain	Gnt	loc.	SiO_2	TiO_2	Al_2O_3	Cr_2O_3	FeO	MnO	NiO	MgO	CaO	Na_2O	Total
cad-C3-10	G9	core	41.89	0.19	20.69	3.55	8.29	0.42	0.01	19.85	5.13	0.04	100.11
cad-C3-11	G9	core	41.94	0.31	20.59	3.33	7.62	0.38	0.01	20.99	4.51	0.07	99.81
cad-C3-12	G9	core	41.92	0.19	20.76	3.53	8.28	0.43	0.01	19.83	5.23	0.05	100.28
cad-C3-13	G9	core	42.00	0.32	21.66	1.69	7.90	0.37	0.01	21.00	4.60	0.04	99.63
cad-C3-14	G9	core	41.76	0.19	20.76	3.54	8.28	0.42	0.01	19.90	5.19	0.04	100.14
cad-C3-15	G3D	core	40.81	0.24	22.74	0.03	16.38	0.31	0.00	13.03	7.24	0.13	100.98
cad-C3-16	G9	core	42.16	0.10	21.28	3.14	7.67	0.38	0.01	20.85	4.42	0.06	100.17
cad-C3-17	G9	core	42.10	0.14	19.89	4.44	7.11	0.31	0.01	20.77	5.08	0.04	99.95
cad-C3-18	G3D	core	40.77	0.24	22.98	0.04	16.41	0.32	0.01	13.03	7.11	0.11	101.10
cad-C3-19	G3D	core	40.97	0.24	23.01	0.05	15.66	0.28	0.01	13.93	6.72	0.13	101.06
cad-C3-20	G4D	core	41.68	0.27	23.11	0.08	11.57	0.32	0.01	17.54	5.70	0.11	100.52
cad-C3-21	G3D	core	40.62	0.26	22.80	0.04	17.97	0.35	0.01	11.78	7.33	0.13	101.35
cad-C3-22	G9	core	42.15	0.23	20.40	4.11	6.85	0.32	0.00	21.02	4.95	0.04	100.12
cad-C3-23	G9	core	42.16	0.20	21.40	2.85	7.37	0.34	0.00	21.09	4.62	0.04	100.12
cad-C3-24	G9	core	42.04	0.31	21.75	2.50	6.89	0.34	0.01	21.52	4.20	0.07	99.69
cad-C5-10	G9	core	41.68	0.15	20.66	3.82	8.59	0.48	0.00	19.80	4.89	0.05	100.23
cad-C5-11	G3D	core	40.91	0.25	23.31	0.04	16.20	0.29	0.00	13.88	6.35	0.13	101.46
cad-C5-15	G9	core	42.09	0.12	21.62	2.91	7.53	0.35	0.01	20.87	4.57	0.04	100.18
cad-C5-16	G9	core	42.10	0.12	21.34	3.25	7.68	0.39	0.01	20.87	4.34	0.06	100.25
cad-C5-19	G9	core	42.07	0.12	21.75	2.42	7.90	0.37	0.00	20.47	4.56	0.04	99.76
cad-C5-20	G9	core	41.65	0.17	20.76	3.45	8.17	0.43	0.00	19.75	5.03	0.04	99.52
cad-C5-21	G9	core	41.71	0.19	20.75	3.52	8.28	0.41	0.01	19.48	5.13	0.04	99.56
cad-C5-22	G9	core	41.83	0.12	21.56	2.41	7.87	0.38	0.01	20.51	4.52	0.04	99.28
cad-C5-23	G9	core	41.81	0.20	20.79	3.54	8.33	0.42	0.01	19.43	5.11	0.04	99.71
cad-C5-24	G9	core	41.32	0.25	20.41	3.63	8.07	0.39	0.01	20.01	4.73	0.06	98.92
cad-C5-25	G9	core	41.80	0.14	21.73	2.39	7.84	0.37	0.00	20.46	4.49	0.03	99.30
cad-C5-29	G3D	core	40.40	0.21	22.64	0.03	16.29	0.30	0.00	13.79	6.15	0.13	100.01
cad-C5-3	G3D	core	40.56	0.26	22.82	0.05	17.01	0.30	0.01	11.37	8.45	0.12	101.02
cad-C5-30	G9	core	41.53	0.18	20.92	3.48	8.27	0.42	0.00	19.77	5.18	0.04	99.84
cad-C5-31	G9	core	41.38	0.19	20.80	3.50	8.31	0.43	0.00	19.60	5.13	0.04	99.43
cad-C5-33	G9	core	41.30	0.13	19.71	4.81	7.53	0.42	0.00	19.91	5.31	0.03	99.21
cad-C5-34	G9	core	41.84	0.17	20.62	3.80	7.29	0.38	0.01	20.72	4.69	0.06	99.67
cad-C5-35	G9	core	42.24	0.20	22.56	1.25	7.77	0.39	0.01	21.15	4.11	0.05	99.80
cad-C5-36	G3D	core	41.39	0.30	22.84	0.05	12.46	0.33	0.00	16.51	6.36	0.09	100.39
cad-C5-37	G9	core	41.80	0.31	20.89	3.40	7.56	0.36	0.00	20.86	4.48	0.07	99.78
cad-C5-38	G9	core	41.82	0.30	20.86	3.37	7.59	0.37	0.01	20.90	4.45	0.07	99.76
cad-C5-39	G9	core	41.73	0.17	21.12	3.43	8.17	0.43	0.01	19.83	5.02	0.04	99.99
cad-C5-40	G3D	core	41.40	0.30	23.10	0.04	12.52	0.33	0.00	16.33	6.43	0.09	100.61
cad-C5-41	G3D	core	41.26	0.31	23.08	0.05	12.53	0.32	0.01	16.35	6.33	0.09	100.41
cad-C5-42	G9	core	41.92	0.18	21.26	3.52	8.30	0.42	0.01	19.78	5.06	0.05	100.53
cad-C5-43	G9	core	41.79	0.20	21.24	3.52	8.31	0.43	0.00	19.74	5.09	0.04	100.41
cad-C5-44	G9	core	41.78	0.19	21.16	3.52	8.23	0.44	0.00	19.83	5.08	0.04	100.33
cad-C5-45	G4D	core	40.63	0.28	22.84	0.15	18.84	0.35	0.00	14.18	3.79	0.12	101.25

Appendix B

Carolina Garnet Data

cont.

Grain	Gnt	loc.	SiO_2	TiO_2	Al_2O_3	Cr_2O_3	FeO	MnO	NiO	MgO	CaO	Na_2O	Total
cad-C5-46	G9	core	41.73	0.16	21.17	3.46	8.19	0.41	0.01	19.82	4.99	0.04	100.05
cad-C5-48	G9	core	41.99	0.12	21.91	2.43	7.85	0.37	0.01	20.68	4.50	0.04	99.94
cad-C5-49	G9	core	41.79	0.18	20.79	3.56	8.32	0.43	0.01	19.62	5.08	0.04	99.86
cad-C5-5	G9	core	41.74	0.11	20.87	3.77	8.22	0.44	0.00	19.41	5.28	0.03	99.92
cad-C5-50	G9	core	41.44	0.19	20.71	3.50	8.27	0.42	0.00	19.80	5.09	0.04	99.52
cad-C5-51	G3D	core	40.53	0.24	22.65	0.02	16.58	0.31	0.01	13.29	6.51	0.11	100.32
cad-C5-52	G1	core	41.79	0.62	21.36	1.86	8.53	0.32	0.00	20.64	4.21	0.09	99.46
cad-C5-53	G9	core	41.98	0.31	20.71	3.27	7.63	0.37	0.01	20.90	4.45	0.07	99.76
cad-C5-54	G9	core	41.70	0.12	20.11	4.17	8.01	0.41	0.00	20.14	4.86	0.05	99.68
cad-C5-55	G9	core	41.47	0.18	20.65	3.49	8.30	0.43	0.01	19.62	5.01	0.04	99.24
cad-C5-56	G9	core	41.71	0.14	21.48	2.43	7.85	0.38	0.00	20.38	4.49	0.04	98.93
cad-C5-57	G3D	core	40.02	0.28	22.40	0.02	18.54	0.33	0.00	10.41	8.37	0.14	100.55
cad-C5-58	G9	core	41.53	0.17	20.85	3.51	8.24	0.43	0.00	19.77	5.06	0.03	99.64
cad-C5-59	G9	core	41.63	0.14	21.69	2.43	7.90	0.37	0.00	20.53	4.52	0.04	99.29
cad-C5-6	G3D	core	40.65	0.24	22.77	0.04	16.88	0.31	0.01	11.44	8.47	0.13	100.99
cad-C5-61	G9	core	41.51	0.20	20.69	3.58	8.29	0.42	0.01	19.67	5.11	0.04	99.57
cad-C5-64	G9	core	41.51	0.10	20.61	3.93	7.74	0.42	0.01	19.98	4.84	0.04	99.21
cad-C5-65	G4D	core	41.23	0.27	23.08	0.07	11.48	0.34	0.01	17.52	5.50	0.10	99.69
cad-C5-67	G9	core	41.51	0.10	20.52	4.02	7.74	0.40	0.01	20.12	4.90	0.03	99.41
cad-C5-68	G3D	core	40.30	0.26	22.69	0.04	18.03	0.34	0.01	11.85	7.17	0.12	100.87
cad-C5-69	G3D	core	39.96	0.24	22.54	0.06	16.89	0.31	0.00	11.43	8.26	0.12	99.88
cad-C5-7	G9	core	42.08	0.16	20.00	4.55	7.07	0.31	0.01	20.79	5.05	0.06	100.15
cad-C5-72	G3D	core	40.15	0.17	22.67	0.02	16.92	0.36	0.01	11.72	7.85	0.11	100.06
cad-C5-74	G3D	core	40.49	0.24	22.71	0.05	16.03	0.29	0.00	13.64	6.19	0.12	99.86
cad-C5-76	G3D	core	39.97	0.23	22.48	0.05	17.94	0.35	0.00	11.63	7.05	0.15	99.92
cad-C5-78	G3D	core	40.00	0.25	22.66	0.04	17.11	0.32	0.01	11.28	8.18	0.13	100.07
cad-C5-79	G4	core	41.56	0.28	23.09	0.24	9.53	0.33	0.00	20.21	3.74	0.06	99.12
cad-C5-8	G3D	core	40.89	0.22	23.04	0.04	16.59	0.32	0.00	13.40	6.46	0.12	101.14
cad-C5-80	G3D	core	40.08	0.17	22.72	0.04	16.93	0.34	0.00	11.74	7.73	0.11	99.93
cad-C5-81	G3D	core	40.09	0.24	22.73	0.06	16.82	0.31	0.01	11.42	8.15	0.12	100.02
cad-C5-82	G3D	core	40.55	0.22	22.99	0.04	16.33	0.31	0.00	12.93	6.95	0.13	100.54
cad-C5-83	G9	core	41.94	0.10	20.96	3.83	7.80	0.41	0.00	20.14	4.83	0.03	100.10
cad-C6-12	G9	core	40.76	0.07	18.47	5.77	7.78	0.41	0.01	18.72	5.97	0.03	98.05
cad-C6-13	G9	core	41.17	0.17	20.38	3.44	8.21	0.42	0.01	19.29	5.00	0.04	98.18
cad-C6-16	G9	core	41.05	0.16	20.41	3.40	8.09	0.42	0.01	19.38	5.03	0.03	98.01
cad-C6-2	G9	core	41.38	0.16	20.59	3.39	8.12	0.43	0.01	19.40	5.01	0.03	98.57
cad-C6-44	G9	core	41.67	0.24	19.70	4.40	7.81	0.40	0.00	19.89	5.05	0.05	99.27
cad-C6-45	G9	core	41.70	0.17	20.57	3.46	8.31	0.42	0.01	19.56	4.98	0.04	99.28
cad-C6-47	G9	core	42.00	0.14	21.40	2.44	7.88	0.38	0.01	20.30	4.57	0.04	99.20
cad C4-1	G9	core	42.46	0.11	21.97	3.13	7.92	0.40	0.01	21.29	4.44	0.06	101.90
cad C4-2	G9	core	42.48	0.21	20.76	4.32	7.35	0.38	0.01	21.14	5.09	0.04	101.82
cad C4-3	G3D	core	41.38	0.21	23.57	0.06	15.83	0.33	0.01	14.52	6.51	0.12	102.61
cad C4-4	G3D	core	41.10	0.22	23.42	0.07	16.44	0.35	0.00	13.51	7.20	0.11	102.52
cad C4-5	G3D	core	41.09	0.23	23.44	0.04	16.60	0.38	0.01	13.53	7.01	0.12	102.53
cad C4-6	G9	core	42.26	0.19	21.43	3.56	8.55	0.45	0.00	20.19	5.24	0.04	101.97
cad C4-7	G9	core	42.33	0.31	21.45	3.33	7.89	0.41	0.01	21.37	4.59	0.07	101.80
cad C4-8	G9	core	41.99	0.18	21.48	3.45	8.47	0.45	0.01	20.16	5.20	0.04	101.46

Appendix B

Carolina Garnet Data

cont.

Grain	Gnt	loc.	SiO_2	TiO_2	Al_2O_3	Cr_2O_3	FeO	MnO	NiO	MgO	CaO	Na_2O	Total
cad C4-9	G9	core	42.20	0.13	22.34	2.44	8.10	0.41	0.00	21.13	4.61	0.04	101.45
cad C4-10	G9	core	42.14	0.18	21.46	3.52	8.59	0.44	0.00	20.24	5.23	0.05	101.92
cad C4-11	G3D	core	41.73	0.30	23.31	0.05	12.84	0.39	0.00	16.69	6.69	0.09	102.18
cad C4-12	G4D	core	42.05	0.29	23.62	0.06	11.83	0.37	0.00	18.10	5.60	0.11	102.14
cad C4-13	G9	core	42.16	0.23	20.79	4.16	8.06	0.46	0.01	20.68	5.10	0.06	101.79
cad C4-14	G9	core	41.95	0.13	20.82	4.12	8.27	0.46	0.01	20.57	4.96	0.05	101.44
cad C4-15	G9	core	42.05	0.31	21.24	3.28	7.82	0.42	0.01	21.21	4.55	0.06	101.01
cad C4-16	G3D	core	40.51	0.20	23.07	0.05	18.28	0.41	0.00	11.33	8.45	0.12	102.50
cad C4-17	G3D	core	41.02	0.22	23.42	0.03	16.50	0.34	0.01	14.02	6.47	0.11	102.22
cad C4-18	G9	core	42.07	0.18	21.36	3.55	8.50	0.49	0.00	20.16	5.25	0.04	101.66
cad C4-19	G9	core	41.95	0.18	21.30	3.54	8.48	0.49	0.01	20.15	5.24	0.04	101.43
cad C4-20	G9	core	42.12	0.13	22.14	2.39	8.11	0.43	0.01	20.91	4.68	0.03	101.00
cad C4-21	G1	core	42.25	0.50	22.51	1.35	9.45	0.40	0.01	20.77	4.14	0.10	101.53
cad C4-22	G9	core	42.03	0.17	21.34	3.44	8.46	0.50	0.00	20.08	5.15	0.03	101.25
cad C4-23	G9	core	42.23	0.15	22.21	2.44	8.17	0.44	0.01	20.89	4.74	0.04	101.36
cad C4-24	G9	core	42.03	0.20	21.30	3.55	8.59	0.47	0.01	19.94	5.28	0.04	101.46
cad C4-25	G9	core	42.13	0.29	21.24	3.34	7.86	0.44	0.01	21.24	4.64	0.06	101.33
cad C4-26	G9	core	41.88	0.14	20.77	4.38	8.06	0.52	0.00	20.28	5.34	0.03	101.44
cad C4-27	G3D	core	40.59	0.21	23.16	0.05	18.28	0.41	0.01	11.19	8.55	0.13	102.64
cad C4-28	G9	core	42.22	0.30	21.34	3.36	7.85	0.43	0.00	21.27	4.65	0.06	101.54
cad C4-29	G3D	core	41.70	0.31	23.26	0.05	12.69	0.38	0.00	16.64	6.60	0.10	101.81
cad C4-30	G4D	core	40.85	0.27	23.12	0.14	18.97	0.42	0.00	14.48	3.92	0.11	102.34
cad C4-31	G12	core	46.44	0.14	14.99	2.70	6.49	0.36	0.01	19.06	10.63	0.52	101.39
cad C4-32	G9	core	42.12	0.30	21.42	3.29	7.86	0.44	0.00	21.14	4.59	0.07	101.29
cad C4-33	G9	core	42.07	0.19	20.41	4.71	7.64	0.44	0.01	20.82	5.04	0.06	101.49
cad C4-34	G9	core	41.90	0.17	21.45	3.45	8.53	0.46	0.00	20.14	5.26	0.05	101.48
cad C4-35	G3D	core	40.97	0.21	23.39	0.05	16.55	0.33	0.01	14.15	6.36	0.11	102.21
cad C4-36	G9	core	42.25	0.31	21.49	3.35	7.85	0.45	0.01	21.11	4.63	0.07	101.58
cad C4-37	G3D	core	40.59	0.21	23.12	0.04	18.36	0.40	0.01	11.25	8.55	0.12	102.72
cad C4-38	G9	core	42.24	0.14	22.29	2.46	8.18	0.43	0.01	20.94	4.76	0.04	101.53
cad C4-39	G9	core	42.39	0.25	21.49	3.20	7.83	0.46	0.00	21.13	4.83	0.06	101.72
cad C4-40	G9	core	42.06	0.17	21.52	3.43	8.45	0.47	0.01	20.12	5.31	0.03	101.64
cad C4-41	G9	core	42.08	0.30	21.31	3.32	7.81	0.42	0.00	21.20	4.67	0.06	101.23
cad C4-42	G9	core	42.30	0.13	22.34	2.44	8.14	0.47	0.00	21.06	4.68	0.04	101.67
cad C4-43	G9	core	41.90	0.25	20.61	4.34	8.06	0.45	0.01	20.49	5.20	0.05	101.42
cad C4-44	G9	core	42.01	0.13	20.77	4.45	8.11	0.47	0.01	20.18	5.35	0.02	101.55
cad C4-45	G9	core	41.94	0.20	21.39	3.53	8.52	0.48	0.01	20.10	5.29	0.04	101.54
cad C4-46	G9	core	41.93	0.18	21.39	3.50	8.50	0.48	0.01	20.03	5.31	0.04	101.41
cad C4-47	G9	core	42.18	0.13	22.23	2.45	8.14	0.44	0.00	20.95	4.69	0.03	101.29
cad C4-48	G9	core	42.08	0.30	21.31	3.36	7.84	0.43	0.01	21.18	4.66	0.06	101.28
cad C4-49	G9	core	42.17	0.32	22.10	2.42	7.85	0.42	0.01	21.17	4.81	0.07	101.41
cad C4-50	G9	core	42.11	0.31	21.35	3.39	7.82	0.42	0.01	21.09	4.70	0.07	101.32
cad C4-51	G9	core	42.27	0.19	22.33	2.52	8.18	0.45	0.00	21.02	4.72	0.05	101.79
cad C4-52	G9	core	41.77	0.08	20.06	5.30	7.98	0.46	0.00	19.91	5.78	0.02	101.41
cad C4-53	G9	core	41.89	0.18	21.41	3.60	8.49	0.48	0.01	19.99	5.38	0.03	101.51
cad C4-54	G9	core	42.31	0.14	22.44	2.41	8.09	0.43	0.01	20.99	4.71	0.04	101.62
cad C4-55	G9	core	42.23	0.14	22.29	2.47	8.09	0.42	0.00	21.07	4.69	0.04	101.49

Appendix B

Carolina Garnet Data

cont.

Grain	Gnt	loc.	SiO_2	TiO_2	Al_2O_3	Cr_2O_3	FeO	MnO	NiO	MgO	CaO	Na_2O	Total
cad C3-1	G9	core	41.89	0.17	21.46	3.44	8.42	0.47	0.00	20.04	5.25	0.04	101.23
cad C3-2	G9	core	41.92	0.19	21.52	3.49	8.46	0.47	0.01	20.06	5.28	0.04	101.49
cad C3-3	G9	core	42.06	0.19	21.47	3.53	8.47	0.47	0.01	20.20	5.31	0.04	101.80
cad C3-4	G4D	core	41.19	0.16	23.61	0.10	17.04	0.36	0.01	14.41	5.87	0.09	102.88
cad C3-5	G9	core	42.12	0.19	21.47	3.55	8.52	0.44	0.01	20.13	5.29	0.03	101.81
cad C3-6	G9	core	42.20	0.14	22.28	2.45	8.21	0.41	0.01	20.93	4.72	0.03	101.43
cad C3-7	G4D	core	40.89	0.16	23.38	0.11	17.12	0.33	0.01	14.10	5.83	0.09	102.07
cad C3-8	G1	core	42.19	0.51	22.37	1.32	9.41	0.37	0.01	20.71	4.14	0.09	101.20
cad C3-9	G9	core	41.93	0.17	21.57	3.44	8.35	0.45	0.00	20.27	5.25	0.04	101.53
cad C3-10	G9	core	41.94	0.18	21.50	3.48	8.51	0.44	0.01	20.16	5.27	0.05	101.60
cad C3-11	G9	core	42.04	0.30	21.28	3.32	7.88	0.38	0.02	21.19	4.60	0.06	101.14
C7-1	G4	core	42.49	0.17	23.51	0.35	7.55	0.35	0.01	22.08	3.97	0.04	100.57
C7-2	G9	core	41.07	0.07	17.33	8.18	7.45	0.43	0.00	19.47	6.09	0.05	100.33
C7-3	G1	core	42.03	0.58	20.36	3.88	6.93	0.31	0.01	21.49	4.78	0.09	100.52
C7-4	G3D	core	40.80	0.22	23.11	0.12	16.61	0.36	0.01	13.22	7.25	0.09	101.78
C7-5	G9	core	41.77	0.29	19.68	5.23	8.02	0.38	0.01	20.08	5.23	0.06	100.81
C7-6	G9	core	41.48	0.11	16.86	9.07	6.73	0.36	0.01	19.97	6.09	0.04	100.79
C7-7	G4D	core	41.56	0.15	23.49	0.16	13.71	0.41	0.00	16.49	5.55	0.08	101.68
C7-8	G9	core	41.60	0.24	18.80	6.33	7.77	0.40	0.01	19.80	5.77	0.06	100.86
C7-9	G3D	core	41.07	0.24	23.14	0.13	11.39	0.23	0.01	12.17	12.71	0.10	101.23
C7-10	G1	core	42.05	0.67	20.60	3.47	7.88	0.33	0.01	20.87	4.72	0.13	100.83
C7-11	G9	core	42.16	0.23	20.89	3.89	7.55	0.41	0.01	21.05	4.48	0.06	100.78
C7-12	G3D	core	41.08	0.18	23.30	0.07	16.21	0.34	0.01	13.80	6.87	0.11	102.02
C7-13	G3D	core	40.93	0.24	23.21	0.05	16.58	0.30	0.01	13.65	6.81	0.13	101.95
C7-14	G11	core	41.88	0.66	19.48	5.17	6.91	0.32	0.01	21.01	5.12	0.09	100.72
C7-15	G9	core	41.82	0.14	20.15	4.91	8.15	0.42	0.00	19.66	5.62	0.04	100.99
C7-16	G9	core	41.85	0.24	20.14	4.75	7.48	0.38	0.01	20.64	5.08	0.06	100.69
C7-17	G11	core	41.62	1.02	18.58	5.43	7.08	0.33	0.01	20.55	5.52	0.11	100.33
C7-18	G1	core	42.14	0.37	20.67	3.57	7.10	0.31	0.01	21.24	4.91	0.06	100.42
C7-19	G9	core	42.41	0.36	21.54	3.08	7.30	0.35	0.01	21.30	4.51	0.08	100.98
C7-20	G9	core	42.06	0.24	20.69	3.97	7.71	0.39	0.01	20.71	4.89	0.04	100.76
C7-23	G9	core	41.51	0.12	20.24	4.74	7.85	0.44	0.00	20.06	5.36	0.04	100.39
C7-24	G9	core	41.83	0.20	20.60	3.61	7.31	0.32	0.02	21.15	4.84	0.05	99.96
C7-31	G9	core	42.02	0.33	20.42	4.27	7.38	0.35	0.00	21.11	4.56	0.07	100.53
C7-34	G3D	core	41.72	0.18	23.74	0.10	8.29	0.17	0.02	15.26	11.51	0.13	101.27
C7-41	G3D	core	40.90	0.21	23.22	0.04	16.35	0.29	0.01	14.13	6.22	0.11	101.52
C7-43	G11	core	41.89	0.56	19.41	5.09	6.78	0.31	0.00	21.22	5.05	0.08	100.45
C7-48	G9	core	42.15	0.15	21.88	2.52	8.04	0.39	0.00	20.84	4.49	0.05	100.53
C7-53	G1	core	42.23	0.84	20.08	3.92	7.11	0.32	0.02	21.29	5.05	0.10	101.04
cad8-1	G9	conc	41.37	0.08	21.57	3.17	8.45	0.45	0.00	19.88	5.84	0.04	100.89
cad8-2	G9	conc	41.32	0.16	21.83	2.65	9.20	0.48	0.01	19.99	5.26	0.05	100.98
cad8-3	G4D	conc	41.72	0.31	23.37	0.28	12.17	0.38	0.00	19.01	4.60	0.08	101.96
cad8-4	G9	conc	41.56	0.15	21.86	2.90	9.23	0.48	0.00	19.65	5.50	0.04	101.41
cad8-5	G9	conc	41.90	0.17	22.29	2.46	9.13	0.45	0.00	20.01	5.30	0.04	101.78
cad8-6	G9	conc	41.70	0.08	22.85	1.59	9.85	0.46	0.00	19.67	4.98	0.03	101.27
cad8-7	G9	conc	41.79	0.15	22.44	2.03	8.12	0.37	0.01	20.95	5.02	0.04	100.96
cad8-8	G9	conc	41.82	0.20	22.47	1.94	8.80	0.39	0.01	20.45	4.94	0.05	101.12

Appendix B

Carolina Garnet Data

cont.

Grain	Gnt	loc.	SiO_2	TiO_2	Al_2O_3	Cr_2O_3	FeO	MnO	NiO	MgO	CaO	Na_2O	Total
cad8-9	G9	conc	41.93	0.16	23.11	1.25	9.99	0.43	0.00	19.65	4.86	0.05	101.47
cad8-10	G12	conc	41.06	0.05	19.65	5.50	7.48	0.41	0.00	19.41	6.84	0.03	100.50
cad8-12	G9	conc	41.25	0.08	22.67	1.52	9.52	0.47	0.00	19.60	4.91	0.03	100.09
cad8-13	G9	conc	41.86	0.06	22.71	1.76	9.75	0.53	0.00	19.45	5.39	0.03	101.59
cad8-14	G4	conc	41.94	0.17	23.52	0.27	11.73	0.41	0.01	18.92	4.80	0.05	101.86
cad8-15	G9	conc	41.42	0.10	20.58	4.29	7.59	0.42	0.01	20.10	5.67	0.05	100.31
cad8-17	G9	conc	41.50	0.16	22.32	1.94	8.55	0.41	0.01	20.20	5.00	0.06	100.20
cad8-18	G9	conc	40.90	0.10	19.67	5.24	7.51	0.40	0.00	19.54	6.25	0.04	99.75
cad8-19	G9	conc	41.40	0.16	22.02	2.32	8.94	0.46	0.00	19.60	5.22	0.04	100.21
cad8-20	G9	conc	41.42	0.06	20.44	4.48	7.38	0.41	0.00	20.02	5.75	0.03	100.08
cad8-21	G9	conc	41.32	0.15	22.42	1.76	9.83	0.49	0.01	19.05	5.00	0.04	100.12
cad8-22	G9	conc	41.46	0.07	20.23	4.82	7.63	0.41	0.01	20.01	5.66	0.03	100.40
cad8-23	G9	conc	41.77	0.04	21.44	3.57	8.42	0.47	0.00	19.73	5.90	0.03	101.41
cad8-24	G9	conc	41.71	0.11	21.32	3.63	8.76	0.47	0.01	19.43	5.90	0.04	101.40
cad9-1	G9	conc	42.06	0.10	22.65	2.02	9.13	0.45	0.00	19.90	5.06	0.03	101.44
cad9-3	G9	conc	42.09	0.22	22.67	1.86	8.41	0.38	0.00	20.65	4.97	0.05	101.34
cad9-4	G9	conc	41.86	0.20	22.38	2.29	8.59	0.40	0.01	20.37	4.98	0.04	101.16
cad9-5	G1	conc	42.18	0.52	22.98	0.91	8.26	0.29	0.00	20.99	4.86	0.06	101.11
cad10-1	G4	conc	42.29	0.36	23.69	0.17	10.38	0.37	0.00	19.87	4.71	0.06	101.94
cad10-2	G3	conc	41.97	0.15	23.61	0.33	9.60	0.30	0.01	18.16	7.54	0.04	101.76
cad10-3	G4	conc	42.30	0.27	23.93	0.12	9.12	0.30	0.00	20.98	4.30	0.06	101.44
cad10-4	G4	conc	42.62	0.11	24.05	0.49	8.19	0.33	0.00	21.04	4.88	0.03	101.78
cad10-5	G4D	conc	41.24	0.28	23.37	0.11	15.08	0.38	0.01	16.82	4.73	0.08	102.15
cad10-6	G4	conc	42.31	0.21	23.83	0.32	8.84	0.38	0.01	20.76	4.75	0.05	101.50
cad10-7	G3	conc	42.07	0.13	23.74	0.32	9.08	0.36	0.00	19.31	6.43	0.05	101.55
cad10-8	G4	conc	42.37	0.21	23.84	0.34	8.82	0.37	0.01	20.80	4.78	0.04	101.62
cad10-9	G4	conc	42.04	0.30	23.75	0.11	11.11	0.35	0.01	19.68	4.39	0.06	101.84
cad10-10	G4	conc	42.18	0.13	23.85	0.28	8.80	0.29	0.00	19.90	5.89	0.03	101.42
cad10-11	G4	conc	42.33	0.12	23.84	0.40	8.60	0.33	0.01	20.74	4.92	0.04	101.37
cad10-12	G3D	conc	40.47	0.27	23.20	0.02	17.36	0.33	0.01	10.85	9.76	0.10	102.43
cad10-13	G3	conc	41.98	0.13	23.58	0.38	9.88	0.36	0.01	18.93	6.06	0.05	101.41
cad10-14	G3	conc	41.84	0.14	23.40	0.54	10.72	0.42	0.01	18.50	6.00	0.04	101.67
cad10-15	G3	conc	42.09	0.08	23.87	0.17	9.36	0.24	0.01	17.16	9.09	0.04	102.15
cad10-16	G4	conc	42.32	0.11	23.84	0.33	9.09	0.39	0.00	19.94	5.40	0.03	101.50
cad10-17	G4D	conc	41.75	0.35	23.62	0.09	12.82	0.33	0.00	18.24	4.49	0.10	101.88
cad10-18	G4	conc	41.78	0.29	23.39	0.19	12.13	0.40	0.01	18.16	5.28	0.06	101.75
cad10-19	G1	conc	42.41	0.44	23.86	0.08	8.34	0.33	0.00	21.18	4.76	0.06	101.52
cad10-20	G4	conc	42.25	0.10	23.86	0.47	8.98	0.38	0.01	20.40	5.03	0.03	101.54
cad10-21	G4D	conc	41.90	0.26	23.75	0.09	12.44	0.37	0.01	18.43	4.70	0.07	102.07
cad10-22	G4D	conc	42.31	0.31	23.84	0.30	8.70	0.35	0.01	21.13	4.21	0.07	101.27
cad10-24	G3	conc	41.64	0.14	23.51	0.25	10.30	0.37	0.00	17.97	7.02	0.04	101.30
cad10-25	G3D	conc	40.96	0.20	23.60	0.03	13.05	0.24	0.00	14.04	9.21	0.09	101.50
cad10-26	G4	conc	42.08	0.20	23.82	0.10	10.22	0.39	0.01	19.78	4.82	0.05	101.52
cad10-27	G4	conc	42.52	0.23	24.06	0.21	7.34	0.34	0.01	21.77	4.74	0.04	101.29
cad10-28	G4	conc	42.04	0.14	23.81	0.41	9.10	0.37	0.01	19.62	5.86	0.04	101.43
cad10-29	G4	conc	42.34	0.18	23.88	0.38	9.04	0.35	0.00	20.73	4.45	0.05	101.44
cad10-30	G4	conc	42.18	0.11	23.92	0.32	8.14	0.28	0.01	20.90	5.01	0.04	100.94

Appendix B

Carolina Garnet Data

cont.

Grain	Gnt	loc.	SiO_2	TiO_2	Al_2O_3	Cr_2O_3	FeO	MnO	NiO	MgO	CaO	Na_2O	Total
cad10-31	G3D	conc	41.18	0.22	23.55	0.04	15.43	0.38	0.00	15.02	6.12	0.08	102.08
cad10-32	G4	conc	42.00	0.23	23.58	0.44	9.05	0.38	0.00	20.33	4.90	0.05	100.98
cad10-33	G4D	conc	41.48	0.21	23.73	0.06	13.16	0.31	0.00	17.83	4.48	0.09	101.43
cad10-34	G4	conc	41.70	0.28	23.46	0.11	10.38	0.35	0.01	19.75	4.45	0.05	100.58
cad10-35	G1	conc	42.18	0.48	22.93	1.02	8.71	0.28	0.01	20.81	4.57	0.07	101.12
cad10-36	G4	conc	42.06	0.26	23.93	0.12	9.13	0.31	0.01	20.87	4.24	0.06	101.05
cad10-37	G4D	conc	41.56	0.29	23.62	0.07	12.14	0.34	0.01	18.16	4.91	0.08	101.23
cad1-1	G9	conc	41.83	0.05	21.90	2.85	8.28	0.48	0.01	19.59	5.60	0.02	100.67
cad1-2	G9	conc	41.93	0.12	21.35	3.36	8.12	0.45	0.00	19.97	5.47	0.02	100.83
cad1-3	G9	conc	41.91	0.15	21.22	3.45	7.86	0.43	0.00	20.33	5.18	0.03	100.63
cad1-4	G9	conc	41.85	0.22	22.15	2.04	9.34	0.53	0.00	19.63	4.83	0.05	100.68
cad1-5	G9	conc	41.99	0.23	22.39	1.81	8.71	0.45	0.00	20.21	4.78	0.03	100.65
cad1-6	G9	conc	42.02	0.26	22.54	1.72	8.77	0.44	0.00	20.25	4.78	0.06	100.87
cad1-7	G9	conc	42.18	0.05	21.82	2.88	7.38	0.36	0.01	20.74	5.22	0.02	100.68
cad1-8	G9	conc	41.62	0.11	20.66	4.24	8.05	0.49	0.00	19.18	6.27	0.03	100.69
cad1-9	G9	conc	41.99	0.05	20.55	4.47	6.94	0.36	0.01	20.37	5.99	0.00	100.79
cad1-10	G9	conc	41.85	0.12	21.87	2.68	8.49	0.47	0.00	19.82	5.28	0.03	100.66
cad1-11	G9	conc	41.98	0.19	21.87	2.63	8.06	0.45	0.00	20.35	5.01	0.04	100.64
cad1-12	G9	conc	41.83	0.21	22.39	1.85	9.16	0.53	0.00	19.69	4.90	0.03	100.64
cad1-13	G9	conc	41.88	0.19	21.97	2.66	7.46	0.37	0.01	20.67	5.15	0.03	100.47
cad1-14	G9	conc	41.88	0.22	22.69	1.64	8.79	0.42	0.00	20.16	4.79	0.05	100.71
cad1-15	G9	conc	42.15	0.22	22.50	1.66	8.77	0.45	0.00	20.12	4.82	0.05	100.76
cad1-16	G9	conc	41.76	0.21	22.54	1.62	9.75	0.51	0.00	19.43	4.82	0.04	100.72
cad1-17	G9	conc	41.85	0.17	22.31	2.12	8.51	0.44	0.01	20.16	4.98	0.03	100.63
cad1-18	G9	conc	41.65	0.20	21.92	2.64	9.19	0.51	0.00	19.45	5.19	0.04	100.85
cad1-19	G9	conc	41.88	0.07	21.78	2.97	7.98	0.44	0.00	20.13	5.34	0.01	100.65
cad1-20	G9	conc	42.03	0.22	21.60	3.14	7.74	0.42	0.00	20.49	5.11	0.04	100.85
cad1-21	G9	conc	41.86	0.18	21.69	2.88	8.71	0.49	0.00	19.77	5.18	0.03	100.85
cad1-22	G9	conc	41.98	0.20	20.51	4.74	6.32	0.33	0.01	21.15	5.49	0.03	100.79
cad1-23	G9	conc	42.01	0.24	22.70	1.53	8.97	0.43	0.01	20.08	4.76	0.05	100.84
cad1-24	G9	conc	41.86	0.14	21.87	2.78	8.40	0.45	0.01	20.03	5.09	0.04	100.73
cad1-25	G9	conc	42.10	0.12	21.56	3.29	8.07	0.42	0.00	20.29	5.26	0.01	101.16
cad1-26	G9	conc	42.09	0.17	21.59	3.29	7.03	0.36	0.01	21.03	5.07	0.02	100.73
cad1-27	G9	conc	41.94	0.16	22.56	2.07	8.04	0.39	0.00	20.62	4.84	0.03	100.71
cad1-28	G9	conc	41.99	0.20	21.71	2.95	8.00	0.46	0.00	20.10	5.26	0.03	100.73
cad1-29	G9	conc	42.04	0.22	21.95	2.65	7.38	0.34	0.02	20.85	5.07	0.03	100.61
cad1-30	G9	conc	41.96	0.10	22.04	2.68	7.32	0.35	0.01	20.78	5.13	0.01	100.42
cad1-31	G9	conc	41.82	0.15	21.63	3.05	8.48	0.47	0.01	19.81	5.33	0.03	100.81
cad1-32	G9	conc	41.90	0.25	22.34	1.79	8.90	0.43	0.01	20.04	4.87	0.04	100.60
cad1-33	G9	conc	41.79	0.25	22.20	2.14	8.78	0.45	0.01	19.90	5.02	0.03	100.61
cad1-34	G9	conc	41.84	0.25	21.11	3.57	7.62	0.41	0.00	20.83	4.78	0.06	100.53
cad1-35	G9	conc	41.78	0.22	21.16	3.47	7.14	0.37	0.01	20.71	5.33	0.02	100.27
cad1-36	G9	conc	41.78	0.24	22.43	1.60	8.93	0.44	0.00	20.13	4.88	0.05	100.54
cad1-37	G9	conc	42.10	0.19	22.68	1.72	8.93	0.44	0.00	20.25	4.78	0.05	101.17
cad1-38	G9	conc	41.96	0.17	22.25	2.28	9.20	0.50	0.00	19.52	5.19	0.03	101.15
cad1-39	G9	conc	42.09	0.19	22.50	1.85	9.06	0.45	0.01	20.19	4.78	0.03	101.21
cad1-40	G9	conc	42.18	0.25	22.40	1.90	9.07	0.47	0.00	20.01	4.90	0.04	101.27

Appendix B

Carolina Garnet Data

cont.

Grain	Gnt	loc.	SiO_2	TiO_2	Al_2O_3	Cr_2O_3	FeO	MnO	NiO	MgO	CaO	Na_2O	Total
cad1-41	G9	conc	41.73	0.03	19.65	5.78	7.44	0.47	0.01	19.22	6.79	0.01	101.18
cad1-42	G9	conc	42.01	0.20	22.26	2.16	9.44	0.51	0.01	19.60	4.83	0.03	101.08
cad1-43	G1	conc	41.72	0.59	21.18	3.12	7.80	0.38	0.01	20.09	5.82	0.04	100.82
cad1-44	G9	conc	42.05	0.18	22.49	1.85	8.56	0.43	0.00	20.27	4.87	0.04	100.78
cad1-45	G11	conc	41.47	0.44	18.80	6.62	6.61	0.38	0.01	19.81	6.66	0.05	100.92
cad1-46	G9	conc	42.20	0.16	22.72	1.78	7.76	0.36	0.00	21.00	4.78	0.03	100.81
cad1-47	G9	conc	42.19	0.25	21.75	2.82	7.32	0.34	0.01	20.84	5.11	0.04	100.74
cad1-48	G9	conc	41.67	0.17	22.12	2.24	8.75	0.46	0.00	19.92	4.92	0.03	100.35
cad1-49	G9	conc	42.13	0.22	22.42	1.91	8.49	0.42	0.01	20.34	4.93	0.04	100.97
cad1-50	G9	conc	42.00	0.21	22.61	1.74	9.17	0.45	0.01	19.98	4.93	0.04	101.17
cad1-51	G9	conc	42.01	0.20	22.21	2.18	8.53	0.44	0.00	19.98	5.13	0.03	100.75
cad1-52	G9	conc	41.99	0.27	22.43	1.94	8.92	0.44	0.01	20.14	4.84	0.04	101.06
cad1-53	G9	conc	41.92	0.26	22.26	1.98	8.76	0.46	0.01	20.12	4.89	0.05	100.77
cad1-54	G9	conc	41.94	0.13	22.61	1.76	9.33	0.49	0.00	19.83	4.95	0.03	101.09
cad1-55	G9	conc	42.09	0.10	21.81	2.86	8.19	0.45	0.01	20.27	5.11	0.01	100.94
cad1-56	G9	conc	42.07	0.19	22.11	2.30	8.68	0.46	0.01	20.01	5.04	0.03	100.93
cad1-57	G9	conc	41.75	0.10	20.99	3.92	8.34	0.52	0.00	19.26	6.06	0.03	101.02
cad1-58	G9	conc	42.12	0.17	22.27	2.19	8.22	0.41	0.01	20.41	4.90	0.04	100.77
cad1-59	G9	conc	42.13	0.20	22.16	2.44	8.45	0.44	0.00	20.34	4.90	0.04	101.18
cad1-60	G9	conc	42.10	0.15	22.74	1.66	9.66	0.50	0.01	19.61	4.90	0.04	101.40
cad1-61	G9	conc	42.33	0.14	22.47	1.93	7.78	0.36	0.01	21.00	4.72	0.00	100.77
cad1-62	G9	conc	42.16	0.25	22.47	1.82	8.61	0.42	0.01	20.34	4.80	0.05	100.96
cad1-63	G9	conc	42.18	0.17	22.38	1.74	8.82	0.43	0.01	20.28	4.79	0.03	100.89
cad1-64	G9	conc	42.00	0.19	22.19	1.95	8.61	0.43	0.00	20.27	4.85	0.03	100.55
cad1-65	G9	conc	42.03	0.20	22.65	1.63	8.72	0.42	0.00	20.28	4.81	0.05	100.83
cad1-66	G9	conc	42.06	0.19	22.09	2.22	8.29	0.44	0.01	20.35	4.92	0.03	100.65
cad1-67	G11	conc	41.70	0.43	19.63	5.14	6.01	0.30	0.01	20.89	5.92	0.02	100.12
cad1-68	G9	conc	41.99	0.23	22.26	1.79	8.87	0.44	0.01	20.26	4.81	0.03	100.72
cad1-69	G9	conc	42.19	0.19	22.27	2.00	7.77	0.37	0.00	21.07	4.76	0.01	100.69
cad1-70	G9	conc	41.98	0.20	21.93	2.20	8.76	0.45	0.01	20.12	4.99	0.03	100.71
cad1-71	G9	conc	41.88	0.17	21.65	2.60	7.97	0.41	0.00	20.64	5.00	0.04	100.40
cad1-72	G9	conc	41.69	0.25	21.78	2.24	8.42	0.45	0.00	20.29	4.95	0.03	100.17
cad1-73	G9	conc	41.72	0.18	22.06	1.84	8.53	0.45	0.00	20.34	4.85	0.03	100.05
cad1-74	G9	conc	41.92	0.14	22.09	2.08	8.53	0.43	0.01	20.31	4.87	0.02	100.47
cad1-75	G9	conc	41.89	0.27	21.85	2.52	8.18	0.45	0.01	20.46	4.97	0.03	100.68
cad1-76	G9	conc	41.96	0.13	22.05	2.24	8.42	0.42	0.01	20.22	5.08	0.01	100.59
cad1-77	G9	conc	41.98	0.23	21.54	2.80	7.53	0.42	0.01	20.82	5.11	0.04	100.52
cad1-78	G9	conc	42.07	0.18	22.11	2.14	8.73	0.45	0.00	20.23	4.94	0.02	100.92
cad1-79	G9	conc	42.16	0.22	22.07	2.21	8.81	0.46	0.01	20.10	4.94	0.03	101.05
cad1-80	G9	conc	41.91	0.10	20.82	3.99	7.91	0.46	0.01	19.85	5.81	0.01	100.92
cad1-81	G9	conc	41.88	0.09	21.19	3.79	8.29	0.55	0.00	19.42	6.01	0.01	101.32
cad1-82	G9	conc	42.10	0.26	22.53	1.72	9.01	0.43	0.00	20.23	4.76	0.05	101.13
cad1-83	G9	conc	41.89	0.16	21.88	2.62	8.86	0.51	0.01	19.45	5.50	0.02	100.95
cad1-84	G9	conc	41.85	0.20	21.78	2.51	9.01	0.49	0.01	19.84	5.15	0.05	100.93
cad1-85	G9	conc	42.04	0.25	22.09	2.04	8.73	0.44	0.01	20.19	4.91	0.04	100.77
cad2-86	G9	conc	42.41	0.24	22.56	1.98	8.68	0.45	0.01	20.39	4.88	0.06	101.70
cad2-87	G9	conc	42.43	0.07	22.53	2.32	8.21	0.45	0.00	20.55	5.24	0.02	101.89

Appendix B

Carolina Garnet Data

cont.

Grain	Gnt	loc.	SiO_2	TiO_2	Al_2O_3	Cr_2O_3	FeO	MnO	NiO	MgO	CaO	Na_2O	Total
cad2-88	G9	conc	42.40	0.08	21.79	3.16	8.00	0.44	0.01	20.30	5.53	0.01	101.78
cad2-89	G9	conc	42.31	0.31	22.16	2.44	8.46	0.45	0.01	20.47	5.01	0.06	101.71
cad2-90	G9	conc	42.17	0.12	20.88	4.29	7.55	0.44	0.00	20.34	5.71	0.04	101.62
cad2-91	G9	conc	42.30	0.20	20.07	5.06	6.02	0.30	0.02	21.37	5.94	0.03	101.37
cad2-92	G9	conc	42.32	0.18	22.11	2.47	8.50	0.47	0.01	20.54	4.96	0.03	101.62
cad2-93	G9	conc	42.16	0.14	21.80	2.69	8.77	0.47	0.01	20.11	5.25	0.02	101.46
cad2-94	G9	conc	42.31	0.12	21.92	2.75	8.84	0.49	0.00	19.99	5.27	0.03	101.77
cad2-95	G9	conc	42.36	0.21	22.40	2.07	9.64	0.52	0.00	20.00	4.83	0.03	102.12
cad2-96	G9	conc	42.41	0.21	22.19	2.32	9.10	0.49	0.01	20.16	5.02	0.03	102.01
cad2-97	G9	conc	42.13	0.08	21.04	3.90	8.20	0.47	0.00	19.90	5.64	0.02	101.46
cad2-98	G9	conc	42.46	0.11	21.72	3.11	8.30	0.46	0.00	20.31	5.29	0.01	101.82
cad2-99	G9	conc	42.43	0.22	22.56	1.89	8.95	0.46	0.00	20.42	4.81	0.05	101.85
cad2-100	G9	conc	42.36	0.13	21.33	3.52	8.78	0.47	0.01	19.85	5.38	0.03	101.94
cad2-101	G9	conc	42.40	0.22	20.57	4.72	6.63	0.34	0.00	20.97	5.75	0.04	101.72
cad2-102	G9	conc	42.58	0.22	22.57	2.06	8.37	0.45	0.00	20.65	4.87	0.06	101.91
cad2-103	G9	conc	42.70	0.08	21.77	3.01	7.43	0.35	0.01	21.02	5.38	0.02	101.83
cad2-104	G9	conc	42.54	0.22	22.62	1.74	9.10	0.44	0.00	20.36	4.70	0.04	101.79
cad2-105	G9	conc	42.70	0.20	21.80	2.93	7.23	0.34	0.01	21.28	5.06	0.03	101.61
cad2-106	G9	conc	42.45	0.13	22.66	1.96	8.42	0.43	0.00	20.68	4.92	0.02	101.72
cad2-107	G9	conc	42.56	0.19	22.68	1.84	8.79	0.44	0.00	20.57	4.80	0.04	101.96
cad2-108	G9	conc	42.43	0.27	22.64	1.88	8.87	0.44	0.00	20.50	4.87	0.06	102.01
cad2-109	G9	conc	42.49	0.24	22.62	1.85	7.97	0.38	0.00	21.06	4.82	0.04	101.52
cad2-110	G9	conc	42.44	0.25	21.72	2.98	7.27	0.35	0.01	21.47	4.89	0.04	101.45
cad2-111	G9	conc	42.04	0.12	21.87	2.85	7.89	0.41	0.00	20.68	5.17	0.02	101.09
cad2-112	G9	conc	42.33	0.22	22.43	1.81	8.73	0.43	0.01	20.49	4.84	0.04	101.38
cad2-113	G9	conc	42.60	0.12	22.51	2.19	7.56	0.37	0.00	21.30	4.86	0.03	101.60
cad2-114	G9	conc	42.33	0.07	21.61	3.36	7.86	0.42	0.01	20.94	4.91	0.03	101.57
cad2-115	G9	conc	42.56	0.09	21.98	2.96	7.18	0.34	0.02	21.22	5.10	0.03	101.50
cad2-116	G9	conc	42.61	0.08	22.48	2.08	7.70	0.37	0.02	21.18	4.85	0.01	101.42
cad2-117	G9	conc	42.35	0.12	20.33	5.01	7.23	0.41	0.01	20.70	5.54	0.03	101.78
cad2-118	G9	conc	42.10	0.16	22.26	2.08	11.67	0.59	0.00	18.39	5.07	0.03	102.40
cad2-119	G9	conc	42.47	0.17	21.37	3.77	8.04	0.46	0.01	20.31	5.35	0.03	102.04
cad2-120	G9	conc	42.67	0.18	22.38	2.24	7.89	0.39	0.01	20.91	5.04	0.03	101.79
cad2-121	G9	conc	42.52	0.17	22.26	2.50	8.47	0.45	0.00	20.38	5.00	0.04	101.84
cad2-122	G9	conc	42.61	0.18	22.12	2.64	8.43	0.43	0.00	20.55	4.92	0.03	101.98
cad2-123	G9	conc	42.66	0.23	22.69	1.78	8.70	0.43	0.02	20.70	4.75	0.04	102.05
cad2-124	G9	conc	42.38	0.11	21.38	3.88	8.26	0.53	0.00	19.56	5.88	0.04	102.08
cad2-125	G9	conc	42.62	0.25	22.84	1.70	8.63	0.42	0.00	20.57	4.73	0.04	101.87
cad2-126	G9	conc	42.55	0.29	22.40	2.16	8.41	0.42	0.00	20.79	4.76	0.03	101.87
cad2-127	G9	conc	42.30	0.19	22.02	2.61	8.90	0.48	0.00	20.00	5.08	0.03	101.66
cad2-128	G9	conc	42.32	0.32	21.42	3.07	7.34	0.34	0.01	20.90	5.40	0.03	101.22
cad2-129	G9	conc	42.32	0.18	20.77	4.29	6.71	0.36	0.01	20.99	5.53	0.02	101.27
cad2-130	G9	conc	42.08	0.04	20.87	4.19	7.80	0.45	0.01	19.97	5.88	0.00	101.36
cad2-131	G9	conc	42.30	0.23	22.32	2.01	8.79	0.45	0.01	20.33	4.86	0.03	101.38
cad2-132	G9	conc	42.22	0.24	21.91	2.46	8.60	0.45	0.00	20.34	4.93	0.05	101.25
cad2-133	G9	conc	42.36	0.19	22.42	1.89	8.84	0.46	0.00	20.40	4.80	0.04	101.44
cad2-134	G9	conc	42.21	0.17	22.62	1.76	9.46	0.49	0.00	19.96	4.73	0.03	101.47

Appendix B

Carolina Garnet Data

cont.

Grain	Gnt	loc.	SiO_2	TiO_2	Al_2O_3	Cr_2O_3	FeO	MnO	NiO	MgO	CaO	Na_2O	Total
cad2-135	G9	conc	42.55	0.27	21.11	3.86	6.50	0.33	0.00	21.34	5.44	0.05	101.52
cad2-136	G9	conc	42.22	0.16	22.37	1.80	9.62	0.50	0.01	19.48	5.39	0.03	101.62
cad2-137	G9	conc	42.58	0.23	22.63	1.70	8.96	0.45	0.01	20.36	4.87	0.04	101.89
cad2-138	G9	conc	42.57	0.10	21.73	3.02	7.92	0.42	0.01	20.63	5.29	0.03	101.74
cad2-139	G9	conc	42.52	0.25	22.56	1.84	8.41	0.43	0.01	20.60	4.87	0.04	101.57
cad2-140	G9	conc	42.58	0.08	20.77	4.71	6.61	0.32	0.01	20.97	5.63	0.02	101.75
cad2-141	G9	conc	42.57	0.07	21.62	3.68	7.73	0.42	0.01	20.56	5.39	0.02	102.12
cad3-142	G9	conc	42.25	0.35	21.77	2.54	7.50	0.35	0.01	21.18	4.87	0.03	100.91
cad3-143	G9	conc	42.07	0.10	21.98	2.48	8.82	0.48	0.01	19.92	5.16	0.03	101.12
cad3-144	G9	conc	42.21	0.20	22.43	1.85	8.69	0.43	0.01	20.38	4.74	0.03	101.01
cad3-145	G9	conc	42.07	0.05	21.84	3.08	8.40	0.50	0.01	19.64	5.48	0.01	101.13
cad3-146	G9	conc	41.97	0.19	22.41	1.93	9.57	0.49	0.01	19.68	4.81	0.06	101.17
cad3-147	G9	conc	41.96	0.09	21.89	2.68	8.59	0.47	0.00	19.49	5.44	0.03	100.71
cad3-148	G9	conc	42.01	0.19	21.44	3.20	7.43	0.40	0.01	20.56	5.37	0.02	100.67
cad3-149	G9	conc	41.56	0.28	18.97	6.37	6.61	0.36	0.00	20.28	6.20	0.01	100.73
cad3-150	G9	conc	41.73	0.06	19.65	5.87	6.38	0.34	0.01	20.70	5.81	0.02	100.67
cad3-151	G9	conc	41.90	0.12	21.57	3.24	7.86	0.41	0.01	20.35	5.24	0.02	100.77
cad3-152	G9	conc	41.82	0.22	22.22	1.95	8.83	0.46	0.01	20.17	4.79	0.03	100.55
cad3-153	G9	conc	41.73	0.18	21.74	2.36	8.65	0.46	0.01	20.19	4.88	0.03	100.30
cad3-154	G9	conc	41.92	0.21	21.90	2.40	8.45	0.45	0.00	20.28	4.89	0.03	100.58
cad3-155	G9	conc	42.08	0.19	22.05	2.39	8.41	0.43	0.00	20.37	4.87	0.03	100.87
cad3-156	G9	conc	41.91	0.15	22.05	2.27	8.68	0.45	0.00	20.19	4.88	0.02	100.63
cad3-157	G9	conc	42.04	0.15	20.58	4.68	6.38	0.33	0.01	21.58	5.00	0.03	100.85
cad3-158	G9	conc	42.04	0.27	19.89	5.29	6.34	0.33	0.01	21.48	4.98	0.02	100.70
cad3-159	G9	conc	42.22	0.20	21.44	3.05	7.53	0.40	0.01	20.86	4.92	0.04	100.71
cad3-160	G9	conc	42.34	0.22	22.16	2.21	8.28	0.42	0.00	20.64	4.81	0.03	101.16
cad3-161	G9	conc	41.94	0.05	19.68	5.99	6.37	0.38	0.01	21.12	5.31	0.01	100.94
cad3-162	G9	conc	42.10	0.18	20.55	4.54	6.79	0.38	0.00	20.65	5.60	0.02	100.90
cad3-163	G9	conc	42.09	0.11	21.68	2.93	8.79	0.55	0.00	19.77	5.24	0.01	101.23
cad3-164	G9	conc	42.24	0.25	22.27	2.21	8.10	0.42	0.00	20.70	4.82	0.05	101.12
cad3-165	G9	conc	41.93	0.07	20.22	5.06	6.37	0.33	0.01	20.76	5.48	0.01	100.31
cad3-166	G9	conc	41.74	0.08	20.87	3.89	8.16	0.48	0.01	19.76	5.46	0.02	100.53
cad3-167	G9	conc	42.00	0.22	22.15	1.92	8.80	0.46	0.01	20.12	4.79	0.04	100.56
cad3-168	G9	conc	41.95	0.20	21.56	2.99	8.23	0.45	0.00	20.23	5.06	0.04	100.79
cad3-169	G9	conc	41.75	0.21	21.53	2.82	8.47	0.48	0.01	20.03	5.07	0.04	100.46
cad3-170	G9	conc	41.89	0.16	20.32	4.57	6.67	0.37	0.01	20.81	5.30	0.03	100.19
cad3-171	G9	conc	41.97	0.18	22.09	2.13	8.49	0.43	0.01	20.38	4.89	0.03	100.64
cad3-172	G9	conc	41.94	0.04	21.40	3.30	7.99	0.44	0.01	20.04	5.47	0.01	100.67
cad3-173	G9	conc	42.07	0.26	20.99	3.50	6.97	0.36	0.02	21.05	5.21	0.04	100.53
cad3-174	G9	conc	42.24	0.28	20.92	3.65	6.35	0.31	0.01	21.89	4.49	0.05	100.26
cad3-175	G9	conc	42.06	0.17	21.97	2.57	8.49	0.45	0.00	20.17	5.03	0.04	100.99
cad3-176	G9	conc	42.29	0.25	22.16	2.44	8.47	0.45	0.00	20.39	4.88	0.05	101.44
cad3-177	G9	conc	41.94	0.11	21.49	3.12	8.61	0.45	0.01	19.80	5.16	0.02	100.75
cad3-178	G9	conc	42.08	0.19	22.39	1.94	9.31	0.51	0.01	19.87	4.90	0.04	101.29
cad3-179	G9	conc	42.29	0.19	21.91	2.79	7.11	0.36	0.00	21.26	4.97	0.04	101.00
cad3-180	G9	conc	41.77	0.10	21.46	3.57	8.36	0.48	0.00	19.37	5.85	0.02	101.03
cad3-181	G9	conc	41.87	0.09	21.03	4.18	8.28	0.53	0.00	19.10	6.13	0.02	101.30

Appendix B

Carolina Garnet Data

cont.

Grain	Gnt	loc.	SiO_2	TiO_2	Al_2O_3	Cr_2O_3	FeO	MnO	NiO	MgO	CaO	Na_2O	Total
cad3-182	G9	conc	42.10	0.26	20.91	3.90	7.46	0.37	0.01	20.27	5.91	0.04	101.27
cad3-183	G9	conc	42.23	0.18	19.80	5.90	5.95	0.33	0.01	21.49	5.18	0.05	101.16
cad3-184	G9	conc	42.14	0.06	21.37	3.76	7.64	0.41	0.00	20.33	5.45	0.02	101.24
cad3-185	G9	conc	42.35	0.23	22.43	1.92	7.51	0.35	0.01	21.02	4.61	0.02	100.49
cad3-186	G9	conc	42.16	0.20	21.42	3.46	6.88	0.35	0.01	20.83	5.22	0.02	100.65
cad3-187	G9	conc	42.09	0.18	21.24	3.52	7.83	0.44	0.00	20.30	5.24	0.04	100.91
cad3-188	G9	conc	41.99	0.24	21.92	2.43	8.41	0.44	0.00	20.23	4.96	0.04	100.72
cad3-189	G9	conc	41.98	0.14	21.95	2.51	8.60	0.46	0.01	20.05	4.98	0.04	100.77
cad3-190	G9	conc	42.03	0.06	21.85	2.96	8.55	0.51	0.00	19.74	5.43	0.02	101.21
cad3-191	G9	conc	41.93	0.09	21.42	3.57	7.81	0.44	0.01	19.83	5.79	0.02	100.96
cad3-192	G9	conc	42.01	0.16	21.18	3.67	7.10	0.35	0.01	20.83	5.19	0.01	100.58
cad3-193	G9	conc	41.97	0.12	22.05	2.52	8.44	0.46	0.00	20.16	5.09	0.03	100.90
cad3-194	G9	conc	42.05	0.25	22.47	1.81	9.21	0.46	0.00	20.04	4.82	0.04	101.20
cad3-195	G9	conc	41.94	0.18	21.66	2.91	8.83	0.50	0.00	19.98	4.97	0.03	101.06
cad3-196	G9	conc	42.39	0.18	22.38	2.06	8.17	0.41	0.01	20.81	4.70	0.03	101.18
cad3-197	G9	conc	42.36	0.13	22.34	2.38	8.41	0.44	0.00	20.44	4.98	0.03	101.55
cad3-198	G9	conc	42.17	0.05	21.70	3.17	7.79	0.43	0.01	20.20	5.58	0.02	101.16
cad3-199	G9	conc	42.16	0.14	21.88	2.75	8.83	0.50	0.01	19.85	5.18	0.02	101.36
cad3-200	G9	conc	42.22	0.25	21.71	3.01	8.42	0.46	0.01	20.33	5.04	0.06	101.56
cad3-201	G9	conc	42.17	0.13	22.53	2.13	8.61	0.46	0.00	20.34	4.95	0.02	101.41
cad3-202	G9	conc	42.27	0.11	22.40	2.47	8.28	0.44	0.00	20.49	5.08	0.02	101.61

Appendix B

Carolina Diamond Descriptions and Carbon Data

Table B.3. Descriptions of 30 diamonds from the Carolina kimberlite, including carbon isotopic analyses.

Sample	Weight (mg)	Colour	Form	Habbit	Surface Features	Resorped	$\delta^{13}C$ (‰)
CAD 01	0.70	ly	D	cry	rt trr dl	r	-5.90
CAD 02	1.50	c	DI	frag	rt h trr	r	-4.09
CAD 03	1.90	lb	DO	cry	ntr h trr dl cs	pr	-5.14
CAD 04a	0.90	c	I	agg	ntr h dl frc h	pr	-4.39
CAD 04b	0.90	lb	I	agg	h trr	r	-4.13
CAD 05	0.90	lg	I	frag	h trr dl	r	-21.40
CAD 06	1.60	ly	OI	agg	h trr	nr	-19.61
CAD 07	1.40	ly	D	cry	h trr frc rt	r	-3.70
CAD 08	0.90	g	I	agg	h trr	pr	-10.13
CAD 09	1.10	g	I	frag	trr h dl	r	-16.61
CAD 10	0.80	c	I	frag	h trr frc	r	-10.06
CAD 11	0.90	lyg	D	frag	h trr	r	-5.59
CAD 12	0.90	g	OI	agg frag	h trr frc	pr	-9.51
CAD 13	1.00	lb	ODI	twn	trr	ur	-12.27
CAD 14	1.70	c	D	frag	h rt	r	-6.18
CAD 15	1.20	lp	DI	agg	rnd	r	-5.03
CAD 16	0.80	g	I	frag	ntr cs h trr	pr	-5.44
CAD 17	1.50	lg	DI	frag	ntr h trr cs	ur	-3.98
CAD 18	0.70	g	I	twn	trr rt frc	r	-8.57
CAD 19	0.90	c	D	slightly flt	h trr	r	-6.04
CAD 20	0.80	g	DOM	twn	ntr h trr	nr	-4.68
CAD 21	0.70	g	DI	frag	h gl	r	-5.01
CAD 22	0.80	c	DI	flt	ntr cs	pr	-5.25
CAD 23	0.80	g	D	cry	rt frc	r	-4.13
CAD 24	0.80	g	DO	cry	h gl	r	-22.35
CAD 25	1.90	lg	D	cry	cs trr cep	r	-3.84
CAD 26	1.10	c	D	elng	cs gl	r	-5.43
CAD 27	1.30	g	DI	frag	trr gl h cs	r	-12.23
CAD 28	2.20	lg	DI	frag	ntr gl trr	ur	-5.10
CAD 29	1.30	ly	DI	flt	h gl ntr trr rt	pr	-8.92
CAD 30	0.90	lg	ODI	frag	ntr trr cs	pr	-4.70

g=grey, c=colourless, b=brown, y=yellow, l=light,
O=octahedra, I=irregular, D=rounded dodecohedra, M=macle frag=fragment, cry=crystal, flt=flat, elng=elongate, twn=twin, agg=aggregate, rt=ruts, trr=terraces, dl=deformation lines, h=hillocks, ntr=negative trigons, cs=corrosion sculptures, frc=fractured, rnd=rounded-no features, gl=growth lines, cep=circular etch pits, r=resorped, pr=partly resorped, ur=uneven resorption, nr=not resorped

Appendix B

Carolina Diamond Nitrogen Data

Table B.4. Nitrogen content and aggregation state, platelet peak area, and the 3107cm^{-1} hydrogen peak area of 230 diamonds from the Carolina kimberlite. Time averaged nitrogen mantle residence temperatures were calculated following Leahy and Taylor (1997), assuming a 1.5Ga lithospheric mantle .

Sample	type IaA (ppm)	type IaB (ppm)	N (ppm)	% B	N. Agg. state	Platelet Area	3107 H area	T[N,1.5Ga]
CAD 01	598.6	339.5	938.2	36.2	IaAB	107.2	0.0	1116.6
CAD 02	1776.4	347.9	2124.3	16.4	IaAB	39.3	1.6	1073.3
CAD 03	816.7	411.5	1228.2	33.5	IaAB	169.5	17.5	1107.5
CAD 04a	563.3	71.1	634.5	11.2	IaAB	14.5	0.0	1090.7
CAD 04b	730.8	0.0	730.8	0.0	IaA	0.0	0.0	-
CAD 5	38.1	17.2	55.3	31.2	IaAB	0.0	6.0	1181.6
CAD 7	1106.8	426.8	1533.6	27.8	IaAB	230.4	2.3	1096.1
CAD 8	239.8	54.5	294.2	18.5	IaAB	0.0	0.0	1122.5
CAD 9	0.0	84.0	84.0	100.0	IaB	0.0	0.0	-
CAD 10	1396.6	15.0	1411.7	1.1	IaA	0.0	8.4	1019.9
CAD 11	604.1	98.9	703.0	14.1	IaAB	95.1	0.6	1094.3
CAD 12	842.1	160.4	1002.5	16.0	IaAB	0.0	3.3	1089.7
CAD 14	123.3	8.3	131.6	6.3	IaA	0.0	15.7	1112.6
CAD 16	887.2	413.6	1300.8	31.8	IaAB	146.8	2.5	1104.3
CAD 17	73.5	0.0	73.5	0.0	IaA	0.0	0.0	-
CAD 18	811.6	252.4	1064.0	23.7	IaAB	0.0	4.7	1099.6
CAD 19	961.0	444.9	1405.8	31.6	IaAB	0.0	0.0	1102.3
CAD 20	637.9	390.3	1028.2	38.0	IaAB	195.2	3.1	1116.3
CAD 21	41.5	0.0	41.5	0.0	IaA	12.6	3.5	-
CAD 22	679.0	219.2	898.3	24.4	IaAB	134.6	13.1	1104.4
CAD 23	892.2	851.5	1743.7	48.8	IaAB	224.3	11.6	1114.3
CAD 24	0.0	47.6	47.6	100.0	IaB	0.0	0.0	-
CAD 25	304.2	426.1	730.3	58.4	IaAB	222.9	5.6	1144.7
CAD 26	457.0	142.1	599.1	23.7	IaAB	92.6	0.3	1113.0
CAD 27	147.5	195.9	343.4	57.0	IaAB	0.0	0.0	1162.3
CAD 28	738.5	204.1	942.6	21.7	IaAB	120.4	0.9	1099.7
CAD 29	703.5	309.6	1013.1	30.6	IaAB	191.8	1.0	1108.8
CAD 30	482.1	344.1	826.2	41.7	IaAB	238.5	3.1	1125.2
CAD05 1	163.0	205.8	368.8	55.8	IaAB	84.1	7.0	1159.2
CAD05 3	562.8	184.8	747.6	24.7	IaAB	109.9	1.3	1109.1
CAD05 4	120.8	316.4	437.2	72.4	IaAB	147.7	0.7	1173.5
CAD05 7	209.4	340.8	550.2	61.9	IaAB	137.1	1.4	1155.5
CAD05 9	585.0	150.5	735.5	20.5	IaAB	81.8	0.8	1103.8
CAD05 10	223.5	249.1	472.6	52.7	IaAB	199.4	2.4	1149.8
CAD05 11	374.2	284.4	658.6	43.2	IaAB	184.6	2.8	1132.2
CAD05 12	494.8	102.5	597.3	17.2	IaAB	73.8	1.3	1103.6
CAD05 14	460.9	283.3	744.2	38.1	IaAB	166.6	3.0	1124.1
CAD05 15	478.7	249.7	728.4	34.3	IaAB	21.3	1.9	1120.7
CAD05 16	592.0	246.9	838.9	29.4	IaAB	97.7	0.9	1112.0

Appendix B

Carolina Diamond Nitrogen Data

cont.

Sample	type IaA (ppm)	type IaB (ppm)	N (ppm)	% B	N. Agg. state	Platelet Area	3107 H area	T[N,1.5Ga]
CAD05 17	300.8	223.5	524.3	42.6	IaAB	166.2	1.7	1137.2
CAD05 18	327.6	541.1	868.7	62.3	IaAB	344.6	6.0	1144.5
CAD05 19	314.6	98.2	412.8	23.8	IaAB	82.7	0.8	1122.0
CAD05 20	250.6	370.2	620.8	59.6	IaAB	0.0	3.2	1150.1
CAD05 21	260.3	208.2	468.5	44.4	IaAB	85.4	2.4	1141.8
CAD05 22	288.2	409.5	697.7	58.7	IaAB	210.8	8.8	1146.2
CAD05 23	523.6	332.5	856.1	38.8	IaAB	164.1	3.6	1121.5
CAD05 24	491.3	211.6	702.9	30.1	IaAB	114.1	6.6	1117.0
CAD05 25	381.0	100.1	481.1	20.8	IaAB	80.2	1.8	1114.2
CAD05 26	572.2	240.4	812.6	29.6	IaAB	172.1	4.8	1112.9
CAD05 27	483.8	151.4	635.2	23.8	IaAB	105.1	3.6	1111.8
CAD05 28	145.7	103.5	249.2	41.5	IaAB	39.5	5.7	1154.6
CAD05 29	395.7	264.7	660.4	40.1	IaAB	129.1	0.7	1129.1
CAD05 32	652.8	63.2	716.0	8.8	IaA	17.4	10.0	1081.9
CAD05 33	412.9	45.4	458.3	9.9	IaA	42.0	4.9	1095.0
CAD05 34	329.2	137.7	466.9	29.5	IaAB	118.9	0.6	1126.1
CAD05 35	385.0	292.0	677.0	43.1	IaAB	166.7	5.1	1131.5
CAD05 36	447.3	179.3	626.6	28.6	IaAB	105.4	0.8	1118.0
CAD05 37	305.5	221.6	527.1	42.0	IaAB	120.4	1.1	1136.5
CAD05 38	33.1	7.0	40.1	17.5	IaAB	15.1	0.5	1170.2
CAD05 39	247.8	288.7	536.5	53.8	IaAB	132.5	1.6	1147.8
CAD05 40	449.5	313.0	762.5	41.0	IaAB	160.7	36.2	1126.5
CAD05 41	451.3	382.5	833.8	45.9	IaAB	284.7	2.9	1129.1
CAD05 42	206.0	508.1	714.1	71.2	IaAB	321.7	5.7	1159.4
CAD05 43	361.4	197.9	559.3	35.4	IaAB	130.8	1.0	1128.2
CAD05 44	40.2	44.4	84.6	52.5	IaAB	18.8	1.9	1193.8
CAD05 46	201.5	195.4	396.9	49.2	IaAB	77.9	2.5	1150.7
CAD05 47	23.0	12.7	35.7	35.6	IaAB	0.0	1.2	1198.4
CAD05 48	551.7	547.4	1099.1	49.8	IaAB	397.5	6.5	1126.3
CAD05 49	452.3	120.7	573.0	21.1	IaAB	73.9	1.3	1110.5
CAD05 50	286.6	108.4	395.0	27.4	IaAB	45.3	0.3	1127.7
CAD05 51	75.8	181.8	257.6	70.6	IaAB	119.6	13.6	1184.9
CAD05 53	217.6	388.4	606.0	64.1	IaAB	61.6	66.1	1155.4
CAD05 54	192.7	228.5	421.2	54.2	IaAB	47.7	3.8	1154.3
CAD05 55	196.2	269.5	465.7	57.9	IaAB	92.7	8.2	1155.4
CAD05B 3	558.3	37.7	596.0	6.3	IaA	59.5	0.9	1077.9
CAD05B 4	0.0	280.7	280.7	100.0	IaB	0.0	6.1	#DIV/0!
CAD05B 5	508.3	351.2	859.5	40.9	IaAB	249.6	3.1	1123.5
CAD05B 7	387.0	417.8	804.8	51.9	IaAB	218.3	5.3	1135.9
CAD05B 8	13.7	5.0	18.7	26.7	IaAB	1.3	0.6	1204.6
CAD05B 9	79.0	15.2	94.2	16.1	IaAB	0.0	0.9	1146.3
CAD05B 10	212.3	548.7	761.0	72.1	IaAB	333.0	5.0	1159.0
CAD05B 11	20.9	1.4	22.3	6.3	IaA	0.0	5.3	1155.9

Appendix B

Carolina Diamond Nitrogen Data

cont.

Sample	type IaA (ppm)	type IaB (ppm)	N (ppm)	% B	N. Agg. state	Platelet Area	3107 H area	T[N,1.5Ga]
CAD05B 15	139.4	82.8	222.2	37.3	IaAB	0.0	1.9	1153.0
CAD05B 16	500.2	596.3	1096.5	54.4	IaAB	334.9	3.7	1130.8
CAD05B 17	456.4	282.1	738.5	38.2	IaAB	158.2	50.9	1124.4
CAD05B 18	690.9	52.0	742.9	7.0	IaA	56.2	3.8	1075.4
CAD05B 19	399.8	223.1	622.9	35.8	IaAB	104.4	4.6	1126.1
CAD05B 21	26.3	12.5	38.8	32.2	IaAB	5.7	1.2	1192.2
CAD05B 22	343.4	345.1	688.5	50.1	IaAB	105.6	1.6	1138.0
CAD05B 24	373.7	232.5	606.2	38.4	IaAB	190.0	3.5	1129.4
CAD05B 25	57.4	91.4	148.8	61.4	IaAB	51.5	1.7	1188.6
CAD05B 26	156.7	62.0	218.7	28.3	IaAB	27.1	3.1	1143.2
CAD05B 27	357.2	227.4	584.6	38.9	IaAB	50.6	3.2	1130.8
CAD05B 28	148.6	59.7	208.3	28.7	IaAB	30.2	4.9	1144.8
CAD05B 29	170.9	323.4	494.3	65.4	IaAB	141.7	14.5	1162.0
CAD05B 30	434.8	139.7	574.5	24.3	IaAB	89.4	14.3	1114.8
CAD05B 32	266.1	459.9	726.0	63.3	IaAB	245.4	3.8	1150.1
CAD05B 33	364.2	84.4	448.6	18.8	IaAB	35.6	13.9	1112.9
CAD05B 34	350.1	155.2	505.3	30.7	IaAB	65.3	2.4	1125.6
CAD05B 35	362.2	247.6	609.8	40.6	IaAB	125.2	12.7	1131.5
CAD05B 36	461.1	287.8	748.9	38.4	IaAB	219.6	2.6	1124.3
CAD05B 37	361.2	197.2	558.4	35.3	IaAB	153.3	2.2	1128.2
CAD05B 38	507.2	773.5	1280.7	60.4	IaAB	455.7	5.5	1133.0
CAD05B 39	415.8	135.5	551.3	24.6	IaAB	87.0	0.9	1116.1
CAD05B 40	532.1	384.5	916.6	41.9	IaAB	237.2	2.1	1123.0
CAD05B 41	545.7	162.4	708.1	22.9	IaAB	75.4	1.7	1108.1
CAD05B 42	159.3	118.0	277.3	42.6	IaAB	73.3	5.2	1152.9
CAD05B 44	460.6	410.4	871.0	47.1	IaAB	181.8	1.9	1129.3
CAD05B 46	218.7	297.7	516.4	57.6	IaAB	0.0	5.7	1152.6
CAD05B 47	916.2	0.0	916.2	0.0	IaA	0.0	3.7	#NUM!
CAD05B 48	291.5	373.2	664.7	56.1	IaAB	0.0	6.4	1144.8
CAD05B 49	380.5	154.0	534.5	28.8	IaAB	0.0	3.4	1122.0
CAD05B 50	330.0	202.5	532.5	38.0	IaAB	89.7	0.7	1132.2
CAD05B 52	298.2	170.1	468.3	36.3	IaAB	72.6	0.5	1133.5
CAD05B 53	36.7	15.0	51.7	29.0	IaAB	12.0	2.0	1180.7
CAD05B 54	248.6	414.0	662.6	62.5	IaAB	221.0	5.7	1151.4
CAD05B 56	34.6	51.1	85.7	59.6	IaAB	6.4	0.6	1201.2
CAD05B 57	42.0	53.4	95.4	56.0	IaAB	33.8	1.6	1194.4
CAD05B 58	66.0	196.1	262.1	74.8	IaAB	118.4	0.3	1190.1
CAD05B 59	209.6	393.3	602.9	65.2	IaAB	0.0	4.4	1156.8
CAD05B 60	287.7	202.5	490.2	41.3	IaAB	86.3	0.6	1137.6
CAD05B 61	445.9	252.6	698.5	36.2	IaAB	171.6	2.3	1123.7
CAD05B 62	438.1	114.3	552.4	20.7	IaAB	72.3	1.2	1110.8
CAD05B 63	462.6	183.6	646.2	28.4	IaAB	149.1	2.8	1117.0
CAD05B 64	383.5	98.1	481.6	20.4	IaAB	123.6	0.2	1113.6

Appendix B

Carolina Diamond Nitrogen Data

cont.

Sample	type IaA (ppm)	type IaB (ppm)	N (ppm)	% B	N. Agg. state	Platelet Area	3107 H area	T[N,1.5Ga]
CAD05B 65	224.5	8.3	232.8	3.6	IaA	0.0	3.0	1085.6
CAD05B 66	165.9	249.0	414.9	60.0	IaAB	155.9	11.5	1160.6
CAD05B 67	265.9	95.8	361.7	26.5	IaAB	10.5	1.4	1128.6
CAD05B 68	302.7	289.5	592.2	48.9	IaAB	121.3	2.0	1140.4
CAD05B 70	309.0	295.7	604.7	48.9	IaAB	98.7	0.8	1139.9
CAD05B 71	252.9	275.9	528.8	52.2	IaAB	96.2	0.8	1146.5
CAD05B 72	236.5	189.9	426.4	44.5	IaAB	130.1	2.3	1144.2
CAD05B 73	239.8	227.2	467.0	48.7	IaAB	48.9	1.6	1146.1
CAD05B 74	331.3	96.5	427.8	22.6	IaAB	51.6	0.8	1119.5
CAD05B 75	240.0	306.7	546.7	56.1	IaAB	196.6	6.1	1149.6
CAD05B 76	371.0	50.4	421.4	12.0	IaAB	25.9	0.3	1101.9
CAD05B 77	72.5	72.0	144.5	49.8	IaAB	50.6	3.2	1177.0
CAD05B 78	185.1	271.3	456.4	59.4	IaAB	13.1	2.8	1157.6
CAD05B 79	53.9	256.1	310.0	82.6	IaAB	67.2	3.4	1198.1
CAD05B 80	193.0	294.1	487.1	60.4	IaAB	88.0	38.3	1156.9
CAD05B 81	153.7	285.4	439.1	65.0	IaAB	92.7	1.9	1164.6
CAD05C 1	309.6	237.1	546.7	43.4	IaAB	145.6	1.3	1137.0
CAD05C 2	182.8	329.7	512.5	64.3	IaAB	128.4	2.2	1159.9
CAD05C 3	245.1	150.8	395.9	38.1	IaAB	92.8	4.3	1139.5
CAD05C 4	150.6	290.5	441.1	65.9	IaAB	137.2	1.1	1165.4
CAD05C 5	256.9	75.7	332.6	22.8	IaAB	44.8	5.6	1125.8
CAD05C 6	882.3	95.9	978.2	9.8	IaA	43.4	1.5	1077.5
CAD05C 7	414.9	364.8	779.7	46.8	IaAB	270.5	1.7	1131.7
CAD05C 8	341.4	84.9	426.3	19.9	IaAB	0.0	2.0	1115.8
CAD05C 9	551.9	278.9	830.8	33.6	IaAB	146.3	0.8	1116.8
CAD05C 10	274.3	428.7	703.0	61.0	IaAB	200.0	3.9	1148.4
CAD05C 11	224.4	140.4	364.8	38.5	IaAB	0.0	6.7	1141.9
CAD05C 12	600.7	151.7	752.4	20.2	IaAB	114.6	1.3	1102.8
CAD05C 13	328.8	368.2	697.0	52.8	IaAB	188.4	0.1	1140.3
CAD05C 14	529.3	116.8	646.1	18.1	IaAB	101.2	2.4	1103.2
CAD05C 17	691.6	175.9	867.5	20.3	IaAB	16.0	4.1	1099.6
CAD05C 18	162.2	80.6	242.8	33.2	IaAB	30.5	4.6	1146.3
CAD05C 19	252.9	317.2	570.1	55.6	IaAB	108.2	1.5	1148.1
CAD05C 21	451.4	99.7	551.1	18.1	IaAB	66.3	6.6	1106.9
CAD05C 22	132.7	146.4	279.1	52.5	IaAB	11.3	3.2	1162.8
CAD05C 23	190.1	95.7	285.8	33.5	IaAB	61.4	2.7	1142.6
CAD05C 24	268.9	264.5	533.4	49.6	IaAB	169.0	1.0	1143.7
CAD05C 25	11.8	12.1	23.9	50.6	IaAB	0.0	2.6	1226.1
CAD05C 27	458.2	443.9	902.1	49.2	IaAB	289.2	3.8	1130.5
CAD05C 28	458.4	590.9	1049.3	56.3	IaAB	329.4	2.7	1133.7
CAD05C 30	248.9	227.3	476.2	47.7	IaAB	89.4	18.8	1144.7
CAD05C 31	775.9	141.5	917.4	15.4	IaAB	26.7	5.1	1090.7
CAD05C 32	183.9	16.2	200.1	8.1	IaA	15.4	4.6	1109.2

Appendix B

Carolina Diamond Nitrogen Data

cont.

Sample	type IaA (ppm)	type IaB (ppm)	N (ppm)	% B	N. Agg. state	Platelet Area	3107 H area	T[N,1.5Ga]
CAD05C 34	122.8	283.2	406.0	69.8	IaAB	21.9	2.1	1172.1
CAD05C 35	259.2	397.3	656.5	60.5	IaAB	238.6	2.8	1149.6
CAD05C 36	482.8	313.4	796.2	39.4	IaAB	81.2	86.0	1123.8
CAD05C 37	279.9	298.7	578.6	51.6	IaAB	141.1	18.2	1143.7
CAD05C 38	414.6	110.2	524.8	21.0	IaAB	3.3	15.1	1112.5
CAD05C 39	416.4	248.4	664.8	37.4	IaAB	98.2	1.7	1126.1
CAD05C 40	438.4	161.2	599.6	26.9	IaAB	117.0	3.0	1117.0
CADJ4 1	65.5	355.9	421.4	84.5	IaAB	112.2	0.8	1193.5
CADJ4 2	51.0	405.5	456.5	88.8	IaAB	244.1	1.8	1201.5
CADJ4 3	393.0	67.7	460.7	14.7	IaAB	26.4	2.0	1105.3
CADJ4 4	457.6	174.4	632.0	27.6	IaAB	90.8	2.4	1116.6
CADJ4 5	408.9	430.1	839.0	51.3	IaAB	237.8	1.3	1134.2
CADJ4 6	205.4	450.6	656.0	68.7	IaAB	8.4	8.2	1158.6
CADJ4 8	434.6	402.2	836.8	48.1	IaAB	236.9	3.2	1131.2
CADJ4 9	334.9	206.9	541.8	38.2	IaAB	82.1	0.0	1131.9
CADJ4 10	493.2	0.4	493.6	0.1	IaA	0.0	6.4	989.0
CADJ4 11	330.8	477.5	808.3	59.1	IaAB	276.4	7.4	1142.9
CADJ4 12	512.5	306.5	819.0	37.4	IaAB	142.6	1.4	1121.2
CADJ4 13	152.0	380.9	532.9	71.5	IaAB	0.0	4.7	1167.3
CADJ4 14	110.6	265.3	375.9	70.6	IaAB	9.3	9.6	1175.1
CADJ4 16	218.2	373.0	591.2	63.1	IaAB	128.5	3.0	1154.9
CADJ4 17	409.9	388.1	798.0	48.6	IaAB	244.2	2.3	1132.9
CADJ4 18	293.1	227.0	520.1	43.6	IaAB	60.1	4.7	1138.5
CADJ4 19	189.8	335.1	524.9	63.8	IaAB	133.8	2.2	1158.7
CADJ4 20	376.5	310.4	686.9	45.2	IaAB	113.3	4.0	1133.2
CADJ4 21	200.1	376.1	576.2	65.3	IaAB	13.8	4.0	1158.0
CADJ4 22	352.7	270.0	622.7	43.4	IaAB	49.5	1.8	1133.8
CADJ4 23	210.9	613.4	824.3	74.4	IaAB	416.5	5.0	1160.0
CADJ4 25	77.5	396.8	474.3	83.7	IaAB	241.5	3.5	1188.8
CADJ4 26	382.8	133.2	516.0	25.8	IaAB	74.9	1.2	1119.3
CADJ4 28	332.5	47.8	380.3	12.6	IaAB	28.1	5.5	1105.6
CADJ4 29	406.1	216.7	622.8	34.8	IaAB	54.9	2.2	1125.0
CADJ4 30	184.6	181.7	366.3	49.6	IaAB	58.2	0.0	1153.1
CADJ4 31	415.0	65.6	480.6	13.6	IaAB	27.3	1.0	1102.3
CADJ4 32	278.2	222.0	500.2	44.4	IaAB	11.2	11.7	1140.1
CADJ4 33	117.4	384.4	501.8	76.6	IaAB	151.9	1.6	1175.7
CADJ4 34	426.7	518.2	944.9	54.8	IaAB	333.0	4.6	1134.8
CADJ4 35	58.1	106.9	165.0	64.8	IaAB	90.5	2.6	1189.7
CADJ4 36	515.7	274.8	790.5	34.8	IaAB	183.7	0.8	1119.3
CADJ4 37	399.9	432.2	832.1	51.9	IaAB	201.6	0.8	1135.1
CADJ4 38	284.9	231.1	516.0	44.8	IaAB	72.5	1.1	1139.8
CADJ4 39	653.8	93.7	747.5	12.5	IaAB	46.5	1.3	1089.9
CADJ4 40	407.6	172.0	579.6	29.7	IaAB	15.5	2.6	1121.1

Appendix B

Carolina Diamond Nitrogen Data

cont.

Sample	type IaA (ppm)	type IaB (ppm)	N (ppm)	% B	N. Agg. state	Platelet Area	3107 H area	T[N,1.5Ga]
CADJ4 41	154.5	325.5	480.0	67.8	IaAB	132.7	3.3	1165.5
CADJ4 42	355.4	105.0	460.4	22.8	IaAB	27.8	1.5	1118.1
CADJ4 43	447.8	115.0	562.8	20.4	IaAB	34.4	1.0	1110.0
CADJ4 45	126.3	277.5	403.8	68.7	IaAB	51.9	1.3	1171.0
CADJ4 46	121.1	269.7	390.8	69.0	IaAB	103.4	2.5	1172.2
CADJ4 47	89.5	246.4	335.9	73.4	IaAB	71.9	3.6	1181.6
CADJ4 48	215.2	289.2	504.4	57.3	IaAB	121.0	2.0	1152.9
CADJ4 49	326.9	242.4	569.3	42.6	IaAB	128.0	8.4	1135.2
CADJ4 50	163.9	101.2	265.1	38.2	IaAB	57.4	5.7	1149.5
CADJ4 52	239.7	315.7	555.4	56.8	IaAB	117.7	1.4	1150.0
CADJ4 54	148.1	343.1	491.2	69.8	IaAB	91.6	1.1	1167.3
CADJ4 55	269.0	261.2	530.2	49.3	IaAB	0.0	4.2	1143.6
CADJ4 56	40.6	7.8	48.4	16.1	IaAB	5.1	6.3	1162.9
CADJ4 57	526.7	479.7	1006.4	47.7	IaAB	361.1	4.5	1126.3
CADJ4 58	128.6	387.7	516.3	75.1	IaAB	152.3	9.4	1172.8
CADJ4 59	357.1	515.5	872.6	59.1	IaAB	7.0	16.4	1141.0

Appendix B

Renard Pb-Pb Clinopyroxene Data

Table B.5. Results of insitu Pb-Pb isotopic analyses of the more radiogenic clinopyroxenes from the Renard kimberlites.

MORE RADIOGENIC CPX

	$^{207}Pb/^{206}Pb$	2σ	$^{206}Pb/^{204}Pb$	2σ	$^{207}Pb/^{204}Pb$	2σ	^{206}Pb (cps)
REN-M1-2-3	0.846	0.008	17.69	0.261	14.97	0.172	47064
REN-T1-7-2	0.823	0.003	18.73	0.114	15.43	0.102	130015
REN-D1-5-1	0.829	0.005	18.46	0.084	15.27	0.092	161958
REN-T1-8-1	0.832	0.001	18.58	0.090	15.46	0.087	131786
REN-T1-9-1	0.832	0.005	18.52	0.126	15.42	0.103	124528
REN-E1-4-1	0.832	0.003	18.79	0.069	15.62	0.069	117319
REN-T1-2-1	0.834	0.003	18.43	0.132	15.42	0.110	118167
REN-M1-12-1	0.836	0.001	18.24	0.060	15.22	0.074	30835
REN-T1-5-1	0.837	0.001	18.51	0.092	15.49	0.086	119595
REN-D1-9-1	0.838	0.002	18.20	0.047	15.24	0.048	164724
REN-T1-7-1	0.839	0.001	18.45	0.053	15.53	0.060	121488
REN-D1-5-2	0.839	0.008	18.28	0.072	15.33	0.031	177353
REN-T1-2-2	0.839	0.001	18.60	0.187	15.58	0.180	110474
REN-T1-1-1	0.843	0.001	18.27	0.087	15.40	0.074	118655
REN-D1-7-1	0.843	0.001	18.15	0.060	15.31	0.062	152991
REN-D1-1-1	0.843	0.005	18.06	0.120	15.28	0.096	231188
REN-A1-2-1	0.844	0.004	17.98	0.171	15.16	0.151	73974
REN-T1-1-2	0.844	0.004	18.23	0.083	15.40	0.087	128844
REN-D1-6-1	0.844	0.005	18.17	0.050	15.32	0.054	168579
REN-D1-4-1	0.845	0.002	18.15	0.163	15.32	0.171	183212
REN-E1-3-1	0.848	0.016	17.97	0.099	15.33	0.192	25664
REN-K1-11-1	0.853	0.004	18.03	0.119	15.45	0.125	63962
REN-E1-1-1	0.853	0.002	18.37	0.101	15.66	0.072	126109
REN-K1-9-1	0.862	0.004	17.80	0.165	15.32	0.189	34726
REN-J1-1-3	0.863	0.007	17.77	0.134	15.39	0.085	127021
REN-J1-2-1	0.870	0.001	17.51	0.126	15.22	0.140	129229
REN-J1-1-2	0.874	0.002	17.55	0.094	15.31	0.124	91262
REN-J1-3-1	0.875	0.003	17.39	0.100	15.22	0.104	138079

Appendix B

Renard Pb-Pb Clinopyroxene Data

Table B.6. Results of insitu Pb-Pb isotopic analyses of the less radiogenic clinopyroxenes from the Renard kimberlites.

LESS RADIOGENIC CPX

	$^{207}Pb/^{206}Pb$	2σ	$^{206}Pb/^{204}Pb$	2σ	$^{207}Pb/^{204}Pb$	2σ	^{206}Pb (cps)
REN-O1-6-1	0.881	0.019	16.59	0.179	14.90	0.121	40422
REN-J1-1-1	0.882	0.002	17.28	0.165	15.25	0.128	127620
REN-M1-1-2	0.904	0.022	16.72	0.284	15.21	0.167	23776
REN-K1-10-1	0.908	0.005	16.92	0.352	15.37	0.288	26391
REN-K1-5-1	0.917	0.002	16.38	0.163	15.00	0.122	25370
REN-B1-8-2	0.929	0.014	16.37	0.187	15.26	0.097	724132
REN-O1-4-1	0.936	0.008	15.63	0.194	14.69	0.158	48568
REN-P1-6-1	0.941	0.003	16.21	0.154	15.25	0.153	40284
REN-O1-3-1	0.948	0.006	15.56	0.201	14.76	0.127	47082
REN-O1-5-4	0.948	0.015	15.81	0.234	14.80	0.266	22237
REN-P1-1-1	0.961	0.006	15.81	0.220	15.22	0.242	35642
REN-B1-7-1	0.964	0.005	15.40	0.200	14.92	0.140	65886
REN-P1-5-1	0.981	0.011	15.46	0.196	15.03	0.150	34916
REN-O1-1-2	0.990	0.012	14.99	0.256	14.78	0.116	30414
REN-B1-12-2	0.995	0.008	14.96	0.232	14.83	0.155	35282
REN-B1-8-1	1.005	0.007	14.79	0.112	14.85	0.110	39495
REN-B1-2-2	1.006	0.006	14.78	0.128	14.86	0.153	55660
REN-B1-10-1	1.006	0.017	14.68	0.147	14.94	0.198	38300
REN-K1-15-1	1.009	0.007	14.50	0.224	14.66	0.214	22358
REN-M1-2-2	1.010	0.008	14.64	0.223	14.61	0.250	27003
REN-B1-3-2	1.025	0.014	14.31	0.093	14.74	0.165	39209
REN-B1-11-1	1.028	0.008	14.31	0.165	14.74	0.167	36773
REN-B1-13-1	1.030	0.009	14.23	0.127	14.65	0.081	32493
REN-B1-12-1	1.045	0.005	14.15	0.159	14.78	0.196	31687
REN-B1-3-1	1.052	0.006	14.02	0.117	14.69	0.041	38439
REN-B1-4-1	1.063	0.006	13.74	0.227	14.60	0.238	35030
REN-B1-5-1	1.068	0.004	13.82	0.077	14.72	0.134	32970
REN-B1-5-2	1.070	0.002	13.84	0.089	14.79	0.112	30809
REN-P1-7-1	1.071	0.004	14.01	0.038	15.01	0.095	21990
REN-P1-8-1	1.072	0.003	13.87	0.168	14.89	0.225	23552
REN-P1-2-1	1.073	0.007	13.83	0.247	14.78	0.168	24326
REN-P1-3-1	1.084	0.004	13.78	0.133	14.85	0.207	23315

Appendix B

SEM Images and Element Analysis of Djerfisherite Bearing Inclusion

Figure B.3. SEM BSE image of the djerfisherite multi-mineral Renard inclusion. The four phases identified for further analysis are shown.

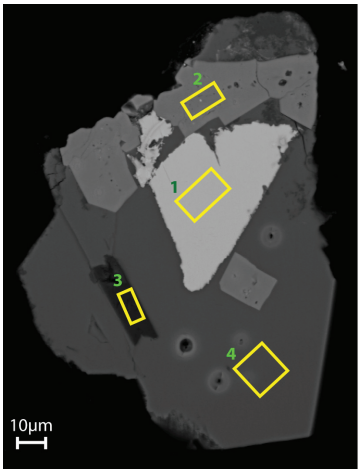

12029-4
Image size:512 x 384
Mag:1443.03198x
HV:20.0kV

Figure B.4. SEM element maps of the djerfisherite multi-mineral inclusion

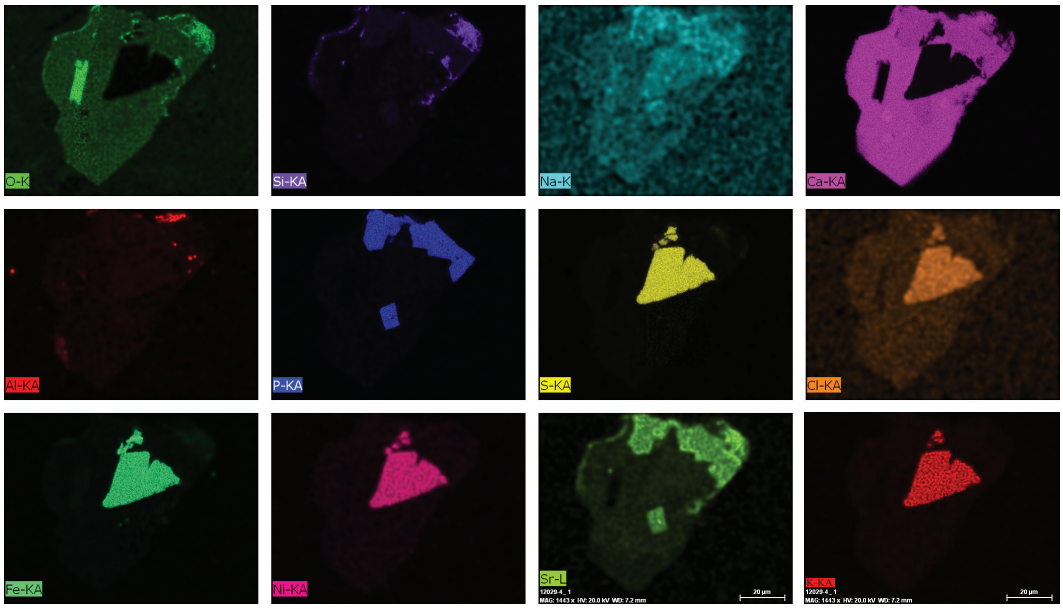

Figure B.5. EDS analysis of the elements present in phase 1 (djerfisherite), with calculated element wt%.

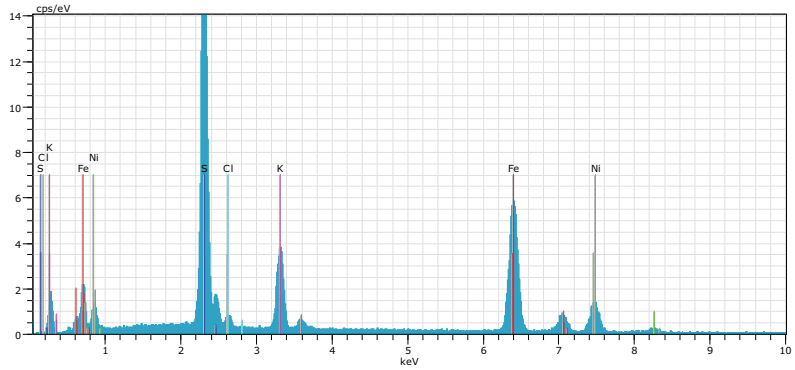

El	AN	Series	unn. C [wt.%]	norm. C [wt.%]	Atom. C [at.%]	Error [wt.%]
Fe	26	K-series	40.26	41.86	33.15	1.1
S	16	K-series	28.86	30.01	41.39	1.1
Ni	28	K-series	16.53	17.19	12.95	0.5
K	19	K-series	9.43	9.81	11.09	0.3
Cl	17	K-series	1.09	1.14	1.42	0.1
		Total:	96.17	100.00	100.00	

Figure B.6. EDS analysis of the elements present in phase 2 (apatite), with calculated element wt%.

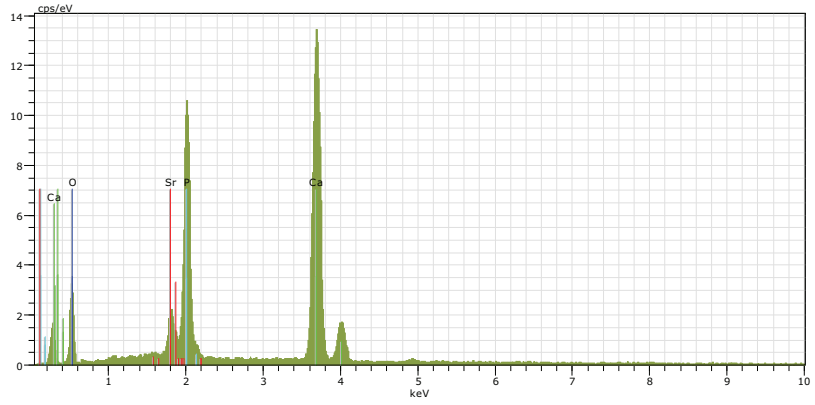

El	AN	Series	unn. C [wt.%]	norm. C [wt.%]	Atom. C [at.%]	Error [wt.%]
Ca	20	K-series	35.29	41.93	26.64	1.1
O	8	K-series	31.21	37.08	59.01	5.7
P	15	K-series	13.06	15.52	12.76	0.6
Sr	38	L-series	4.61	5.48	1.59	0.2
		Total:	84.16	100.00	100.00	

Figure B.7. EDS analysis of the elements present in phase 3 (dolomite), with calculated element wt%.

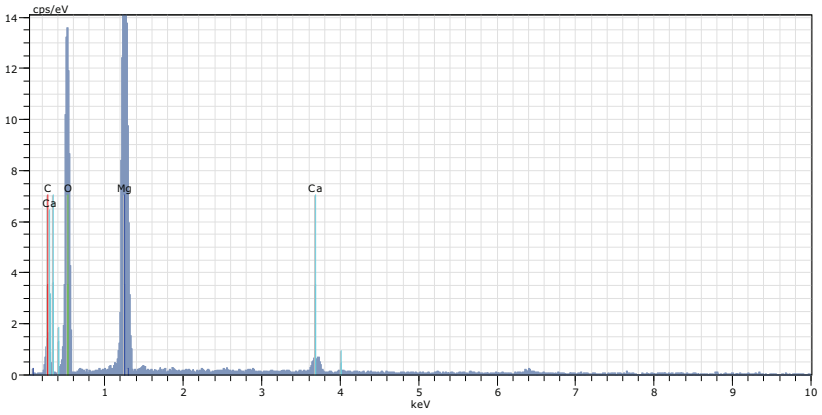

El	AN	Series	unn. C [wt.%]	norm. C [wt.%]	Atom. C [at.%]	Error [wt.%]
O	8	K-series	44.68	51.99	55.61	7.0
Mg	12	K-series	26.23	30.51	21.49	1.5
C	6	K-series	13.29	15.46	22.03	3.6
Ca	20	K-series	1.75	2.04	0.87	0.1
		Total:	85.95	100.00	100.00	

Figure B.8. EDS analysis of the elements present in phase 4 (calcite), with calculated element wt%.

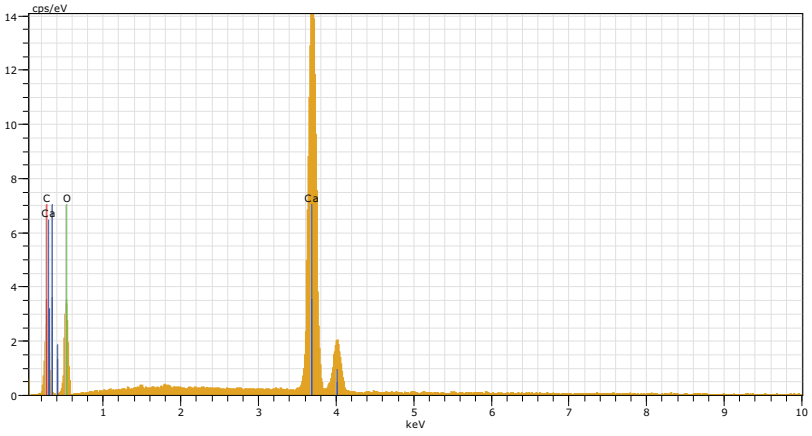

El	AN	Series	unn. C [wt.%]	norm. C [wt.%]	Atom. C [at.%]	Error [wt.%]
Ca	20	K-series	44.51	43.47	21.89	1.3
O	8	K-series	41.25	40.28	50.80	6.8
C	6	K-series	16.65	16.26	27.31	2.8
		Total:	102.41	100.00	100.00	

Appendix B

Element Maps of Sulphide bearing inclusions

Figure B.9. Element maps from the JEOL8900-JXA Superprobe of Renard sulphide inclusions.

12006b - 6

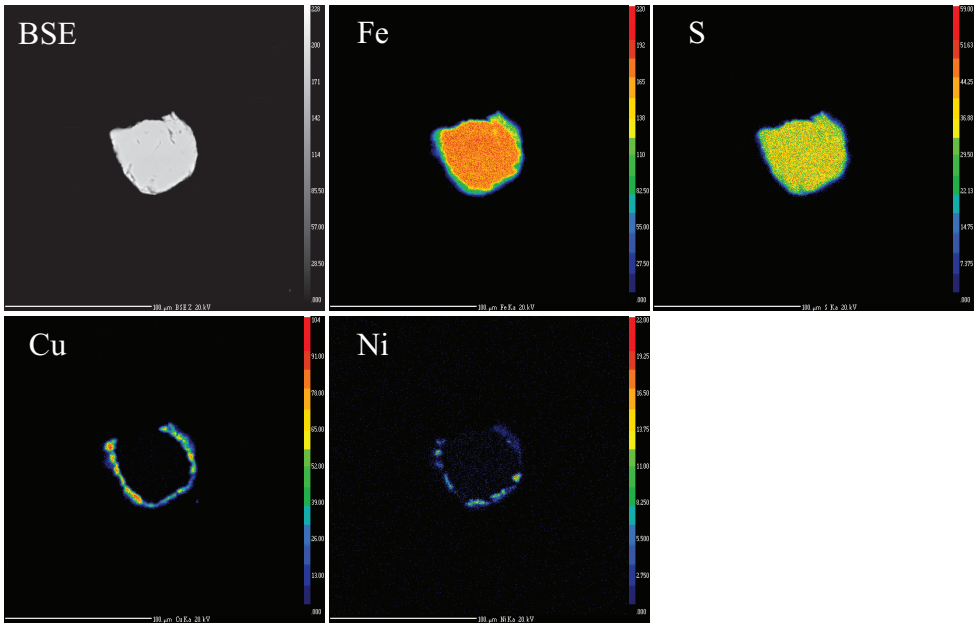

12006b - 7

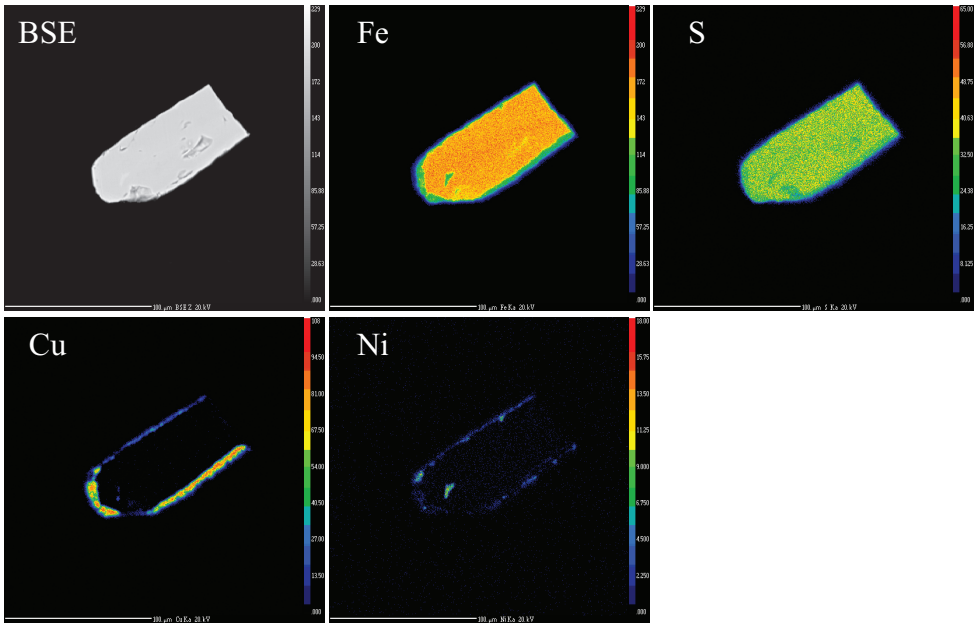

Appendix B

Element Maps of Sulphide bearing inclusions

12029 - 9

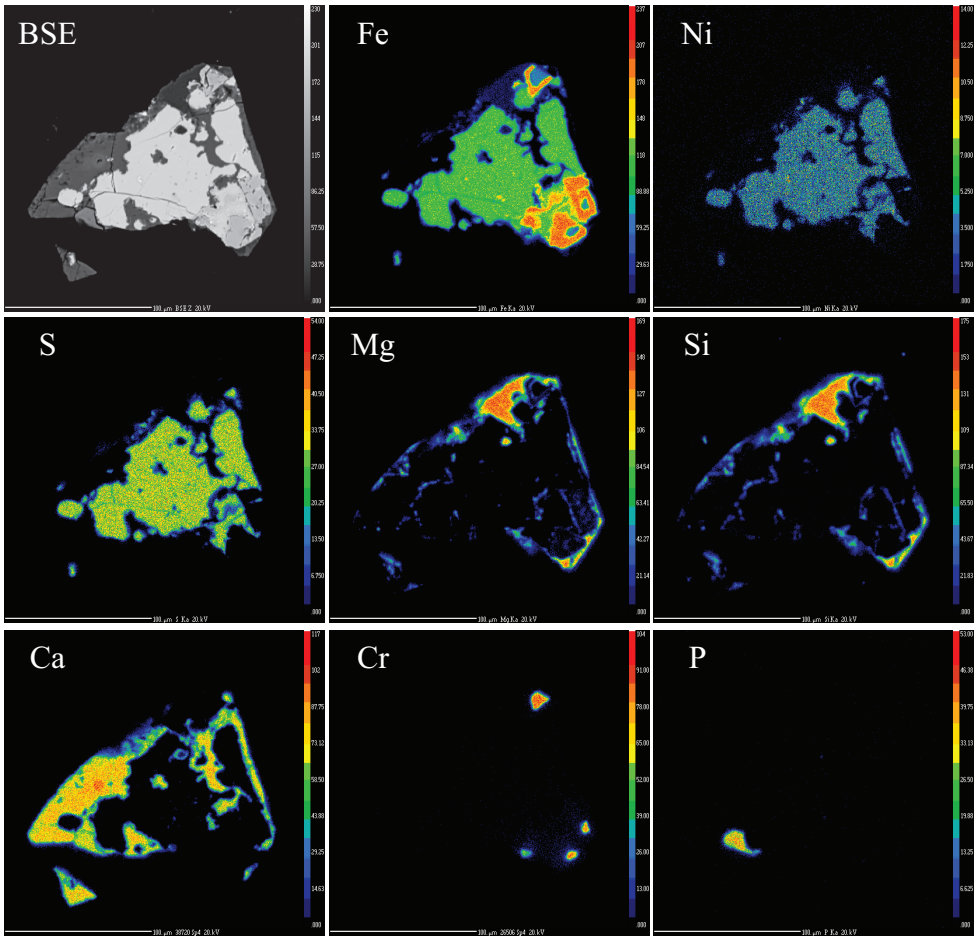

Appendix B

Element Maps of Sulphide bearing inclusions

12029 - 10

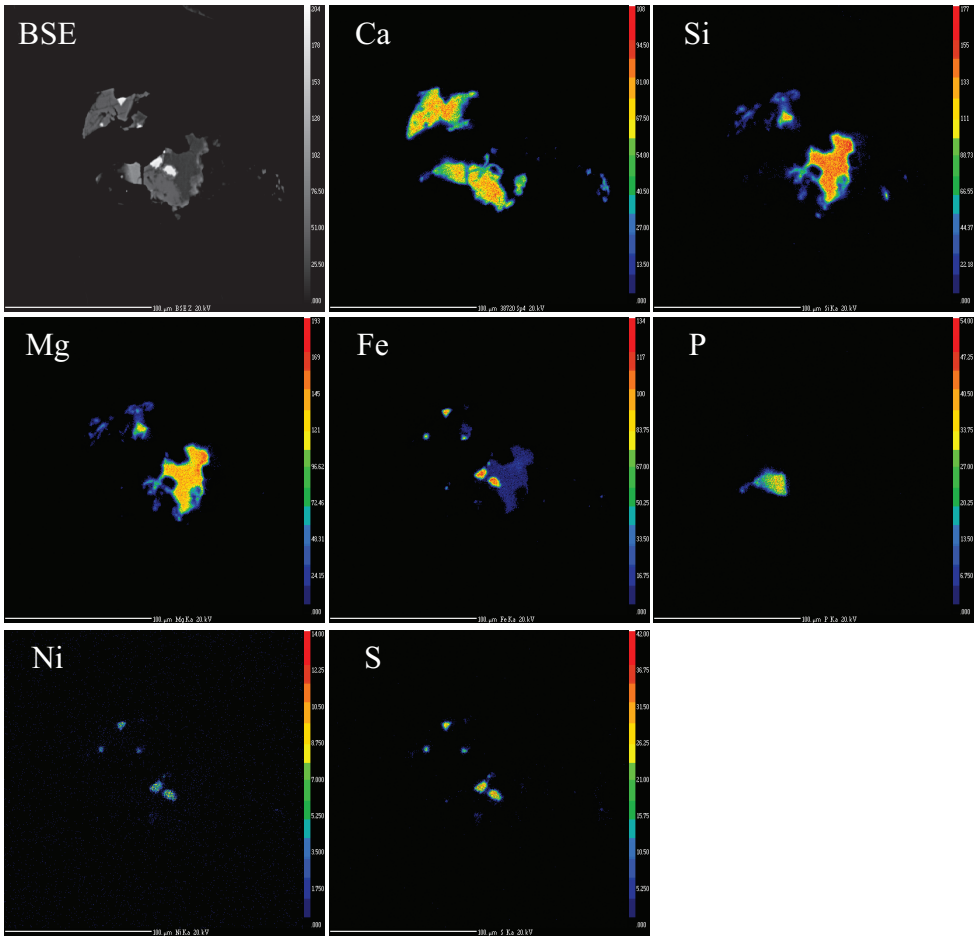

Appendix B

Element Maps of Sulphide bearing inclusions

12029 - 11

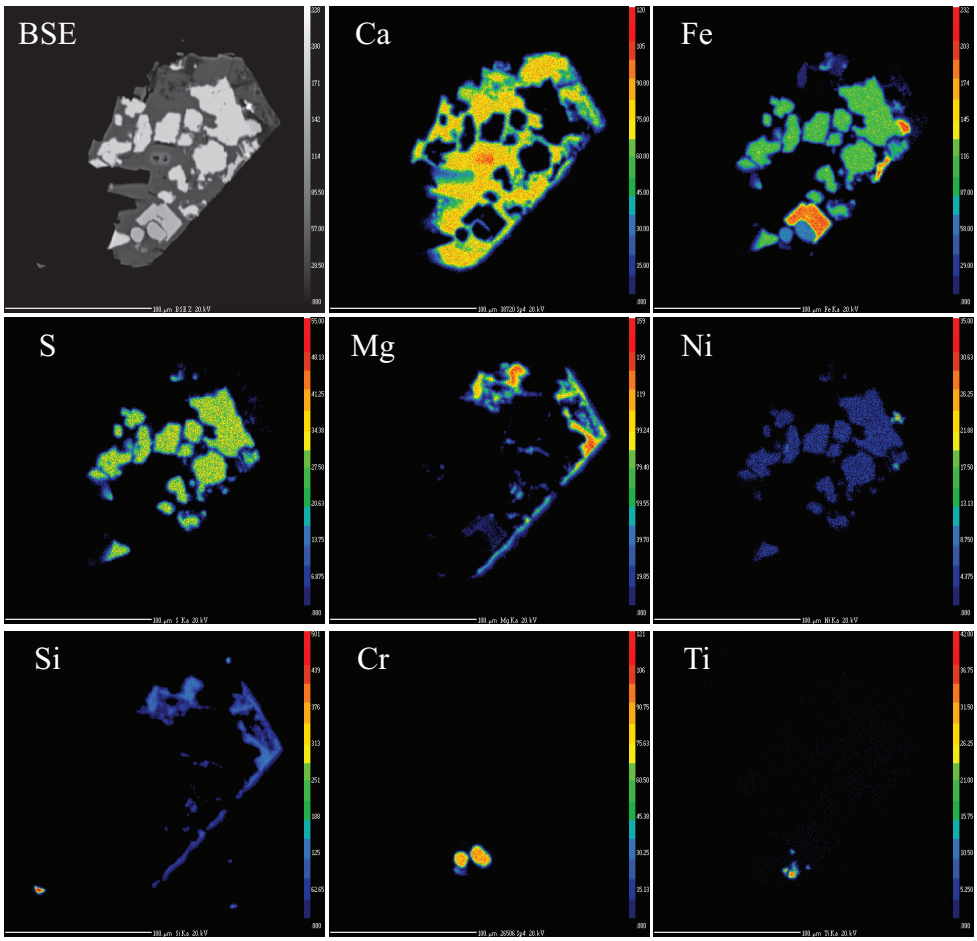

Appendix B

Element Maps of Sulphide bearing inclusions

12036a - 4

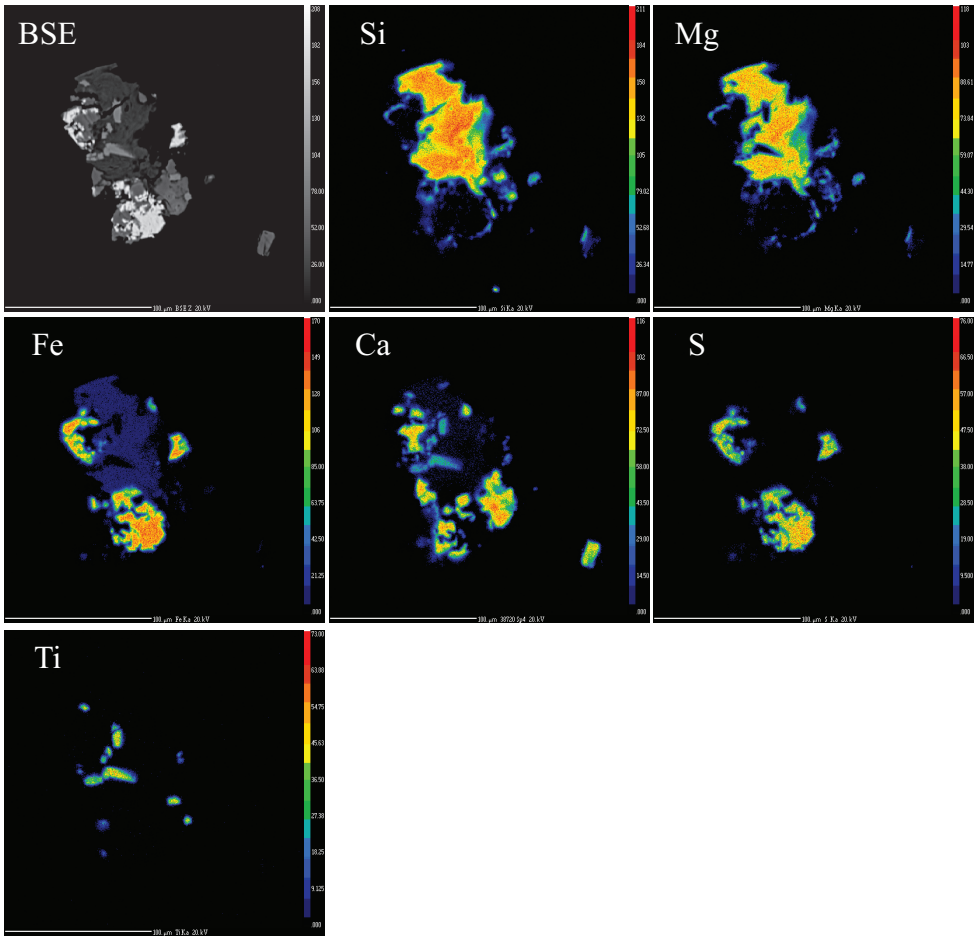

Appendix B

Element Maps of Sulphide bearing inclusions

13530b - 3

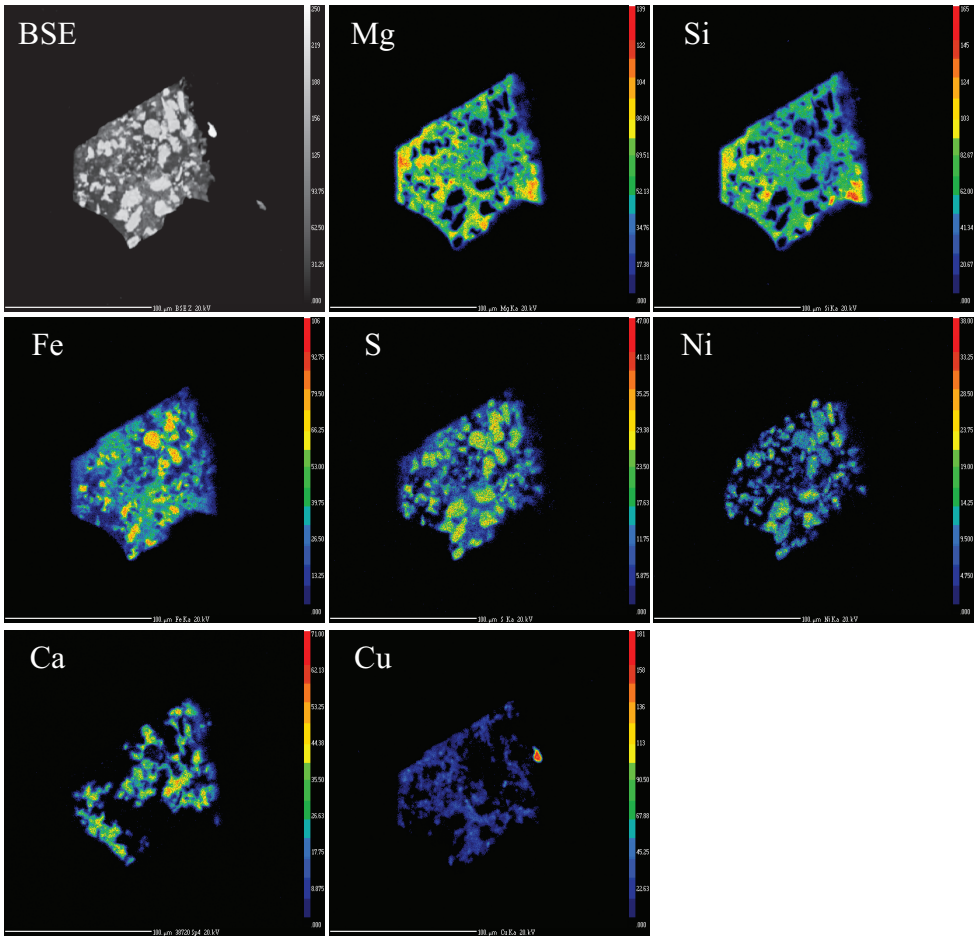

Appendix B

Element Maps of Sulphide bearing inclusions

12029 - 9

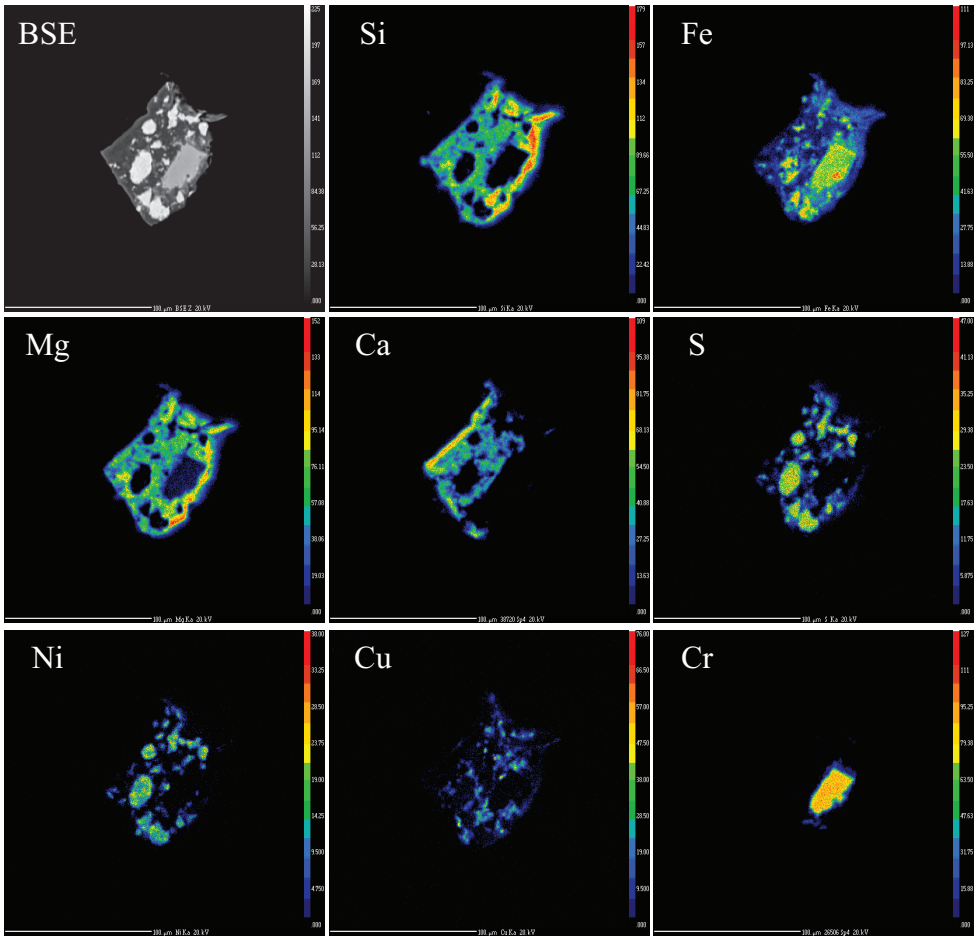

Appendix C

Diamond Desciptions

Appendix C

Diamond Morphologies

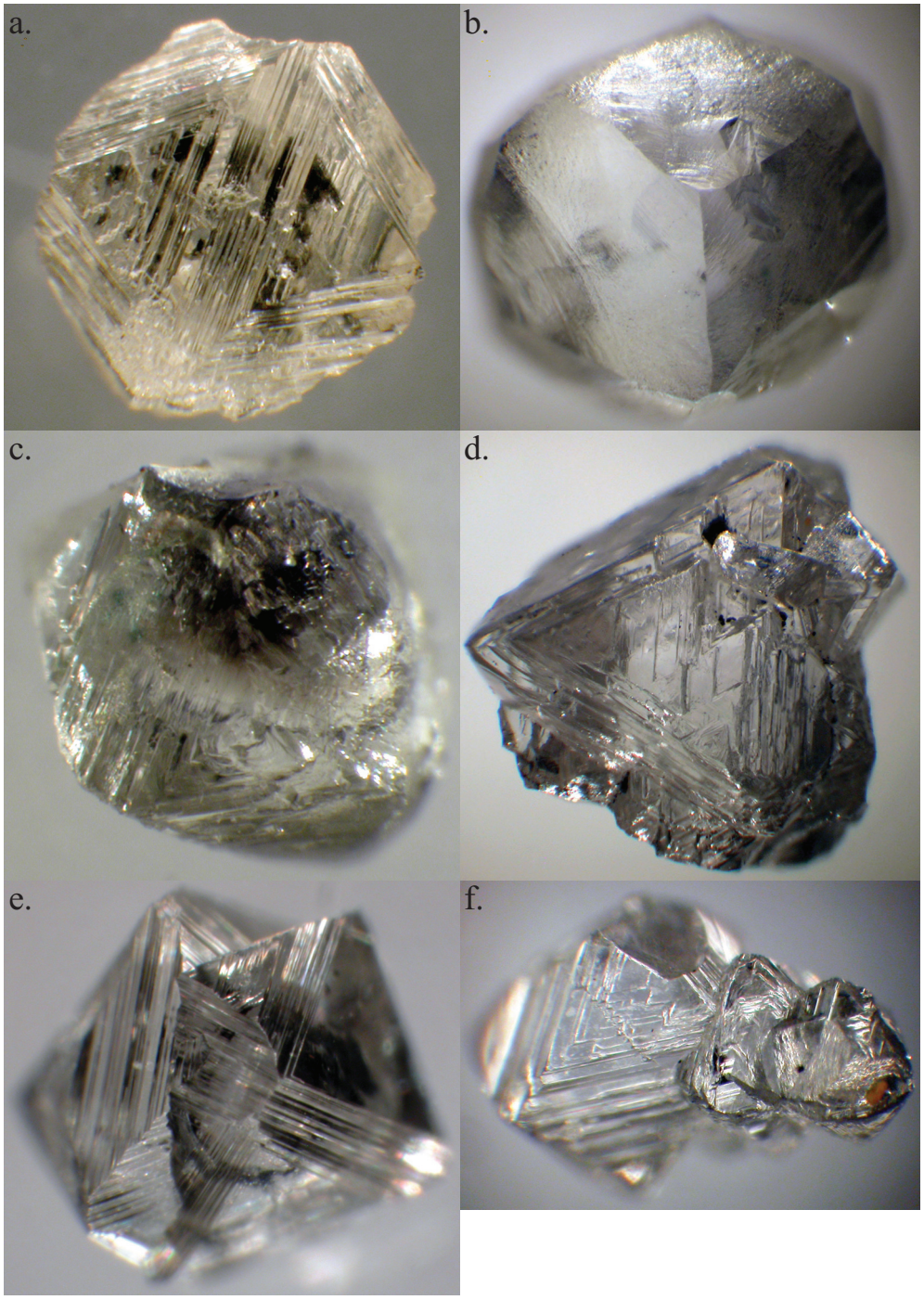

Figure C.1. a) Octahedra. b) Rounded dodecahedra. c) Pseudohemimorphic. d) Macle. e) 2 stone aggregate. f) 3 stone aggregate.

Appendix C

Diamond Inclusions

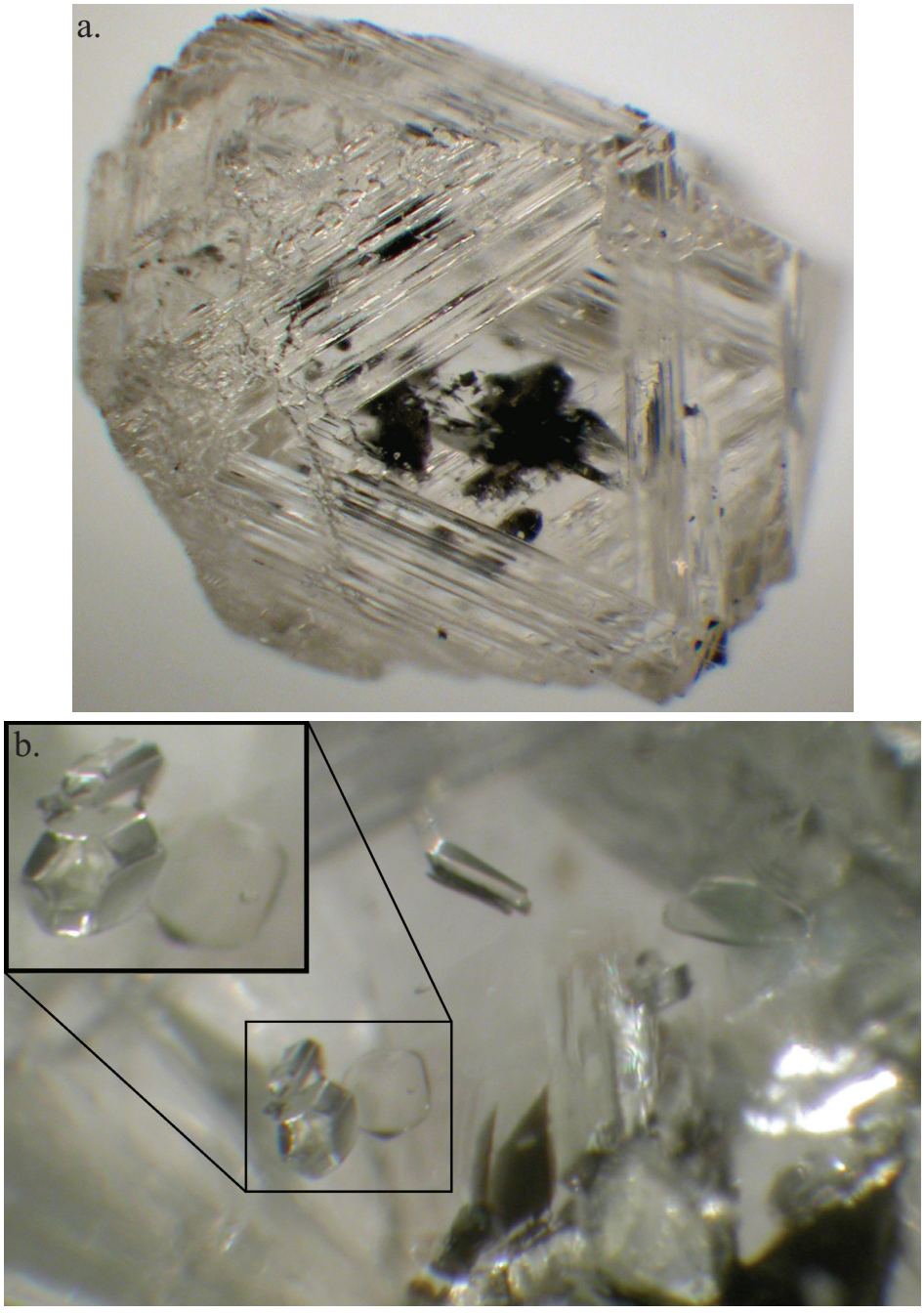

Figure C.2. a) Sulphide inclusion. b) Colourless inclusions showing imposed morphology.

Appendix C

Diamond Inclusions

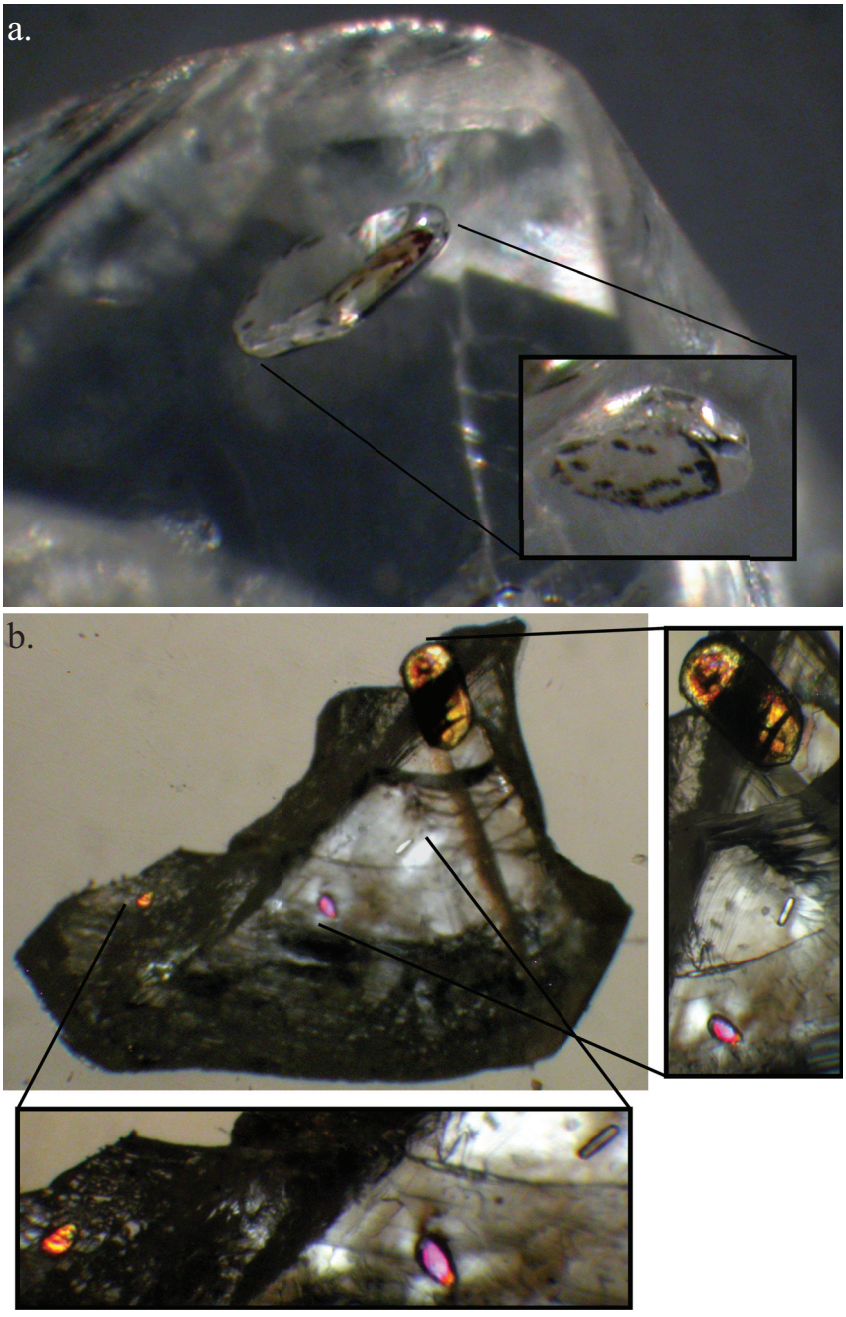

Figure C.3. a) Colourless inclusion showing imposed morphology, with hexagonal graphite plates forming on the surface. b) Colourless inclusions under crossed polarised light

Appendix C

Diamond Inclusions

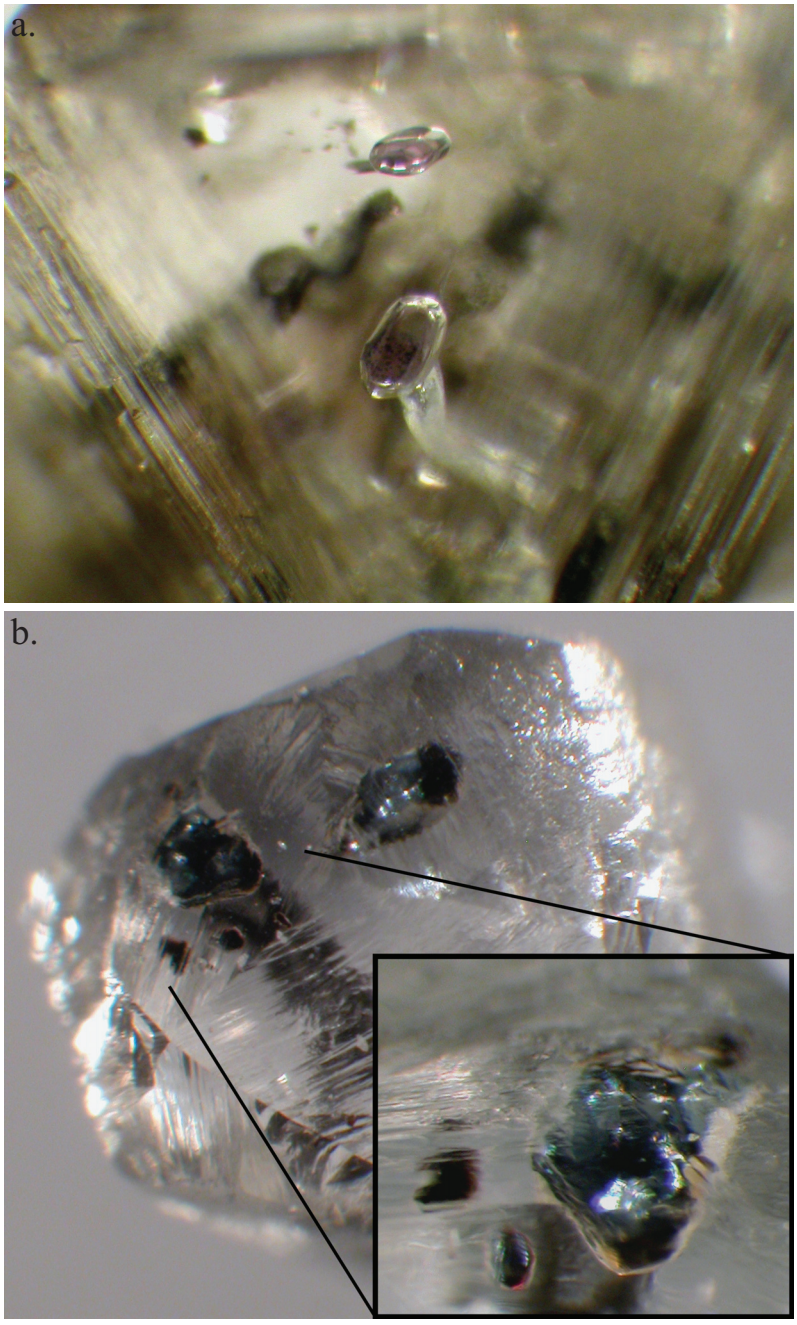

Figure C.4. a) Pink peridotitic garnet inclusions. b) Cherry red chromite inclusions.

Appendix C

Diamond Surface Features

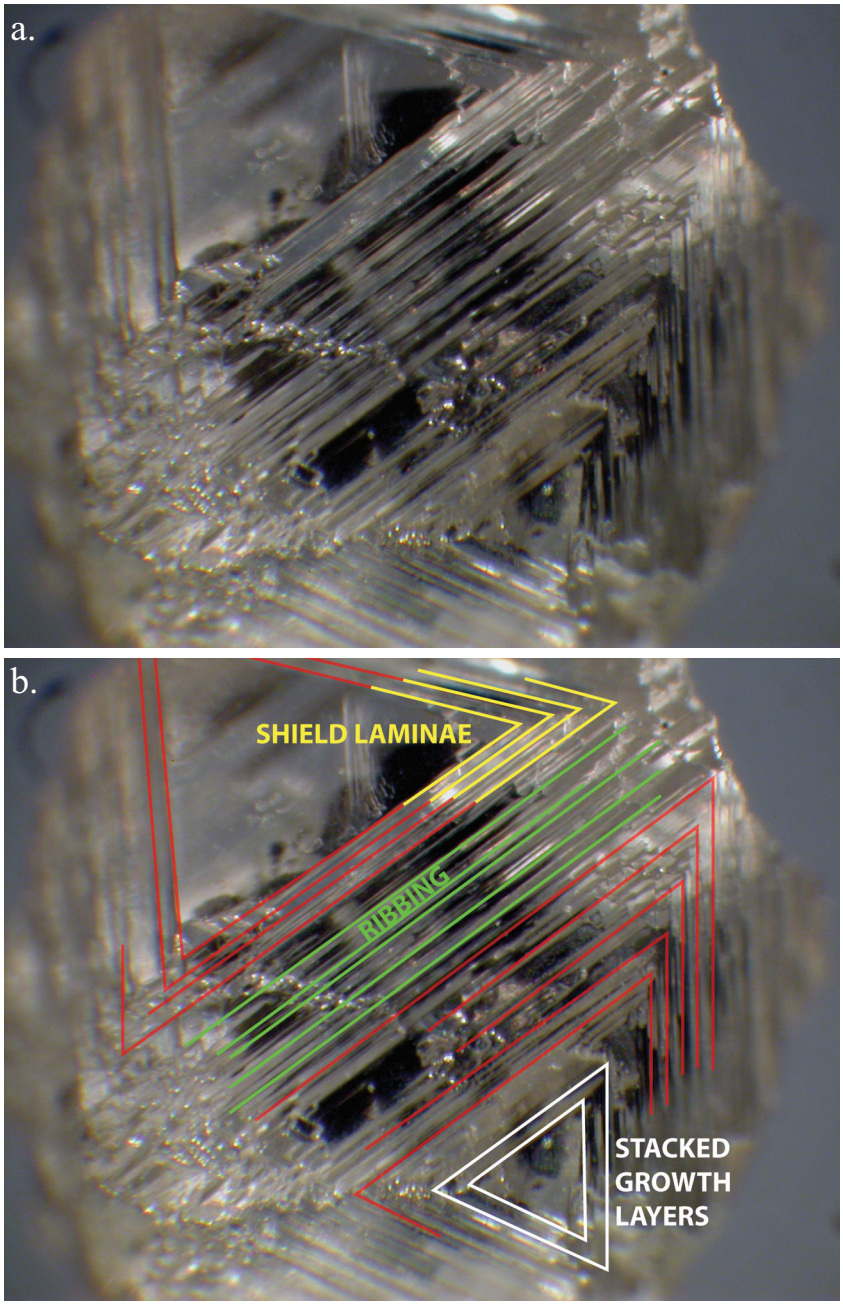

Figure C.5. a) b) Octahedral diamond showing stacked triangular growth layers with shield laminae, which form ribbing between faces.

Appendix C

Diamond Surface Features

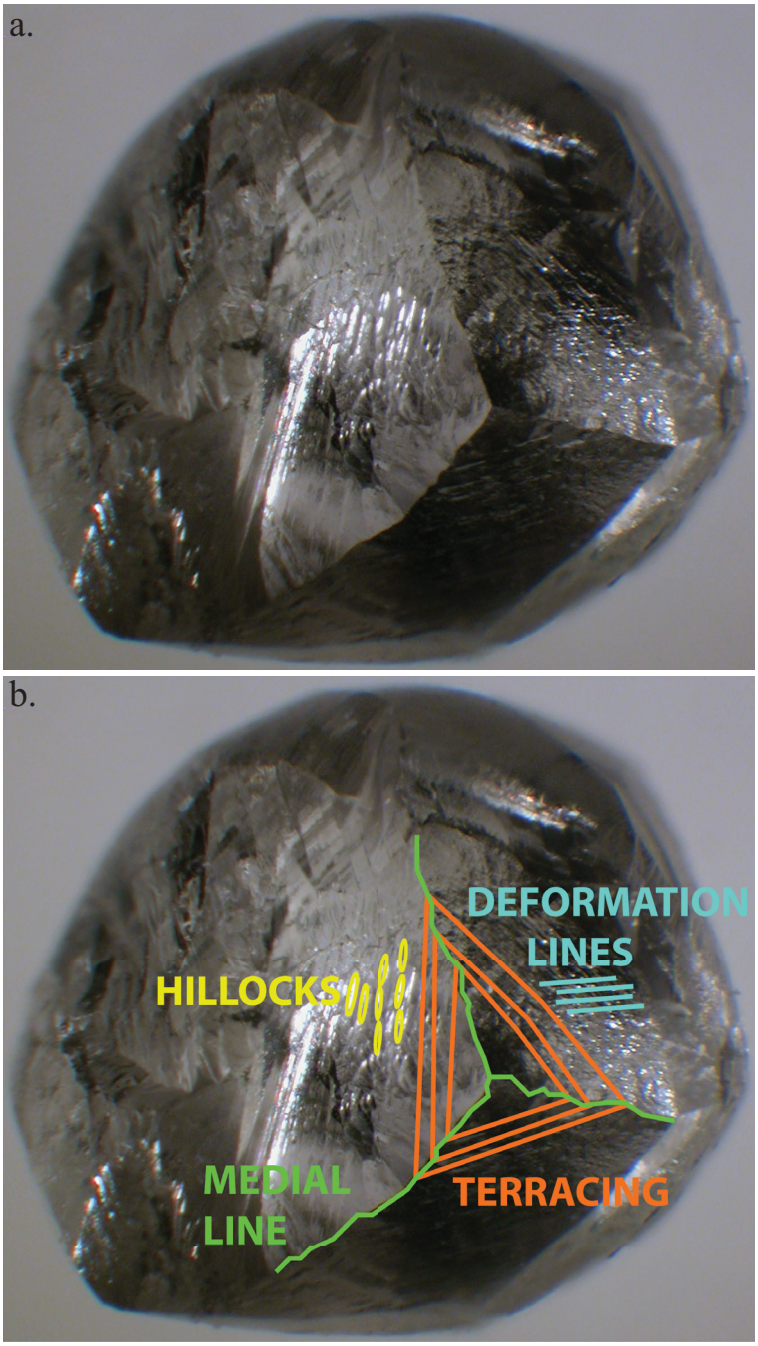

Figure C.6. a) b) Rounded dodecahedral diamond with terracing, medial lines and hillocks on resorbed faces. Deformation lines cross-cut the terracing.

Appendix C

Diamond Surface Features

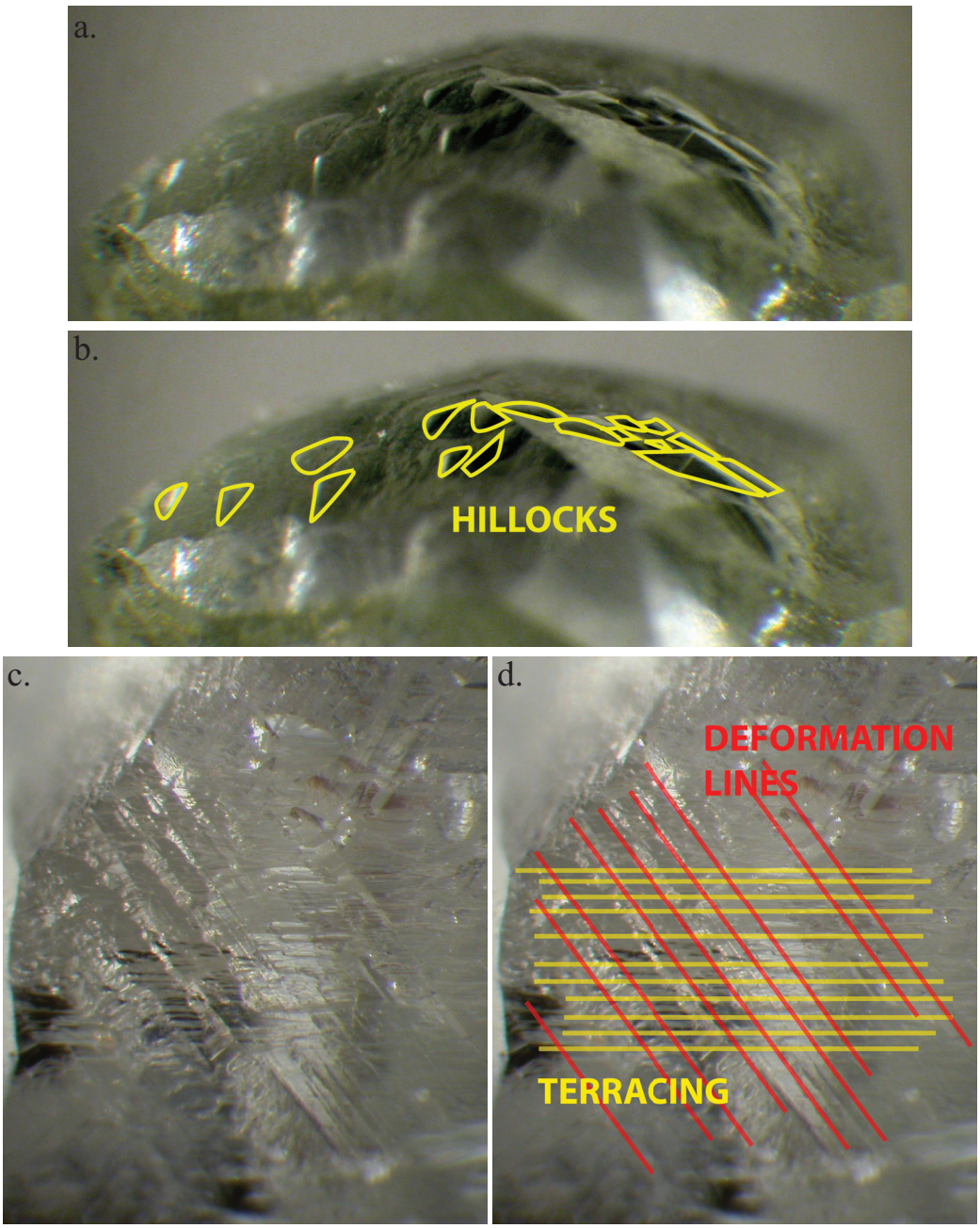

Figure C.7. a) b) Large rounded and pyramidal hillocks are observed. c) d) Terracing on the rounded dodecahedral faces cross cut by deformation lines.

Appendix C

Diamond Surface Features

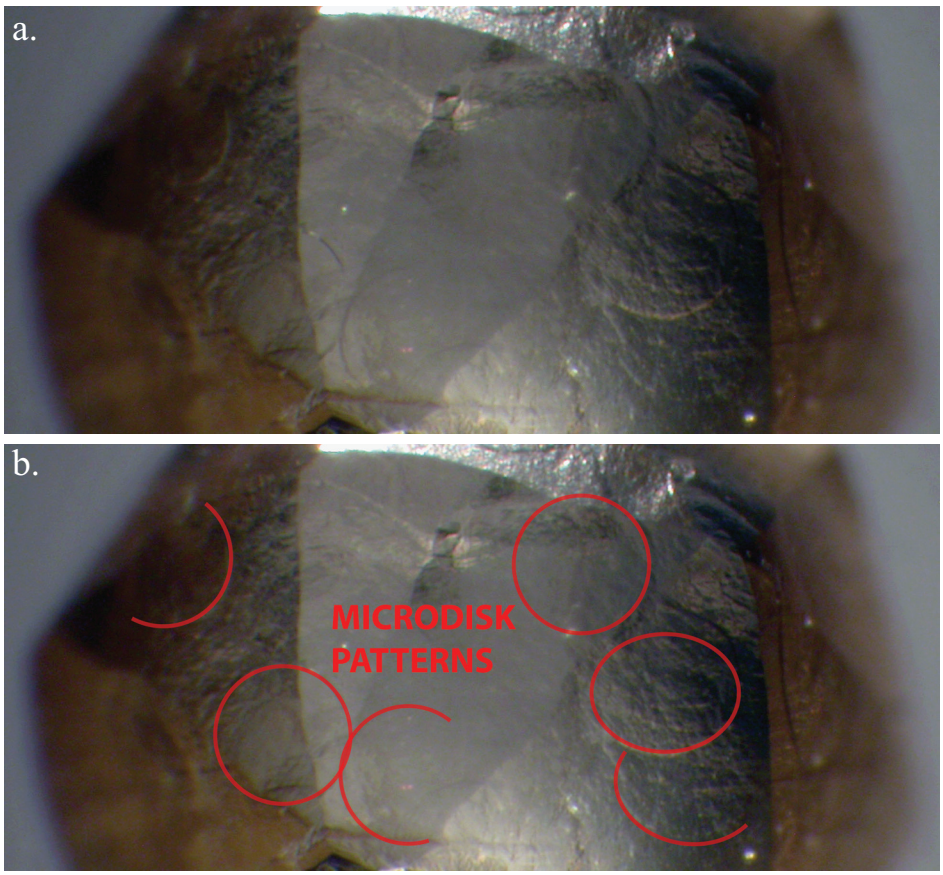

Figure C.8. a) b) Circular microdisk patterns are observed on the rounded dodecahedral stone.

Appendix C

Diamond Surface Features

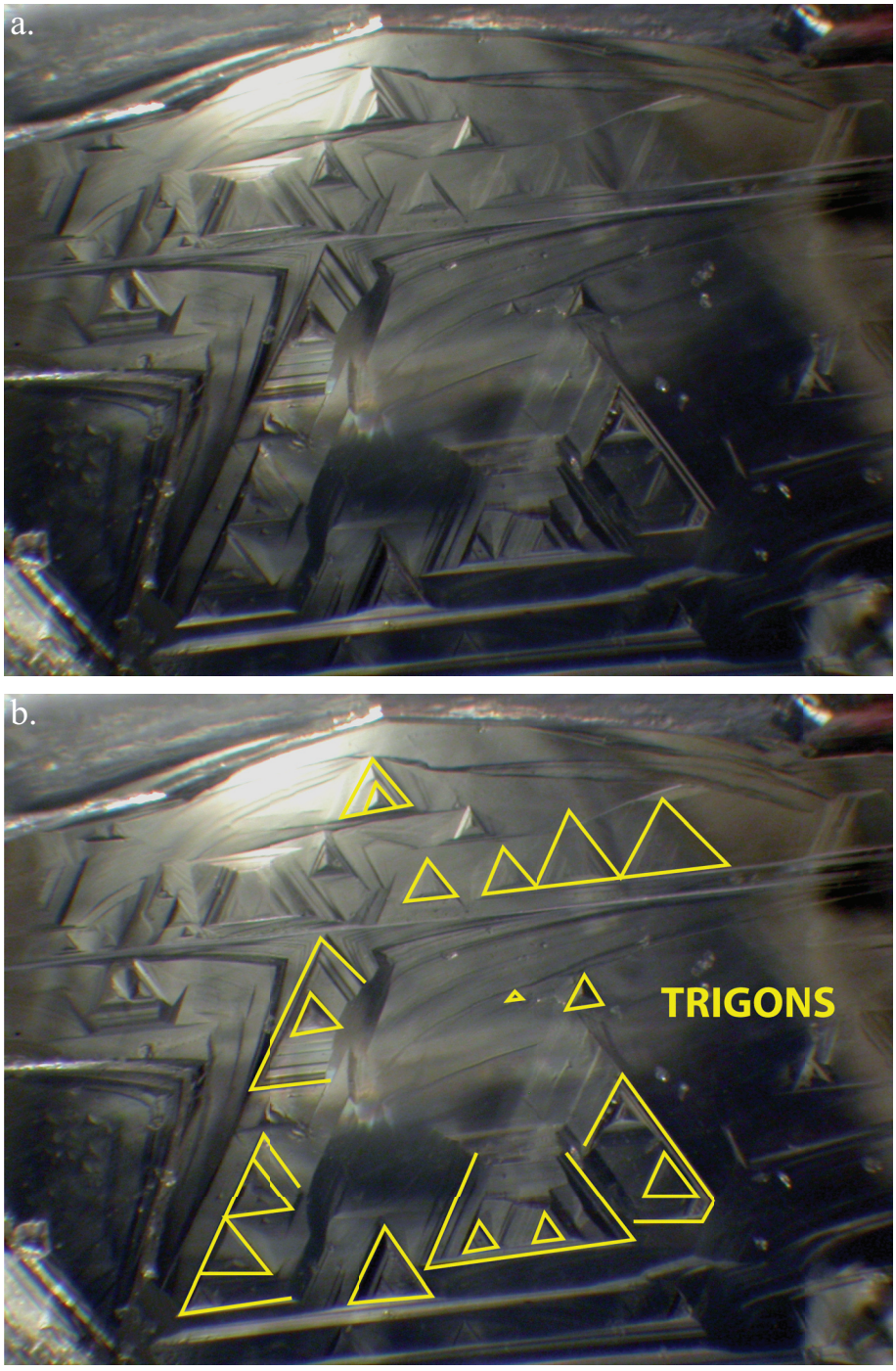

Figure C.9. a) b) Multiple trigons are observed. The majority are flat bottomed.

Appendix C

Diamond Surface Features

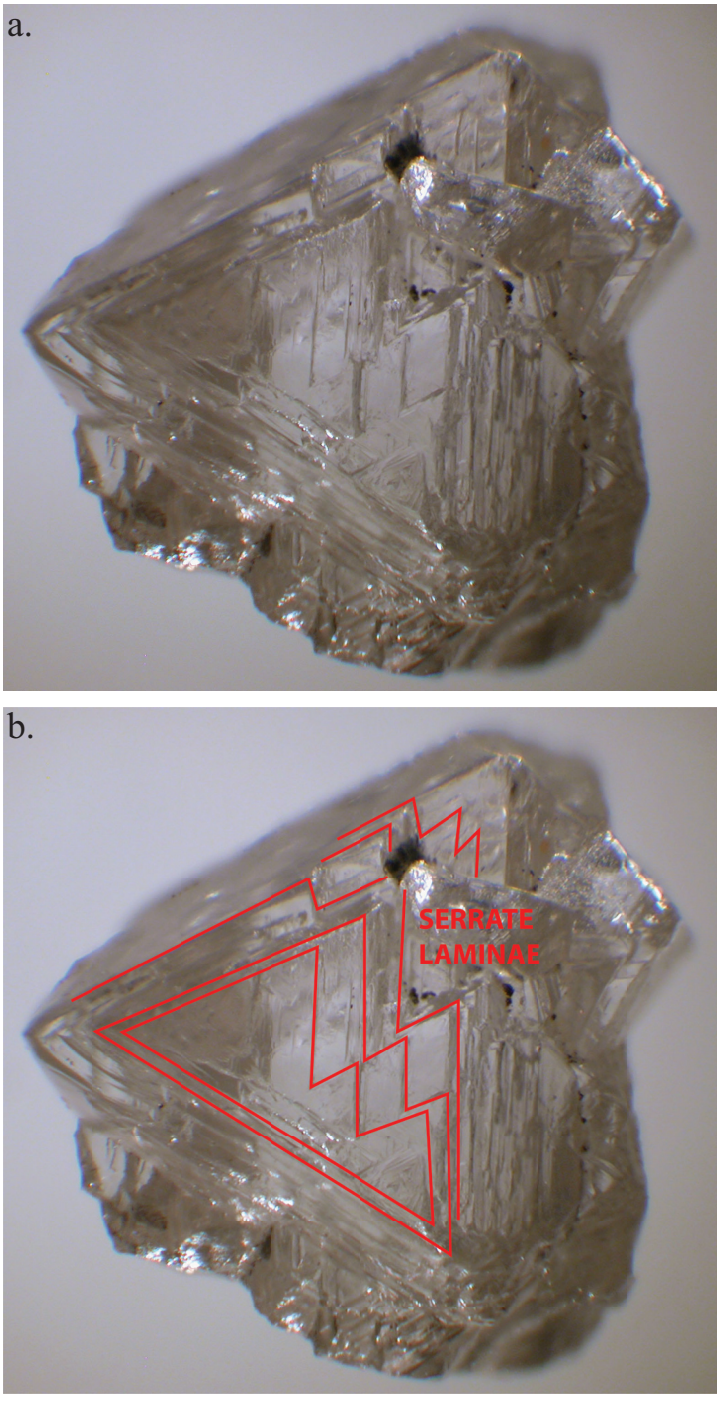

Figure C.10. a) b) Stacked growth layers showing serrate laminae.

Appendix C

Diamond Surface Features

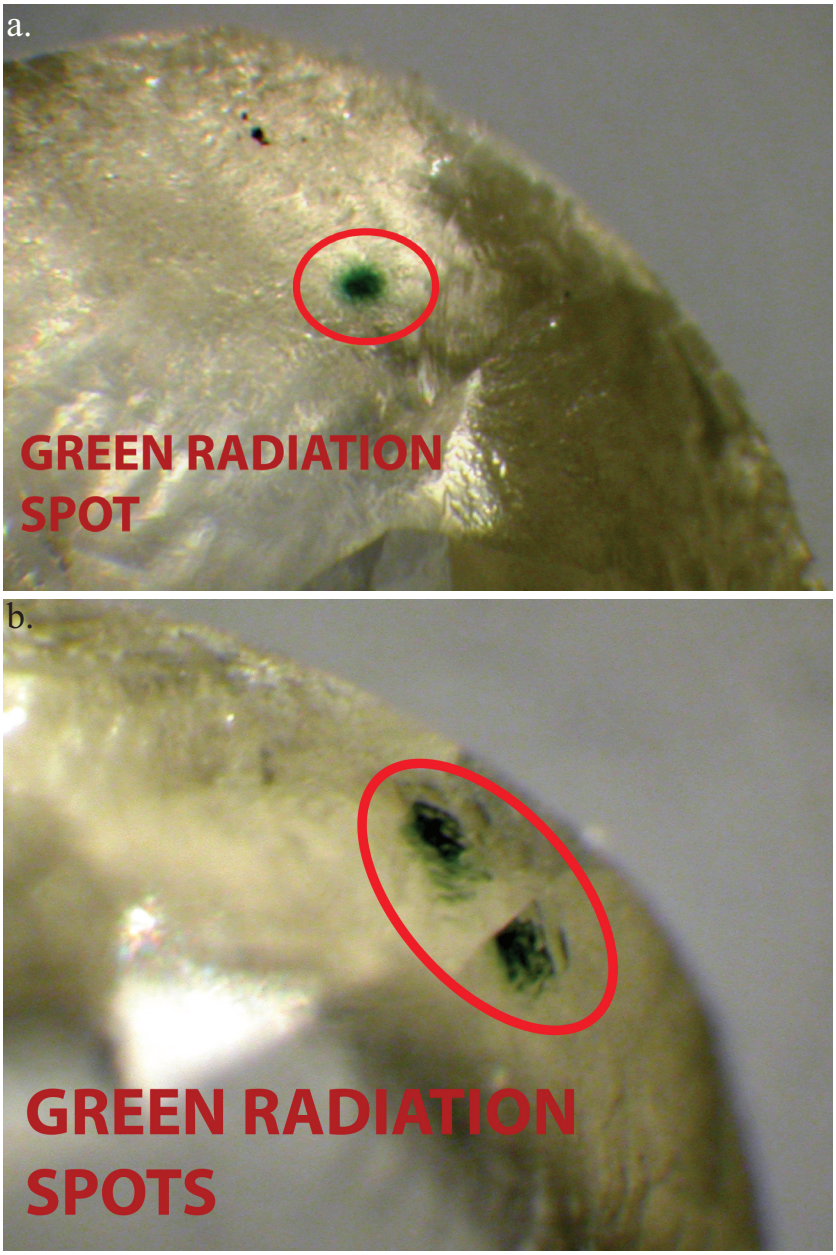

Figure C.11. a) b) Green radiation spots are visible on the surface of the diamond.

Appendix C

Diamond Surface Features

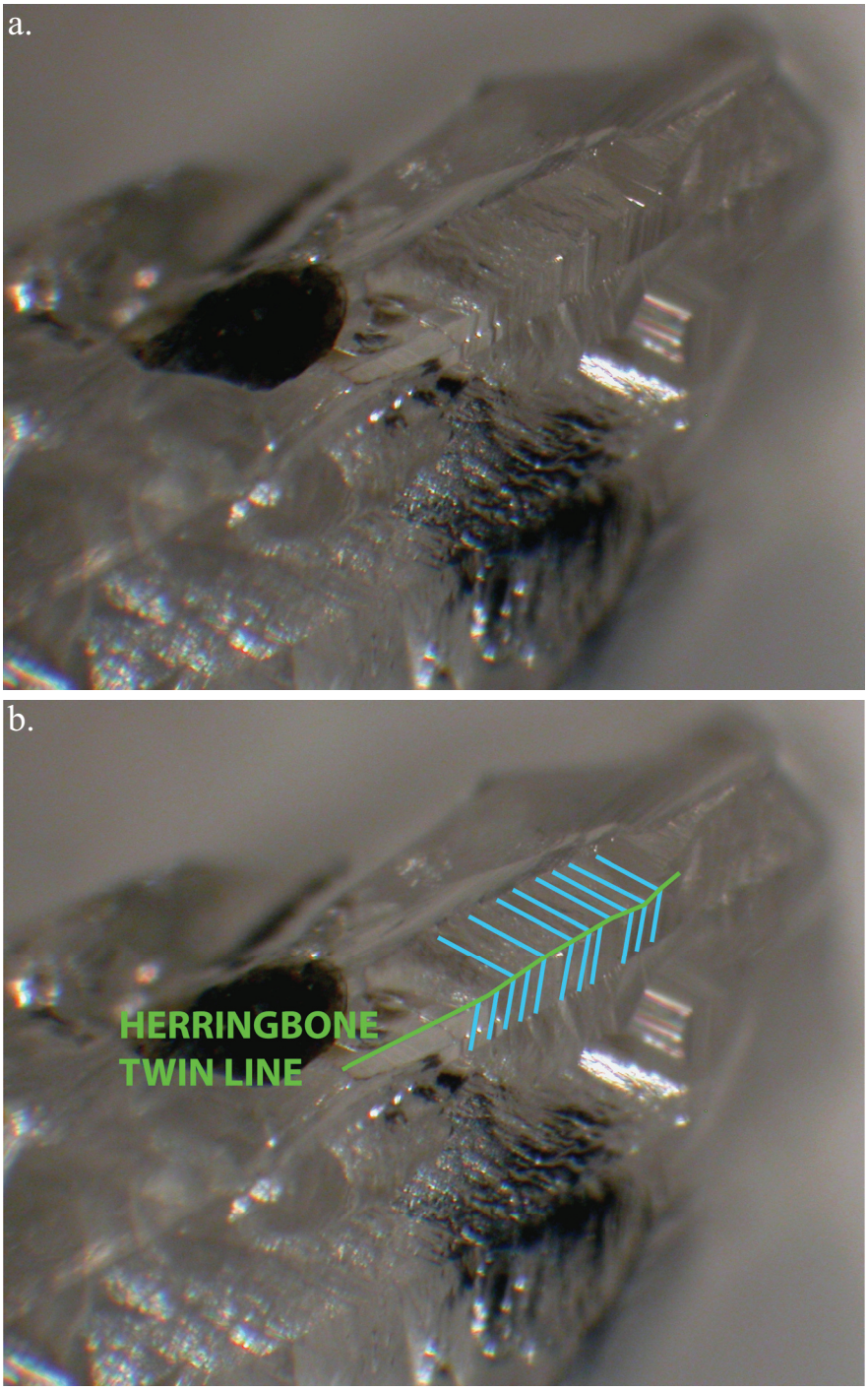

Figure C.12. a) b) A prominent herringbone twin line is observed on the triangular macle stone.

Appendix C

Diamond Surface Features

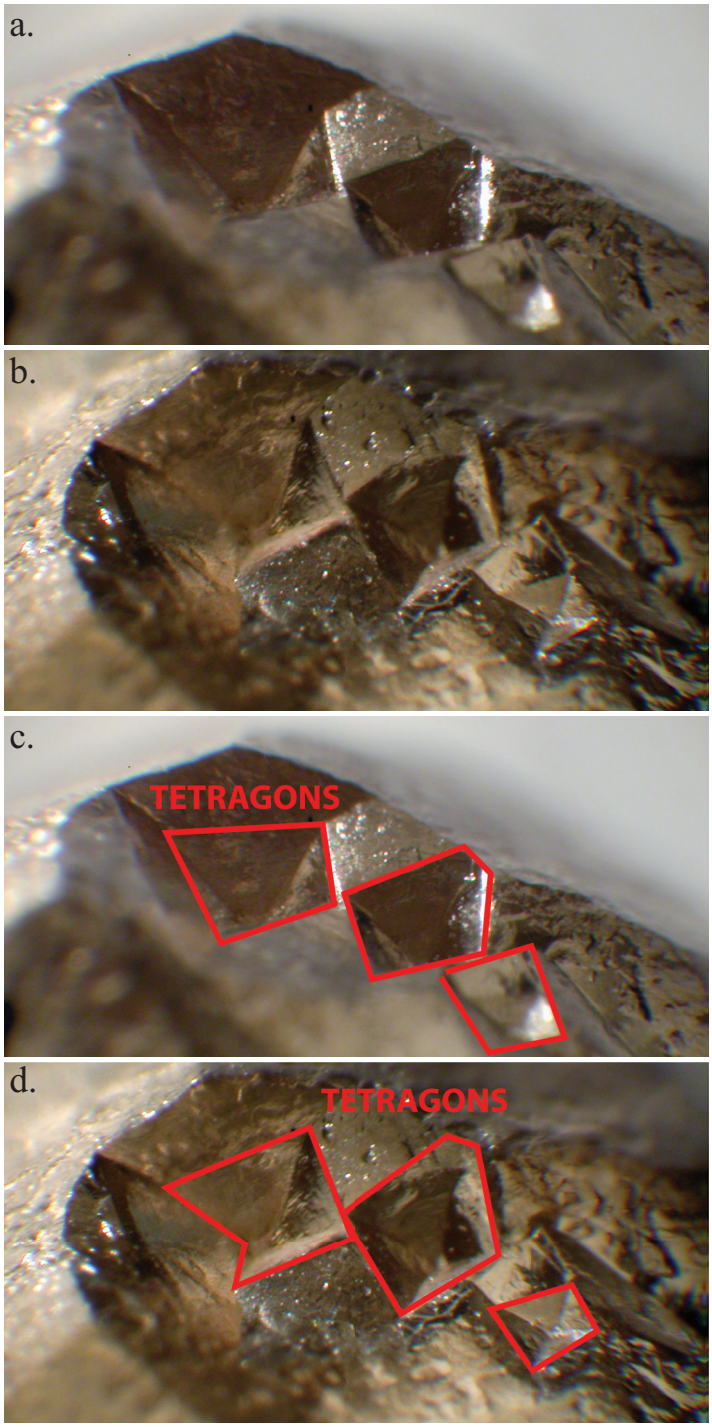

Figure C.13. a) b) c) d) On a broken cubic face tetragons have developed.

Appendix D

Additional Figures

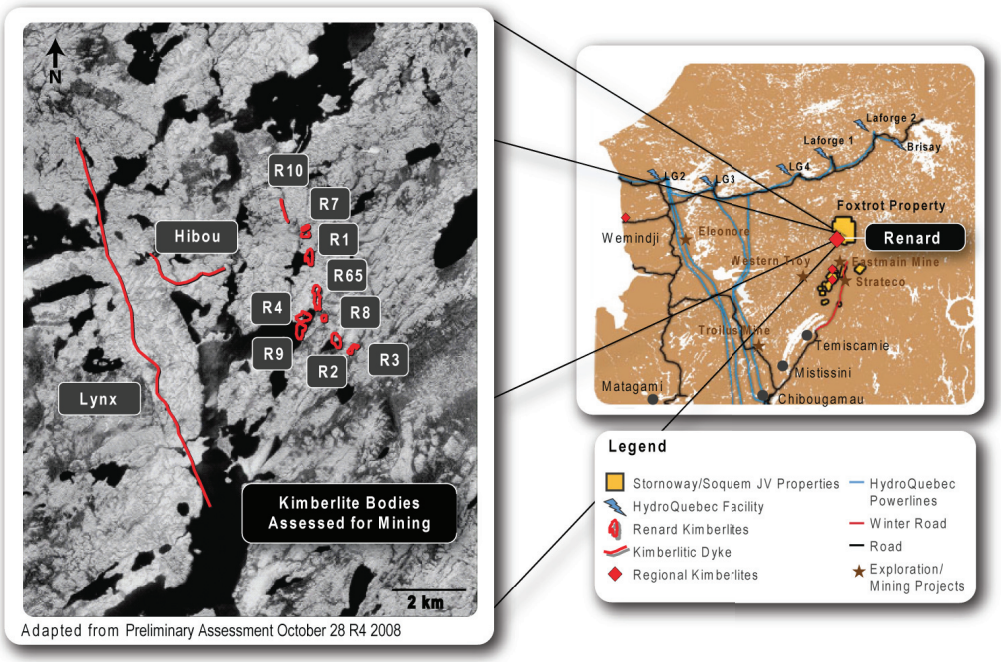

Figure D.1. A map showing the 8 kimberlite pipes, trending North-west/South-east, and the Lynx and Hibou Dykes to the west.

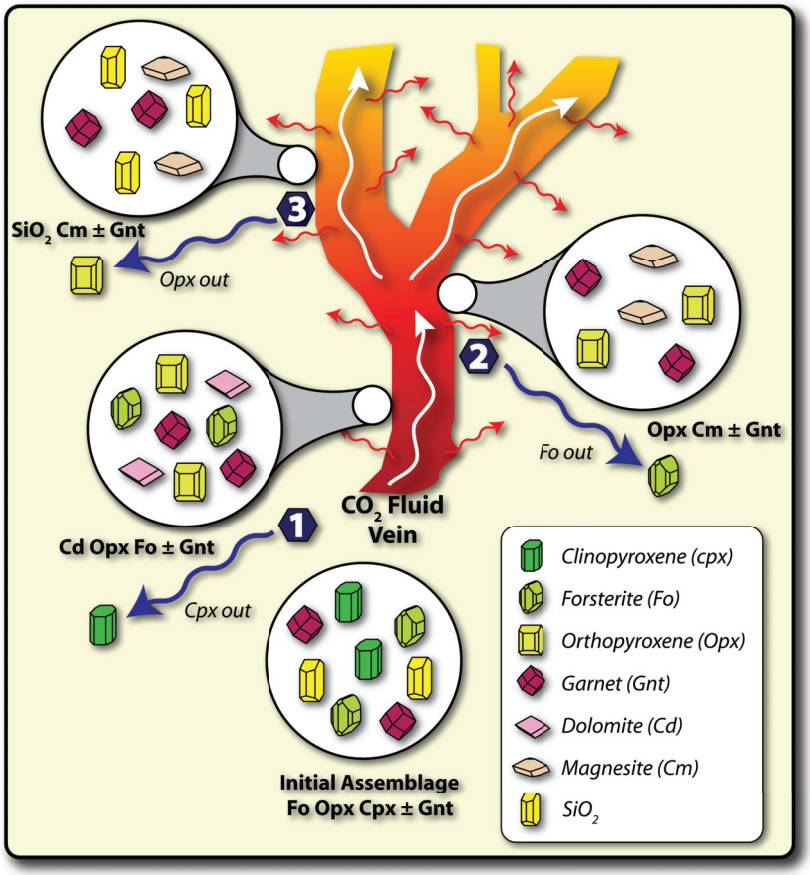

Figure D.2. Carbonation model, following the reactions of Wyllie and Huang (1976)

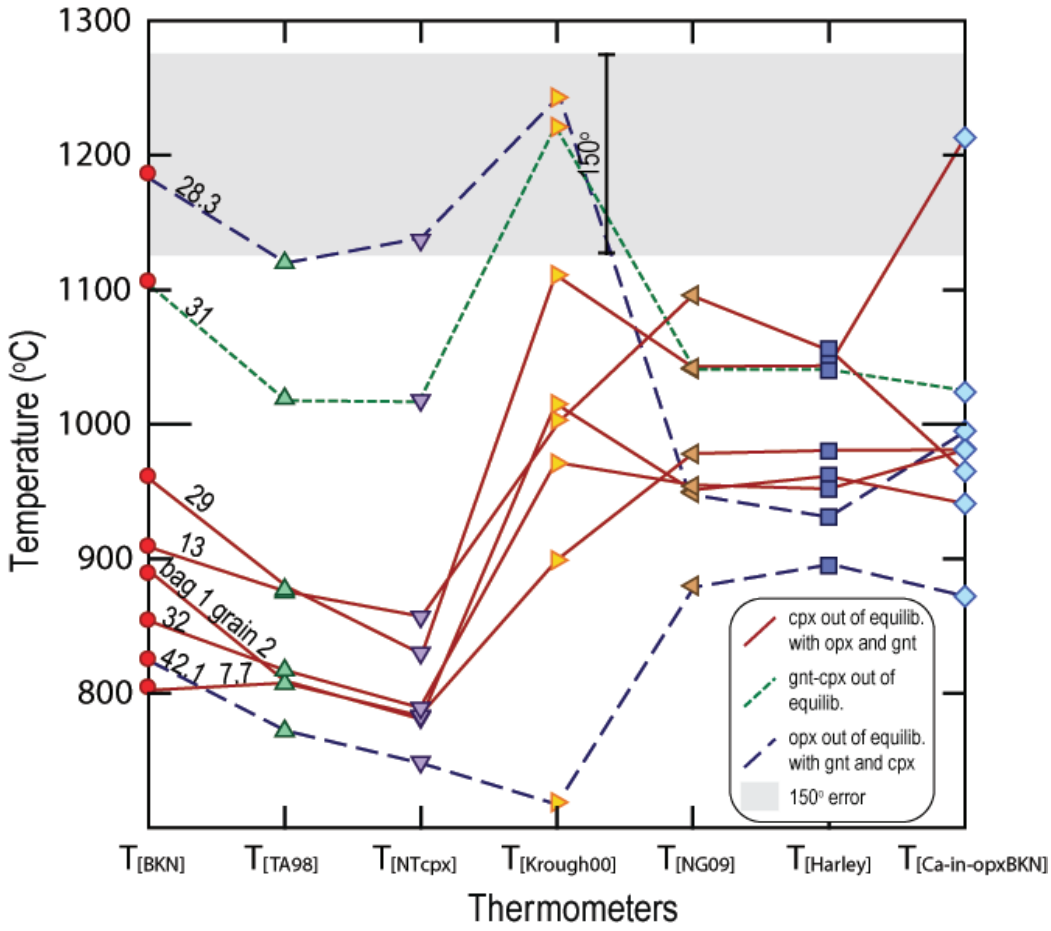

Figure D.3. Plot showing different thermometer combinations for disequilibrium comparison. 150°C is used as a first approximation of disequilibrium, this number varies with different thermometers which have different precisions.

T_{BKN} – Brey and Kohler (1990) (cpx-opx) thermometer; T_{TA98} – Taylor (1998) thermometer; T_{NT} – Nimis and Taylor (2000) thermobarometer; $T_{KROUGH00}$ – Krough (Ravna, 2000) thermometer; T_{NG09} – Nimis and Grütter (2010) thermometer; T_{Harley} – Harley (1984) Thermometer; $T_{Ca\text{-}in\text{-}opxBKN}$ – Brey and Kohler (1990) thermometer.